CHARACTERIZATION OF MIXED WETTABILITY AT DIFFERENT SCALES AND ITS IMPACT ON OIL RECOVERY EFFICIENCY

Final Report

August 4, 1999 – August 3, 2003

By

Mukul M. Sharma
George J. Hirasaki

September 2003

Work Performed under Contract No. DE-AC26-98BC15205

Chandra Nautiyal
Project Manager
U. S. Department of Energy
National Petroleum Technology Office
Tulsa, Oklahoma

Prepared by
The University of Texas at Austin
and
William Marsh Rice University

EXECUTIVE SUMMARY

1. PROJECT OBJECTIVES

The objectives of the this research project were to:

- Quantify the pore scale mechanisms that determine the wettability state of a reservoir,
- Study the effect of crude oil, brine and mineral compositions in the establishment of mixed wet states,
- Clarify the effect of mixed - wettability on oil displacement efficiency in waterfloods,
- Develop a new tracer technique to measure wettability, fluid distributions, residual saturations and relative permeabilities.

2. PROJECT TASKS

The project tasks are summarized below.

Task 1: Mechanisms of Establishment of Mixed-Wetting States

Task 2: Stability of Wetting Films and its Impact on Mixed Wetting States

Task 3: Effect of Wettability on Displacement Efficiency and Imbibition Behavior

Task 4: Use of Interfacial Tracers to Characterize Mixed Wet States

Task 5: Wettability Up-Scaling

3. ACCOMPLISHMENTS

The accomplishments of this project are discussed in detail in this report. In this section a summary of the accomplishments are provided below.

3.1 Effect of Brine Salinity and Crude Oil Properties on Oil Recovery and Residual Saturations

Centrifuge experiments were conducted on Berea cores to measure the drainage and imbibition relative permeabilities in two phase and three phase systems. Three crude oils, Prudhoe Bay and Shell Mars A1 and A20 crude were used in our tests. No effect on oil recovery was obtained in the drainage experiments when the crude oil was displaced by air at connate water. However in the imbibition experiments the oil recovery increased

significantly with the salinity of the connate brine. The salinity of the displacing brine had no significant influence on the oil recovery. The relative permeability curves obtained during drainage were also found to be insensitive to the salinity of the brine. However the imbibition relative permeability curves show strong salinity dependence. A comparison of the two crude oils and a non-polar mineral oil indicates that the more water-wetting Mars crude oil shows a higher oil relative permeability at the same bond number compared to the mixed-wetting Prudhoe Bay crude oil. The salinity dependence of the residual saturations and the relative permeabilities clearly indicate that the change in wetting properties of the rocks surfaces from water-wet to mixed-wet during the drainage process is an important factor controlling the imbibition relative permeability curves. This clearly suggests that the performance of waterfloods will be strongly affected by the composition of the crude oil and its ability to wet the rock surfaces, the salinity of the connate brine in the reservoir, and the height above the o/w contact.

3.2 Effect of Capillary Pressure, Salinity, and Aging on Wettability Alteration in Sandstones and Limestones

Core flow tests (Berea sandstone and Texas Cream limestone) were performed with a range of fluids under different conditions to identify the factors influencing the residual wetting and non-wetting phase saturations and oil recovery. Results of the tests conducted with Prudhoe Bay and Moutray crude oil show that remaining water (S_{wr}) and residual oil saturation vary systematically with Bond number for both sandstone and limestone samples. Differences in the shape of the wetting phase capillary desaturation curves are observed during primary and secondary drainage. This suggests that the distribution of fluids in the rock during secondary drainage is different from primary drainage due to a change in wettability of the core from a water-wet state to mixed-wet state. These trends were not observed with decane. Both limestone and sandstone cores become more susceptible to wettability alteration as the salinity is increased. The wettability index (Aw-Ao, water Amott-oil Amott) decreases from 0.56 (0.3% brine) to 0.2 (20% brine) in a limestone core with Prudhoe Bay crude oil. Aging the samples for 20-30 days with Moutray crude oil shows results in a change in the wettability of the cores. The oil recovery increases by 10-15% to more than 95% in both Berea and limestone cores. These results show that with time

the crude oil changes the wettability of the core from strongly water wet to mixed wet, which leads to a higher oil recovery. Experiments with samples of sandstone and limestone aged with Prudhoe Bay crude oil and brine of different salinities also show similar trends.

3.3 Investigating the Role of Crude Oil Components on Wettability Alteration

The surface forces between a crude-oil and its components (oil, resin and asphaltenes) and a glass substrate have been measured in brine of different salinity and pH using an atomic force microscope. The force vs. distance curves are used to measure the critical disjoining pressure for wettability alteration, i.e., departure from water-wet conditions. The measured data are compared with the classical DLVO theory to explore the nature of interaction of these components with mineral substrates.

The results indicate that the resins and asphaltenes obey the DLVO theory i.e. the stability of the brine film decreases with increasing brine salinity and increases with increasing solution pH. The opposite trend is observed with increasing salinity for the non-polar (pentane soluble) fraction and for the crude oil itself. This deviation from DLVO predictions indicates that for non-polar oils, hydrophobic interactions may play an important role in the interaction of oils with minerals and, therefore, in wettability reversal.

3.4 Influence of Wettability and Saturation on Liquid-Liquid Interfacial Area in Porous Media

The knowledge of the area of interfaces between phases is important to understand and quantify many flow and transport processes in porous media. In this work we apply the interfacial tracer technique to study the dependence of fluid/fluid interfacial area on saturation and wettability. The interfacial area between the wetting and non-wetting phases (brine and decane) in unconsolidated porous media (glass beads) was measured using an anionic surfactant (3-phenyl decyl benzene sulfonate) as an interfacial tracer. The beads are water wet; treating them with organosilane rendered them oil wet. The measurements were done at a series of steady-state fractional flows, providing data at intermediate as well as residual saturations. Flow rates were kept low so that capillary forces controlled the fluid configurations. We observe significant differences in interfacial areas as a function of wetting phase saturation as the wettability is changed from water-wet to oil-wet. During

primary drainage, measured interfacial area increases monotonically with decreasing water saturation in a water-wet medium. In contrast, the interfacial area measured in the oil wet porous medium increases with decreasing decane saturation, reaches a maximum and decreases as the residual decane saturation is achieved. The oil-wet experiment is qualitatively consistent with theoretical results, which predict the existence of a maximum in fluid/fluid interfacial area during drainage. The water-wet experiment is consistent with theoretical predictions that include the area of grains in pores that have been drained. We conclude that in the water-wet experiments, the tracer adsorbs at the interface between nonwetting phase and the wetting films on grains. In the oil-wet experiments, either the oil films are not sustained at high water saturation, or the tracer does not adsorb at them, possibly prevented by steric hindrance.

3.5 Experimental and Theoretical Basis for a Wettability-Interfacial Area-Relative Permeability Relationship

Using an interfacial tracer technique, our experiments show qualitatively different trends of total interfacial area between the wetting and non-wetting phases as a function of saturation, depending on whether the system is strongly or weakly wetted. A strongly wetted system is defined as one in which the wetting phase can spread as a thin film on the solid surface. We assess the relative contributions of fluid/fluid and fluid/solid interfaces to the total area using thermodynamic arguments. The fluid/solid contribution to area plays a crucial role in explaining the measurements.

The influence of interfacial area on relative permeability is not straightforward. Simple analysis based upon pore-level distribution of phases in a model porous medium allows quantifying the differences in the relative permeabilities for both weakly and strongly wetted systems, measured simultaneously with the interfacial area. Relative permeability correlates with fluid/solid area but not with fluid/fluid interfacial area.

3.6 Phase Behavior Modeling of Hydrocarbon-Methanol-Water Mixtures by Peng-Robinson and SAFT Equations of State

The phase behavior of mixtures of hydrocarbons, and polar fluids is important because such fluid mixtures are commonly encountered in field applications such as the

mixing of injected and reservoir fluids in near-wellbore treatments. The phase behavior of such fluid mixtures is difficult to model using currently available equations of state.

In this study, phase behavior data were measured both to help interpret coreflood experiments and for testing of equation-of-state models used in compositional simulation studies of methanol well treatments. The Peng-Robinson equation-of-state and the SAFT equation-of-state were used to model this new phase behavior data. The Peng-Robinson equation-of-state does better than the SAFT equation-of-state for hydrocarbon mixtures. The binary interaction coefficients had to be adjusted in both models to match the experimental data when methanol and water are in the mixture. The SAFT EOS required less tuning to match data from hydrocarbon-methanol mixtures. SAFT EOS, as expected, agrees with the data better than the Peng-Robinson EOS when water is in the mixture.

3.7 SAFT Based Interfacial Tension Model with Gradient Theory

SAFT equation of state is used with the generalized van der Waals gradient theory to evaluate the inhomogeneous influence parameter c for several non-polar and polar mixtures, which give an excellent agreement with the pure component interfacial tensions. Interfacial tensions of several binary mixtures are also computed. A mixing interaction coefficient similar to the binary interaction coefficient for bulk fluids had to be introduced in certain cases so as to obtain better predictions. The effect of high temperature and pressure on the interfacial tension of methane-water and CO2-water mixtures is also presented.

3.8 Estimation of Relative Permeability Curves and Wettability from Transient Pressure Drop Measurements

In this chapter a method is provided for the rapid determination of relative permeability curves and wettability from simple displacement experiments. The results for core flood experiments conducted on Texas Cream limestone and Berea sandstone are presented that illustrate the methodology.

The peak in the transient pressure drop response during displacement is found to be a very sensitive indicator of the curvature of the relative permeability curves. A simple curve-fitting algorithm is used to obtain the best fit to the transient pressure response during primary drainage and imbibition to obtain the water and oil exponents in a Corey type

relative permeability model. It is shown that these exponents of the relative permeability curves provide a good initial estimate of the curvature of the relative permeability curves, which, in addition to the relative permeability end-points, can be used in reservoir simulators.

The ratio of dimensionless end-point pressure drop during primary drainage, normalized by viscosity ratio, to the dimensionless pressure drop during secondary imbibition is defined as a new wettability indicator. For oil-wet rocks, the Relative Permeability Wetting Index (RPWI) is greater than one, whereas, for water-wet rock the RPWI is less than one. For intermediate wet rock, the wetting index is observed to be close to one.

The methodology provided in this paper gives a rapid and convenient way of estimating both wettability and relative permeability curves without having to conduct capillary pressure or steady state relative permeability experiments, which can be very time consuming.

3.9 Enhanced Imbibition into Oil-Wet Matrix

Oil recovery by water flooding in fractured formations is often dependent on spontaneous imbibition. However, spontaneous imbibition is usually insignificant in oil-wet, carbonate rocks. Sodium carbonate and anionic surfactant solutions are evaluated for enhancing oil recovery by spontaneous imbibition from oil-wet carbonate rocks. Crude oil samples must be free of surface-active contaminants to be representative of the reservoir. Calcite, which is normally positively charged, can be made negative with sodium carbonate. The ease of wettability alteration is a function of the aging time and temperature and the surfactant formulation.

3.10 Effects of Asphaltene Polydispersity on its Phase Behavior In Oil

In this study, we investigated the effects of asphaltene polydispersity on the thermodynamic phase behavior of oil. At this stage of the research, we represented polydisperse asphaltene in SAFT with four pseudo-components: the n-C_{3-5} (the resins), the n-C_{5-7}, the n-C_{7-15}, and the n-C_{15+} sub-fractions. Using an extension of the monodisperse SAFT asphaltene parameter fitting procedure, we were able to assign a set of SAFT parameters to represent each of the four sub-fractions. The volume fractions of precipitants at asphaltene

instability onset calculated using these parameters qualitatively agree with experimental findings.

SAFT calculations show that the lower molecular weight asphaltenes and resins play a large role in stabilizing higher molecular weight asphaltenes in oil. This is despite the inclusion of only dispersion interactions in the SAFT model. Resin's stabilizing effects on polydisperse asphaltene is greatest in the region of incipient asphaltene instability; when sufficiently large amounts of n-alkane precipitants are added, similar amounts of asphaltenes would precipitate regardless of the presence of resins in the oil. An analysis of the mass distribution of the asphaltene sub-fractions in the precipitated phase shows that the largest asphaltenes will precipitate first, followed by the precipitation of smaller asphaltenes upon further oil dilution.

TABLE OF CONTENTS

LIST OF FIGURES

LIST OF TABLES

1. Effect of Brine Salinity and Crude Oil Properties on Oil Recovery and Residual Saturations

Filoco, P. R., and Sharma, M. M.

SPE paper 49320, presented at the 1998 SPE Annual Meeting in New Orleans, LA, September 1998.

ABSTRACT

Centrifuge experiments were conducted on Berea cores to measure the drainage and imbibition relative permeabilities in two phase and three phase systems. Three crude oils, Prudhoe Bay and Shell Mars A1 and A20 crude were used in our tests. No effect on oil recovery was obtained in the drainage experiments when the crude oil was displaced by air at connate water. However in the imbibition experiments the oil recovery increased significantly with the salinity of the connate brine. The salinity of the displacing brine had no significant influence on the oil recovery. The relative permeability curves obtained during drainage were also found to be insensitive to the salinity of the brine. However the imbibition relative permeability curves show strong salinity dependence. A comparison of the two crude oils and a non-polar mineral oil indicates that the more water-wetting Mars crude oil shows a higher oil relative permeability at the same bond number compared to the mixed-wetting Prudhoe Bay crude oil. The salinity dependence of the residual saturations and the relative permeabilities clearly indicate that the change in wetting properties of the rocks surfaces from water-wet to mixed-wet during the drainage process is an important factor controlling the imbibition relative permeability curves. This clearly suggests that the performance of waterfloods will be strongly affected by the composition of the crude oil and its ability to wet the rock surfaces, the salinity of the connate brine in the reservoir, and the height above the o/w contact.

INTRODUCTION

Oil recovery in petroleum reservoirs is greatly affected by fluid-rock and fluid-fluid interactions. Surface chemical interactions directly control rock wettability, capillary pressure curves and relative permeabilities.

It has been generally accepted in the past that while relative permeability to the oil is higher in water-wet rocks the ultimate oil recovery may be higher in mixed-wet and oil-wet rocks. This lower residual oil saturation has been attributed to the presence of thin wetting films of oil on the surfaces of the rock grains[1,2,3]. Such continuous wetting oil films allow the oil to drain over a long period of time with very low trapped oil saturations left behind as disconnected oil ganglia. This mechanism has been used to explain high oil recoveries observed in reservoirs in which gravity drainage is the major recovery process. The ultimate oil recovery at the end of a waterflood has been shown to either increase or decrease with increasing oil-wetness [4,5]. In three phase systems an alternative explanation for these high oil recoveries is the drainage of oil films spreading on water in the presence of gas in the pore space. There are, however, a very limited number of studies to substantiate this claim.

Earlier studies [5] have demonstrated the importance of brine salinity in oil recovery by waterflooding. Core flow tests clearly show that for some crude oils the residual oil saturation obtained at the end of a waterflood depends on the salinity of the brine used. The reasons for this are as yet unclear.

The importance of wettability in determining oil recovery and relative permeability curves is well established [2]. The conditions under which mixed-wettability states are achieved is less well understood. Recent studies conducted by Basu and Sharma [7,8,9,10] and Buckley et al.[3] point to the importance of crude oil composition in wettability alteration. This dependence on the capillary pressure can be explained on the basis of the critical disjoining pressure that has been measured for both mineral oil and crude oils [7,10]. At capillary pressures above the critical disjoining pressure thin brine films that wet the mineral grains are ruptured and the crude oil-wets the grain surfaces. Since the critical disjoining pressure is a function of the properties of the brine and the crude oil and the curvature of the mineral grains there can be a wide range of pressures over which film rupture occurs. It is expected that convex surfaces will be dewet at the lowest capillary pressures in accordance with the augmented Young-Laplace equation [11,12]. This selective dewetting of surfaces can give rise to mixed-wetting conditions over a range of capillary pressures. With this conceptual framework the rock is expected to get progressively more oil-wet as the capillary pressure is increased i.e. the connate water saturation is decreased. This is consistent with the fact that reservoirs tend to be more oil-wet higher in the structure [11].

The objectives of this research are to perform centrifuge coreflow tests with a range of fluids under different conditions of wettability and to clearly identify the factors that influence: (1) the remaining wetting phase saturation at the end of primary drainage, (2) the residual intermediate-wet phase saturation during secondary drainage, (3) the relative permeability to the non-wetting phase during imbibition (waterflooding) and, (4) the residual non-wetting phase saturation at the end of the imbibition cycle. A sequence of drainage and imbibition cycles are conducted using the centrifuge for two and three-phase systems. The relative permeability curves, the residual saturations, and the capillary desaturation curves for water and oil-wet Berea cores for various fluid pairs obtained are presented and discussed in the context of known fluid properties.

The relative permeability and the residual saturations can be expressed as functions of the capillary number and Bond number [13,14] and incorporated in numerical reservoir simulators. The results show that the centrifuge method is a fast and reliable method for obtaining the desired residual saturations as a function of the Bond number or the equivalent trapping number [15,16,17,18,19]. In regions of low relative permeability (near end points) and in reservoirs where gravity drainage controls the recovery process the centrifuge method offers some clear advantages over other displacement methods [20].

EXPERIMENTAL METHODS

Fluids Used The fluid systems (water/oil/air) were chosen with the objective of evaluating the effect of their properties on relative permeability and residual saturations. The fluid systems were carefully prepared by allowing them to be in contact with each other for at least 12 hours. This allows mass transfer to take place between phases prior to the fluids entering the core. This minimizes transient effects associated with mass transfer of partitioning components in the core. The interfacial tension of the fluids were measured as described below. The spreading coefficient calculated from the interfacial tension measurements, is defined as [21]:

$$S = \sigma_{wg} - (\sigma_{og} + \sigma_{ow}) \qquad [1.1]$$

The aqueous phase used was brine (NaCl), different concentrations and cation types were tested. In some cases a small amount (2%) of isobutanol was added to the brine in order to

change its initial spreading coefficient from positive to negative. The gas phase is always air. The fluids were pre-equilibrated before use in the centrifuge, contact angle and IFT experiments.

The oil phases used were Soltrol (mineral oil), dodecane, dodecene, Prudhoe Bay crude oil, and Shell A-1 and A-20 crude oils. The mineral oil, dodecane and dodecene are alkenes with well known compositions, the Prudhoe Bay and Shell crudes provide us crude oils with a range of acid and base numbers.

Core Preparation A total of 104 core plugs (2.5 cm in diameter and 2.5 cm in length) were cut from a large optically homogenous slab of Berea sandstone using tap water as the cutting fluid. The core plugs were dried in an air-oven at 100°C for at least 24 hours and then evacuated and saturated in a dessicator during a period of five hours prior to weighing. The core porosities varied from 19.9% to 23.6% and the absolute permeability varied from 180mD to 220mD.

Berea sandstone in its original state is water-wet. To artificially render the cores oil-wet the cores were treated with a wettability altering agent, Quilon C. This is a fatty acid chromium complex manufactured by DuPont, that binds irreversibly to negatively charged surfaces such as silica leaving a hydrophobic surface of hydrocarbon tails. Details of the core treatment procedure are given in Appendix A. The treated cores showed very reproducible results and the original porosity was reduced by less than 1%.

Interfacial Tension Measurements The interfacial tension between brine and crude oil was measured by a ring tensiometer. The ring was flamed and immersed in brine. Crude oil was poured on the brine and the tension was measured for the ring passing from the brine to the oil phase (see Ref. 21 for details).

Centrifuge Experiments A Beckman high-speed ultra-centrifuge equipped with a stroboscope, an electrical timer, and a device for mounting the cores in the centrifuge for drainage and imbibition was used in our experiments. The fluid production from the cores is observed through a transparent window with the help of a stroboscope. A video camera was placed over the observation window of the centrifuge to record the fluid production data at early time. It is very important to accurately record the fluid production in the first few

minutes of each test. The fluid production was recorded manually by viewing the tape in slow motion. O'Meara and Lease[19] solved the same problem using an automated centrifuge apparatus that used a linear photodiode array in conjunction with a microcomputer to image and identify liquids recovery from centrifuged core samples.

The centrifuge method consists of increasing the centrifuge speed in steps and measuring at each step the amount of fluid produced from a core as a function of time and at equilibrium when flow has ceased. At each speed, the equilibrium saturation and capillary pressure can be used to obtain the capillary pressure curve, and the transient behavior can be used to infer the relative permeability of the displaced phase.

The cores, previously dried and weighed, are saturated with the specified brine using a dessicator. A drainage centrifuge displacement is run, displacing the brine with crude oil until a "residual" water saturation is achieved. The volume of wetting phase collected as a function of time is recorded at each centrifuge speed. The remaining water saturation at each rpm is also recorded to obtain the capillary desaturation curve for the wetting phase.

The imbibition test is conducted by displacing the crude oil with a displacing brine that may be different from the "residual" brine depending on the objective of the test. The early time displacement data is recorded with the video-camera for more precise readings and subsequent displacement data is recorded visually. For our test conditions relatively little flow occurs after 2 or 3 hours. To ensure equilibrium the core is spun at each rpm for at least 20 hours.

In order to obtain approximately the same residual water saturation the drainage tests should be run at the same bond number so the rpm used for each set of fluids is a function of the density of the brine and interfacial tensions. The same is true for the imbibition tests when similar displacement conditions are needed for different brine salinity or for different crudes.

The bond number is defined as [22],

$$N_B = \frac{kg(\rho_{l'} - \rho_l)}{\sigma_{ll'}} \qquad [1.2]$$

The trapping number is defined as [22],

$$N_{Tl} = \frac{\left| \underline{\underline{k}}.\nabla.\Phi_{\lambda'} + g(\rho_{l'} - \rho_l)\nabla D \right|}{\sigma_{ll'}} \qquad [1.3]$$

The capillary desaturation data can be represented by a relation of the form [22]

$$S_{lr} = S_{lr}^{high} + \frac{S_{lr}^{low} - S_{lr}^{high}}{\left(1 + T_l N_{Tl}\right)^n} \qquad [1.4]$$

Values of S_{lr}^{high} and S_{lr}^{low} are obtained experimentally, *n* is assumed to be 1 (unless stated otherwise) and T_l is a fitting parameter.

The relative permeability curves for the displaced phase were calculated using the method presented in Ref. 15. This method provides an easy analytical way of analyzing the data. The analytical analysis of centrifuge data has two main limitations: the inability to measure the relative permeability of the displacing phase, and the assumption that the viscosity of the displacing phase is small. These are discussed in detail in Ref. 15.

RESULTS

Figure 1.1 shows a capillary desaturation curve where the non-wetting phase is air or dodecane. The remaining water saturation at high bond numbers is slightly lower when the water is displaced by air (0.08) as compared to dodecane (0.14). On the other hand at low bond numbers the remaining water saturation is higher when air is the displacing phase. The data is in general consistent with that reported by Omoregie [20].

When the wetting phase is changed from water to dodecene (Figure 1.2) the remaining wetting phase saturation is higher for the water than the dodecene at a given bond number (air being the non-wetting phase in both cases). This may be expected since the mineral surfaces are much more “water-wet” than “dodecene wet” in the presence of air i.e. the dodecene-mineral interfacial energy is higher than the water-mineral interfacial energy. As a consequence it is much more difficult to remove thin films and pendular rings of water from the pore space than the dodecene.

Important differences in the shape of the wetting phase capillary desaturation curve are seen when our data is compared with data from the literature [23,24,25,26] obtained using both centrifuge displacement and dynamic displacement methods for desaturating the core (Figure

1.3). It is observed that all the centrifuge data (unfilled data points) appear to follow a slightly different trend than the dynamic displacement data (filled points). This rather remarkable grouping of data from a wide variety of sources using a wide variety of fluids seems to suggest that the two methods may provide systematically different "residual" wetting phase saturations at comparable bond and capillary numbers. The centrifuge method appears to provide systematically lower wetting phase saturations than the displacement technique. We conjecture that this may be due to insufficient time being allowed for equilibrium to be attained in the dynamic displacement experiments. Additional work needs to be done to better understand these differences.

The capillary desaturation curves for oil in oil-wet cores and water in water-wet cores look very much the same (Figure 1.4). This clearly suggests that the single most important factor controlling the capillary desaturation curve is the wettability of the porous medium.

Relatively small changes in the remaining water saturation after primary drainage are seen if the oil is changed from a non polar mineral oil to a crude oil (Figure 1.5). Changing the composition of the brine in the core from 3% to 20% sodium chloride also does not have a significant impact on the residual brine saturations.

In three-phase systems the residual saturation of the intermediate wet phase is also observed to decrease systematically with bond number. Figure 1.6 is a capillary desaturation curve showing the effect of spreading on the remaining oil saturation as a function of bond number. In this 3-phase system the oil (dodecane or dodecene) is the intermediate wetting phase. The results show consistently that the spreading system reaches a lower remaining oil saturation. For the spreading system the remaining oil saturation approaches zero at a bond number of approximately 1.E-04. This is consistent with previous results reported for three-phase systems [27]. In spreading systems the oil maintains phase continuity till very low oil saturations and can, therefore, be drained to near zero residual saturation [28,29,30,31]. Higher oil recoveries may, therefore, be expected for spreading oils.

The oil recovery achieved in these systems by a drainage process (air displacing oil at connate water saturation) is found to be independent of the salinity of the brine used. Figure 1.7 shows relative permeability curves obtained from the drainage displacement data for two different salinities. Almost identical curves are obtained for the Shell A20 crude at 0.3% and 3% salt concentration. Similar results were obtained with the other crude oils.

It can be concluded from the above experiments that the oil recovery during drainage for a given rock at a fixed bond number (or trapping number) is largely dependent on the spreading coefficient and not on individual interfacial tensions.

The results for imbibition show dramatically different results. The oil recovery during imbibition for a Prudhoe Bay crude oil is shown in Figure 1.8 for three different salinities. It is evident that significantly higher oil recoveries are obtained for the lower salinity brines. Similar results have been reported by Morrow et al.[5] in dynamic displacement experiments.

In the above experiments the salinity of the initial water was the same as that of the water injected during the waterflood. To check if the salinity of the connate water was the critical factor we varied the connate water salinity while keeping the salinity of the waterflood water the same. As seen in Figure 1.9 the oil recovery for the lower salinity connate water was again significantly higher than that for the high salinity connate water.

To check the influence of the waterflood water salinity the connate water salinity was held constant in the next set of experiments. As seen in Figure 1.10 the oil recovery does not change as the waterflood water salinity is changed from 0.3% to 20% for a fixed connate water salinity of 3%. This suggests that the oil recovery is not sensitive to the salinity of the injected brine. Indeed the oil recovery appears to be primarily determined by the salinity of the connate water.

To confirm these trends, experiments were conducted with three other oils. Figure 1.11 shows the oil recovery results for Shell A-1 crude oil during a waterflood. The same qualitative trends are observed. Higher oil recovery is achieved with lower connate salinity brines. The shape of the oil recovery curve is, however, quite different than that seen in Figure 1.10.

Results for Shell A-20 crude also show similar effects. However, when the tests were run for dodecene, the trends were less obvious (Figure 1.13). Only a very small difference was seen in the oil recovery as the connate brine salinity was changed from 3% to 20 %. Clearly the composition of the oil phase plays an important role in determining the relative magnitude of the salinity effect. For example, the Shell A-1 crude oil shows a bigger difference in the oil recovery when the connate brine salinity is changed from 3% to 20 % while the Prudhoe Bay crude shows a smaller effect (Figure 1.14) and the dodecene shows

the smallest effect (Figure 1.13).

DISCUSSION

The tests clearly show that the oil recovery is greater for lower connate brine salinities. Tests using 0.3% NaCl brine show an oil recovery of over 70% while the 20% NaCl brine shows a 57% oil recovery for the Prudhoe Bay crude. The oil-wet core showed an oil recovery of only 46%.

We can speculate about the reasons for the increase in oil recovery with decreasing salinity. Figure 1.8 shows that the oil recovery is lowest for the oil-wet sample. This effect of wettability is clearly more pronounced than that of salinity. It is also noted that the salinity of only the connate water appears to be important. This suggests that changes in connate water salinity may cause changes in the wettability of the pore space during the drainage process. The ability of the oil to rupture thin brine films is determined by the critical disjoining pressure for the water film bounded by the oil-water and the mineral water interfaces [7,8,9,10]. Repulsive disjoining pressures such as those caused by electrostatic repulsion or hydration forces can stabilize films. This will promote water-wetness. As the salinity is increased, electrostatic repulsion decreases due to screening of the surface charges [21]. Higher salinity should, therefore, result in less stable brine films. However, this is not observed experimentally. Adhesion tests [3] show less adhesion (more stable brine films) at higher salinities. AFM experiments[7,8,10] also show higher critical disjoining pressures (more stable brine films) at higher salinities. This can be attributed to changes in hydrophobic/hydration forces with salinity. Clearly these short range forces must become more repulsive as the salinity us increased.

The higher stability of brine films at higher salinity suggests suggest that low connate water salinity will cause cores to become mixed-wet (more oil-wet). Mixed-wet cores show lower residual oil saturations than strongly water-wet or oil-wet cores (Ref. 4) *i.e.* they have higher oil recoveries. This is the likely explanation for the trend observed with salinity. Figure 1.17 summarizes this trend.

What role does the composition of the oil play? It has been shown by direct measurements of critical disjoining pressure [7,8,10] that the Π_{crit} increases with salinity for some oils. Data presented by Basu and Sharma[7,8,10] indicates that for non-polar mineral oils

(octadecane etc.) and some crude oils the brine films become more stable as the salinity is increased. This is inconsistent with DLVO theory (a theory of surface forces that accounts for electrostatic and van der Waals interactions) and can only be explained by invoking hydrophobic interactions about which relatively little is known. However, for some crude oils and for the polar fractions of crude oils, electrostatic interactions dominate hydrophobic interactions and the brine films become less stable as the salinity is increased [8]. For highly acidic or basic oils (large acid or base numbers) where the surface charge density at the oil-water interface is large, electrostatic interactions are expected to dominate and the trends seen in our experiments can be explained in terms of the instability of brine films at high salinity. Prudhoe Bay crude has a high base number and presents a positively charged oil-water interface. For oils that do not contain acidic or basic groups the picture becomes less clear and the salinity dependence may be different. Indeed many such oils (eg. dodecene) do not show any salinity dependence.

Table 1.1 shows a comparison of the acid and base numbers of the crude oils used. It can be clearly seen that the crude oils with the high base numbers are observed to show mixed-wet behavior. This can be attributed to the electrostatic destabilization of the wetting brine films on the mineral grains[32]. High base numbers lead to a positive charge on the oil-water interface under neutral pH conditions. With the silica-water interface being negatively charged for pH values greater than 3 there is a net electrostatic attraction between the mineral-water and oil-water interfaces. This attractive disjoining pressure will cause destabilization of brine films and lead to mixed-wet conditions[32].

Differences are also observed in the breakthrough curves and oil recoveries for different crude oils at the same salinity. Figure 1.16 shows that the higher base number Mars A20 crude shows a lower oil recovery than the low base number Mars A1 crude. This fits in with the general trend that the more oil-wet the rock gets during primary drainage the lower the oil recovery will be during imbibition. No differences in oil recovery are seen during secondary drainage.

If the pore space is progressively made more oil-wet due to film rupture as the capillary pressure is raised, the pores rendered oil-wet will be the larger pores, as pointed out by Melrose and others [11,12]. This implies that the waterflooding brine sees a different porous medium than the connate water sees during primary drainage when the rock was water-wet.

As a consequence the waterflood water will tend to go into the largest of the oil-wet pores and of course continue to flow through the smallest pores which have not been contacted by oil during drainage and are hence still water-wet. This creates a very different fluid distribution than would be achieved if the core were oil-wet to begin with. Waterflood water will, therefore, be excluded from the intermediate size pores that have been rendered oil-wet. The fraction of such pores of course depends on the capillary pressure (trapping number) imposed during drainage. This reassignment of pore occupancy caused by changes in wettability during drainage is a likely reason for a larger fraction of the oil being bypassed during imbibition but not during drainage.

This leads to the conclusion that it is no longer sufficient to know what the original wettability of the rock is but rather to be able to track changes in the wettability as the rock undergoes cycles of drainage and imbibition.

The role of crude oil composition on the salinity dependence of the wettability and oil recovery is a difficult problem to resolve. We have clearly shown that for some crude oils the oil recovery is sensitive to the connate brine salinity while in mineral oils no such dependence is observed. The salinity dependent oil recovery during waterflooding is not limited to acidic crudes since both Shell A1 and A20 (high base number) crudes show a clear salinity dependence. For Prudhoe Bay crude, the oil recovery data (at high capillary pressures) indicate that the brine films become more stable as the salinity is increased. This is consistent with the AFM and adhesion tests (Refs. 3,7) conducted at low capillary pressure indicate that the critical disjoining pressure increases with salinity (less adhesion of oil). DLVO theory (a theory of surface forces that accounts for electrostatic and van der Waals interactions) is unable to explain the increase in brine film stability with salinity. It has been speculated [8] that hydration forces [9] and hydrophobic interactions are responsible for this observation. This effect of salinity on the brine film stability for different crude oils needs to be investigated further.

CONCLUSIONS

Centrifuge experiments were conducted to investigate the dependence on residual wetting phase saturation and relative permeability on fluid properties. In two phase systems the remaining wetting phase saturation shows a slight dependence on the surface energies of

the fluid-solid interface. It is shown that in three-phase systems the residual intermediate wetting phase saturation is independent of the individual interfacial tensions and depends primarily on the spreading properties of the fluids. The oil displacement and relative permeabilites during secondary drainage are independent of the brine salinity.

Imbibition (waterflood) experiments show a strong salinity dependence. Higher oil recoveries are obtained for lower connate brine salinities. All three crude oils studied showed similar results. For the non-polar mineral oils no salinity dependence was detected. The salinity of the connate water was found to be the primary factor controlling the oil recovery. We attribute this dependence to alteration of the wettability to mixed-wet conditions from water-wet conditions.

NOMENCLATURE

D = depth, L

g = gravitational constant, Lt^{-2}

$\underline{\underline{k}}$ = permeability tensor, L^2

k = permeability, L^2

N_B = bond number

N_{Tl} = trapping number of phase l

S_{lr} = residual saturation of phase l

$S_{lr}^{high}, S_{lr}^{low}$ = residual saturation of phase l at high and low N_{Tl}, L^3/L^3 PV

T_l = trapping parameter for phase l

Greek Symbols

$\nabla.\phi_l$, = flow potential gradient

ρ_l = density of phase l, mL^{-3}

$\sigma_{ll'}$ =interfacial tension between phase l and l' mt^{-2}

ϕ_l = potential of phase l, $mL^{-1}t^{-2}$

Subscripts

l = displaced phase

l' = displacing phase

r = residual

Superscripts

high = high trapping number

low = low trapping number

REFERENCES

1. Anderson, G. W.: "Wettability Literature Survey - Part 5: The Effects of Wettability on Relative Permeability," *JPT* (November 1987) 1453.
2. Salathiel R.A.: "Oil Recovery by Surface Film Drainage in Mixed-Wettability Rocks," *JPT* (Oct. 1973) 1216.
3. Buckley, J. S., Liu, Y. and Monsterleet, S.: "Mechanisms of Wetting Alteration by Crude Oils," SPE 37230, Presented at the SPE International Symposium on Oilfield Chemistry, Houston (Feb. 1997).
4. Morrow, N. R.: "Wettability and its Effect on Oil Recovery", JPT (Dec. 1990) 1476.
5. Tang, G. Q. and Morrow, N. R.: "Effect of Temperature, Salinity and Oil Composition on Wetting Behavior and Oil Recovery by Waterflooding," paper SPE 36680 presented at the SPE Annual Technical Conference and Exhibition, Denver, Colorado (Oct. 6-9, 1996).
6. Dullien F.A.L. *et al*.: "The Effects of Surface Roughness on the Capillary Pressure Curves and the Heights of Capillary Rise in Glass Bead Packs," *J. Coll. Int. Sci.,* 127(2), 362-372, 1989.
7. Basu, S.; Sharma, M.M.; "Characterization of Mixed Wettability States in Oil Reservoirs

by Atomic Force Microscopy", SPE Journal, Vol. 2, SPE 35572, 427-435, December1997.

8. Basu, S.; Sharma, M.M.; "Investigating the Role of Crude-Oil Components on Wettability Alteration Using Atomic Force Microscopy," SPE Journal, Vol. 4, No. 3, 235-241, Sept. 1999.
9. Das, S.K.; Sharma, M.M.; Schechter, R.S.; "Solvation Force in Confined Molecular Fluid Using Molecular Dynamics Simulation," The Journal of Physical Chemistry, 100, No. 17, 7122-7129, May 1996.
10. Basu, S.; Sharma, M.M.; "Measurement of Critical Disjoining Pressure for Dewetting of Solid Surfaces", Journal of Colloid and Interface Science, 181, 443-455, August 1996.
11. Jerauld, G.R., Rathmell, J.J.: "Wettability and Relative Permeability of Prudhoe Bay: A Case Study of Mixed-wet Reservoirs", SPE Reservoir Engineering, (Feb. 1997) 58.
12. Melrose, J.C.: "Interpretation of Mixed Wettability States in Reservoir Rocks", SPE 10971, Presented at the 1982 SPE Annual Conference and Exhibition, New Orleans (Oct 1982).
13. Dumoré, J. M. and Schols, R.S.: "Drainage Capillary-Pressure Functions and the Influence of Connate Water," *Soc. Pet. Eng. J.* (Oct. 1974) 437-444.
14. Dykstra, H.: "The Prediction of Oil Recovery by Gravity Drainage," *JPT* (May 1978) 818.
15. Hagoort, J.: "Oil Recovery by Gravity Drainage," *SPEJ* (June 1980) 139.
16. Hirasaki, G.J., Rohan, J.A., and Dudley, J.W.: "Interpretation of Oil-Water Relative Permeabilities from Centrifuge Experiments," SPE Advanced Technology Series, Vol. 3, N°. 1 (March, 1995).
17. Hirasaki, G.J.: "Dependence of Waterflood Remaining Oil Saturation on Relative Permeability, Capillary Pressure, and Reservoir Parameters in Mixed-wet, Turbidite Sands," paper SPE 30763 presented at the SPE Annual Technical Conference and Exhibition, Dallas, Texas (Oct. 22-25, 1995).
18. Johnson, E. F., Bossler, D. P., and Naumann, V. O.: "Calculation of Relative Permeability from Displacement Experiments", *Trans*., AIME (1959) **216**, 370-372.
19. O'Meara, D. J., Jr. and Lease, W. O.: "Multiphase Relative Permeability Measurements Using an Automated Centrifuge," paper SPE 12128 presented at the SPE Annual

Meeting, San Francisco, Oct., 1983.

20. Omoregie, Z.S.: "Factors Affecting the Equivalency of Different Capillary Pressure Measurement Techniques", SPE 15384, Presented at the 61st Annual SPE Conference and Exhibition, New Orleans (Oct. 1986).
21. Adamson, A. W.: *Physical Chemistry of Surfaces*. Interscience Publishers (1997).
22. Pope G. A. et al.: "Modelling Relative Permeability Effects in Gas Condensate Reservoirs", SPE 49266, Presented at the Annual SPE Conference and Exhibition, New Orleans (Sept. 1998).
23. Gupta, S. P., and Trushenski, S.P.: "Micellar Flooding – Compositional Effects in Oil Displacement", SPE 7063, SPEJ (April 1979), 116.
24. Mohanty, K. K., and Salter, S. J.: "Multiphase Flow in Porous Media: 3. Oil Mobilization Transverse Dispersion and Wettability, SPE 12127, Presented at the Annual SPE Conference and Exhibition, San Francisco (Oct. 1983).
25. Bhuyan, D.: "Effect of Wettability on Capillary Desaturation Curves", M.S. Thesis, University of Texas at Austin, 1986.
26. Delshad et al.: "Effect of Capillary Number on the Residual Saturation of Three Phase Micellar Solution", SPE 14911, Proceedings of the SPE/DOE Symposium on Enhanced Oil Recovery, Tulsa (1986).
27. Kalaydijian, F. *et al*.: "The Role of Wettability and Spreading in Gas Injection Processes under Secondary Conditions," de Haan, H.J. (ed.), *New Developments in Improved Oil Recovery*, Geological Society Special Publication No. 84, 63-71, 1995.
28. Nenniger, E. JR. and Anderson Storrow, J.: "Drainage of Packed Beds in Gravitational and Centrifugal-force Fields," *AIChEJ*., **4(3)**, 305-316, 1958.
29. Oren, P. E. and Pinczeweski, W.V.: "The Effect of Film Flow on the Mobilization of Waterflood Residual Oil by Gas Flooding," *proc*. of the 1991 European IOR-Symposium, Stavanger, Norway, May 21-23.
30. Oren, P. E. and Pinczewski, W.V.: "The Effect of Wettability and Spreading on Recovery of Waterflood Residual Oil by Immiscible Gas Flooding," *SPEFE* (June 1994) 149.
31. Richardson, J. G., Sangree, J. B., and Snider, R.M.: "Oil Recovery by Gravity Segregation," *JPT* (Jun. 1989) 581.
32. Dubey, S.T. and Doe, P.H.,: "Base Number and Wetting Properties of Crude Oils", SPE

Reservoir Engineering, (Aug 1993), 195.

APPENDIX A

The following steps were followed to obtain strongly oil- wet cores. The cores previously dried and weighed were evacuated for "five" hours. The cores were then vacuum saturated and submerged in a solution of Quilon C (20%) in isopropyl alcohol in a dessicator. The system was kept in vacuum for "three" hours and left to adsorb on the pore surfaces overnight. After being weighed the cores were heated to dryness overnight at a temperature of 80°C. The oil-wetness of the Quilon C treated cores was tested by a spontaneous imbibition test. The brine saturation changes by only 4% during spontaneous imbibition indicating that the core was still mixed-wet but with large oil-wet domains.

TABLE 1.1. PROPERTIES OF THE CRUDE OILS USED

CRUDE OIL	Acid number / Base number	DENSITY kg/m3	VISCOSITY cp	WETTABILITY FROM LITERATURE
Shell A-1 (Pink)	1.93 / 2.22	0.909	250	Water-wet
Shell A-20 (Terracota)	0.24 / 2.60	0.859	42	Mixed-wet
Prudhoe Bay	0.15 / 2.28	0.91	22	Mixed-wet

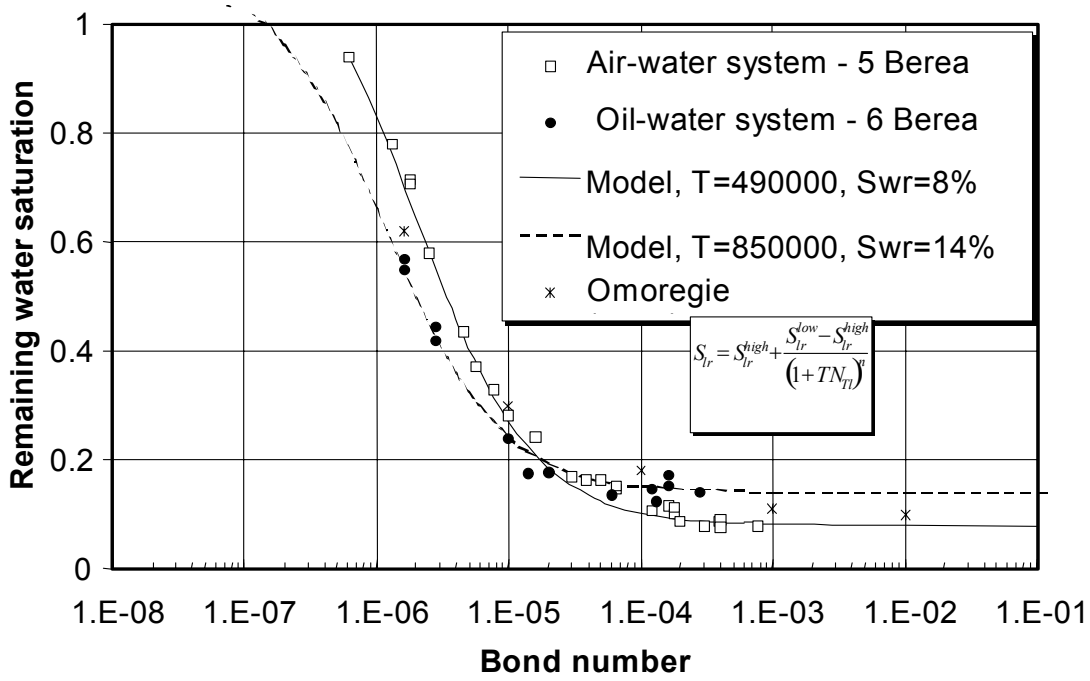

Figure 1.1 Wetting phase capillary desaturation curve, (two phase, Berea). The plot shows the effect of changing the non-wetting phase during primary drainage.

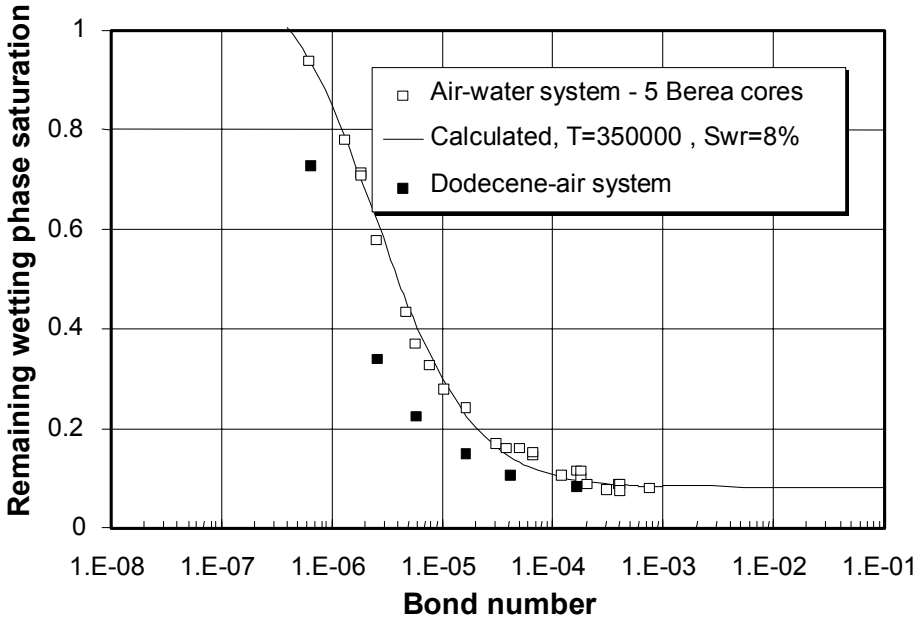

Figure 1.2 Wetting phase capillary desaturation curve, (two phase, Berea). The plot shows the effect of changing the wetting phase.

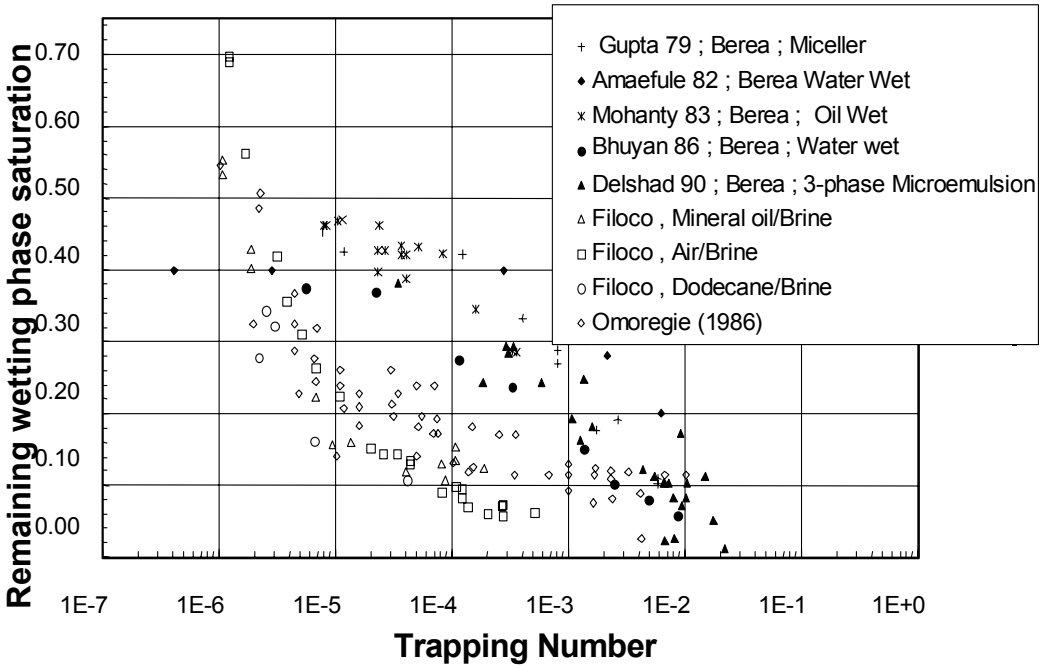

Figure 1.3 Comparison of centrifuge and displacement wetting phase desaturation curve, (two phase, Berea).

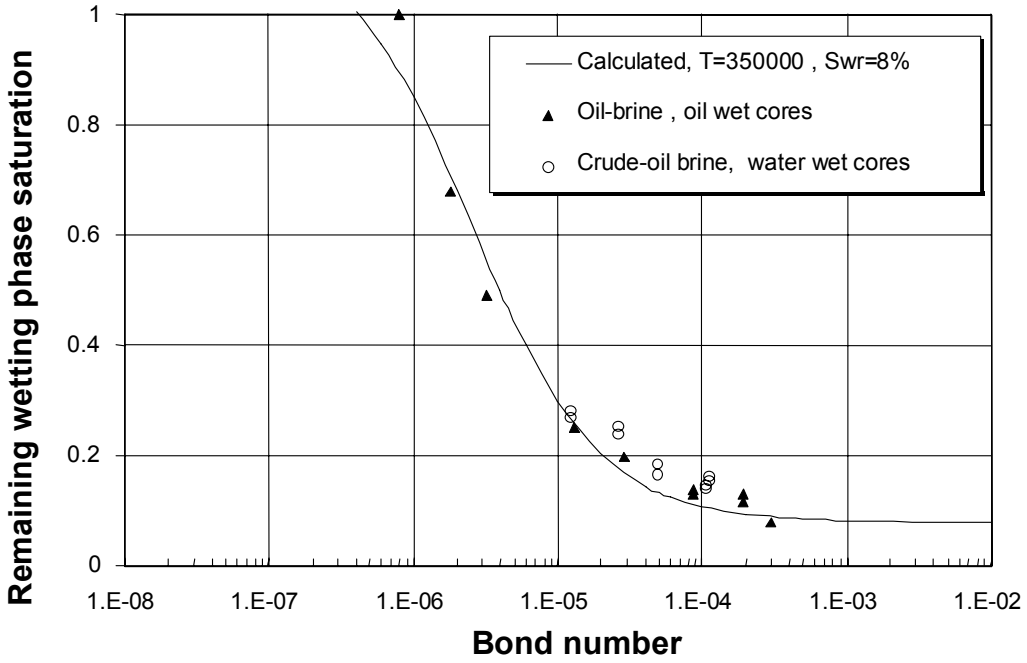

Figure 1.4 Effect of core wettability on capillary desaturation curves.

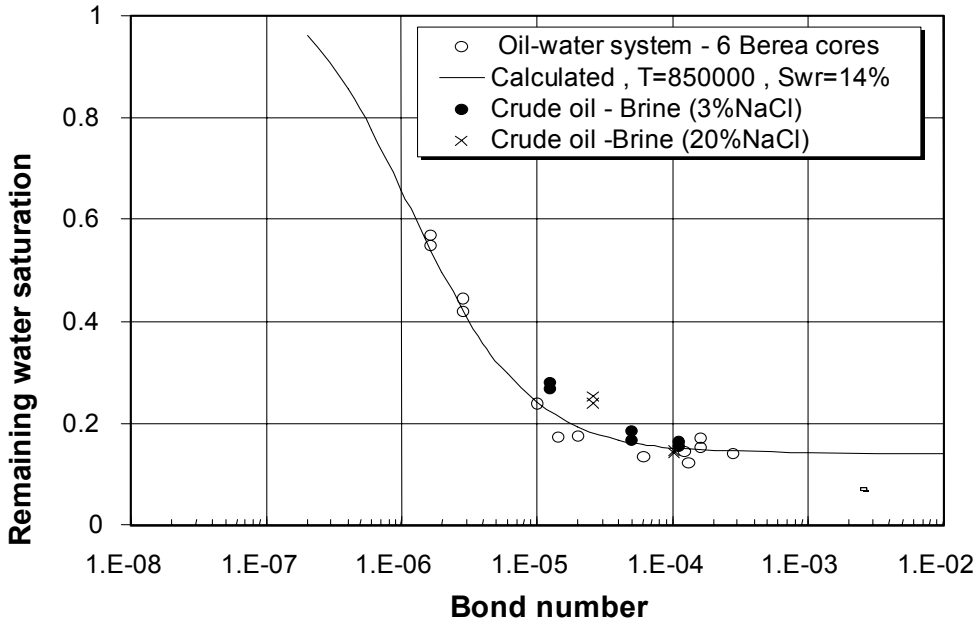

Figure 1.5 Capillary desaturation curves, (two phase, Berea). Changing the oil from a non-polar mineral oil to a crude oil (Prudhoe Bay) and /or changing the salinity of the resident brine does not change the capillary desaturation curve for the wetting phase (brine) during primary drainage.

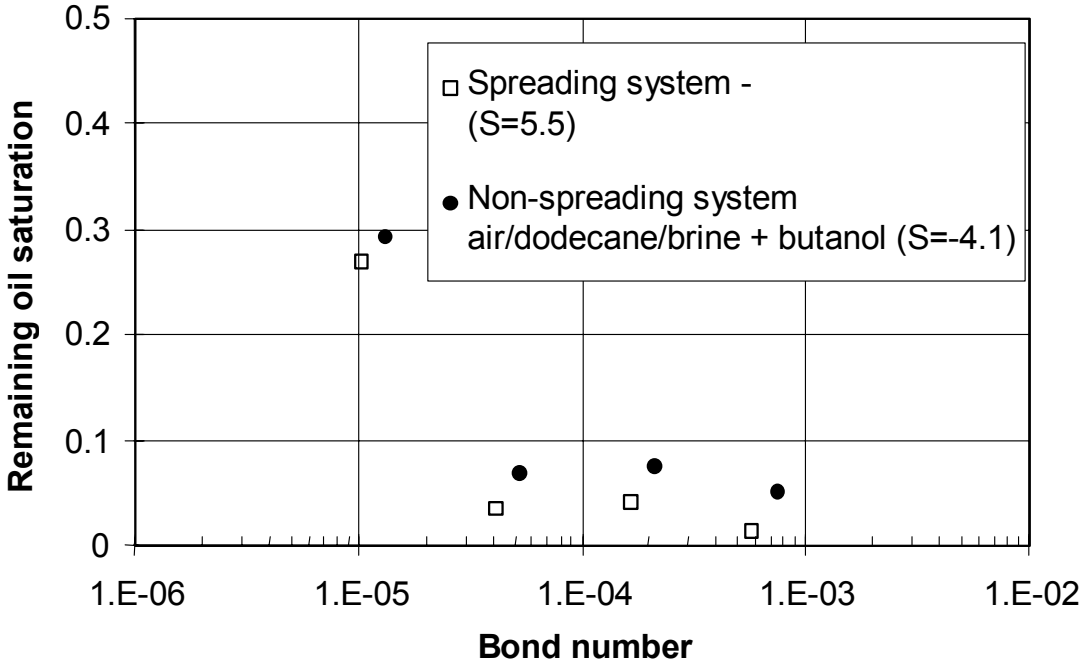

Figure 1.6 Effect of spreading on capillary desaturation curve for the intermediate wetting phase. Positive spreading coefficients result in lower remaining oil saturation. (three phase, Berea).

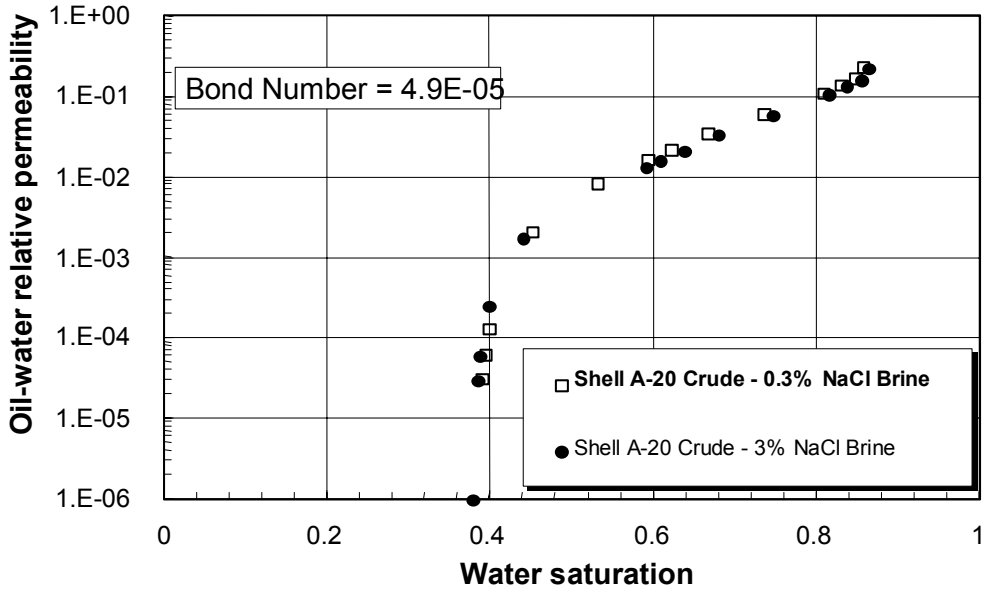

Figure 1.7 Effect of brine salinity on drainage relative permeability to oil, (two phase, Shell A-20 Crude). Salinity of the injected and connate brine is equal.

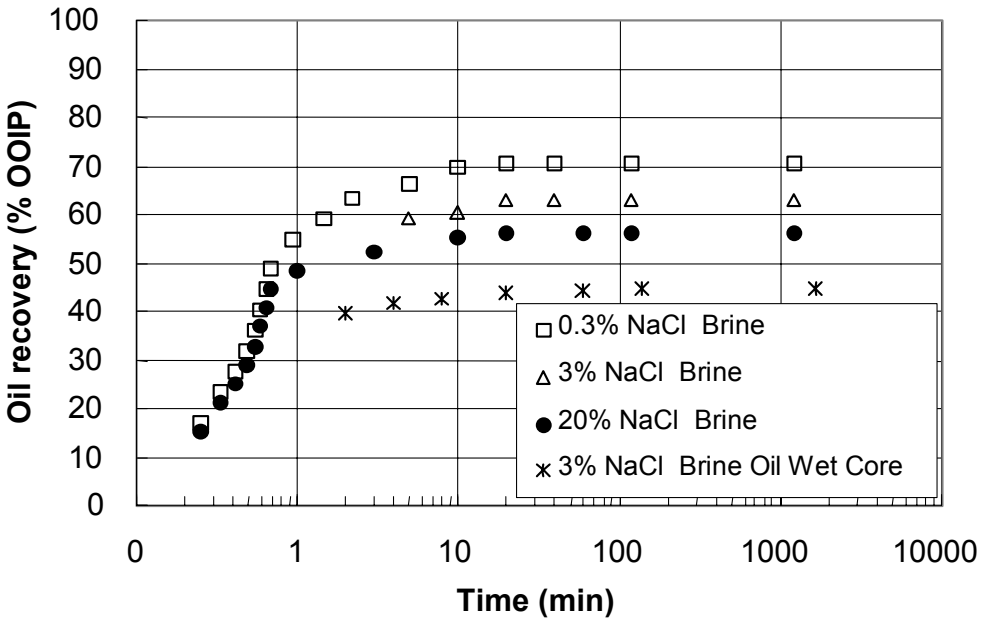

Figure 1.8 Effect of brine salinity on oil recovery by waterflood (Prudhoe Bay crude, Berea). Salinity of the injected and connate brine is equal.

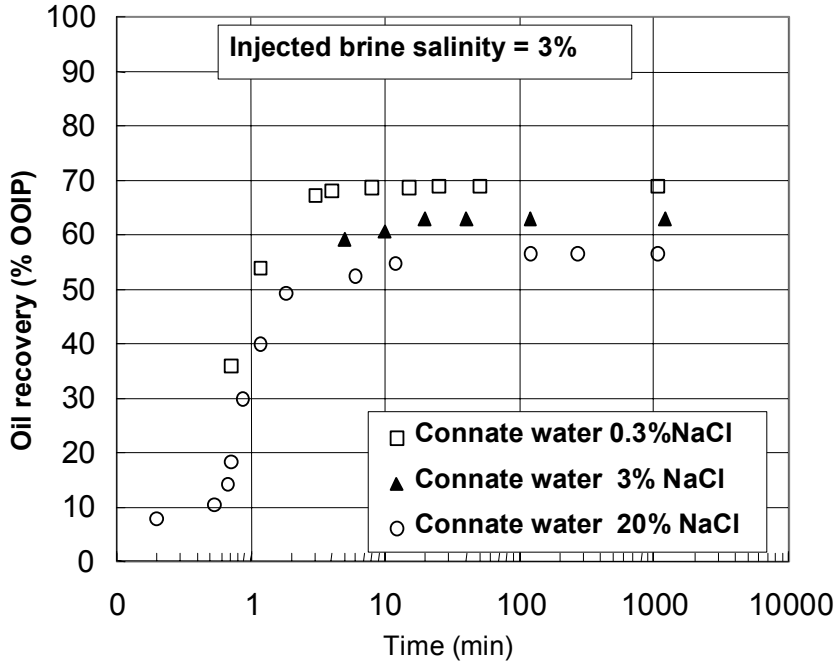

Figure 1.9 Effect of connate brine salinity on oil recovery, by waterflood (Prudhoe Bay Crude, Berea.)

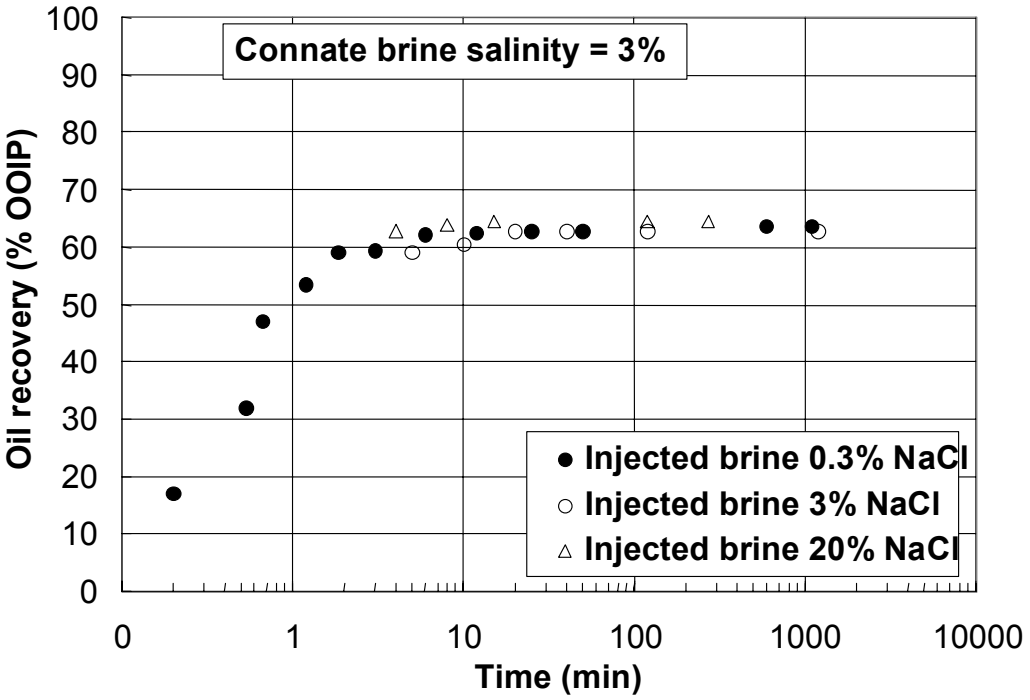

Figure 1.10 Effect of injected brine salinity on oil recovery by waterflood (Prudhoe Bay Crude, Berea).

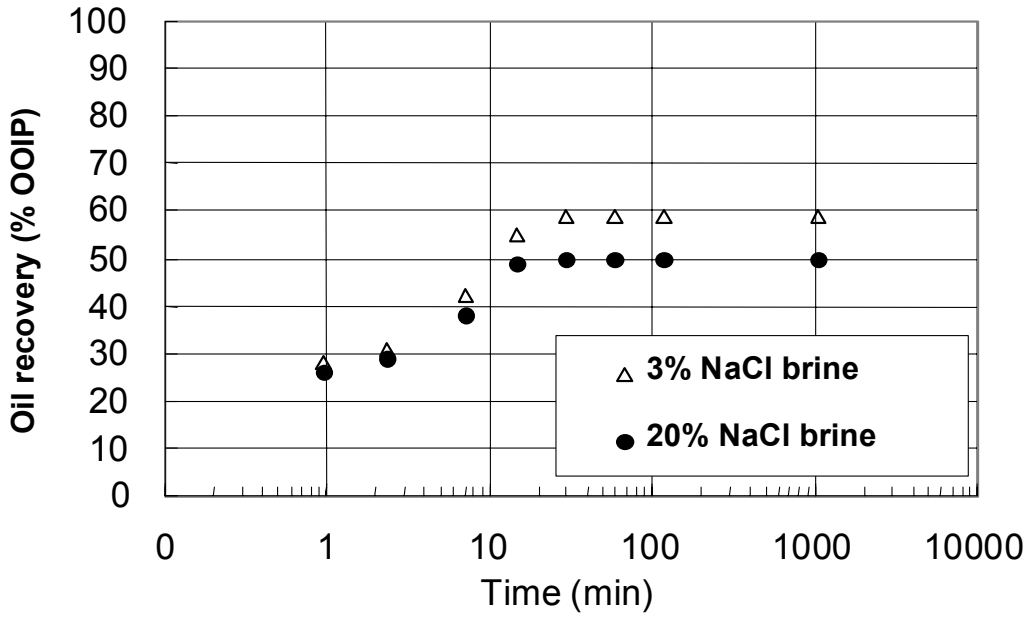

Figure 1.11 Effect of brine salinity on oil recovery by waterflood (Shell A-1 Crude, Berea). Salinity of the injected and connate brine is equal.

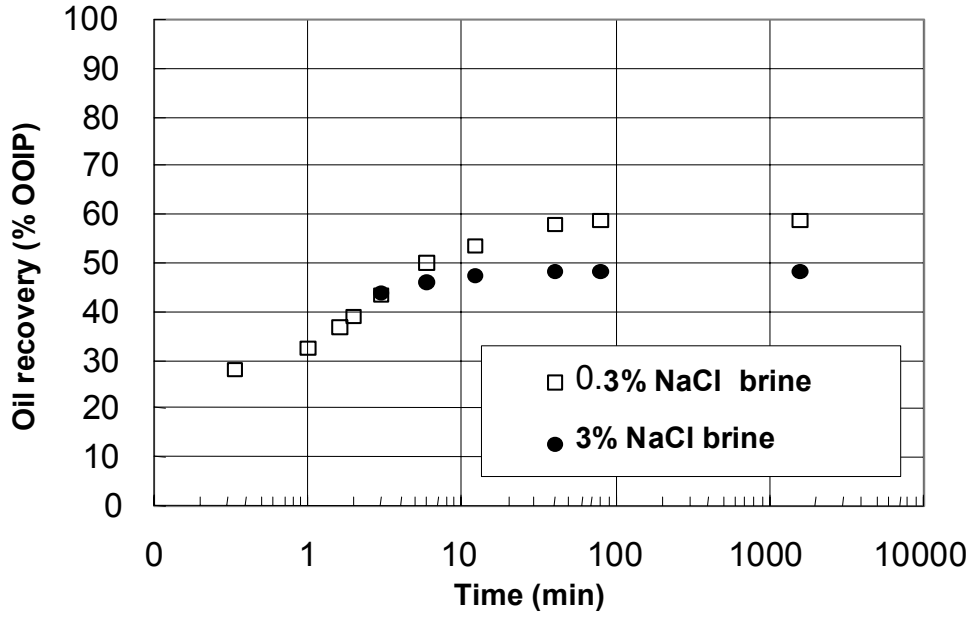

Figure 1.12 Effect of brine salinity on oil recovery by waterflood (Shell A-20 Crude, Berea). Salinity of the injected and connate brine is equal.

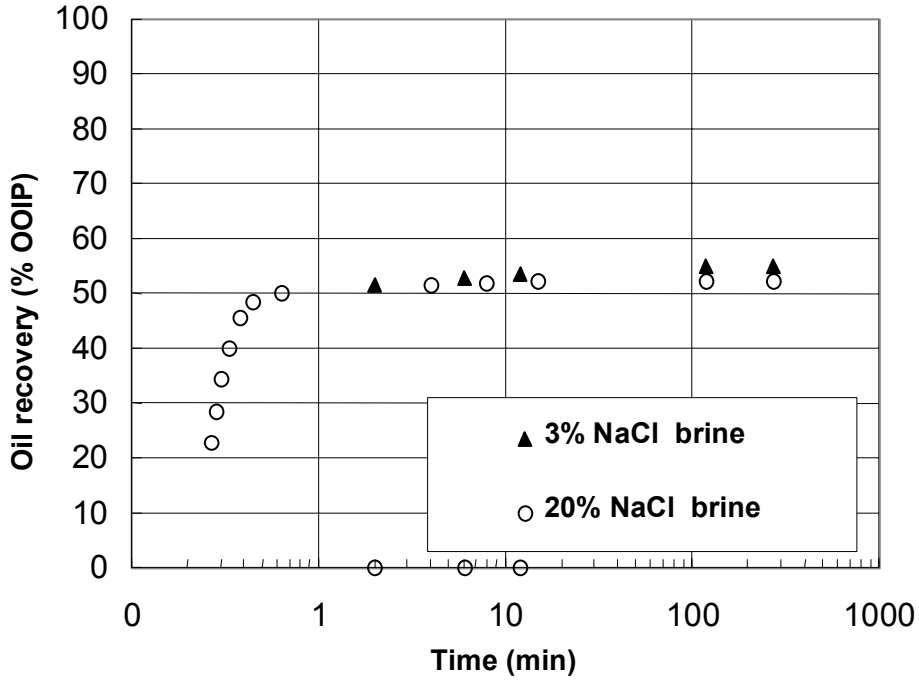

Figure 1.13 Effect of brine salinity on oil recovery by waterflood (Dodecene, Berea). Salinity of the injected and connate brine is equal.

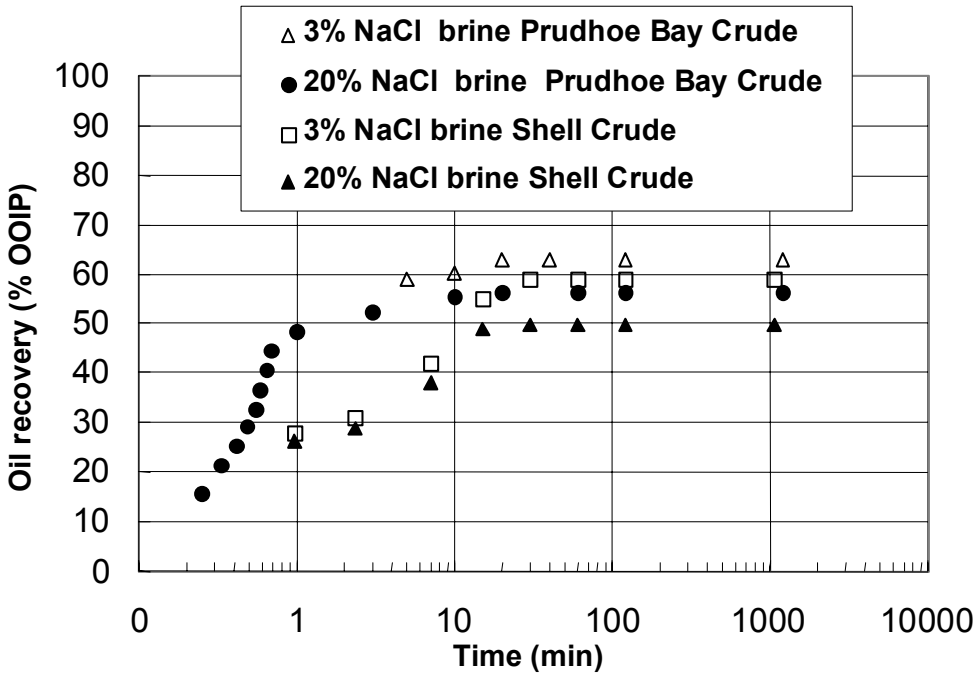

Figure 1.14 Effect of oil type and brine salinity on oil recovery by waterflood (Prudhoe Bay/Shell A-1 Crude, Berea).

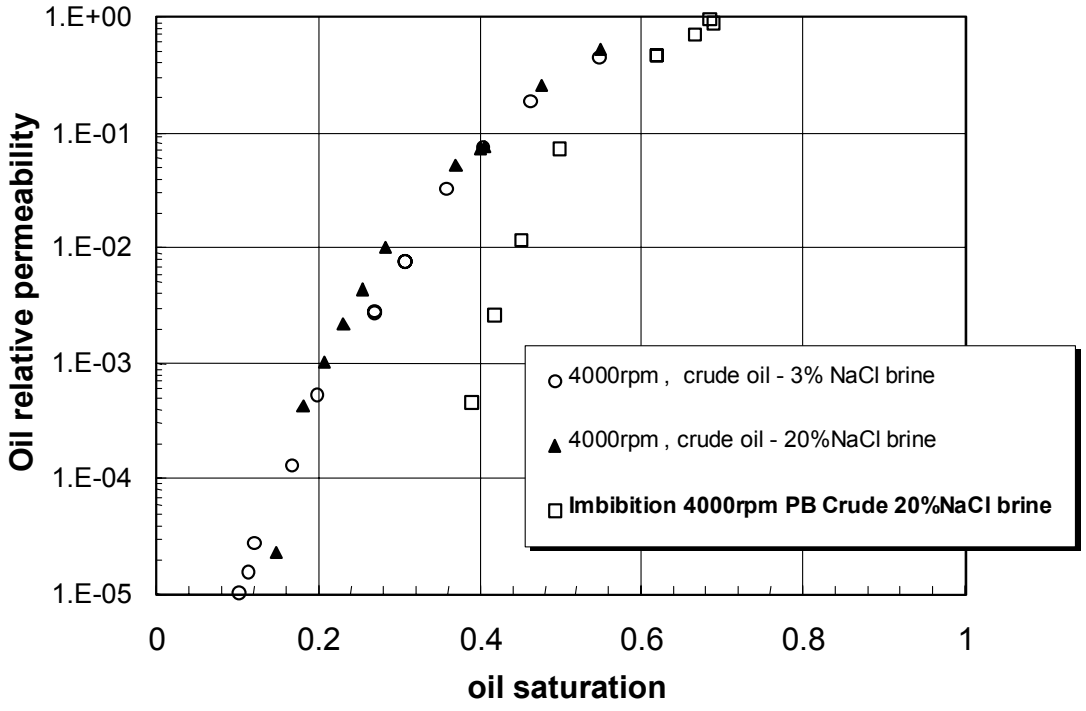

Figure 1.15 Imbibition and drainage oil relative permeabilities, (Prudhoe Bay Crude, Berea).

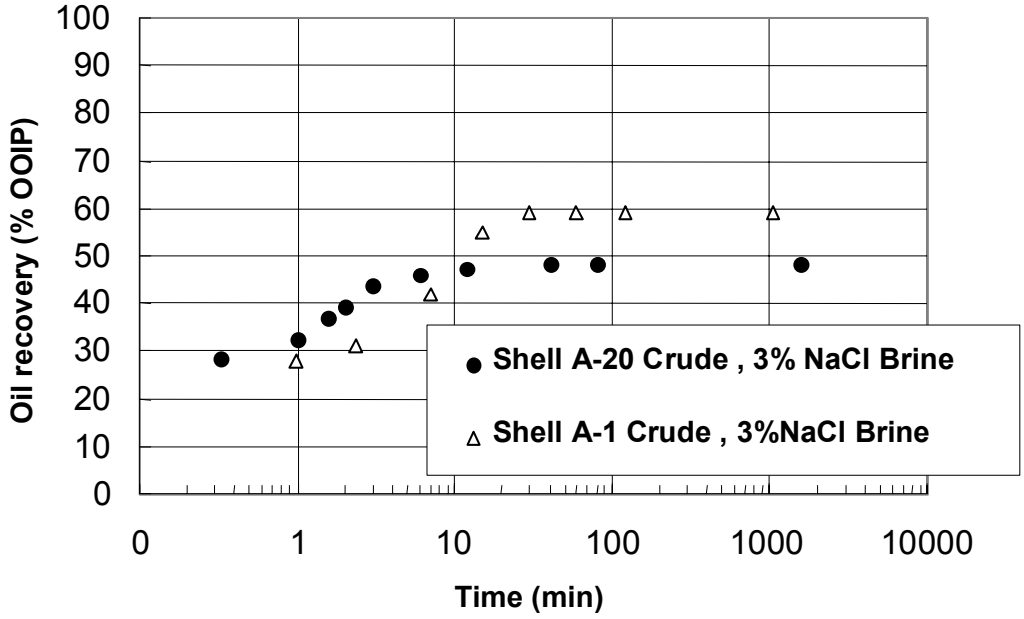

Figure 1.16 Comparing oil recovery by waterflood for Shell A-1 and A-20 Crude (3% NaCl Brine salinity, Berea).

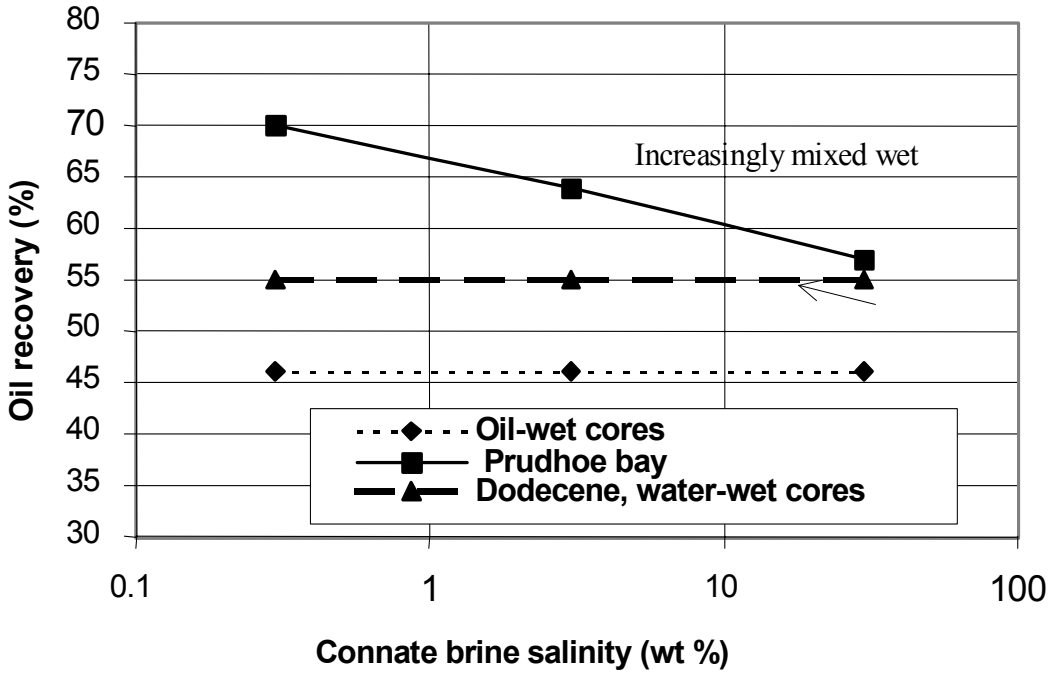

Figure 1.17 Effect of connate brine salinity on oil recovery.

2. Effect of Capillary Pressure, Salinity, and Aging on Wettability Alteration in Sandstones and Limestones

Chattopadhyay, S., Jain, V., and Sharma, M. M.

SPE paper 75189, presented at the SPE/DOE Thirteenth Symposium on Improved Oil Recovery held in Tulsa, Oklahoma, 13–17 April 2002.

ABSTRACT

Oil recovery in petroleum reservoirs is greatly affected by fluid –rock and fluid-fluid interactions. These surface chemical interactions directly control rock wettability, capillary pressure curves and relative permeabilities. Centrifuge coreflow tests (Berea sandstone and Texas Cream limestone) were performed with a range of fluids under different conditions to identify the factors influencing the residual wetting and non-wetting phase saturations and oil recovery. Results of the tests conducted with Prudhoe Bay and Moutray crude oil show that remaining water (S_{wr}) and residual oil saturation vary systematically with Bond number for both sandstone and limestone samples. Differences in the shape of the wetting phase capillary desaturation curves are observed during primary and secondary drainage. This suggests that the distribution of fluids in the rock during secondary drainage is different from primary drainage due to a change in wettability of the core from a water-wet state to mixed-wet state. These trends were not observed with decane. Both limestone and sandstone cores become more susceptible to wettability alteration as the salinity is increased. The wettability index (Aw-Ao, water Amott-oil Amott) decreases from 0.56 (0.3% brine) to 0.2 (20% brine) in a limestone core with Prudhoe Bay crude oil. Aging the samples for 20-30 days with Moutray crude oil shows results in a change in the wettability of the cores. The oil recovery increases by 10-15% to more than 95% in both Berea and limestone cores. These results show that with time the crude oil changes the wettability of the core from strongly water wet to mixed wet, which leads to a higher oil recovery. Experiments with samples of sandstone and limestone aged with Prudhoe Bay crude oil and brine of different salinities also show similar trends.

INTRODUCTION

Oil recovery in reservoirs is greatly affected by fluid-fluid and fluid-rock interactions. These interactions control rock wettability, capillary pressure and relative permeabilities. Wettability is a significant issue in multiphase flow problems ranging from oil migration from source rocks to enhanced oil recovery processes.[1] It has been generally observed in the past that relative permeability to the oil is higher in water-wet rocks, however, the ultimate oil recovery is higher in mixed-wet rocks. This lower residual oil saturation has been attributed to the presence of thin wetting films of oil on the surfaces of the rock grains[2,3], that allows the oil to drain over a long period of time. The ultimate oil recovery at the end of a waterflood has been shown to either increase or decrease with increasing oil-wetness.[4]

The importance of wettability in determining oil recovery and relative permeability curves is well established.[2] The conditions under which mixed-wettability states are achieved is less well understood. Recent studies conducted by Basu and Sharma[5,6] and Buckley et al.[1] point to the importance of crude oil composition in wettability alteration. Polar crude oil components can absorb on mineral surfaces and alter their wetting properties. Polar components of crude oil can absorb by different mechanisms, depending upon factors that include brine composition, solvent quality of the oil, aging time and type of oil.[1] In addition the wettability state has been shown to be a function of the height above the oil-water contact[7] or capillary pressure. The dependence on the capillary pressure can be explained on the basis of the critical disjoining pressure that has been measured for both mineral oil and crude oils.[5,8] When capillary pressures above the critical disjoining pressure are reached, thin brine films that wet the mineral grains are ruptured and the crude oil comes in contact with the grain surfaces. Since the critical disjoining pressure is a function of the properties of the brine and the crude oil and the curvature of the mineral grains there can be a wide range of pressures over which film rupture occurs. This leads to selective dewetting of surfaces as convex surfaces will be dewet at the lowest capillary pressures in accordance with the augmented Young-Laplace equation. This gives rise to mixed-wetting conditions over a range of capillary pressures and the rock becomes more oil-wet as the capillary pressure is increased. This is consistent with the fact that reservoirs tend to be more oil-wet higher in the structure.[7]

Crude oil aging time and temperature can also impact the imbibition process.[9] The

extent of wetting alteration is a function of both the duration and temperature at which a core containing connate water is aged in the oil.[10] The wettability with respect to water decreases with an increase in aging temperature and decrease in initial water saturation.[11] The potential for improved displacement increases with wettability alteration from strongly to weakly water-wet conditions.[12] Earlier studies[13,14] have demonstrated the importance of brine salinity in oil recovery by waterflooding. Core flow tests clearly show that for some crude oils the residual oil saturation obtained at the end of a waterflood depends on the salinity of the connate brine used.[15] The reasons for this are as yet unclear. However, it is conjectured that changes in salinity can alter rock wetting that results in changes in the residual oil saturation.

The objective of this research is to clearly identify the factors that influence: (1) the residual wetting and non-wetting phase saturations, (2) the impact of salinity on wettability, and (3) the impact of aging on residual saturations and wettability. Sequences of drainage and imbibition cycles are conducted using the centrifuge for two-phase systems. Research shows that the centrifuge method is a fast and reliable method for obtaining the desired residual saturations as a function of the Bond number or the equivalent trapping number.[16-18] In regions of low relative permeability (near end points) and in reservoirs where gravity drainage controls the recovery process the centrifuge method offers some clear advantages over other displacement methods.

EXPERIMENTAL METHODS

Fluids Used. The fluid systems (brine/oil) were chosen with the objective of evaluating the effect of fluid properties on residual wetting and non-wetting phase saturations and wettability before and after aging. All chemicals used were of analytical grade and were used as received from the manufacturer without any further purification. Brine solutions were prepared using deionized water (Milli-Q Plus, Millipore Corp., Bedford, WA). The oil phases used were decane, Prudhoe Bay (AK93) and Moutray crude oil. Prudhoe Bay and Moutray crude are very well studied oil with a lot of data available in the literature. Table 2.1 shows some properties of the crude oils.[19]

The solution chemistry of the fluid systems play a crucial role in defining the

interfacial properties and wettability as surface active components from the oil are dissolved into the brine, changing these properties. The brine at different salinities used in the experiments was pre-equilibrated with the crude oils by letting the liquids stand in contact with each other for at least 72 hours prior to conducting any experiment. This allows mass transfer to take place between phases, minimizing transient effects associated with mass transfer of partitioning components in the core.

Core Preparation. A total of 50 core plugs (2.5 cm in diameter and 2.5 cm in length) were cut from a large optically homogenous slab of Berea sandstone and Texas Cream limestone using tap water as the cutting fluid. The core plugs were dried in an air-oven at 100°C for at least 24 hours. They were weighed and then evacuated and saturated in a dessicator. The cores were weighed again after saturating them with brine. Core porosities varied from 19.7% to 21% for Berea and 17% to 20 % for the Texas Cream limestone and the absolute permeability varied from 180 mD to 220 mD for the Berea sandstone and 10 mD to 15 mD for the limestone.

Interfacial Tension Measurements. The interfacial tension between brine and crude oil was measured by a DuNouy ring tensiometer. The instrument consists of a platinum-iridium ring supported by a stirrup attached to the beam of a torsion balance. The flamed ring was placed at the interface of two liquids or at the surface of a liquid with air. It was than pulled upward until it breaks free of the liquid and moves into the second liquid or into the air. The force that is just required to break the ring free of the liquid/liquid or liquid/air interface is proportional to the surface tension. The instrument reading is the apparent interfacial or surface tension.

Centrifuge Experiments. A Beckman high-speed ultra-centrifuge (maximum speed of 20,000 rpm) equipped with a stroboscope, an electrical timer, and a device for mounting the cores in the centrifuge for drainage and imbibition was used in our experiments. The fluid production from the cores is observed through a transparent window with the help of a stroboscope.

The combined USBM-Amott method[20] consists of increasing the centrifuge speed in

steps and at each step measuring the amount of fluid produced from a core as a function of time and at equilibrium when flow has ceased. At each speed, the equilibrium saturation and capillary pressure can be used to obtain the capillary pressure curve, and the transient behavior can be used to infer the relative permeability of the displaced phase. A drainage centrifuge displacement is run, displacing the brine with crude oil until a residual brine saturation is achieved. The volume of wetting phase collected as a function of time is recorded at each centrifuge speed. After the drainage cycle, the core is subjected to spontaneous imbibition, whereby the core is kept in a reservoir of brine and the spontaneous drainage of crude oil from the core is measured. The forced imbibition test is conducted in the centrifuge by displacing the crude oil with brine using imbibition centrifuge buckets. The early time displacement data is recorded with the video-camera for more precise readings and subsequent displacement data is recorded visually. For our test conditions relatively little flow occurs after 2 or 3 hours. To ensure equilibrium the core is spun at each rpm for at least 4 hours. Following the imbibition cycle, a spontaneous drainage test is conducted, whereby the core is kept in a bath of crude oil and the spontaneous drainage of brine from the core is measured. Subsequently the secondary drainage cycle is conducted in the centrifuge. Figure 2.1 gives all the steps of the experiment.

After the secondary drainage cycle, the core is aged in the crude oil for 20-25 days at room temperature at connate water saturation. Then another set of spontaneous imbibition (step2), forced imbibition (step3), spontaneous drainage (step4) and forced drainage (step5) cycles are conducted with the core to observe the impact of aging on the capillary destauration curves and wettability of the cores.

The wettability changes in the core are measured by calculating Water and Oil Amott and USBM indices. The Water and Oil-Amott indices are calculated as

$$W_{Amott} = \frac{\Delta S_w(\text{step2})}{\Delta S_w(\text{step2} + \text{step3})} \qquad [2.1]$$

$$O_{Amott} = \frac{\Delta S_w(\text{step4})}{\Delta S_w(\text{step4} + \text{step5})} \qquad [2.2]$$

and the USBM index is calculated as

$$W_{USBM} = LOG \frac{\text{Area under the curve 5}}{\text{Area under the curve 3}} \quad [2.3]$$

where the steps are given in Figure 2.1.

The capillary pressure at any rpm is given by

$$P_c = \frac{\Delta\rho\omega^2}{2}\left(r_2^2 - r_1^2\right) \quad [2.4]$$

where P_c = capillary pressure at core inlet, dynes/cm^2, r_1 = radius of core inlet face measured from the center of rotation, cm, r_2 = radius of core outlet face measured from the center of rotation, cm, ω = angular velocity (= $2\pi N/60$, where N = centrifuge speed in revolutions per minute), radians/second and $\Delta\rho$ density difference between the wetting and non-wetting phases, gm/cm^3.

RESULTS AND DISCUSSION

Table 2.2 shows the surface and interfacial tension of the different fluid systems and Table 2.3 shows the properties of the cores used in this work. The capillary desaturation curves are presented in terms of a dimensionless Bond Number, which is given as

$$N_b = \frac{1.0823x10^{-13} kNr_c\Delta\rho}{\sigma} \quad [2.5]$$

where r_c is the core radius (cm), k is the permeability (mD) and □ is the interfacial tension (dynes/cm). Presenting the results as a Bond number allows for a direct comparison of capillary pressure curves among different systems. Figure 2.2 shows a capillary desaturation curve between decane and 3% brine in Berea sandstone. The figure shows that there are no significant differences between the primary and secondary drainage curves. A residual water saturation of 0.19 and 0.205 is achieved with decane in Berea during primary and secondary drainage cycles, respectively.

Important differences in the shape of the wetting phase capillary desaturation curves are observed (primary vs secondary drainage) when crude oil is used as the non-wetting

phase. When the non-wetting phase is changed from decane to crude oil (Figure 2.3), no change is residual water saturation is observed during primary drainage for different types of brines in Berea. However, there are significant differences between the primary and secondary drainage curves. The salinity of the brine primarily impacts the secondary drainage curves (Figure 2.4). The water saturation is higher during secondary drainage for the same Bond numbers and more brine is trapped during secondary drainage in brine/Moutray/Berea systems. The water saturation is generally higher with increase in the salinity of the brine (increase from 4% NaCl + 0.5% $Cacl_2$ brine to 4% NaCl + 2% $Cacl_2$ brine), however the differences are more significant during the secondary drainage. The increase in the brine salinity increases the difference between S_{wr} of primary and secondary drainage from 0.04 (4% NaCl + 0.5% $Cacl_2$ brine) to 0.11 (4% NaCl + 2% $Cacl_2$ brine).

Similar results were observed in Limestone/Prudhoe Bay/brine system (Figure 2.5). The primary drainage curve at different brine salinities (3% NaCl to 20% NaCl) shows no differences. The residual water saturation in limestone is higher than that from Berea because of differences in the permeability (Berea has a high permeability of 150-200mD, whereas limestone has a permeability of only 5-10mD). However similar to the Berea-Moutray system the secondary drainage curves show higher water saturation as compared to primary drainage at the same Bond numbers (Figure 2.6). Moreover, increase in the salinity from 0.3% NaCl to 20% NaCl increases the difference between S_{wr} of primary and secondary drainage from 0.10 to 0.16.

When brine is equilibrated with non polar oils (such as decane) there is no change in the solution chemistry of the brine, whereas when brine is equilibrated with polar crude oils, the composition of the brine is altered because of solubilization of components from the crude oil into the brine. These changes in the brine solution and the presence of polar compounds could explain the differences observed during primary and secondary drainage and the changes observed with increasing salinity of the brine. The pore space progressively becomes more oil-wet due to film rupture as the capillary pressure is raised. Hence the brine (during imbibition) and the oil (during secondary drainage) sees a different porous medium, which is now mixed wet or partially oil wet. As a consequence the brine during imbibition would tend to go into the largest of the oil-wet pores and of course continue to flow through the smallest pores which have not been contacted by oil during drainage and hence are still

water-wet. This creates a very different fluid distribution (Figure 2.7) than would have been achieved if the core were oil-wet to begin with. Brine is thus excluded from the intermediate size pores that have remained oil-wet. The fraction of such pores depends on the capillary pressure imposed during drainage. The reassignment of pore occupancy caused by changes in wettability during primary drainage is a likely reason for the large fraction of the water being trapped during secondary drainage. As a result considerable differences in S_{wr} between primary and secondary drainage were observed.

The primary and secondary drainage (Figure 2.8) curves in the Limestone/Moutray/Brine of NaCl and $Cacl_2$ show that there are differences in the drainage curves with increase in salinity. Significant higher brine saturations are observed during primary drainage with the increase in the $Cacl_2$ concentration in the brine from 0.5% to 2%. However, these differences recede in the secondary drainage cycle.

Figure 2.9 shows the primary and secondary imbibition capillary desaturation curves in a Berea/Moutray/Brine system. The secondary imbibition cycle is conducted after aging the cores for 20-25 days. The figure shows that the residual oil saturation decreases after aging the cores and is also a function of brine salinity. Aging the cores made them more mixed-wet and hence more oil was recovered during the imbibition cycle. The oil saturation is higher for a lower brine salinity for both the primary and secondary imbibition curves. Increasing the salinity leads to more oil recovery.

Figure 2.10 shows the capillary desaturation curves for limestone/Prudhoe Bay oil/brine systems. Similar to Berea cores lower oil saturation is observed in the limestone cores after aging, with oil recovery of more than 95%. Similar trends were observed with Moutray oil/brine systems (Figure 2.11).

Tables 2.4 and 2.5 show the residual saturations and wettability indices of the systems studied in this research before and after aging, respectively. The water and oil Amott indices calculated before and after aging and USBM indices are listed in the tables. The indices show that with Moutray oil, both the Berea and limestone cores exhibit more water-wet behavior with increasing salinity. However with Prudhoe Bay oil, the water-wetness decreases with increasing brine salinity. Limestone cores with brine of 20% NaCl concentration spontaneously imbibes oil, which was not observed with any other core. Thus cores become less water-wet and more oil-wet with increase in brine salinity. Both limestone

and sandstone cores become more susceptible to wettability alteration with aging and become less water-wet. The oil recovery increases by 10-15% to more than 95% in both sandstone and limestone cores. These results show that with time the crude oil changes the wettability of the core from strongly water-wet to mixed-wet condition, which leads to higher oil recovery. This change is also evident from the differences observed in residual oil saturation observed during primary and secondary imbibition.

Similar results showing the impact of salinity have been observed by Filoco and Sharma (1999). Jadhunandan and Morrow (1994) have reported similar results for Berea/Moutray oil/brine systems, where aging made the cores more oil-wet with increasing brine salinity. The ability of the oil to rupture thin brine films is determined by the critical disjoining pressure, whereas repulsive forces caused by electrostatic repulsion or hydration forces can stabilize films. As salinity is increased thin wetting films become increasingly unstable as the double layer repulsion is screened by the ions, leading to a mixed-wettability condition, which becomes more permanent with aging of the core.

Basu and Sharma[6,8] have shown that for non-polar mineral oils and some crude oils the brine films become more stable as the salinity is increased. However, when electrostatic interactions dominate hydrophobic interactions, the brine films become less stable with increase in salinity. These explanations substantiate the results observed with AK93 crude oil, which has a high base number and presents a positively charged oil-water interface. However, Moutray oil does not show similar trends as the cores show more water wet behavior with increase in salinity unlike the results observed in AK93.

CONCLUSIONS

Centrifuge coreflow tests (Berea sandstone and Texas Cream limestone) were performed with a range of fluids (decane and crude oils) under different conditions to identify the factors influencing the residual wetting and non-wetting phase saturations and oil recovery. The following conclusions were reached:

1. Significant differences were observed between primary and secondary wetting phase capillary desaturation curves, when crude oils was used as the non-wetting phase. The water saturation is higher during secondary drainage for the same bond numbers and

more brine is trapped. However, when pure hydrocarbon, decane was used as the non-wetting phase there are no significant differences between the drainage curves.

2. Aging impacts the residual oil saturation, which decreases with aging. Oil recovery of around 95% is observed in aged cores.
3. Aging impacts the wettability indices. Aging the cores made them more mixed-wet and hence more oil was recovered. Both limestone and sandstone cores become more susceptible to wettability alteration as the salinity is increased.
4. Residual oil saturation to a waterflood decreases with an increase in connate brine salinity.
5. Higher residual brine saturations are observed in limestone cores as compared to sandstone cores because of the differences in the lithology. The lower permeability of the limestone cores leads to higher brine saturations at the same bond numbers as compared to sandstone cores.

REFERENCES

1. Buckley, J. S., Liu, Y. and Monsterleet, S.: "Mechanisms of Wetting Alteration by Crude Oils," SPE 37230, Presented at the SPE International Symposium on Oilfield Chemistry, Houston (Feb. 1997).
2. Anderson, G. W.: "Wettability Literature Survey - Part 5: The Effects of Wettability on Relative Permeability," *JPT* (November 1987) 1453.
3. Salathiel R.A.: "Oil Recovery by Surface Film Drainage in Mixed-Wettability Rocks," *JPT* (Oct. 1973) 1216.
4. Morrow, N. R.: "Wettability and its Effect on Oil Recovery", JPT (Dec. 1990) 1476.
5. Basu, S.; Sharma, M.M.; "Characterization of Mixed Wettability States in Oil Reservoirs by Atomic Force Microscopy", SPE Journal, **Vol. 2**, SPE 35572, 427-435, December1997.
6. Basu, S.; Sharma, M.M.; "Investigating the Role of Crude-Oil Components on Wettability Alteration Using Atomic Force Microscopy," SPE Journal, **Vol. 4**, No. 3, 235-241, Sept. 1999.
7. Jerauld, G.R., Rathmell, J.J.: "Wettability and Relative Permeability of Prudhoe Bay: A Case Study of Mixed-wet Reservoirs", SPE Reservoir Engineering, (Feb. 1997) 58.

8. Basu, S.; Sharma, M.M.; "Measurement of Critical Disjoining Pressure for Dewetting of Solid Surfaces", Journal of Colloid and Interface Science, 181, 443-455, August 1996.
9. Tang, G. Q. and Morrow, N. R.: "Effect of Temperature, Salinity and Oil Composition on Wetting Behavior and Oil Recovery by Waterflooding," paper SPE 36680 presented at the SPE Annual Technical Conference and Exhibition, Denver, Colorado (Oct. 6-9, 1996).
10. Zhou X.et al.: "The Effect of Crude-Oil Aging Time and Temperature on the rate of Water Imbibition and Long Term Recovery by Imbibibition" Presented at the 1993 SPE Annual Technical Conference and Exhibition, Houston, Oct. 3-6.
11. Jadhunandan P. P.:"Effect of Wettability on Waterflood Recovery for Crude-oil/Brine/Rock Systems" Presented at the 66th Annual Technical Conference and Exhibition, Dallas, Oct 6-9, 1991.
12. Villard J. et al.: "Wetting and Waterflood Oil Recovery of a Moderatley Viscous Crude Oil", 1993 SCA Conference paper
13. Dumoré, J. M. and Schols, R.S.: "Drainage Capillary-Pressure Functions and the Influence of Connate Water," *Soc. Pet. Eng. J.* (Oct. 1974) 437-444.
14. Dykstra, H.: "The Prediction of Oil Recovery by Gravity Drainage," *JPT* (May 1978) 818.
15. Filoco, P.R., and Sharma, M.M.: "Effect of Brine Salinity and Crude Oil Properties on Relative Permeabilities and Residual Saturations", SPE paper 49320, presented at the 1998 SPE Annual Meeting in New Orleans, LA, September, 1998.
16. Hirasaki, G.J.: "Dependence of Waterflood Remaining Oil Saturation on Relative Permeability, Capillary Pressure, and Reservoir Parameters in Mixed-wet, Turbidite Sands," paper SPE 30763 presented at the SPE Annual Technical Conference and Exhibition, Dallas, Texas (Oct. 22-25, 1995).
17. Johnson, E. F., Bossler, D. P., and Naumann, V. O.: "Calculation of Relative Permeability from Displacement Experiments", Trans., AIME (1959) **216**, 370-372.
18. Melrose, J.C.: "Interpretation of Mixed Wettability States in Reservoir Rocks", SPE 10971, Presented at the 1982 SPE Annual Conference and Exhibition, New Orleans (Oct 1982).
19. Buckley, J.S.: "Mechanisms and Consequences of Wettability Alteration by Crude Oils",

Ph.D. Thesis, Department of Petroleum Engineering, Heriot-Watt University, Edinburgh, UK, 1996.

20. Sharma, M.M., and Wunderlich, R.W.: The Alteration of Rock Properties Due to Interactions With Drilling Fluid Components, SPE paper 14302, presented at the 60th Annual Conference and Exhibition of the Society of Petroleum Engineers held in Las Vegas, NV, September 22-25, 1985.
21. Jadhunandan, P.P, and Morrow, N.R.: "Effect of Wettability on Waterflood Recovery for Crude-oil/Brine/Rock Systems", SPE paper 22597, 1994.

Table 2.1: Properties of the Crude Oils

Crude Oil	Acid number / Base number	Density kg/m3	Viscosity cp	Wettability from Literature
Prudhoe Bay	0.14 / 2.42	0.91	22	Mixed-wet
Moutray	0.56/0.90	0.845	5.23	-

Data from ref 19.

Table 2.2: Properties of the cores used in the research

Sample ID	Length, cm	Diameter, cm	Pore volume, ml	Porosity	Saturating liquid
B18-D	2.52		2.274	18.93	3% NaCl
B2M10 0.5% CaCl2	2.54	2.466	2.339	19.28	4% NaCl+0.5% CaCl2
B4M2 2% CaCl2	2.51	2.468	2.30	19.16	4% NaCl+2% CaCl2
LS5AK93 0.3B	2.527	2.463	2.419	19.37	0.3% NaCl
LS7AK93 3B	2.517	2.451	2.453	20.67	3% NaCl
LS1AK93 20B	2.512	2.461	2.99	25.07	20% NaCl
LS3M10 0.5% CaCl2	2.476	2.387	2.91	26.25	4% NaCl + 0.5% CaCl2

LS1M2 2% CaCl2	2.463	2.413	2.813	24.97	4% NaCl+2% CaCl2

Table 2.3: Surface and interfacial tension of the fluid systems used in the experiments

Fluid Systems	Air	Brine
0.3 % NaCl brine	69	-
AK93	29.6	19
3 % NaCl brine	70	-
AK93	31	12
20 % NaCl brine	71	-
AK93	29.5	16
4 % NaCl +0.5% $CaCl_2$ brine	62.4	-
Moutray	27.1	8.3
4 % NaCl +2% $CaCl_2$ brine	64.7	-
Moutray	28	9
3 % brine	68.5	-
Decane	25.4	40.2

Table 2.4: Wettability indices and residual saturations for the experiments conducted

Berea							
Saturating Brine Concentration	Displacing Fluid	Water Amott	Oil Amott	USBM Index	Swr: Prim. Drainage	Sor: Prim. Imbibition	Swr: Sec. Drainage
3% NaCl	Decane	0.462	0		0.19	0.242	0.208
4% NaCl + 0.5% $CaCl_2$	Moutray	0.181	0	-0.21	0.17	0.124	0.224
4% NaCl + 2% $CaCl_2$	Moutray	0.363	0	-0.04	0.184	0.037	0.283
Limestone							
0.3% NaCl	AK 93	0.556	0	0.349	0.5	0.156	0.597
3% NaCl	AK93	0.5	0	0.255	0.41	0.039	0.651
20% NaCl	AK93	0.467	0.136	0.178	0.42	0.083	0.55
4% NaCl + 0.5% $CaCl_2$	Moutray	0.242	0	0.42	0.312	0.12	0.364
4% NaCl + 2% $CaCl_2$	Moutray	0.276	0	0.459	0.32	0.16	0.35

Table 2.5: Wettability indices and residual saturations for the aged samples.

Berea					
Saturating Brine Concentration	Displacing Fluid	Water Amott	Oil Amott	Sor: Sec. Imbibition (aged)	Swr: Sec. Drainage (aged)
4% NaCl + 0.5% $CaCl_2$	Moutray	0	0	0.017	0.32
4% NaCl + 2% $CaCl_2$	Moutray	0.06	0	0.005	0.213
Limestone					
0.3% NaCl	AK 93	0.528	0	0.008	0.517
3% NaCl	AK93	0	0	0.03	0.63
20% NaCl	AK93	0.166	0	0.05	0.55
4% NaCl + 0.5% $CaCl_2$	Moutray	0	0	0.035	0.278
4% NaCl + 2% $CaCl_2$	Moutray	0.014	0	0.036	0.36

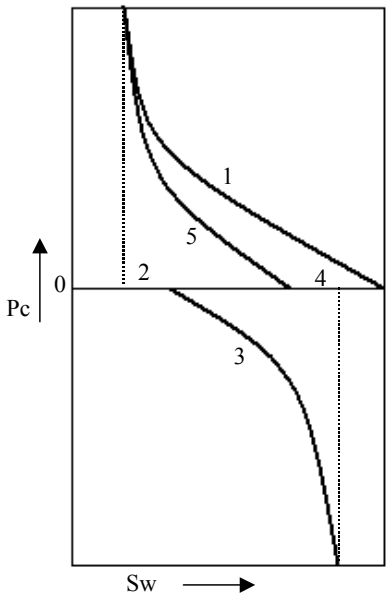

Figure 2.1: Sequence of the experimental steps conducted in this research; 1: Primary drainage, 2. Spontaneous imbibition, 3: Primary imbibition, 4: Spontaneous drainage, 5: Secondary drainage.

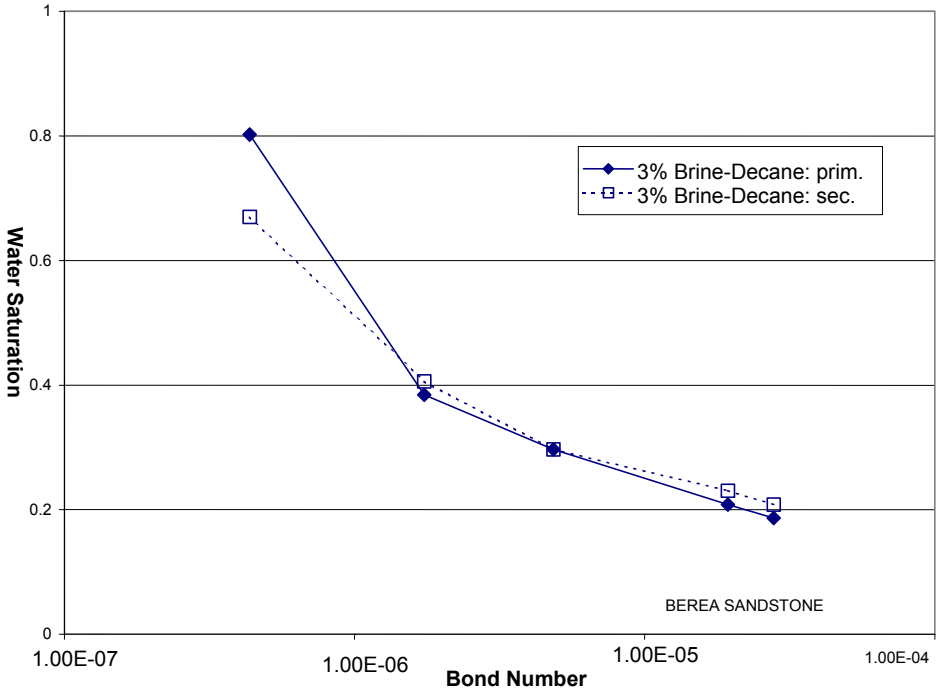

Figure 2.2: Wetting phase drainage capillary desaturation curves in a 3% brine-decane-Berea system.

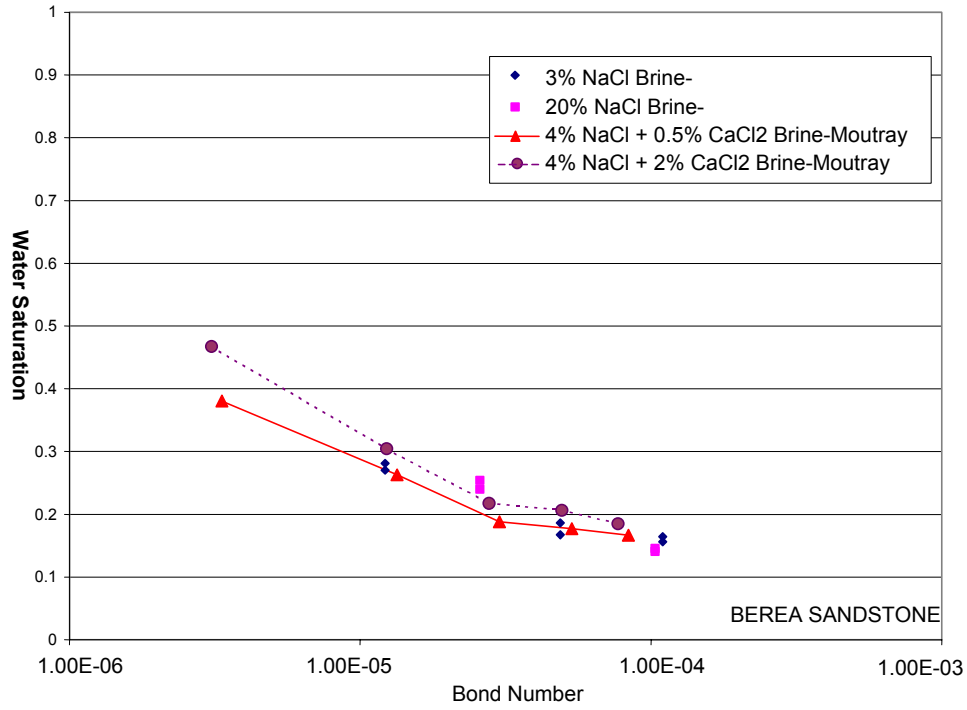

Figure 2.3: Wetting phase capillary desaturation curves in brine-crude oil-Berea system. (Brine-AK93-Berea data is from Reference 15)

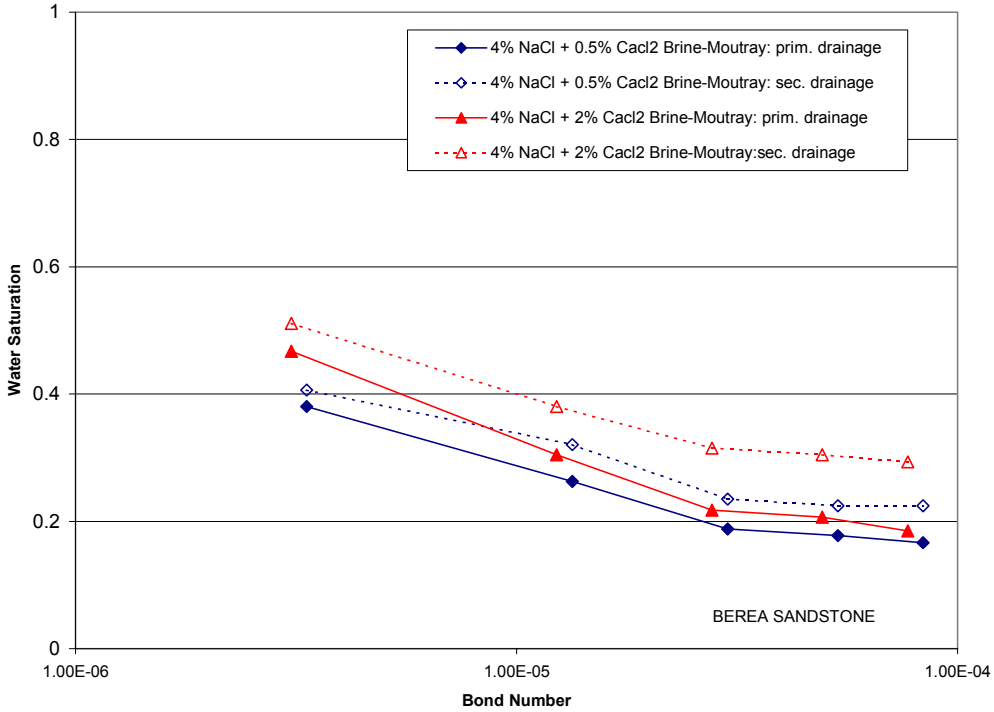

Figure 2.4: Wetting phase drainage capillary desaturation curves in brine-Moutray-Berea system.

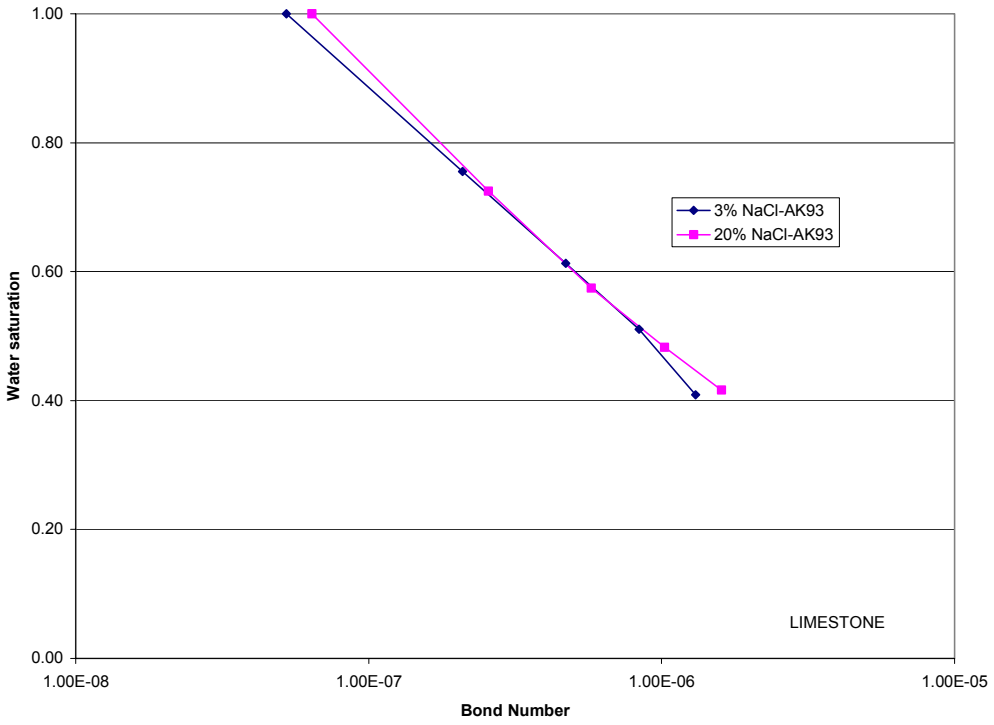

Figure 2.5: Wetting phase primary drainage capillary desaturation curves in brine-AK 93-limestone system.

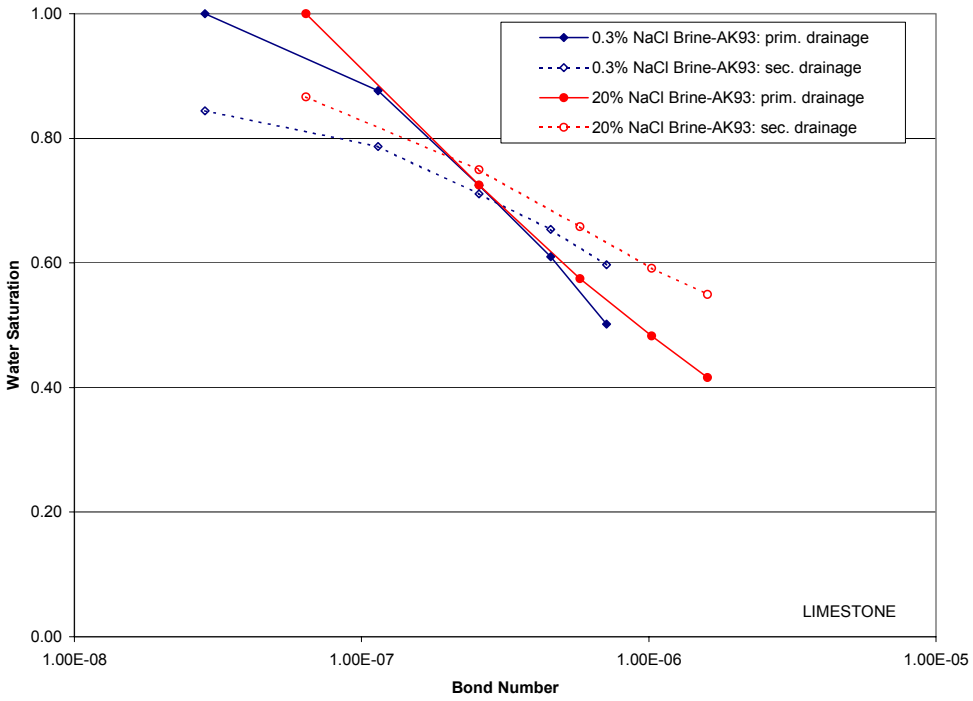

Figure 2.6: Wetting phase drainage capillary desaturation curves in brine-AK 93-limestone system.

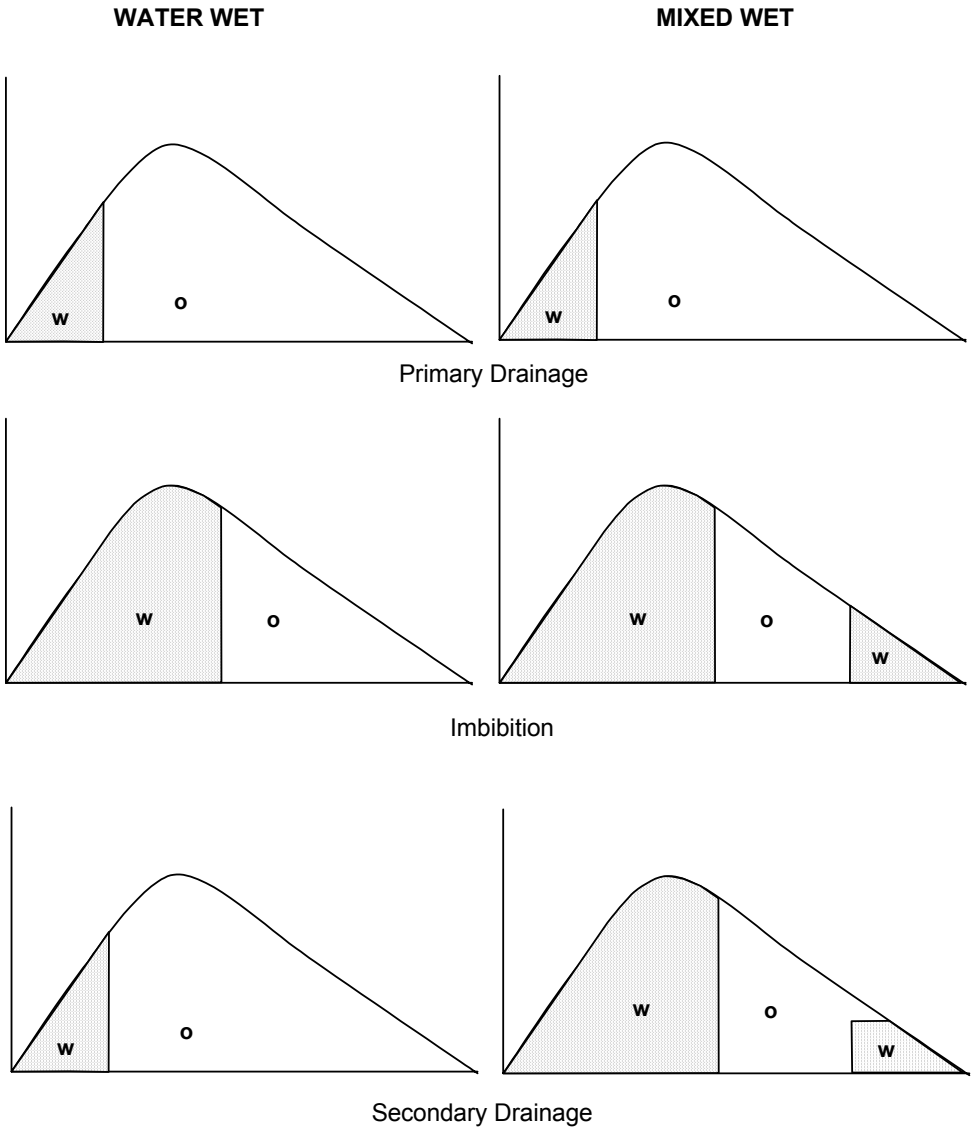

Figure 2.7: Proposed mechanism of the change of wettability of the curve from water-wet to mixed wet during drainage and imbibition process.

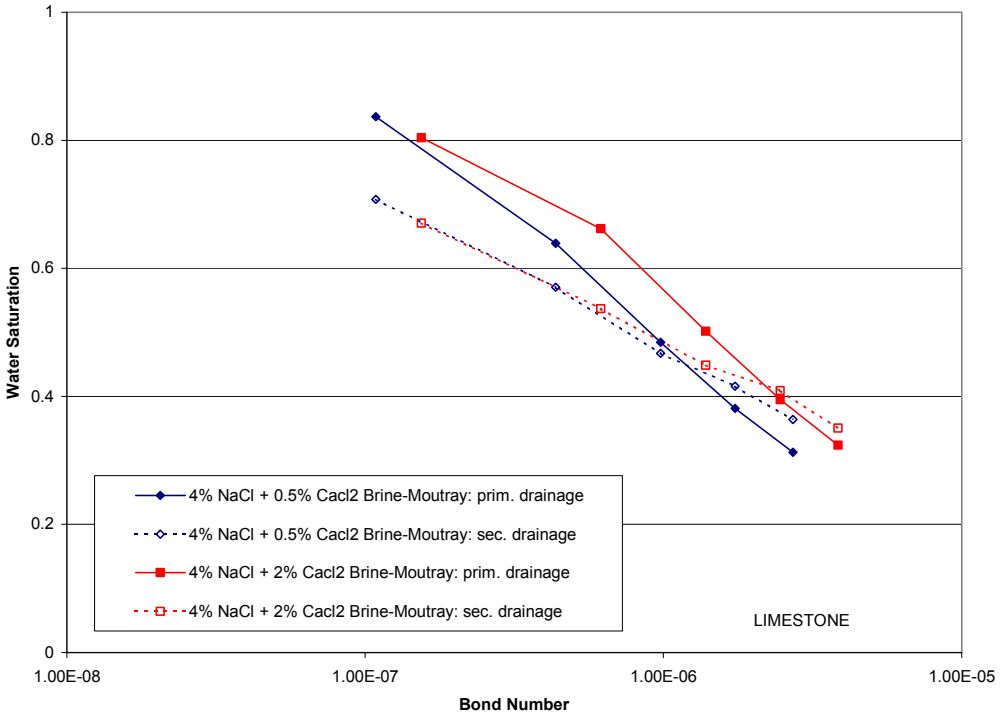

Figure 2.8: Wetting phase drainage capillary desaturation curves in brine-Moutray-limestone system.

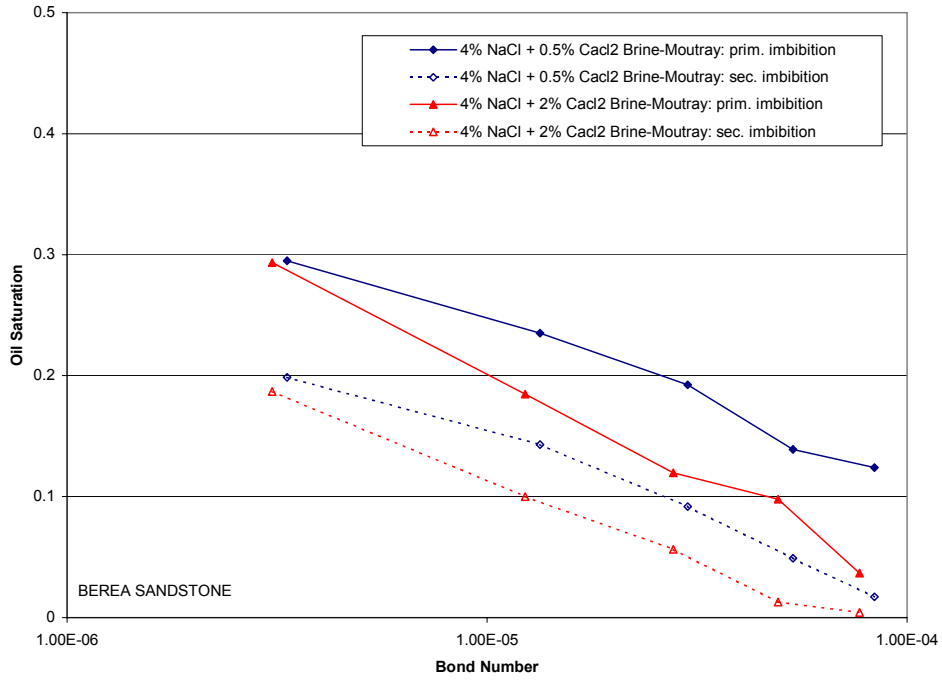

Figure 2.9: Non-wetting phase capillary desaturation curves in brine-Moutray-Berea system.

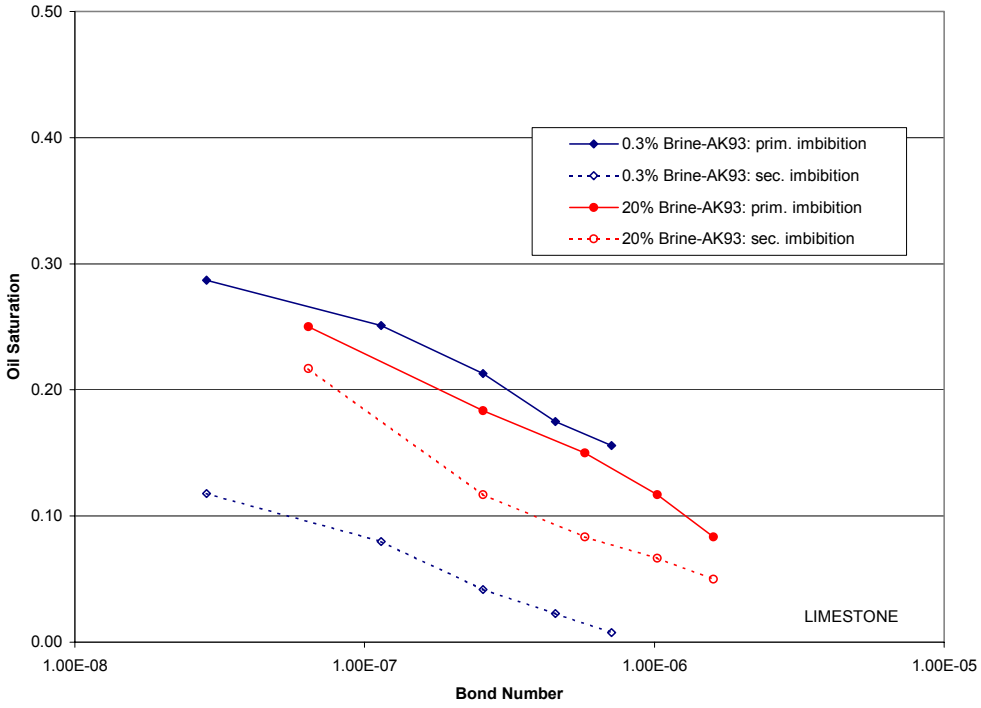

Figure 2.10: Non-wetting phase capillary desaturation curves in brine-AK 93-limestone system.

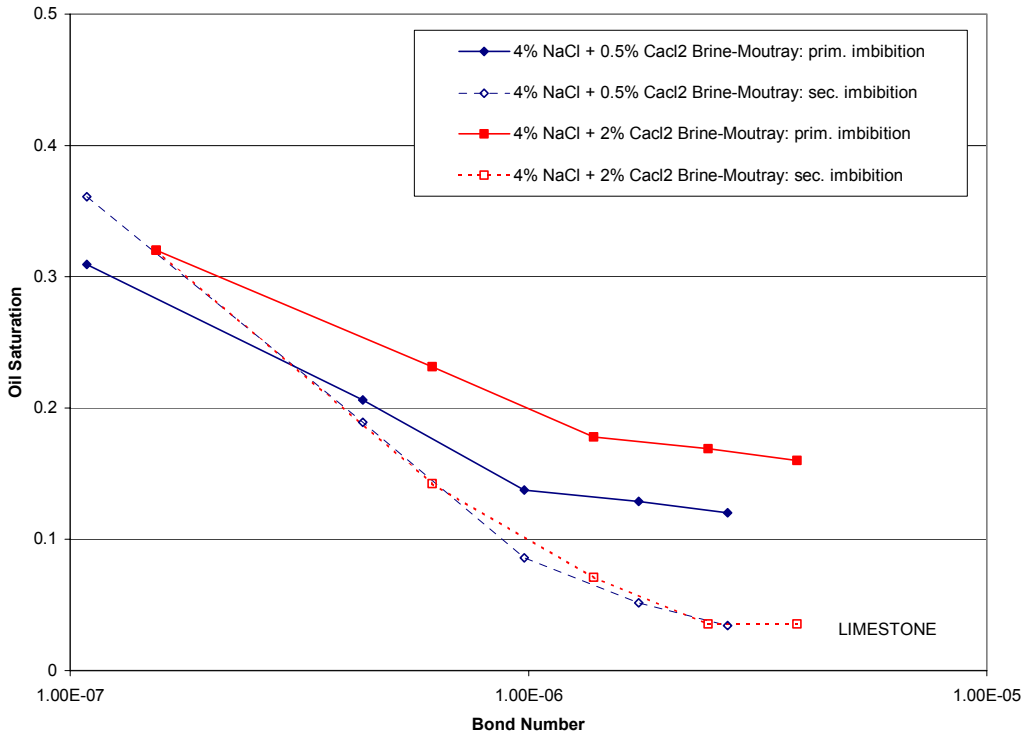

Figure 2.11: Non-wetting phase capillary desaturation curves in brine-Moutray-limestone system.

3. Investigating the Role of Crude Oil Components on Wettability Alteration

Basu, S. and Sharma, M. M.

Presented in SPE Journal, Vol. 4, No. 3, 235-241, Sept. 1999.

ABSTRACT

The surface forces between a crude-oil and its components (oil, resin and asphaltenes) and a glass substrate have been measured in brine of different salinity and pH using an atomic force microscope. The force vs. distance curves are used to measure the critical disjoining pressure for wettability alteration, i.e., departure from water-wet conditions. The measured data are compared with the classical DLVO theory to explore the nature of interaction of these components with mineral substrates.

The results indicate that the resins and asphaltenes obey the DLVO theory i.e. the stability of the brine film decreases with increasing brine salinity and increases with increasing solution pH. The opposite trend is observed with increasing salinity for the non-polar (pentane soluble) fraction and for the crude oil itself. This deviation from DLVO predictions indicates that for non-polar oils, hydrophobic interactions may play an important role in the interaction of oils with minerals and, therefore, in wettability reversal.

INTRODUCTION

The contribution of surface-active polar components in crude-oils in determining the wetting preference of reservoir rock minerals for oil or water is well-documented. These compounds are mainly concentrated in the polar fractions of the crude-oil, i.e. the asphaltenes and resins.[1-5] Many investigators have suggested that the wettability of reservoir rock is directly related to the adsorption and/or deposition of these petroleum heavy ends on mineral surfaces.[6-9] Wettability alteration studies have mainly focused on understanding the adsorption of resins and asphaltenes on model mineral surfaces. It is conjectured that once adsorbed on the mineral surface, they permanently change the preference of the mineral surface for the oil phase. The variability in wetting properties of reservoirs has been attributed to factors such as the proportion of asphaltenes and resins in the crude-oil, the

stability of the intervening water film, and the mineralogy of the rock surface.

The wettability reversal phenomenon has been studied in the past by investigating the conditions that cause the adsorption and desorption of crude-oil components on reservoir rock surfaces. The crude oil fractions that are most strongly adsorbed to mineral surfaces are the polar fractions. Many researchers have clearly demonstrated their effect in changing the wetting properties of mineral surfaces once they are adsorbed.[9] However, it is unclear how these molecules gain access to the mineral surface. Their role in destabilizing aqueous films separating the crude-oil and the mineral surface is also not known. There is a great deal of uncertainty about factors such as the size and complexity of molecular structural arrangements of these organic molecules and their physico-chemical interactions with rock surfaces in a reservoir fluid medium. One measure of these interactions is the surface forces acting between two interacting phases across a fluid medium. It is well known that surface forces determine the contact angle at a three-phase contact line (Frumkin-Derjaguin theory[10,11]) and that these forces primarily quantify the wetting properties of reservoir minerals. The force vs. distance curves provide information regarding the ability of these crude-oil fractions to break water films under different conditions, thereby, altering the wettability of the rock surface.[12,13]

In the past, studies on understanding the intermolecular and surface interactions causing the collapse of thin brine films confined between an oil and a mineral phase have met with limited success.[14,15] This was primarily due to a lack of quantitative measurements of the surface force vs. distance curves. Recently, Basu and Sharma[16] have demonstrated the feasibility of measuring these interaction forces between crude-oil and mineral substrates in an aqueous medium using an Atomic Force Microscope (AFM). The dewetting of pre-existing brine films on glass and mica substrates for different conditions of oil composition, brine chemistry, and surface morphology was systematically studied. The results of their work clearly show the importance of surface forces on wettability reversal phenomenon in oil/brine/mineral systems in oil reservoirs.[17] In this paper, the experimental technique developed in Reference 17 has been used to measure the surface force versus distance curves for asphaltenes, resins, and oils interacting with glass surfaces in brine. It is observed that the composition of the oil phase plays an important role in the stability of the brine films.

Asphaltenes and Resins Crude oil can be fractionated into different components and in different ways based either on molecular weight or polarity. Fractionation in a refinery is typically based on molecular weight with the highest molecular weight components being in general less volatile than the lower molecular weight components. For the purposes of wettability alteration it is the polarity of the molecules that is of primary concern to us. For this reason we fractionate the crude oil on the basis of their solubility in various solvents i.e. on the basis of molecular polarity. The fraction of crude oil, insoluble in heptane but soluble in benzene or toluene is referred to as the asphaltene fraction; the heptane soluble fraction of the crude oil consists of oils and resins. The heptane soluble fraction is further fractionated by eluting a silica gel column with pentane to obtain the oil fraction, with benzene to obtain the aromatic fraction and with methanol to obtain the resin fraction. This fractionation procedure with minor variations has been used extensively in the literature.[18,19] The oils, therefore, consist of the non-polar fraction of the crude oil. The resins constitute the low molecular weight polar fraction whereas the asphaltene fraction consists of the high molecular weight polar fraction of the crude oil.

Although the skeletal structure of the asphaltene fraction (obtained from various crude-oils) has been extracted by analytical methods, their structural arrangement is still not fully known. It consists of high molecular weight compounds made up of condensed polycyclic aromatic rings bearing alkyl side-chains with oxygen (O), nitrogen (N), or sulphur (S) present in the cyclic structure in small proportions. The resins have more aliphatic chains rendering them more soluble in crude-oil compared to asphaltene. The asphaltenes and resins are often referred to as the NSO fraction because of the presence of the hetero-atoms (N, S, and O). It is thought that the polarity induced by the presence of heteroatoms in the organic molecule makes them interfacially-active.[20] A detailed discussion on the chemical composition and structural arrangement of these fractions is given elsewhere.[21]

The asphaltene fraction is known to be surface-active and behave in many ways similar to a surfactant molecule. The kinetics of micellization is very slow because of their size, structural heterogeneity and chemistry. This results in slow interfacial adsorption of these fractions when deposited on a mineral surface.[18,19] A deposited layer of asphaltenes strongly affects the wetting preference of the reservoir rock, changing it from water-wet to

oil-wet. The mechanism of asphaltene precipitation has been studied through changes in mixture refractive index[17] and observing the adsorption process through molecularly thin adsorbed water films.[15]

Asphaltenes are insoluble in the oil fraction of the crude and are more likely to separate out than any other component of the crude-oil. The resins, on the other hand, are more soluble in the oil phase and help to keep the asphaltenes dispersed. It is thought that both the aromaticity and polarity of resins is, in part, responsible for the peptization (dispersion) of asphaltenes in the crude-oil. Loss of the resin and aromatic fractions results in asphaltene flocculation and precipitation. The ability of the asphaltenes to precipitate and separate out of the crude-oil makes them an important fraction for the study of reservoir wettability.

It is conjectured that a stable brine film, separating the crude-oil and the rock surface, prevents the oil phase from coming into physical contact with the rock surface. Under some conditions, the wetting film destabilizes or breaks and the crude-oil is exposed to the rock surface. The polar constitutents in the interfacially active fractions (asphaltenes and resins) get irreversibly adsorbed on the rock surface with the hydrocarbon structures exposed to the oil phase. This changes the natural hydrophilic character of the mineral surface and renders it hydrophobic perhaps permanently. The mechanism by which the NSO compounds partition to the oil/brine interface and rupture the brine film is the primary focus of our study.

The balance between the intermolecular forces in the brine film and the capillary pressure at the crude-oil/brine interface primarily determines the stability of this wetting film. The intermolecular forces are a result of the interaction between the oil/brine interface and the brine/mineral interface across the water film. The surface forces consists of van der Waals interactions which are primarily attractive, electrostatic interactions which for two negatively charged interfaces are repulsive, and structural interactions which can be either attractive or repulsive. While our outstanding of the van der Waals and electrostatic interactions is reasonably complete, structural interactions are not very well understood. When the two interacting surfaces are hydrophilic, the structural force is referred to as the hydration force. The hydration force is essentially repulsive and increases with ionic strength. Recently, the origin of the hydration forces was adequately explained by accounting for dielectric saturation effects occurring in the intervening brine film.[24,25]

When one of the interacting surfaces is hydrophobic, the structural force can be attractive and is referred to as hydrophobic force.[26] Since the crude-oil water interface is hydrophobic, the attractive structural forces play an important role in the brine film (in) stability. It is our lack of understanding of hydrophobic forces that limits our ability to interpret the experimental data presented in this paper.

The main objectives of our work are to (a) measure the interaction of crude-oil fractions with a model mineral surface, and (b) study their role in rupturing thin brine films on mineral substrates. The surface force vs. distance curves have been measured with asphaltenes and resins in brine to understand their impact on reservoir rock wettability. Experiments were conducted for different brine salinity and pH to characterize the effect of brine chemistry. The results reveal contrasting trends in the stability of the thin aqueous layer at different brine conditions when compared with those for crude-oil. These curves are analyzed to understand the role played by these compounds in the physico-chemical interactions between crude-oil and mineral substrates in brine. The disjoining pressure isotherms have been compared with those obtained from the DLVO theory to explore the nature of interaction and surface characteristics of these components.

EXPERIMENTAL PROCEDURES

An Atomic Force Microscope[27] (AFM) was used to measure forces between crude-oil fractions and glass substrates in brine as a function of separation distance. The measurement techniques used in this work are the same as the film stability tests described in an earlier paper.[16] The capability of this apparatus to measure weak intermolecular forces with precision has been exploited to measure disjoining pressure isotherms between surfaces of interest. A planar glass substrate was placed on the piezoelectric scanner that moves in the vertical direction (z axis). The oil phase was placed at the tip of the cantilever, in the form of a pendant drop, above the glass surface. Using a fluid cell, the cantilever (with the oil phase in place) and the mineral surface was immersed in brine. When the piezoelectric scanner moves closer to the cantilever tip, it deflects due to the chemical interactions between glass and oil. The tip deflection vs. z position of the piezo curves, displayed by the computer assembly, can be converted to surface force vs. distance curves. The stiffness constant of the cantilevers used in our measurements varied from 0.042 ± 0.006 Nm^{-1} to 0.32 ± 0.05 Nm^{-1}.

Cantilevers with a spring constant of 0.042 Nm^{-1} was used in experiments where small forces were recorded (< 0.05 Nm^{-1}) in the interest of acquiring greater detail in the measured tip deflection curves. Cantilevers with higher spring constants were used for systems with large forces (> 0.05 Nm^{-1}) to expand the coverage of the measurable data.

Crude-oil samples, fractionated into three fractions (asphaltenes, resins, and oils), were obtained from Mobil Oil Corporation. The elemental composition of the crude oil and the three fractions are shown in Table 3.1.

Cantilever Tip Preparation. The force curves were measured with crude-oil, asphaltenes, and resins at different brine salinity and pH. For measurements with crude-oil and resins, the specific crude-oil fraction was attached to the cantilever tip. The oil phase is attached to the cantilever tip in the form of a pendant drop. The higher viscosity and lower density of the oil phase compared to water keeps the oil drop stable on the tip when immersed in brine. Figure 3.1 shows an SEM photograph of the tip with the resin drop in place.

When measuring forces with asphaltenes, the tip was prepared in a slightly different way. The asphaltene crystals were first dissolved in toluene. A 15 μm diameter glass microsphere was glued to the cantilever tip with an epoxy hardener mix. The cantilever probe with the colloidal sphere was dipped into the organic solvent containing dissolved asphaltene. The tip is then removed and held for a couple of hours till the toluene evaporates and the asphaltene (solute) is left deposited on the microsphere. Figure 3.2 shows a SEM micrograph of the glass sphere coated with asphaltene. The asphaltene-coated microsphere has surface irreglarities as expected because the asphaltenes have a crystalline structure. It should be pointed out that a very small area (nm^2) of the tip interacts with the underlying glass substrate. We expect that the surface will behave like a rough surface with surface asperities leading to smaller measured disjoining pressures.[16]

Surface Preparation and Cleaning Procedures. Glass microslides were used for the force measurements with crude oil and its fractions. The glass substrates were glued to the magnetic disks (supplied with the Nanoscope E AFM) using an epoxy hardener mix. The substrates and the cantilevers were treated with methanol, isopropanol, and acetone followed

by rinsing with deionized water before each measurement to remove any contaminants. The same procedures were used for cleaning the fluid cell except that it was not treated with acetone (because it has a corrosive action on the reflective material coating the cell). The magnetic disk (with the glass substrate) and the cantilever were then mounted on the piezoelectric scanner and the fluid cell, respectively. The methodology used for the AFM measurements and the data analysis used to obtain the force curves for oil/brine/mineral systems is discussed in detail elsewhere[16].

DLVO Force Computations The intermolecular forces in a thin liquid film confined between surfaces have traditionally been quantified by the DLVO theory.[28,29] The theory classifies these intermolecular forces into the electrical double layer force, Π_{el}, and the van der Waals force, Π_{vdW}. The net pressure, Π, which is called the disjoining pressure, is the sum of these two forces or

$$\Pi = \Pi_{vw} + \Pi_{el} \qquad [3.1]$$

In this case, a curved surface (oil drop) interacts with a flat surface (mineral substrate). The Derjaguin approximation[30] is used to convert measured forces to interaction energy per unit area,

$$W = \frac{F}{2\pi R} = \int_h^\infty \Pi \, dh \quad , \qquad [3.2]$$

where E is the interaction energy per unit area, F is the force between the interacting bodies, h is the film thickness, and r is the radius of curvature of the oil drop. The force curves are plotted as F/R vs. h.

The electrostatic interactions between the mobile ions in the thin film and the charged surface sites give rise to a double layer of oppositely charges ions in the solution. The electrical double layer formed at the interface interacts with the double layer at other interfaces. This causes an overall increase in counter-ion concentration in the film resulting in an osmotic force. The electrical double layer force, Π_{el}, is repulsive for negatively charged surfaces, and can be expressed as[29],

$$\Pi_{el} = 64\pi n_o kT \tanh\left(\frac{e\zeta_1}{kT}\right)\tanh\left(\frac{e\zeta_2}{kT}\right)\exp(-\kappa h), \qquad [3.3]$$

where n_O is the number density of ions in the bulk solution, k is the Boltzmann constant, T is the temperature of the system, ζ_1 and ζ_2 are the zeta potentials at the interfaces, and κ is the Debye length. This equation is derived assuming that the electrical potential at the center of the thin film for overlapping double layers can be represented as the sum of the electrical potentials at that position for non-interacting double layers. This equation is valid for a film thickness h > 5-7 nm.

The van der Waals forces are attractive when the dielectric permittivity of the liquid interlayer is smaller than that of the confining phases. These forces are mainly attributed to induced dipole-induced dipole interactions between molecules, also known as the London-dispersion interactions. The retarded van der Waals forces, Π_{VW}, are calculated using the relation,

$$\Pi_{vw} = \frac{-A\left(\frac{15.96h}{\lambda} + 2\right)}{12\pi h^3 \left(\frac{5.32h}{\lambda} + 1\right)^2}, \qquad [3.4]$$

where A is the Hamaker constant and λ is the London wavelength (1000 Å). The Hamaker constant used for calculating Π_{vdW} between glass and a hydrocarbon phase interacting across an aqueous medium is 2.0 x 10^{-21} J.[26]

The DLVO theory is able to predict the magnitude of measured surface forces up to a separation distance ranging from 5 to 50 nm, depending upon the physico-chemical characteristics of the interacting surfaces and the chemistry of the liquid interlayer. In many cases, the measured forces at smaller film thickness are not predicted by this theory. These non-DLVO forces, commonly known as structural forces, are extremely large and dominate the surface force components at separation distances smaller than 10 nm. These forces have important implications in stabilizing and destabilizing thin films in oil reservoirs.

RESULTS AND DISCUSSION

AFM experiments were performed to obtain surface force curves with crude-oil and its fractions, resins and asphaltenes, on planar glass substrates in an aqueous NaCl solution. The measured force vs. distance curves are presented for different salinity and pH of the aqueous medium. The main purpose of these measurements is to investigate the differences

in behavior between the crude-oil fractions on the wettability reversal of mineral surfaces. To study the effect of brine chemistry (salt concentration and pH) on wetting film stability, measurements were made at three different salt concentrations - 0.01M, 0.1M, 1M - each at a pH of 5.5 and 8.

In this work, the brine film is considered unstable if it collapses spontaneously when the non-wetting (oil) phase is brought in close physical proximity to the underlying mineral surface. A metastable film does not break until the capillary pressure applied on the non-wetting phase exceeds the critical disjoining pressure for film rupture. The wetting brine films are referred to as stable films if they do not break even when very high capillary pressures are applied.

Effect of Brine Salinity. Measured force curves with resins and asphaltenes at 0.01M, 0.1M, and 1M NaCl concentrations against glass surfaces are shown in Figures 3.3 and 3.4, respectively. The curves show a decrease in repulsion with increasing salt concentration for asphaltenes and resins. In both cases, the brine films are metastable at 0.01M NaCl and unstable at 1M NaCl. At 0.1M NaCl, the aqueous films are metastable with asphaltenes whereas they are unstable with resins. The film thickness at rupture, h_r, decreases with increasing salt concentration. The results are in qualitative agreement with the DLVO theory which predicts a decrease in disjoining pressure and film rupture thickness with increasing salt concentration. The plotted data also indicates the absence of additional repulsive hydration forces that can stabilize thin films. This matter will be dealt with in later sections.

Brine films with crude-oil reveal decreasing h_r with increasing brine salinity (Fig. 3.5). The films are completely unstable for the whole range of NaCl concentrations. The film rupture thickness decreases (a trend of increasing stability) with increasing salinity. Figure 3.6 shows metastable and stable films for 0.01 M and 0.1 M brine salinity, respectively, at pH 8. Because of the absence of hysteresis in the AFM curves, the zero reference for the separation distance is not obtained. Therefore, the measured data points are not shown in the plot and a solid line represents the force curve. This shows that for the crude oil, film stability increases with increasing salt concentration. These opposing trends in film stability between the crude-oil and the polar fractions of the crude show that the surface-active fractions (resins and asphaltenes) behave differently than the crude oil.

Effect of Brine pH. The aqueous wetting films show an increase in stability with increasing solution pH with the resin and asphaltene fractions. Figure 3.7 shows an increase in repulsive intermolecular forces with resins with increasing solution pH. This is expected since the solution pH strongly influences the surface charge density. Decreasing the concentration of potential-determining H^+ ions increases the concentration of deprotonated surface groups. The higher surface charge density gives rise to a higher concentration of mobile counter-ions in the aqueous film through Coulombic interactions. This causes a higher osmotic or electrical double layer force.

The decrease in repulsion with increasing brine salinity at a higher solution pH (pH 8) is still observed, similar to the trend obtained at pH 5.5. This is in direct agreement with the results obtained from the DLVO theory which predicts a decrease in electrical double layer forces due to surface charge screening effects at a higher ion concentration. Notably, there is an absence of any additional repulsive structural or hydration forces at small distances of separation at the higher solution pH.

Figure 3.8 shows the effect of solution pH on the surface force between crude-oil and glass. The increase in the repulsive force with brine pH is consistent with the DLVO theory. The qualitative trends essentially are in agreement with previously reported measurements with similar (oil/brine/rock) systems.[16,17]

Differences in Force Curves (Resins vs Asphaltenes) Similar film stability results are obtained for both asphaltenes and resins. Films are more stable at 0.01M brine salinity with resins compared with asphaltenes on glass surfaces. However, the films become less stable at 0.1M and 1M salt concentration with resins. Film stability is more sensitive to changes in pH for resins as compared with asphaltenes. A larger increase in disjoining pressure is obtained with resins when the pH is raised from 5.5 to 8, as shown in Figure 3.4. However, changes in brine chemistry cause similar changes in force curves for both the polar fractions. This indicates that the interfacial properties of these fractions have similar characteristics when in contact with an aqueous phase.

Comparisons with Force-Curves For Crude-Oil Figure 3.9 shows a comparison of force curves between crude-oil, asphaltenes, and resins. The brine films are most stable with

asphaltenes and least stable with crude-oil for the same brine chemistry and mineralogy of the solid surface. For a brine salinity and pH of 0.01M and 5, the asphaltenes reveal metastable films whereas unstable films result in the case of crude-oil. For some salinities and pH values resins may show more stable films (Figure 3.7). For crude oils, increasing salt concentration and solution pH has a stabilizing effect on the aqueous films as observed in Figures 3.5 and 3.6. In similar experiments conducted earlier, we have also reported such trends.[16] The wetting films were shown to become more stable with increasing salt concentration and pH with crude-oils obtained from different reservoirs. NSO compounds, on the other hand, show a less stable water film with increasing brine salinity.

Comparisons with DLVO Theory Good quantitative and qualitative predictions with DLVO theory are obtained with resins and asphaltenes for 0.01M brine at a pH of 5.5 and 8, as shown in Figures 3.10 and 3.11. The ζ-potentials for glass is obtained from Ref. 14. Comparisons with the theory were made only for 0.01M brine salinity since the Poisson-Boltzmann equation, which assumes point charges, is not valid at high brine salinities and pH. Overall, the force vs. distance curves obeyed the DLVO theory very well. The calculated ζ-potentials for resins and asphaltenes are provided in the figure legends. The disjoining pressure decreases with increasing ion concentration and increases with increasing solution pH. Higher H^+ favors the dissociation of fixed charge groups on surfaces and causes a higher surface charge density. On the other hand, charge-screening at higher salt concentrations reduces the effective surface charge density and, therefore, the counter-ion concentration and electrical potentials in the thin film.

In related recent work[31], it has been shown that the interaction of asphaltenes with a mineral substrate depends on the composition of the brine. Surface imaging studies on aged mica conducted with an AFM revealed that the weight of adsorbed asphaltene aggregates on the mineral surface increased with brine salinity and decreased with solution pH.[31] This indicates that the brine films are more unstable at higher salt concentration and low pH in order for the asphaltenes in the oil phase to gain access to the underlying mica surface.

Structural Forces Qualitative agreement with DLVO force curves indicates that

structural forces are not dominant in the intermolecular interactions between the polar fractions and glass. The brine film invariably ruptures in all force measurements with resins and asphaltenes. Good agreement between theory and experiments at low brine salinity and pH indicate the absence of hydrophobic forces. Structural or non-DLVO forces do not appear to play a significant role in determining film rupture for these polar crude-oil components.

In contrast with the polar fractions the experimental trends indicate that structural forces have a strong influence on film stability in the case of crude-oils and alkanes. Hydrophobic interactions, that are primarily attractive, cause unstable films at low brine salinity and pH (Fig. 3.5). On the other hand, extremely short-range repulsive hydration forces result in stable films at high brine salinity and pH (Fig. 3.6). The trend of increasing water wetness with increasing salinity is observed in simple adhesion tests for a variety of crude oils[23]. Similar results have also been obtained using the AFM with octadecane, Moutray and Prudhoe Bay crude-oils.[17]

It is now well established that the interaction of a non-polar surface (oil-water) with a polar surface (glass-water) may be dominated by hydrophobic interactions (attractive).[26] This is the most likely reason for the instability of the brine film with the crude oil. Hydrophobic forces do not arise when two polar surfaces interact. As a result the resin and asphaltene fractions show good agreement with the DLVO calculations.

The dependence of hydrophobic forces on salinity is not well known. Our limited set of experiments suggests that the hydrophobic attractive forces increase as the salinity decreases.

CONCLUSIONS

The surface force vs. distance curves for asphaltenes and resins follow the trends predicted by the DLVO theory where the critical disjoining pressure decreases with increasing brine salinity and decreasing pH. This trend of decreasing film stability with increasing brine salinity and decreasing pH suggests that for the polar fractions of the crude-oil electrostatic interactions play a dominant role.

In the presence of a non-polar oil, however, hydrophobic interactions (attractive) become important and the brine film is more unstable. Increasing the pH or the salinity

results in more stable films. The increase in film stability with salinity is consistent with the behavior observed for octadecane and two other crude oils[16] but is not explainable on the basis of DLVO theory. Perhaps the explanation lies in the variation of the hydrophobic force with salinity.

REFERENCES

1. Clementz, D.M.: "Interactions of Petroleum Heavy Ends with Montmorillonite," *Clays and Clay Minerals* (1976) **24**, 312-319.

2. Donaldson, E.C. and Crocker, M.E.: "Characterization of the Crude Oil Polar Compound Extract," DOE Report Investigations, DOE/BETC/RI-80/5, (October, 1980).

3. Czarnecka, E. and Gillot, J.E.: "Formation and Characterization of Clay Complexes With Bitumen From Athabasca Oil Sand," *Clays and Clay Minerals* (1980) **28**, 197-203.

4. Collins, S.H. and Melrose, J.C.: "Adsorption of Asphaltenes and Water on Reservoir Rock Minerals," paper SPE 11800 presented at the 1983 SPE Intl. Symposium on Oilfield and Geothermal Chemistry, Denver, June 1-3.

5. Cuiec, L.: "Rock /Crude-Oil Interactions and Wettability: An Attempt to Understand Their Interrelation," presented at the 1984 SPE Annual Technical Conference and Exhibition, Houston, TX, Sept. 16-19.

6. Lowe, A.C., Philips, M.C., and Riddiford, A.C.: "On the Wettability of Carbonate Surfaces by Oil and Water," *J. Cdn. Pet. Tech.* (1973) **12**, 33-40.

7. Lyutin, L.V., and Burdyn, T.A.: "Adsorption of Asphaltenes in a Stratum and Its Effect on Permeability and Oil Production," *Tr., Vses. Neftegasov. Nauch.-Issled. Inst.* (1970) **53**, 117-130.

8. Berezin, V.M., Yarygina, V.S., and Dubrovina, N.A.: "Adsorption of Asphaltenes and Tar From Petroleum by Sandstone," *Neftepromysyl. Delo* (1982) **5**, 15-17.

9. Dubey, S.T. and Waxman, M.H.: "Asphaltene Adsorption and Desorption From Mineral Surfaces," SPE Res. Eng. (1991) 389-395.

10. Frumkin, A.N.: "Wetting and Adherence of Bubbles," *Zh. Fiz. Khim.* (1938) **12**, 337-345.

11. Derjaguin, B.V.: "Theory of Capillary Condensation and Related Capillary Effects. Calculation of Spreading Action of Polymolecular Liquid Films," *Zh. Fiz. Khim.* (1940) **14**, 137-147.

12. Hirasaki, G.J.: "Interfacial Phenomena in Petroleum Recovery," N.R. Morrow (ed.), Ch.2, pp. 23-76, Marcel Dekker, New York (1991).

13. Hirasaki, G.J.: "Interfacial Phenomena in Petroleum Recovery," N.R. Morrow (ed.), Ch.3, pp. 77-99, Marcel Dekker, New York (1991).

14. Buckley, J.S., Takamura, K., and Morrow, N.R.: "Influence of Electrical Surface Charges on the Wetting Properties of Crude Oils," *Soc. Pet. Eng. Res. Eng.* (1989) **4**, 332-340.

15. Kaminsky, R., Bergeron, V., and Radke, C.J.: "Thin Films, Asphaltenes, and Resrvoir Wettability," presented at the 1993 World Congress on Emulsions, Paris, France, Oct. 19-22.

16. Basu, S. and Sharma, M.M.: "Direct Measurement of Critical Disjoining Pressure for Dewetting of Solid Substrates," *J. Colloid Interface Sci.* (1996), **181**, 443-455.

17. Basu, S. and Sharma, M.M.: "Characterization of Mixed-Wettability States in Oil Reservoirs by Atomic Force Microscopy," paper SPE 35572, presented at the 1996 SPE Annual Technical Conference and Exhibition, Denver, CO, Oct. 6-9..

18. Sheu, E.Y. , De Tarm, M.M., Storm, D.A., and DeCania, S.J.: "Aggregation and Kinetics of Asphaltenes in Organic Solvents," *Fuel* (1992) **71**, 299-302.

19. Sheu, E.Y., De Tar, M.M., and Storm, D.A.: "Interfacial Properties of Asphaltenes," *Fuel* (1992) **71**, 1277-1281.

20. Speight, J.G., and Moschopedis, S.E.: "Chemistry of Asphaltenes," J. W. Bunger and C. Norman (eds.), Ch. 1, pp. 1-16, Advances in Chemistry, Series 195 (1981).

21. Tissot, B.P and Welte, D.H.: "Petroleum Formation and Occurrence," pp. 375-414, Springer-Verlag Berlin Heidelberg, New York (1984).

22. Buckley, J.S.: "Microscopic Investigation of the Onset of Asphaltene Precipitation," *Fuel Sci. & Tech. Internat.* (1996) **14**, 55-74.

23. Buckley, J.S.: "Chemistry of Crude Oil/Brine Interface," presented at the 1994

International Symposium on Reservoir Wettability and Its Effect Recovery, Laramie, WY, Sept. 21-23.

24. Basu, S. and Sharma, M.M.: "Effect of Dielectric Saturation on Disjoining Pressure in Thin Films of Aqueous Electrolytes," *J. Colloid Interface Sci.* (1994), **165**, 355-362.

25. Paunov, V.N., Dimova, R.I., Kralchevsky, P.A., Broze, G., and Mehreteab, A.: "The Hydration Repulsion Between Charged Surfaces as an Interplay of Volume Exclusion and Dielectric Saturation Effects," *J. Colloid Interface Sci.* (1996), **182**, 239-248.

26. Israelachvili, J., "Intermolecular and Surface Forces", Academic Press (1991).

27. Binnig, G., Quate, C.F., and Gerber, C.: "Atomic Force Microscope", *Phys. Rev. Lett.* (1986) **56**, 930-933.

28. Derjaguin, B.V., and Landau, L.: *Acta Physicochim.* (1941) **14**, 633.

29. Verwey, E.J.W., and Overbeek, J.Th.G.: "Theory of the Stability of Lyophobic Colloids," Elsevier, Amsterdam, The Netherlands (1948).

30. Derjaguin, B.V.: *Kolloid Zeits.* (1934) **69**, 155.

31. 31.Steve Yang, George Hirasaki, Subhayu Basu, and Ravi Vaidya, "Mechanisms for Contact Angle Hysteresis and Advancing Contact Angles," presented at the 5th International Symposium on Evaluation of Reservoir Wettability and Its Effect on Oil Recovery, Trondheim, Norway, June 22-24, 1998.

Table 3.1--Elemental composition of crude oil and its fractions

	Crude Oil	Oil	Asphaltenes	Resins
Carbon (%)	84.14	83.91	80.84	80.55
Hydrogen (%)	10.79	11.59	8.25	9.42
Oxygen (%)	0.49	0.20	1.26	1.79
Nitrogen(%)	0.38	0.02	1.06	0.66
Sulfur (%)	4.27	2.24	8.05	5.92
Total NSO(%)	5.14	2.46	10.37	8.37

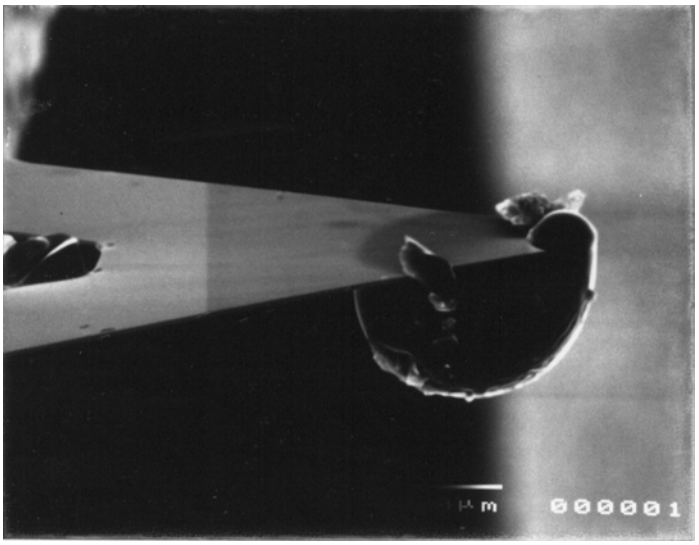

Figure 3.1 A SEM photograph of a drop of resin hanging on the cantilever tip.

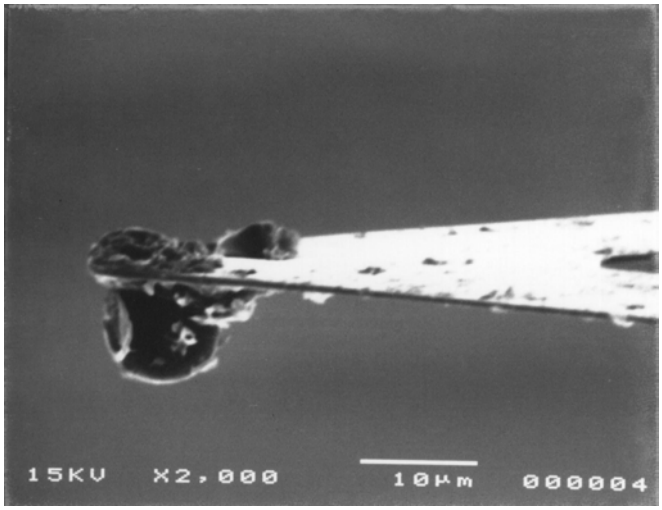

Figure 3.2 A SEM photograph of 10 µm diameter glass microsphere glued on the cantilever and coated with asphaltenes.

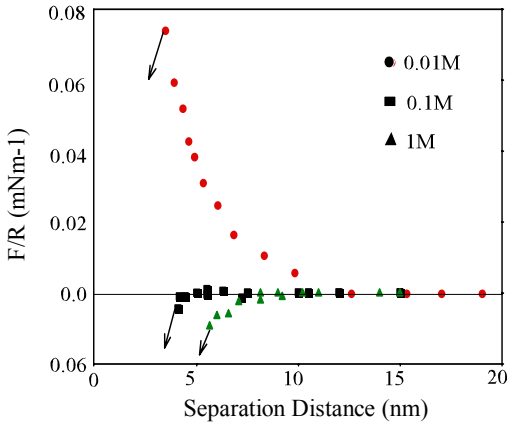

Figure 3.3 Measured surface force curves with resins at pH 5.5. The arrows indicate the separation distance where the intervening brine film ruptured and the hydrocarbon phase gained access to the underlying glass surface. The curves suggest decreasing film stability with increasing brine salinity (consistent with DLVO theory).

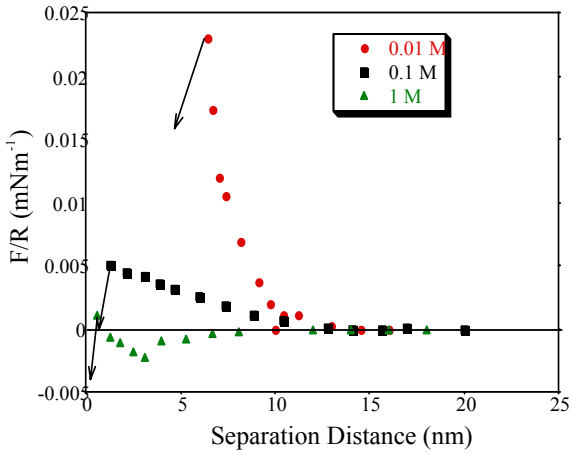

Figure 3.4 Measured surface force curves with asphaltenes at pH 5.5. The arrows indicate the separation distance where the intervening brine films ruptured and hydrocarbon phase adhered to the underlying glass surface. The curves suggest decreasing film stability with increasing brine salinity salinity (consistent with DLVO theory).

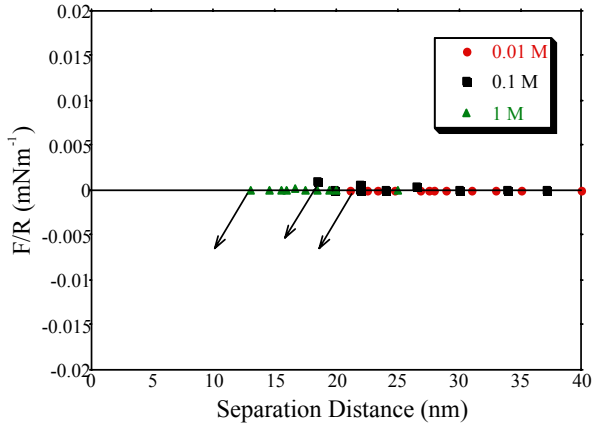

Figure 3.5 Measured surface force curves with asphaltenes at pH 5.5. The arrows indicate the separation distance where the intervening brine films ruptured and hydrocarbon phase adhered to the underlying glass surface. The curves suggest increasing film stability with increasing brine salinity.

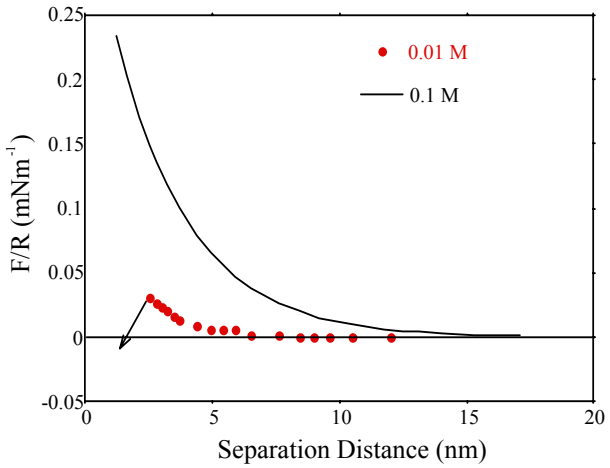

Figure 3.6 The measure forces with crude-oil at a solution pH of 8. The brine film become stable at a higher solution pH compared with those obtained at a pH of 5.5 (Fig. 5). Due to the inherent limitations in the AFM measurements in calculating the separation distance for completely stable films, solid line is drawn to illustrate this effect.

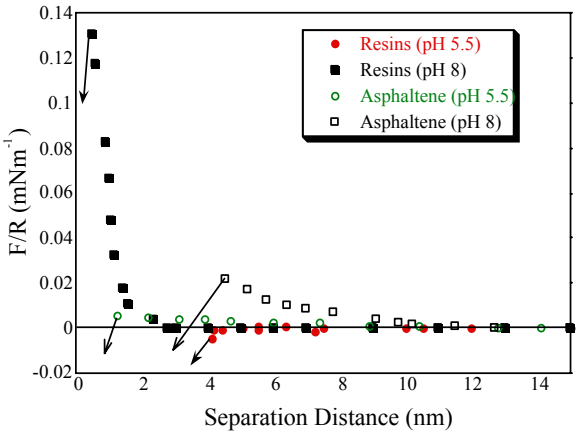

Figure 3.7 Effect of brine pH on measured surface force curves with asphaltenes and resins in 0.1M brine. The increase in stability of brines films is more with resins than with asphaltenes.

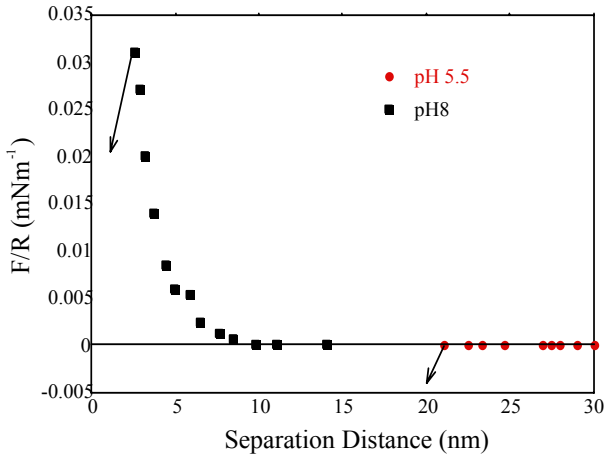

Figure 3.8 Effect of brine pH on measured surface force curves with crude-oil on glass in 0.01M brine. The stability of brine films increases with increasing solution pH.

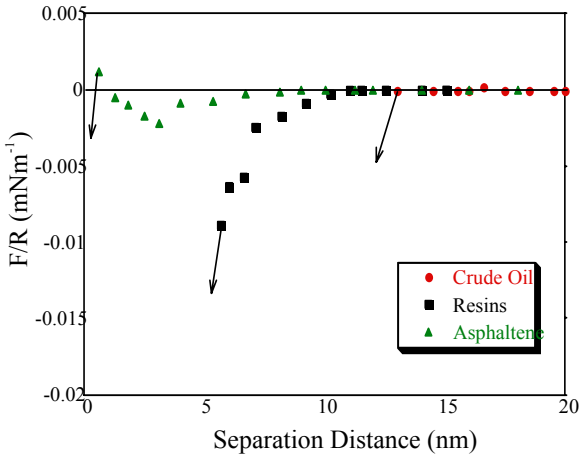

Figure 3.9 Comparison of measured surface force curves with crude-oil, asphaltenes, and resins in 1M brine at pH 5.5. The brine films are least stable with crude-oil and the most stable with asphaltenes.

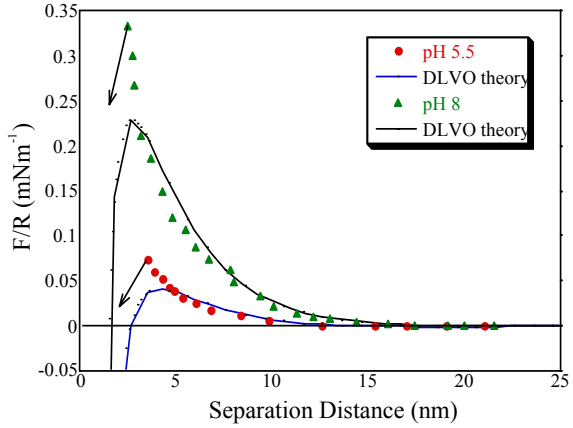

Figure 3.10 Comparison of measured surface force curves for resins with DLVO theory in 0.01M brine. The theory predicts slightly larger film rupture thickness. At pH 5.5, ζ_{glass} = -65 mV and ζ_{resins} = -2.6 mV; at pH 8, ζ_{glass} = -75 mV and ζ_{resins} = 5.3 mV)

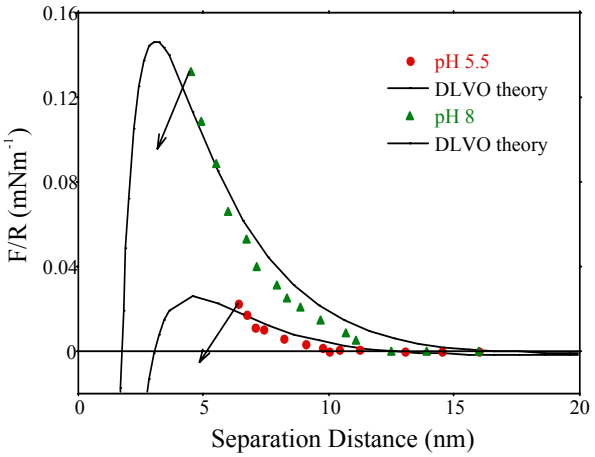

Figure 3.11 Comparison of measured surface force curves for asphaltenes with DLVO theory in 0.01M brine. The theory predicts slightly larger film rupture thickness. At pH 5.5, z_{glass} = -65 mV and $\zeta_{asphaltenes}$ = -2.2 mV; at pH 8, ζ_{glass} = -75 mV and $\zeta_{asphaltenes}$ = -4.2 mV)

4. Influence of Wettability and Saturation on Liquid-Liquid Interfacial Area in Porous Media

Jain, V., Bryant, S. and Sharma, M. M.

Presented in Environmental Science and Technology, 2003.

ABSTRACT

The knowledge of the area of interfaces between phases is important to understand and quantify many flow and transport processes in porous media. In this work we apply the interfacial tracer technique to study the dependence of fluid/fluid interfacial area on saturation and wettability. The interfacial area between the wetting and non-wetting phases (brine and decane) in unconsolidated porous media (glass beads) was measured using an anionic surfactant (3-phenyl decyl benzene sulfonate) as an interfacial tracer. The beads are water wet; treating them with organosilane rendered them oil wet. The measurements were done at a series of steady-state fractional flows, providing data at intermediate as well as residual saturations. Flow rates were kept low so that capillary forces controlled the fluid configurations. We observe significant differences in interfacial areas as a function of wetting phase saturation as the wettability is changed from water-wet to oil-wet. During primary drainage, measured interfacial area increases monotonically with decreasing water saturation in a water-wet medium. In contrast, the interfacial area measured in the oil wet porous medium increases with decreasing decane saturation, reaches a maximum and decreases as the residual decane saturation is achieved. The oil-wet experiment is qualitatively consistent with theoretical results, which predict the existence of a maximum in fluid/fluid interfacial area during drainage. The water-wet experiment is consistent with theoretical predictions that include the area of grains in pores that have been drained. We conclude that in the water-wet experiments, the tracer adsorbs at the interface between nonwetting phase and the wetting films on grains. In the oil-wet experiments, either the oil films are not sustained at high water saturation, or the tracer does not adsorb at them, possibly prevented by steric hindrance. Interpretation of interfacial tracer experiments

therefore requires care: for some mass transport processes, the thin films of wetting phase on grains will not behave the same as macroscopic volumes of wetting phase.

INTRODUCTION

Knowledge of interfacial areas is important to better understand and quantify many flow and transport processes in unsaturated/saturated porous media. Mass transfer rates for processes such as adsorption, dissolution, and volatilization are proportional to solid-fluid and fluid-fluid interfacial areas. Interfacial areas are also important for modeling colloidal and microbial transport. The air-water interfacial area is important for modeling remediation processes like soil-vapor extraction in vadose zone. Air-water interfaces serve as sorption sites for colloids and bacteria, subsequently retarding their transport in unsaturated media. Similarly, knowledge of liquid-liquid interfacial area is important in estimating the contaminant flux between non-aqueous phase liquids (NAPL) and water for various remediation processes such as surfactant enhanced aquifer remediation (SEAR). Knowledge of interfacial areas, therefore, facilitates the quantification and numerical simulation of a variety of flow and transport processes (1-2).

Multiphase transport in porous media is characterized by means of several macroscopic transport properties such as relative permeability, capillary pressure and dispersivity. These properties have been found experimentally to depend upon parameters such as fluid saturations, fluid properties, saturation history and pore space morphology. Alpak et. al. (3) have modified the Carmen-Kozeny equation to model two-phase relative permeabilites, which includes a dependence on solid-liquid and liquid-liquid interfacial areas. However, they have no independent measurement of interfacial areas to validate their model. Moreover, a standard assumption in modeling is that the flowing aqueous phase is in local chemical equilibrium with the oil phase. Depending on the flow rate, the oil saturation and the ratio of surface area to volume of the oil phase, this assumption may not be valid. Moreover, the area of the liquid-liquid interface is likely to vary with oil saturation (4-5), and this effect is not accounted for in standard kinetic models.

The objective of this research was to apply the tracer technique to study the effect of fluid saturation, wettability and hysteresis on interfacial area and to model the impact of liquid-liquid interfacial area on relative permeability. Interfacial tracers (6) can be used to

measure the specific oil-water interfacial area in a porous medium. Because so little experimental data is available for liquid-liquid interfacial area, this paper presents a series of experiments with interfacial tracers in order to better define the possible range of interfacial areas over different saturations for varying types (water-wet and oil-wet) of porous media. The measurements are done not just at the end points, but also for intermediate saturations, where both phases are flowing. Throughout the experiments, capillary forces dominated viscous forces ($N_{Ca} \sim 10^{-6}$). Thus the measurements are relevant to fluid configurations arising in situations such as NAPL contamination events, tracer injection for NAPL volume estimation, and pump-and-treat remediation.

BACKGROUND

Most models for fluid transport in porous media employ a "lumped" parameter for interphase mass transport. The lumped parameter includes an interfacial area and a mass transfer coefficient (7), as it is difficult to measure independently the interfacial area on which or through which the adsorption, dissolution etc is occurring. This would be less of a problem if the interfacial area were constant. However, experiments show that interfacial areas vary with non-wetting phase saturation.

There are many theoretical studies, which have modeled air-water or liquid-liquid interfacial area in porous media as a function of pressure and saturation by assuming a specific pore geometry (8-10). Others have used thermodynamic arguments to relate the area of fluid/fluid and fluid/solid interfaces to the area under drainage and imbibition curves (4,11). Some experimental measurements of air-water interfacial area in unsaturated porous media as a function of saturation have been reported. Karkare and Fort (12) used a hydrophobic surfactant (1-tetradecanol) to study its impact on water movement and then calculated air-water interfacial area as the number of molecules of surfactant required to initiate water movement multiplied by area of each surfactant molecule. Kim et. al. (13) developed a miscible displacement technique using interfacial tracers to measure the interfacial areas. The interfacial tracer technique can be used as a simple, nondestructive measurement method for obtaining the specific oil-water interfacial area in both laboratory and field settings (6,14). Anionic surfactants are used as interfacial tracers at concentrations below the critical micelle concentration (CMC), to minimize solubilization and mobilization

of the oil phase. These interfacial tracers accumulate at the oil-water or air-water interface by adsorption, however they do not partition into the oil or air phase.

Schaeffer et al. (15) measured air-water interfacial area as a function of capillary pressure and water saturation. They measured interfacial areas greater than that observed by Kim et al. (13) and attributed this to inclusion of thin films in their measurements. Faisal et al. (16) developed a new method to measure air-water interfacial area using the surfactant adsorption concept. Their experimental results show that the air-water interfacial area increases with decreasing water saturation during the drainage cycle. The imbibition cycle area differs from the corresponding drainage area at the same water saturation. Schaeffer et al. (15) observed no relation between interfacial area and water saturation in the imbibition cycle.

Bradford and Leij (4) inferred air-oil and air-water interfacial area from drainage and imbibition experiments in unconsolidated media that were imperfectly wetted (contact angle > 0) or of mixed wettability (some grains water-wet, others oil-wet). The work by Saripalli et al. (6) involved measuring the liquid-liquid interfacial area at residual non-wetting phase saturation for water-wet and oil-wet sands. However, the interfacial tracer technique has not previously been applied to measure the area between two liquids in a porous medium as a function of saturation and wettability. The objective of this study is to measure liquid-liquid interfacial area as a function of saturation in different wettability states (water-wet and oil-wet).

Initial experimental evidence strongly indicates that the specific oil-water interfacial area exhibits changes as a function of the wetting state of the porous medium. Results of the column experiments conducted by Saripalli et al. (6) using interfacial tracers demonstrate that the specific oil-water interfacial area (per unit pore volume) varied from 86 cm^2/cm^3 to 272 cm^2/cm^3 depending upon which phase was initially present in the column. Estimation of the interfacial area from measured capillary pressure-saturation curves (4) indicate that similar hysteresis is observed in interfacial area as is observed in capillary pressure curves during primary drainage and imbibition. Moreover, they estimated that interfacial area is smaller for a mixed wet system as compared to water-wet or oil-wet system. We note that if the liquid/liquid configurations are controlled by capillary forces in a perfectly wetted system, the identity of the wetting phase (e.g. water or oil) should be immaterial; the trend of

area as a function of saturation should be the same for drainage (or imbibition) in a water-wet system as for drainage (or imbibition) in an oil-wet system.

THEORY

The basis of the interfacial tracer method is the following idealization: the retardation of an interfacial tracer with respect to a conservative tracer is proportional to the sorbed concentration of the interfacial tracer within the porous medium. In practice, the retardation of the interfacial tracer is also impacted by its mobility along the interface (17). Interface mobility consists of two components: Marangoni flux due to concentration gradient and convection due to shear at the interface. Here we have assumed that the convection effect is very small and the interface mobility is small compared to the bulk pore velocity and subsequently has no effect on the retardation factor. The retention factor, R_{ift}, accounts for sorption onto the porous medium and adsorption at the wetting-nonwetting phase interface:

$$R_{ift} = 1 + \frac{\rho K_d}{S_w} + \frac{K_o}{S_w} \qquad [4.1]$$

ρ: bulk density of solid, g/cm^3; K_d: sorption coefficient onto the solid matrix, cm^3/g; S_w: wetting phase or water saturation; K_o (dimensionless): adsorption coefficient at the wetting-nonwetting phase interface. K_o is a function of the interfacial area and the chemical affinity of the tracer for the interface.

K_d can be estimated from a tracer experiment conducted in a water-saturated column in the absence of non-wetting phase. The Gibbs adsorption equation relates the adsorbed concentration of the tracer (C^i_{ads}) at the oil-water interface to the bulk concentration:

$$C^i_{ads} = \Gamma a_i = K_o C_w \qquad [4.2]$$

where a_i is the oil-water interfacial area (cm^2/cm^3) and Γ, surface excess of the tracer (mol/cm^2) is given as,

$$\Gamma = -\frac{1}{2RT}\left(\frac{\partial \gamma}{\partial C_w}\right)_T C_w \qquad [4.3]$$

R: ideal gas constant, erg mol^{-1} K^{-1}; T: absolute temperature, K; γ: interfacial tension, dyne/cm.

Surface excess of the tracer can be determined using interfacial tension data. Since γ is a nonlinear function of C_w, the interfacial adsorption isotherm is nonlinear too. However, it can be used to estimate K_o using equations 4.2 and 4.3:

$$K_o = \frac{\Gamma a_i}{C_w} = -\frac{a_i}{2RT}\left(\frac{d\gamma}{dC_w}\right) = -\frac{a_i \beta}{2RTC_w} \qquad [4.4]$$

where β is obtained by fitting the following equation: $\gamma = \alpha - \beta \ln(C_w)$ to measurements of γ at various C_w.

For a step-input tracer experiment the retardation factor is calculated by measuring the area above the breakthrough curve, given as (6):

$$R_{ift} = \frac{\mu_{ift}}{\mu_{con}} \qquad [4.5]$$

where the subscripts 'ift' and 'con' refer to interfacial and conservative tracers respectively and μ is (6)

$$\mu = \int_0^\infty (1 - C^*)dt \qquad [4.6]$$

Here $C^*(t) = C(t)/C_w$ is the normalized concentration of the tracer monitored at the column outlet; C_w is the influent tracer concentration.

The retardation factor is obtained from the analysis of the effluent history of the tracers using equations 5 and 6 and the interfacial area is calculated by using equations 4.1 and 4.4.

MATERIALS AND METHODS

Materials Flow experiments were conducted in glass columns packed with cleaned glass beads (Potter Industries, Brownwood, TX). The glass beads were cleaned using 0.1 M HCl and 15% H_2O_2 in order to remove surface impurities such as metal ions and to oxidize the organic matter. The glass beads were then thoroughly washed with water to remove the residual acid and peroxide, and then oven-dried before storing them in a clean beaker for use in column experiments. The glass beads were made oil-wet using silane and chloroform following the procedure described in detail by Lewis (18).

Water was used as the aqueous phase and decane was the organic phase. Experiments were conducted with decane loaded in different ways (e.g. water loaded first vs decane loaded first) in columns packed with water-wet or oil-wet glass beads. Potassium iodide (KI), and pure 3-phenyl decyl benzene sulfonate (C_{10} 3-ϕ LAS), an anionic surfactant were used as conservative and interfacial tracers, respectively. C_{10} 3-ϕ LAS is a 10 carbon, linear alkyl benzenesulphonate, with the benzene ring at the third carbon position. All the chemicals used in this research were obtained from Aldrich chemical company, Milwaukee, WI, except the interfacial tracer. The surfactant tracer was purified in the chemistry department at the University of Texas at Austin. T-stilbene was the conservative organic phase soluble tracer. Based on the results of Saripalli et al. (6) and Kruger et al. (19), C_{10} 3-ϕ LAS used in this study should have very weak sorption on to the porous medium, be insoluble in the organic phase and also have no chromatographic separation.

Methods Aqueous solutions were prepared at different surfactant concentrations and the interfacial tension between the aqueous surfactant solutions and decane was measured using a ring tensiometer.

The column was a chromatography (Kontes, Vineland, NJ) glass column (diameter: 2.5 cm and length: 30 cm), fitted with PTFE shielded O-rings, metal screens, and a variable length teflon fitting at one end, which can be used to control the packed length of the column and has a single outlet for both the fluids exiting the column. Figure 4.1 shows the setup for the column experiments. The other end fitting was modified from one inlet to two inlets, to facilitate simultaneous flow of oil and water. A 100 mesh metal screen was present on each end of the column to prevent migration of fines and to distribute fluids evenly in the column.

The glass column was dry packed on a vibrating table. The column was packed in increments, so that the glass beads packed densely. A consistent porosity was achieved by this method. The column was then evacuated for 1 hour. It was then flooded with CO_2 gas and again evacuated for ½ hour and then saturated with deaerated and de-ionized water. Subsequently, the column was flushed with 2-3 pore volumes of deaerated water before the tracer experiments were conducted. The gross weight of the column without glass beads and the column with glass beads was measured. The dry weight of the beads packed in the

column was obtained from the difference in weight, which was used to obtain the overall porosity and pore volume of the column.

The permeability of the column to water was measured using pressure transducers (Cole Parmer, Vernon Hills, IL) connected to the inlet and outlet lines of the column. The electrical signal from the pressure transducer was converted into pressure and recorded on a chart recorder. Measurements were made at different flow rates (1-4ml/min) and the average permeability was computed.

The retardation factor was determined from effluent concentration histories (concentration of tracer exiting the column vs. time). The effluent concentrations were measured directly in a flow-through measurement cell plumbed into the experimental apparatus. This provides the requisite resolution for determining retardation of the concentration front and eliminates many of the data quality concerns that would arise if discrete samples were collected and then analyzed in batch mode. To eliminate the possibility of overlapping absorption peaks, the tracers were injected in separate slugs.

A step input of KI at a concentration of 25 mg/L (C_w) was initially injected until it was observed in the effluent. The flow-rate through the column was maintained at 1 ml/min during the tracer experiments. The tracer was followed by water and once no more KI was observed in the effluent, the column was flushed with another 2-3 pore volumes of water and the process was repeated with a step input of C_{10} 3-ϕ LAS at a concentration of 50 mg/L (C_w). The injected concentration was far below the CMC of the surfactant (600 ppm). Because of the low injection concentration of the tracer, we did not anticipate nor did we observe any mobilization or solubilization of the oil, which would have changed the interfacial area as the tracer was injected in the column. The effluent was analyzed using an online UV detector (Ocean Optics, Model: CHEM2000-UV-VIS) for continuous detection of KI (wavelength: 221 nm) or LAS (wavelength: 217 nm). Each data point (concentration in effluent at a given time) was the average of 25 scans of the contents of the in-line sample cuvette (Hellma Scientific, 18 μl volume), taken over a 0.04 minute interval. The scanning and averaging were carried out automatically by the spectrophotometer system that includes a data acquisition card and software. Data were logged directly to a PC.

A calibration curve was prepared for each tracer that relates measured absorbance to known tracer concentration. The response was almost perfectly linear. Measurements in the

range of interest, i.e. greater than 1% of the injected concentration, show high accuracy. The calibration curve was used to obtain the effluent concentration profile.

Initial tracer tests were conducted to calculate the background sorption of interfacial tracer onto the glass beads. Decane being lighter than water was introduced into the column from the top. A connate water saturation of about 30% was obtained. Subsequently, the column was flushed with 4-5 pore volumes of water from the bottom at increasing flow rates (1ml/min-4ml/min) to reduce the column to a residual decane saturation. After establishing residual decane saturation, the tracer experiments were conducted following the procedure described above.

Next, the decane saturation in the column was increased by flowing decane through the column, while reducing the water flow rate, keeping the total flow rate through the column constant at 1ml/min. At each fractional flowrate, water and decane were simultaneously injected into the column for 35-40 pore volumes to achieve steady state saturations in the column. The permeability to liquid phases was measured at each stage, followed by the tracer experiments. Water saturation at each fractional flowrate was obtained from the conservative tracer profile, and retardation of the interfacial tracer was calculated relative to the conservative tracer. The residual water saturation was obtained by using T-stilbene as the conservative tracer in oil. At this point water is present as residual phase in the column. The following fractional flows of water were used in the experiments: f_w = 1, 0.75, 0.50, 0.25, 0. When both phases were simultaneously flowing through the glass beads, slugs of decane and water formed in the effluent line (slug size depending upon the f_w) and subsequently passed through the UV measurement cell, Figure 4.1. The detector gives a signal when the cell was filled with tracer solution (size of the signal depending upon the concentration) and a significantly high detector signal was observed when it was filled with decane. The high frequency of data accumulation helps in creating an effluent history, even after eliminating the decane data points at different times, without losing consistency.

RESULTS AND DISCUSSION

Interfacial tension measurements The interfacial tension (IFT) between decane and different concentrations of C_{10} 3-ϕ LAS surfactant was measured using a ring tensiometer.

As shown in Figure 4.2, the IFT decreases with increase in surfactant concentration. The slope (β) is required to calculate K_o as shown in equation 4.6. β was obtained by fitting the interfacial tension data (Figure 4.2) and K_o has a value of 8.16 times 10^{-4} times a_i for a 50mg/L injection concentration of the C_{10} 3-ϕ LAS tracer in the column experiments.

Retardation measurements A typical effluent history as a function of pore volumes injected (dimensionless time) is shown in Figure 4.3. As the figure shows, there was a small retardation of C_{10} 3-ϕ LAS tracer as compared to the conservative KI tracer. Hence sorption of LAS onto the porous medium, although small, can not be completely neglected in calculating the retardation factor and the interfacial area. Similar initial sorption experiments conducted with silanized glass beads show that the tracer absorbed to a small extent onto the glass beads, which does not have a major impact on the tracer profile.

Repeated injections of tracers (KI and C_{10} 3-ϕ LAS) were conducted in water saturated columns to establish the accuracy and repeatability of the effluent history. Injected concentrations of the tracers used ranged from 25 to 50 mg/l. The standard deviation of the replicate analysis of tracer concentration was of the order 10^{-3} mg/l, so that the method detection limit was of the order 10^{-4} mg/l. The precision of concentration measurements obtained from the UV spectrophotometer was better than 1%. Two sets of replicate analyses on each of the two tracers (KI and LAS) were conducted. The results of the replicate effluent histories and batch studies show good reproducibility of the data and the high accuracy of the detectors. The retardation factor R_{ift}, was obtained by analyzing the effluent concentration profile of the tracers. Calculations showed that the arrival time of dimensionless concentration 0.5 in the effluent provides a convenient approximation to the moment defined in Equation 4.6. This approximation typically introduces less than 1% error due to the symmetry of the effluent concentration history and the high frequency of sampling (one measurement every 0.05 seconds).

Repeat injections of C_{10} 3-ϕ LAS tracer were conducted in columns at residual decane saturation to observe the impact of flow stoppage and flowrate. Results indicate that the changes in flowrate (reduction from 1ml/min to 0.25 ml/min) and flow stoppage (15 hrs) had no impact on the effluent history. Thus, mass transfer limitations are not governing the sorption of surfactant.

Figure 4.3 also highlights the impact of residual decane on the retardation of LAS in a glass column. The presence of residual decane saturation results in KI tracer breakthrough before 1 pore volume (earlier than in a water saturated column). The C_{10} 3-ϕ LAS profile is delayed relative to the KI profile, due to the sorption of surfactant onto the porous medium and also at the water-decane interface. Equation 4.1, which includes sorption of tracer onto the porous medium, was used to calculate the interfacial area between the water and decane in all the experiments.

Table 4.1 shows the experimental conditions for the four main experiments for which results are presented in this paper. Experiments ww1 and ww2 were conducted using water-wet glass beads, while in experiments ow3 and ow4, oil-wet beads were used. The glass beads were made oil-wet using the silanation method described earlier. In the ww1 experiment the interfacial area was measured at a succession of steady states during primary drainage (ww1a). In primary drainage the non-wetting phase displaces the wetting phase from a porous medium initially completely saturated with wetting phase. The fractional flow of water was decreased in steps and the interfacial area measured at each of 4 fractional flows during the primary drainage. Oil-water interfacial areas were also subsequently measured, during secondary imbibition (ww1b) and secondary drainage (ww1c). (Secondary imbibition refers to displacement of nonwetting phase by wetting phase from a medium initially at residual wetting phase saturation. In water wet glass beads, water is the wetting phase and decane is the non-wetting phase and vice versa in oil-wet glass beads. During secondary drainage, non-wetting phase displaces the wetting phase from a medium initially at residual nonwetting phase saturation.) In the ww2 experiment the column was reduced to residual decane saturation and the specific interfacial area was measured during secondary drainage, i.e. the water flowrate was decreased and decane flowrate increased, until residual water saturation was achieved. However, unlike the other experiments, the liquids were injected from bottom up, thus creating an unstable displacement process. Experiments ow3 and ow4 were conducted with oil-wet beads. In experiment ow3, interfacial area was measured during primary drainage, where water displaced decane. Experiment ow4 is similar to ww1b; however, the non-wetting phase (water) was first loaded into the column, and the interfacial area was measured during the imbibition cycle.

Figure 4.4 compares the changes in interfacial area measured during primary drainage in columns packed with 400 μm water-wet (ww1a) and oil-wet glass beads (ow3). There are significant differences in the two curves. In experiment ww1a, reducing the water fractional flow through the column decreases the water saturation in the column. As the figure shows, a decrease in water saturation leads to a monotonic increase in the interfacial area. The total interfacial area calculated and measured here evidently includes contributions from the thin water films covering the glass beads. This result is consistent with changes in air-water interfacial area observed in other studies (13, 15-16).

However, the interfacial area measured during primary drainage in oil-wet beads shows significant differences from the water-wet curve. In the early stages the behavior is similar. The area increases from 50 cm^2/cm^3 to 95 cm^2/cm^3 with an increase in water (non-wetting phase) saturation from 10% to 25%. However, unlike for water-wet beads, as drainage continues the interfacial area reaches a maximum and then declines, reaching 45 cm^2/cm^3 at the residual decane saturation (28%). This result suggests that the tracer does not see the decane films or that such films are not sustained over the glass beads as the decane saturation decreases. There are no reported literature values to compare our results of interfacial area for an oil-wet medium. The observed maximum in area is however consistent with theoretical predictions which do not include thin films (9, 20-21).

The differences in the two cases can also be explained by comparing the morphology of the phases in the porous medium. Consider the drainage endpoint, when the trapped wetting phase exists as pendular rings at grain contacts, as lenses in pore throats, and/or as islands (connected volumes spanning one or more pores). A pendular ring at a contact between two spheres of radius R contributes an area of 18 to 20 R^2 per unit ring volume (22). Similarly, a lens contributes an area of about 5 R^2 per unit lens volume. Islands contribute of order 1 R^2 per unit phase volume (21). In our bead packs R = 200 μm and porosity is 0.40. If all the irreducible wetting phase saturation (S_{wr} = 0.27) exists as pendular rings, then we would expect an interfacial area $a_{nw} = 20\frac{R^2}{R^3 ring} \times 0.25\frac{R^3 ring}{R^3 PV} \times 0.40\frac{R^3 PV}{R^3 Bulk} \times \frac{1R}{0.02cm} = 100\frac{cm^2}{cm^3}$. This is comparable to the surface area of the beads, i.e. $\frac{3(1-\phi)}{R} = \frac{3 \times 0.6}{0.02cm} = 90\frac{cm^2}{cm^3}$. At higher wetting phase

saturations, when more of the wetting phase is connected, we would expect smaller areas. In contrast, the measured area at a wetting phase saturation of 0.40, when the water fractional flow is 0.25, is 200 cm^2/cm^3. We conclude that the wetting film on the surface of drained pores contributes to the measured area. Evidently such films of water can accommodate the hydrophilic end of the tracer molecules in sufficient numbers to influence the retardation.

This hypothesis is reinforced by the measurements made during drainage in the oil-wet bead pack. A decane film is unlikely to be able to accommodate the 10-to-12 carbon alkyl group of the tracer molecule in large numbers, and thus we expect little retardation due to sorption at this interface. Moreover, a hypothetical distribution of the irreducible wetting phase saturation (S_{wr} =0.27) into equal volumes of pendular rings, lenses and larger islands of connected decane would yield an interfacial area contributions of 36, 9, and 2, respectively, in units of cm^2/cm^3 bulk. The sum of these contributions is close to the measured value. Thus the wetted bead surface does not appear to contribute significantly to the measured area in the oil-wet experiments.

The implication of these results is that the area of wetting films on surfaces of drained pores can be much larger than the area of the interface between macroscopic phase volumes. If the film contribution is included in the measurement, it can lead to substantial errors in interpreting mass transfer data, for example. Most measurement techniques, or at least their common application in water-wet systems, include the film contribution (21).

The relative permeability measured during primary drainage in these experiments is shown in Figure 4.5 and the values are given in Table 4.2. In the experiment ww1a the water relative permeability decreases gradually, while the decane relative permeability increases, with decreasing wetting phase saturation. The wetting phase (decane) relative permeability decreases sharply in experiment ow3, as compared to that in ww1a, where water is the wetting phase. The nonwetting phase relative permeability increases similarly in both the experiments (ww1a and ow3). The presence of films and changes in interfacial area impacts the relative permeability.

The interfacial area measured during secondary imbibition in columns packed with water-wet (ww1b) and oil-wet (ow4) glass beads is given in Figure 4.6. During secondary imbibition, the behavior of the water-wet bead pack is qualitatively very similar to the drainage curve, Figure 4.4. In the experiment, ww1b, the interfacial area decreases with

increasing wetting phase saturation. This is consistent with the area being dominated by the contribution of wetting films, which necessarily decreases as the wetting phase saturation increases. Also, the wetting phase is present in high surface area morphologies (pendular rings at grain contacts, lenses in pore throats) at the beginning of the imbibition, and those volumes are reconnected to the bulk wetting phase (which has a much lower area/volume ratio) during imbibition. The area at water fractional flow of 0.25 is 200 cm^2/cm^3, similar to the value obtained at the same fractional flow rate during drainage. Tracer transport is thus influenced by wetting films as well as by rings, lenses and islands of wetting phase.

The imbibition curve observed in experiment ww1b is different from the results of Schaefer et al. (15) who report that as imbibition begins after drainage, interfacial area decreased rapidly, then stayed constant till a saturation of 0.5, then increased to a maximum near S_w = 0.65 before gradually declining again. This result is also different from the water-decane interfacial area observed here and shown in Figure 4.6. In contrast, the area measured during imbibition in the oil-wet bead pack increases monotonically.

For the water-wet experiment, the initial value (50 cm^2/cm^3) is quite close to the drainage endpoint value, Figure 4.4. The area at a fractional flow of water of 0.75 is 100 cm^2/cm^3, similar to the value obtained during drainage at the same fractional flow. But at smaller fractional flows of water, the area continues to increase, rather than decrease as it did during drainage. A contribution from wetting films would account for the magnitude of the area measured at residual nonwetting phase saturation in Figure 4.6. No such contributions were evident either at the beginning of secondary imbibition or during the drainage experiment. The reason for this hysteresis remains unclear and will be the subject of further investigation.

Figures 4.7 shows the changes in water-decane interfacial area as a function of saturation in columns packed with water-wet glass beads measured during different cycles. This figure highlights the impact of hysteresis observed in capillary pressure curves and interfacial area as a function of saturation. The total interfacial area measured during primary imbibition (ww1b) shows hysteresis effects. The water saturation is lower during the imbibition process than drainage at the same capillary pressure. Therefore, due to the presence of trapped decane and the lower water saturation, the interfacial area measured during imbibition (ww1b) is higher than that measured during drainage (ww1a). The figure also shows that the interfacial area measured during secondary drainage (ww1c) is higher

than measured during primary drainage. During primary drainage there is no trapped non-wetting phase, however during subsequent cycles the non-wetting phase is present as trapped ganglia. These ganglia increase the total interfacial area as observed in Figure 4.7. These results agree well with the pore scale network modeling done by Reeves and Celia (9) and Held and Celia (23).

Figure 4.8 compares changes in interfacial area and residual decane saturation as a function of grain size. The residual decane saturation decreases with increasing grain size, which leads to a decrease in the specific interfacial area. The water-decane interfacial area for 3-mm glass beads is 22 cm^2/cm^3 as compared to 50 cm^2/cm^3 for 0.4-mm glass beads. This is very much expected as the specific solid surface area increases with decrease in grain size, which also leads to an increase in the specific liquid-liquid interfacial area. Film area is at a minimum at residual decane saturation. Faisal et al. (16) observed similar results in their air-water experiments with glass beads ranging from 0.25mm to 0.75mm diameter.

Figure 4.9 compares gravity stable (ww1c) and unstable (ww2) displacements and the impact on interfacial area. In experiment ww2, water and decane were injected from the bottom of the column in the upward direction. However, decane being lighter than water creates an unstable displacement front, which results in fingering along preferential flow paths. A large amount of water is left bypassed by decane. Figure 4.9 shows that decreasing the water saturation from 82% to 61% increases the interfacial area from 50 cm^2/cm^3 to 190 cm^2/cm^3. A comparison of results (ww1c vs ww2) shows that in experiment ww2, higher water saturations were achieved at the same fractional flow rates. However, similar results for interfacial areas were obtained in both experiments. This shows that fingering and an unstable drainage process results in higher water saturations at the same fractional flow. This leads to a higher saturation of trapped and disconnected i.e. an increase in the total interfacial area.

These results show the range of interfacial areas that could be expected for different saturations and wettability. The research forms the basis for developing a process whereby liquid-liquid interfacial area could be measured where both the phases are flowing and saturation is controlled by the fractional flow rate. The application of these data will serve as a baseline for future work on more heterogeneous porous media, notably soils/rocks with a wider distribution of grain sizes. These data can be compared with pore-scale model

predictions. The resulting data can be used to characterize the constitutive relationships between a_i, S_w and relative permeability and to verify and advance the mathematical models. Interphase mass transfer rates are proportional to liquid-liquid interfacial area. Our results show that wettability significantly impacts the value of area inferred from interfacial tracer experiments and its dependence on saturation. In a water-wet medium, the interfacial tracer technique included the contribution of water films on the glass beads; the resulting trend in area as a function of saturation can be explained by the morphology of the wetting phase. However, during primary drainage in an oil-wet medium, the area inferred from the interfacial tracer technique exhibited a clear maximum at intermediate saturation. This observation is consistent with theoretical predictions that do not include the film of wetting phase on the beads, but the reason for difference in behavior from the water-wet system is unclear. Similarly difficulties arise in interpreting the trend in areas measured during imbibition. Hence in order to estimate the mass transfer rates, its important to understand the history (wettability, saturation, flow of fluids through the porous media etc) of the system, and further research is needed to account for the transport of interfacial tracers in such systems.

ACKNOWLEDGEMENTS

Funding for this work was provided by the Department of Energy under grant DE-AC26-98BC15205 for the project “Characterization of Mixed Wettability at Different Scales and Its Impact on Oil Recovery Efficiency”. Additional support was provided by EPA (R827116/01/0) and with funds from the State of Texas as part of the program of the Texas Hazardous Waste Research Center (THWRC, 069UTA0803). This paper has not been subject to agency review and therefore does not necessarily reflect the views of the sponsoring agency, and no official endorsement should be inferred.

REFERENCES

1. Miller, C. T., Poirer-McNeill, M. M., Mayer, A. S., *Water Resources Research*, **1990**, 26, 2783-2796.
2. Wan, J., Wilson, J. L., *Water Resources Research*, **1994**, 30, 857-864.

3. Alpak, F. O., Lake, L. W., Embid. S. M., presented at *SPE Annual Technical Conference and Exhibition: 'Reservoir Engineering'*, Oct 3-Oct 6 **1999**, Houston, TX, USA, 193-203.
4. Bradford, S. A., Leij, F. J., *Journal of Contaminant Hydrology*, **1997**, 27, 83-105.
5. Johns, M. L., Gladden, L. F., *Journal of Colloid and Interface Science*, **1999**, 210, 261-270.
6. Saripalli, K. P., Kim, H., Rao, P. S. C., Annable, M. D., *Environmental Science and Technology*, **1997**, 31(3), 932-935.
7. Powers, S. E., Loureiro, C. O., Abriloa, L. M., Walter, W. J., Jr., *Water Resources Research*, **1991**, v. 27, no. 4, 463.
8. Gvirtzman, H. Roberts, P. V., *Water Resources Research*, **1991**, 27, 1165-1176.
9. Reeves, P. C., Celia, M. A., *Water Research Resources*, **1996**, 32 (8), 2345-2358.
10. Cary, J. W., *Journal of Contaminant Hydrology*, **1994**, 15, 243-248.
11. Morrow, N, *Industrial and Engineering Chemistry*, **1970**, 62, 32-56.
12. Karkare, M. V., Fort, T., *Langmuir*, **1996**, 12, 2041-2044.
13. Kim, H., Rao, P. S. C., Annable, M. D., *Water Resources Research*, **1997**, 33(12), 2705-2711.
14. Annable, M. D., Jawitz, J. W., Rao, P. S. C., Rai, D. P., Kim, H., Wood, A. L., *Ground Water*, **1998**, 36(3), 495-502.
15. Schaefer, C. E., Dicarlo, D. A., Roberts, P. V., Blunt, M. J., American Society of Mechanical Engineers, *Heat Transfer Division, (Publication) Heat Transfer Division - 1999 (The ASME International Mechanical Engineering Congress and Exposition)* Nov 14-Nov 19, **1999**, v364-2, Nashville, TN, USA, Sponsored by: ASME, ASME Fairfield, NJ, 93-97.
16. Faisal Anwar, A. H. M., Bettahar, M., Matsubayashi, U. *Journal of Contaminant Hydrology*, **2000**, 43, 129-146.
17. Kim, H., Rao, S. C., Annable, M. D., *Soil Science Society American Journal*, **1999**, 63, 1554-1560.
18. Lewis, M. G., Masters Thesis, Department of Petroleum and Geosystems Engineering, The University of Texas at Austin, **1988**.
19. Kruger, C. J., Barber, L. B., Metge, D. W., Field, J. A., *Environmental Science and Technology*, **1998**, 32(8), 1134-1142.

20. Berkowitz, B., Hansen, D. *Transport in Porous Media*, **2001**, 45, 303-319.
21. Bryant, S., Johnson, A., In *Chemicals in the Environment: Fate, Impacts, and Remediation, ACS Symposium Series v.* 806, Robert L. Lipnick, Robert P. Mason, Margaret L. Phillips and Charles U. Pittman Jr., eds., **2001**, 26-41.
22. Johnson, A., MS Thesis, Dept. of Chemical Engineering, The University of Texas at Austin, **2001**.
23. Held, R. J., Celia, M. A., *Advances in Water Resources*, **2001**, 24, 325-343.

Experiment name	Type of porous media	Phase first loaded	Measurement of interfacial area
ww1a	Water-wet	water	Prim. drainage
ww1b	Water-wet	water	Prim. imbibition
ww1c	Water-wet	water	Sec. drainage
ww2	Water-wet	water	Sec. Drainage (bottom loading)
ow3	Oil-wet	oil	Prim. drainage
ow4	Oil-wet	water	Sec. imbibition

Table 4.1: Conditions of column experiments

Experiment name	Porosity	Saturated permeability, 10^{-5}, cm^2	Pore volume	Swr	Sor
ww1a	0.35	4.29	39.5	25%	-
ww1b	0.35	4.29	39.5	25%	22%
ww1c	0.35	4.29	39.5	23%	22%
ww2	0.346	4.95	41	60%	18%
ow3	0.367	5.22	40.5	-	30%
ow4	0.36	3.34	40.6	22%	28%

Table 4.2: Results from column experiments

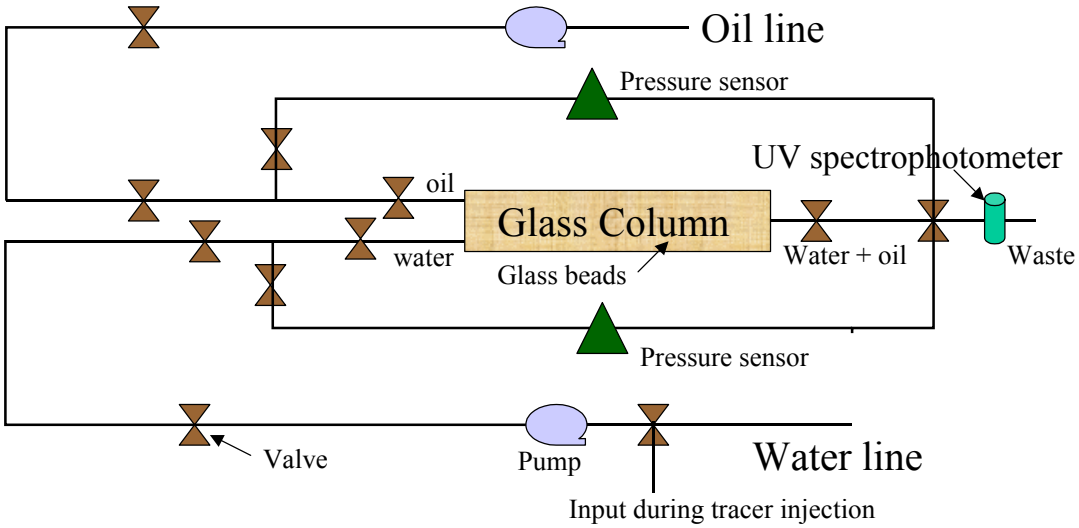

Figure 4.1 Experimental setup for column experiments.

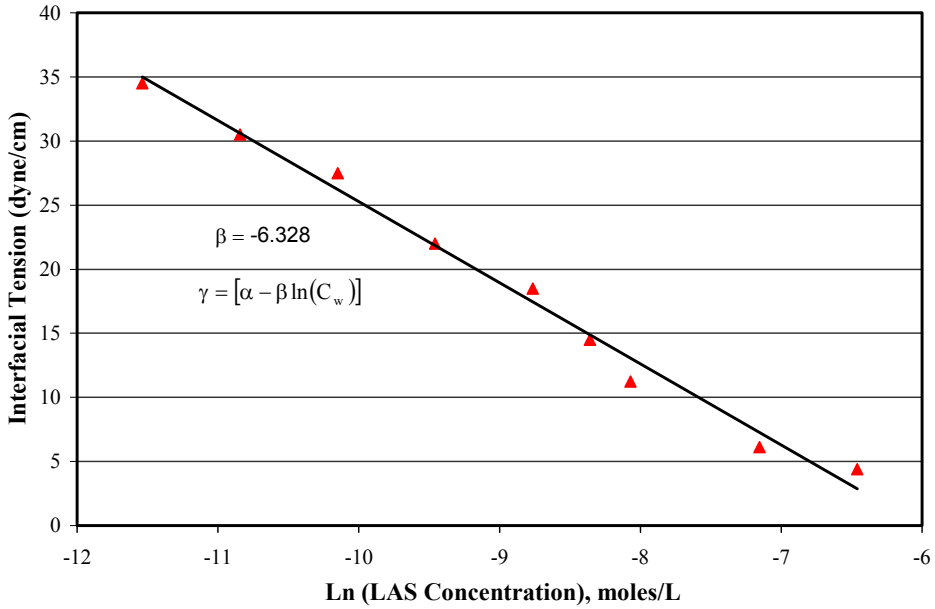

Figure 4.2 Interfacial tension plotted against Ln concentration to obtain the adsorption coefficient.

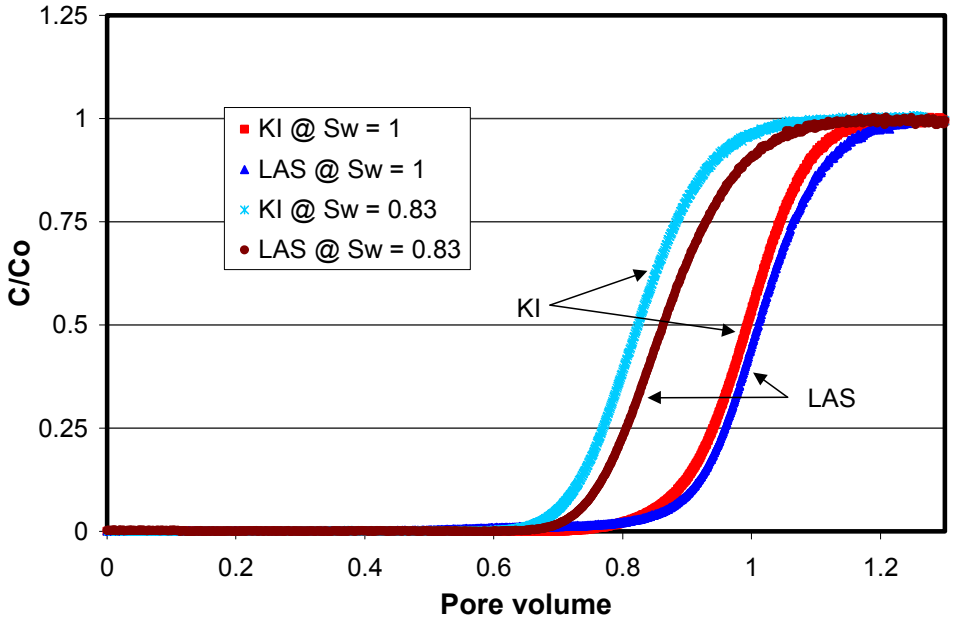

Figure 4.3 Comparison of effluent profile of LAS surfactant and KI showing the impact of residual decane in a column packed with water-wet glass beads.

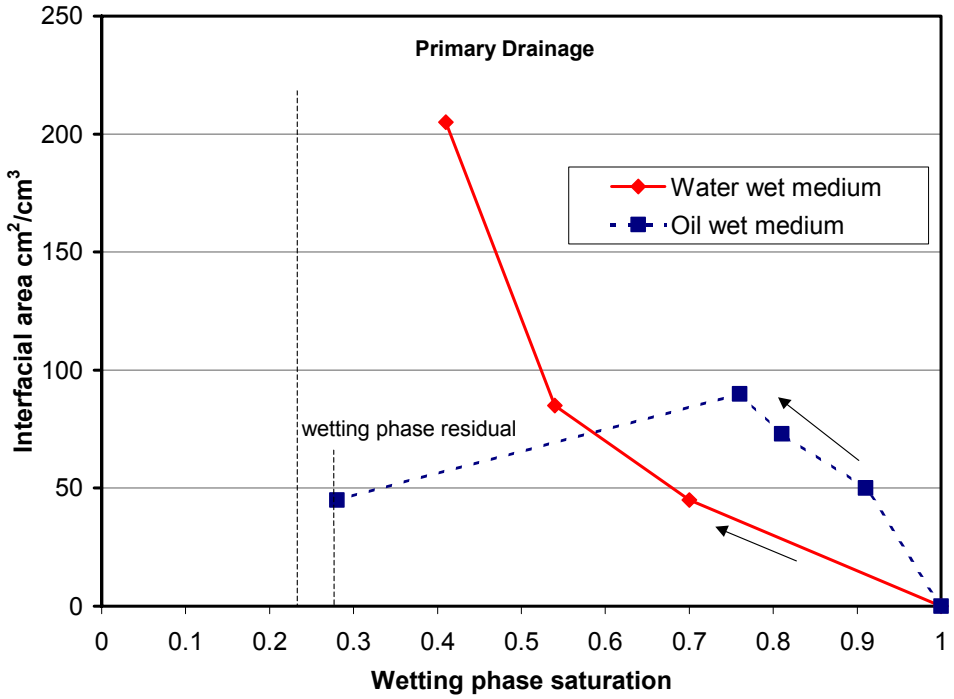

Figure 4.4 Change in interfacial area between water and decane as a function of wetting phase saturation in columns packed with water-wet (ww1a) and oil-wet (ow3) glass beads, measured during primary drainage.

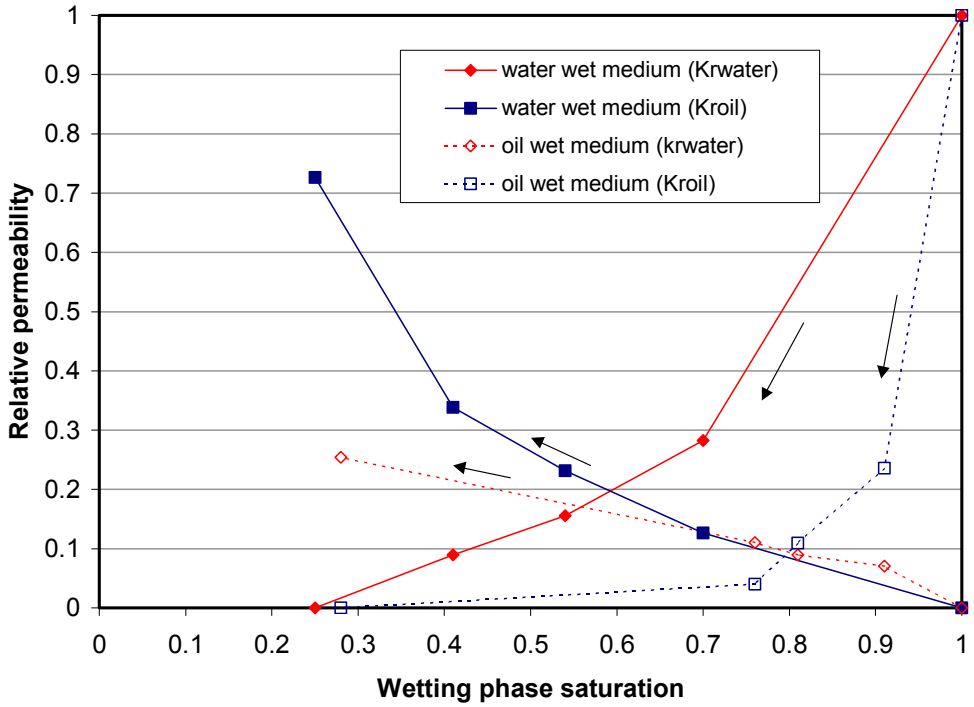

Figure 4.5 Comparison of relative permeability measured during primary drainage in columns packed with water-wet (ww1a) and oil-wet (ow3) glass beads.

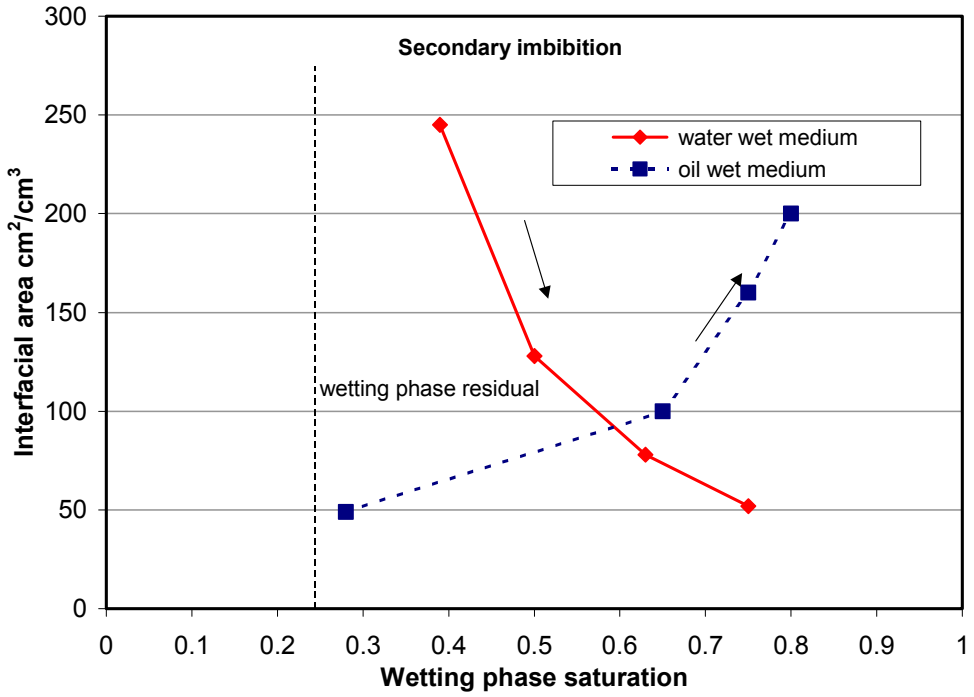

Figure 4.6 Change in interfacial area between water and decane as a function of saturation in columns packed with water-wet (ww1b) and oil-wet (ow4) glass beads, measured during secondary drainage.

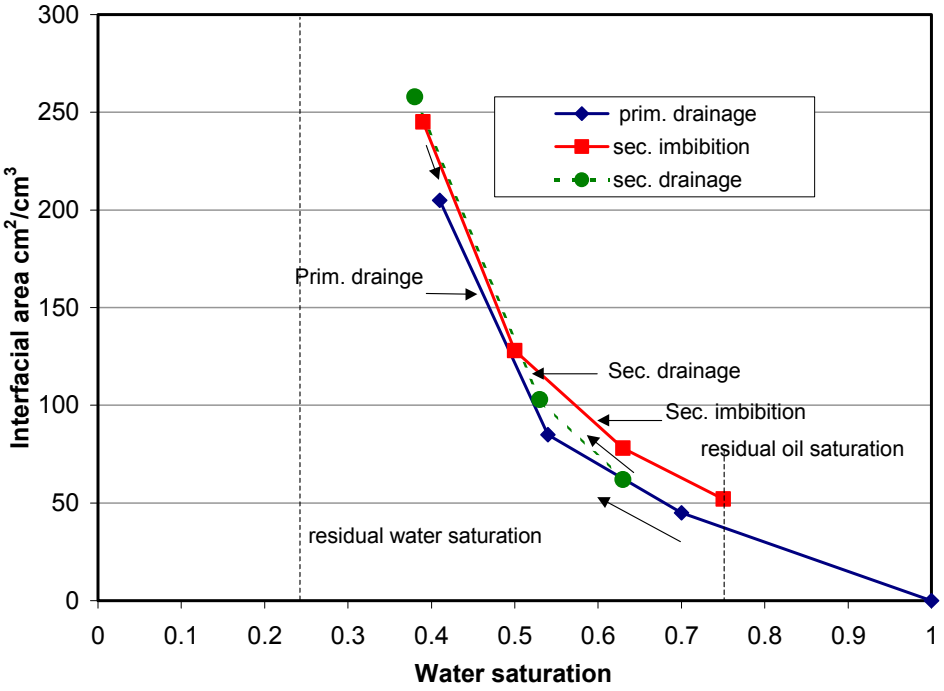

Figure 4.7 Change in interfacial area between water and decane as a function of saturation in column packed with water-wet (ww1) glass beads, measured during different cycles.

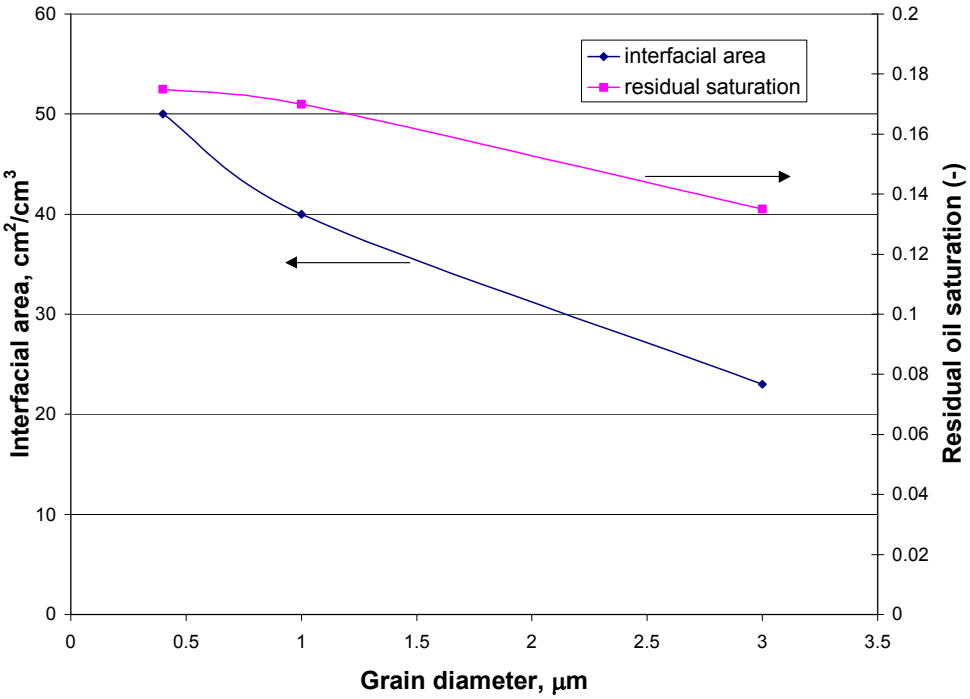

Figure 4.8 Change in interfacial area between water and decane at residual decane saturation as a function of glass bead size.

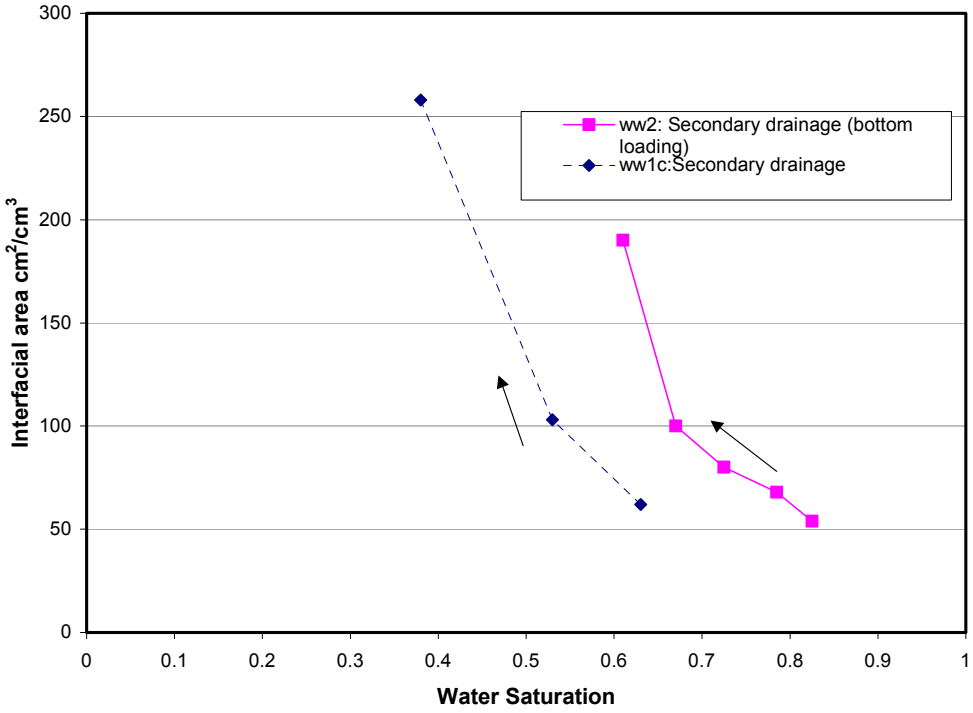

Figure 4.9 Comparison of interfacial area measured during secondary drainage in columns packed with water-wet glass beads, highlighting the impact of unstable loading of fluids in the column.

5. Experimental and Theoretical Basis for a Wettability-Interfacial Area-Relative Permeability Relationship

Mikhail Gladkikh, Vivek Jain, Steven Bryant, and Mukul Sharma,

SPE 84544 presented at the SPE Annual Technical Conference and Exhibition held in Denver, Colorado, U.S.A., 5 – 8 October 2003.

ABSTRACT

Using an interfacial tracer technique, our experiments show qualitatively different trends of total interfacial area between the wetting and non-wetting phases as a function of saturation, depending on whether the system is strongly or weakly wetted. A strongly wetted system is defined as one in which the wetting phase can spread as a thin film on the solid surface. We assess the relative contributions of fluid/fluid and fluid/solid interfaces to the total area using thermodynamic arguments. The fluid/solid contribution to area plays a crucial role in explaining the measurements.

The influence of interfacial area on relative permeability is not straightforward. Simple analysis based upon pore-level distribution of phases in a model porous medium allows quantifying the differences in the relative permeabilities for both weakly and strongly wetted systems, measured simultaneously with the interfacial area. Relative permeability correlates with fluid/solid area but not with fluid/fluid interfacial area.

INTRODUCTION

Relative permeability is a measure of the ability of the porous medium to conduct fluid flow when multiple fluid phases are present. It is intuitively clear that the relative permeability to a phase should increase as the phase saturation increases, and experiments have validated this expectation. Consequently it is routine to parameterize relative permeabilities only in terms of fluid saturations. Yet a first-principles analysis[1] as well as a long history of experimental work both teach that relative permeability is more complicated property, the composite effect of pore geometry, wettability, fluid distribution, saturation history, and contact areas (fluid-fluid interfacial area and solid-fluid area).

Evaluation of the influence of contact areas and wettability on relative permeability, e.g. by Alpak *et al.*[2], has been hindered by the lack of independent measurements of areas between phases in a porous medium. In this paper we present the results of such measurements in strongly wetted and weakly wetted systems and interpret the data in terms of a simple thermodynamics analysis.

Many results presented in the literature have established the connection between the wettability of the system (expressed usually in terms of contact angle) and relative permeabilities. To our knowledge, very little work has been done to investigate the relationship between wettability, interfacial area and two-phase relative permeability.

THERMODYNAMIC ANALYSIS OF INTERFACIAL AREA

The behavior of the interfacial area between phases during drainage/imbibition experiments depends upon the wettability of the system. Wetting phase will spread over the grain surface, if the following condition holds:

$$\gamma_{WS} + \gamma - \gamma_{NS} < 0 \quad \text{or} \quad S = \frac{\gamma_{WS} + \gamma}{\gamma_{NS}} < 1 \qquad \text{.....(1)}$$

where γ_{WS}, γ_{NS} and γ are the interfacial tensions between wetting phase/solid grain, nonwetting phase/solid grain and wetting/nonwetting phases. The fraction in Eq. 1 is called the spreading coefficient S. If $S<1$, wetting phase will form thin films on the surface of solid grains. For the case $S>1$ wetting phase will remain at grain surfaces in the form of drops, and a contact angle can be defined as follows:

$$\cos\theta = \frac{\gamma_{NS} - \gamma_{WS}}{\gamma} \qquad \text{.....(2)}$$

Simple thermodynamic analysis for the free energy of the system during drainage or imbibition[3,4] demands qualitatively different behavior of W-NW interfacial area for the strongly and weakly wetted systems. In a strongly wetted system, W spreads and thin films are present. In a weakly wetted system, W phase is in the form of drops. Schematic trends of qualitative behavior of the interfacial area at different conditions are shown on **Figures 1 – 4**. In these figures A_g is the total surface area of the grains; A_{total} is the total interfacial area (including contributions from thin films, if they exist); A_{film} is the area of thin films alone; and A is the area of bulk interfaces. There are two important points in the analysis. First, for

the strongly wetted system two types of fluid-fluid interface contribute to the interfacial area: bulk interface between phases, and thin films. For the case of a weakly wetted system there are no films. Thus qualitatively different behavior arises in the trends of interfacial areas: compare A_{total} on Figs 1 and 2 and A on Figs 3 and 4. Secondly, the interfacial area cannot exceed total grain area. This fact can be used to gauge the accuracy of the method of measuring interfacial areas, though unfortunately the total grain area itself can be very hard to measure and quantify.

Influence of Wettability

According to conventional wisdom, oil wet rocks exhibit higher values of relative permeability to water, and water wet rocks exhibit higher oil relative permeability. This is because NW phase tends to occupy larger pores, so that at the same water saturation relative permeability to water is larger when it is NW phase. The usual behavior of the relative permeabilities as functions of water saturation for strongly wetted systems (zero contact angle) in oil wet and water wet cases is shown on **Figure 5**. The relative positions of the crossover points ($k_{r,oil} = k_{r,water}$) for each case in Fig 5 are the consequence of NW phase occupying larger pores. But this shift in crossover point disappears when relative permeabilities are plotted against W phase saturation. The different values of oil saturation when relative permeability to it is zero should be readily identified with residual NW phase saturation in the case of water wet system and irreducible W phase saturation for the case of oil wet; that is why the second is usually smaller.

So, this common explanation of the influence of wettability on relative permeabilities has nothing to do with the analysis presented in this paper, and represents just another way of data interpretation. All else being equal, strongly wetted systems should exhibit the same relative permeability curves when plotted vs. wetting phase saturation.

The wettability (value of contact angle) affects the form of pendular rings and menisci and so influences the critical curvatures (curvature of the meniscus when it just moves into or out of a pore) for both drainage and imbibition. This effect shifts the capillary pressure – saturation curve, but does not affect the dependence of relative permeability on W phase saturation. The differences in the values of interfacial tensions also do not affect fluid flow (and so, relative permeabilities). Rather, relative permeability to W phase depends on

the fraction of pores and pore throats completely filled with W phase. Relative permeability to NW phase depends on (1) the fraction of pores/pore throats that contain NW phase and (2) the sizes of parts of pore throats available for NW phase flow. The latter are complicated by the fact that W phase forms pendular rings at grain contacts, thus restricting the size of the pore throat, as illustrated in **Figure 6**.

Strongly Wetted vs. Weakly Wetted Systems

We define strongly wetted systems as ones in which the spreading coefficient *S* for the solid surface is less than unity. The main difference between strongly wetted and weakly wetted systems is that in the former, the W phase remains connected at any saturation and capillary pressure. At small saturations this hydraulic connectivity is provided by the presence of thin films. In principle, such a system can be driven to as low a value of W saturation as desired. Because the bulk W phase, which at small saturations exists in the form of pendular rings around grain contacts, remains connected by the films, these rings can diminish indefinitely as the capillary pressure is increased. The contribution of thin films to flow is small because their thickness may only be a few molecular diameters. The presence of films thus does not significantly affect relative permeability curves. In weakly wetted systems, the W phase loses its bulk connectivity and can be trapped as rings and other morphologies[7]. This trapping leads to the irreducible W phase saturation.

The above suggests that the wettability (strong vs. weak, or equivalently the presence vs. absence of W phase films) affects relative permeability only when the growth/shrinkage of pendular rings is significant. This is the case at small W phase saturations. For high W phase saturations, most pendular rings are in direct contact with the W phase in neighboring pores. Thus even in the absence of thin films their form adjusts to the current capillary pressure. In effect, then, there is no difference between the strongly and weakly wet situations at high W saturation.

The qualitative behavior of the relative permeability curves, based upon the above considerations, is shown on **Figure 7** for primary drainage. The differences in wettability do not have a significant impact on relative permeability curves at high W phase saturations. Differences arise when pendular rings and lenses of W phase become trapped in the weakly wetted system. A trapped ring does not shrink as capillary pressure increases and therefore

contains more W phase than a ring in a strongly wetted medium. At a given saturation, therefore, more of the W phase volume in a strongly wetted medium exists as pores completely filled with W phase. The smaller size of pendular rings in a strongly wetted system also implies larger cross-sectional areas in the pore throats available for the flow of NW phase. This yields higher relative permeability for the W phase in strongly wetted systems. We hypothesize that this is the primary influence on the NW phase relative permeability.

The strongly wetted system also has a lower irreducible W phase saturation (which ideally can go to zero as the capillary pressure goes to infinity) and higher relative permeability to NW phase in this irreducible state. This is because of the same effect as was considered above: pendular rings are all hydraulically connected and their volume can be reduced (which decreases irreducible saturation), which, in turn, increases pore throat constrictions, available for the flow of NW phase.

For the case of imbibition, **Figure 8**, the above arguments are still valid, only now, pendular rings grow in the strongly wetted system. The rings remain smaller than their counterparts in a weakly wetted system until the capillary pressure reaches the value at which the rings were trapped in the weakly wetted system. This again suggests larger values of relative permeabilities to both W and NW phases at low W phase saturations. At higher W saturations all trapped pendular rings regain connectivity. This restores hydraulic conductivity to the W phase in a weakly wetted system. All pendular rings now adjust their sizes to the current capillary pressure, and thus the difference between strongly/weakly wetted systems disappears.

Experiments - Materials and Methods

The above analysis of the behavior of interfacial area and qualitative predictions of relative permeabilities in strongly/weakly wetted systems now allows us to interpret results of experiments in which interfacial area and relative permeabilities are measured simultaneously on samples of different wettability.

Flow experiments were conducted in glass columns packed with cleaned glass beads (Potter Industries, Brownwood, TX). The glass beads were cleaned using 0.1M HCl and 15% H_2O_2 in order to remove surface impurities such as metal ions and to oxidize the organic

matter. The glass beads were then thoroughly washed with water to remove the residual acid and peroxide, and then oven-dried before storing them in a clean beaker for use in column experiments. The glass beads were made oil-wet using silane and chloroform following the procedure described in detail by Lewis[8].

Water was used as the aqueous phase and decane was the organic phase. Experiments were conducted with decane loaded in different ways (e.g. water loaded first vs decane loaded first) in columns packed with water-wet or oil-wet glass beads. Potassium iodide (KI), and pure 3-phenyl decyl benzene sulfonate (C_{10} 3-ϕ LAS), an anionic surfactant were used as conservative and interfacial tracers, respectively for measuring interfacial area. C_{10} 3-ϕ LAS is a 10-carbon, linear alkyl benzenesulphonate, with the benzene ring at the third carbon position. All the chemicals used in this research were obtained from Aldrich chemical company, Milwaukee, WI, except the interfacial tracer. The surfactant tracer was purified in the chemistry department at the University of Texas at Austin. T-stilbene was the conservative organic phase soluble tracer.

The column was a chromatography (Kontes, Vineland, NJ) glass column (diameter: 2.5 cm and length: 30 cm), fitted with PTFE shielded O-rings, metal screens, and a variable length teflon fitting at one end, which can be used to control the packed length of the column and has a single outlet for both the fluids exiting the column. **Figure 9** shows the setup for the column experiments. The inlet end fitting was modified from one inlet to two inlets, to facilitate simultaneous flow of oil and water. A 100 mesh metal screen was present on each end of the column to prevent migration of fines and to distribute fluids evenly in the column.

The glass column was dry packed on a vibrating table. The column was packed in increments, so that the glass beads packed densely. A consistent porosity was achieved by this method. The column was then evacuated for 1 hour. It was then flooded with CO_2 gas and again evacuated for ½ hour and then saturated with deaerated and de-ionized water. Subsequently, the column was flushed with 2-3 pore volumes of deaerated water before the tracer experiments were conducted. The gross weight of the column without glass beads and the column with glass beads was measured. The dry weight of the beads packed in the column was obtained from the difference in weight, which was used to obtain the overall porosity and pore volume of the column.

The permeability of the column to water was measured using pressure transducers

(Cole Parmer, Vernon Hills, IL) connected to the inlet and outlet lines of the column. There are two separate inlet lines to the column for water and decane phase and one common outlet line from the column. The pressure was measured as differential pressure between the two-inlet lines and outlet line giving pressure drop for wetting and nonwetting phases. Three pressure transducers were connected in parallel to cover the range of differential pressure expected during the measurements. The electrical signal from the pressure transducer was converted into pressure and recorded on a chart recorder. Measurements were made at different flow rates (1–4 ml/min) and the average permeability was computed.

The procedure for measuring interfacial area is described in Jain *et al*[5]. The retardation factor required for measuring interfacial area was determined from effluent concentration histories (concentration of tracer exiting the column vs. time). The effluent concentrations were measured directly in a flow-through measurement cell plumbed into the experimental apparatus. This provides the requisite resolution for determining retardation of the concentration front and eliminates many of the data quality concerns that would arise if discrete samples were collected and then analyzed in batch mode. To eliminate the possibility of overlapping absorption peaks, the tracers were injected in separate slugs.

Initial tracer tests were conducted to calculate the background sorption of interfacial tracer onto the glass beads. Decane being lighter than water was introduced into the column from the top. A connate water saturation of about 30% was obtained. Subsequently, the column was flushed with 4-5 pore volumes of water from the bottom at increasing flow rates (1– 4ml/min) to reduce the column to residual decane saturation. After establishing residual decane saturation, the tracer experiments were conducted. Next, the decane saturation in the column was increased by flowing decane through the column, while reducing the water flow rate, keeping the total flow rate through the column constant at 1ml/min. At each fractional flowrate, water and decane were simultaneously injected into the column for 35-40 pore volumes to achieve steady state saturations in the column. The permeability to liquid phases was measured at each stage, followed by the tracer experiments. Water saturation at each fractional flowrate was obtained from the conservative tracer profile, and retardation of the interfacial tracer was calculated relative to the conservative tracer. The residual water saturation was obtained by using T-stilbene as the conservative tracer in oil. At this point water is present as residual phase in the column. The following fractional flows of water

were used in the experiments: f_w = 1, 0.75, 0.50, 0.25, and 0.

RESULTS AND DISCUSSION

The results of the experiments are shown on **Figures 10** and **11** for the interfacial area and on **Figures 12** and **13** for the relative permeabilities. Comparing the measurements in Figs 10 and 11 with the curves in Figs 1 – 4, it is evident that the water-wet medium is a strongly wetted system, i.e. thin films of water are present on grain surfaces, and that the oil-wet medium is a weakly wetted system. The measured interfacial area reaches a maximum then decreases during drainage in the weakly wetted medium, whereas it monotonically increases for the water-wet medium. This classification is also confirmed by the imbibition experiment in the water wet medium, where interfacial area monotonically decreases. For the oil-wet system, however, the measurement shows a monotonic increase in interfacial area during imbibition. Assuming that the system was weakly wetted in this case as in the corresponding drainage experiment, we would expect the trend to exhibit a maximum, similar to that of Fig 4. It is conceivable that a decrease in interfacial area would be observed if it were possible to reduce the NW saturation further.

Relative permeabilities to both water and oil are presented on Fig 12 for primary drainage and on Fig 13 for secondary imbibition. Decreasing water saturation decreases permeability of the column to water, while it increases the decane permeability. The relative permeability is presented as a function of wetting phase saturation; hence the crossover points do not indicate the wettability of the column. The previous classification of water wet medium as strongly wetted and oil wet medium as weakly wetted implies a qualitative correspondence of the data with the predicted trends in Figs 7 (primary drainage) and 8 (secondary imbibition).

For primary drainage, Fig. 12, we find qualitative agreement with the predictions. Relative permeability to the W phase remains smaller for the weakly wet medium than for the strongly wet medium during all stages of drainage. The behavior of relative permeabilities to both phases at low W phase saturation agrees well with the predicted trends. As predicted, irreducible W phase saturation is smaller for the water wet medium (strongly wetted), and relative permeabilities to both phases are lower for the oil wet (weakly wetted) medium (compare to Fig 7). However, the large differences between the two systems for high

W phase saturation (a factor of 4 at S_w = 0.75) cannot be explained by the presented considerations alone.

For secondary imbibition, Fig. 13, the agreement with Fig 8 is not good. While the trends in relative permeabilities to the both phases are consistent with predictions at low W phase saturation (viz., relative permeabilities to both phases are smaller for the weakly wetted (oil wet) system), the observed values of these quantities do not agree with the predictions at high W phase saturation: relative permeability to NW phase is larger for the weakly wetted (oil wet) system, while relative permeability to W phase is smaller for the same medium. Also, the residual NW phase saturation is much higher for the strongly wetted (water wet) system (25% in comparison with 15% in the oil wet (weakly wetted) medium). These discrepancies cannot be explained by our analysis. Moreover, the large difference in the residual saturations suggests that the number of pores with NW phase trapped during imbibition is different for water-wet and oil-wet media. A possible factor is the different saturation history preceding imbibition in the water-wet and oil-wet experiments.

For comparison we have also plotted the results of Embid[6] in Figs 12 and 13. She measured relative permeabilities in steady-state experiments in which the oil phase was decane and the water was 1% NaCl brine. The media were water-wet sandpacks and a chemically treated sandpack that was moderately oil-wet. The wettability of each system was estimated from measurements of brine-oil contact angles on glass slides that were pretreated in the same way as the sands. The contact angle for primary drainage in the water wet system was less than 5^o, which suggests strongly wet behavior in this case. For the other experiments much larger values of contact angles were measured, indicating weakly wet behavior.

Embid's results are consistent with the behavior of a weakly wetted system. Unfortunately, she did not measure primary drainage in a weakly wetted system; relative permeabilities during secondary drainage are shown instead. In this case (Fig 12) there is a large difference between relative permeabilities to the wetting phase at the beginning of drainage (high wetting phase saturation) for water and oil wet systems, whereas relative permeability to the nonwetting phase remains roughly the same. This can be explained by the difference between primary and secondary drainage, rather than the above analysis for systems with different wettabilities, which predicts the same values of relative permeabilities at high wetting phase saturations. For the same value of saturation and relative permeability

at the beginning of drainage, the nonwetting phase forms flow channels with some dendritic regions through the medium. For primary drainage, these regions must be adjacent and connected to this channel, whereas for secondary drainage regions with residual nonwetting phase exist that are disconnected from the network of pores through which the NW phase is flowing. This creates additional obstacles for the flow of the wetting phase in comparison with primary drainage.

The dependence of relative permeabilities upon interfacial area during our experiments is shown on **Figure 14** for primary drainage and on **Figure 15** for secondary imbibition. For primary drainage in the water wet medium (strongly wetted system) there is a strong correlation between these parameters: relative permeability to the wetting phase decreases and to the nonwetting phase increases while interfacial area increases during primary drainage. This is not surprising, since the interfacial area in this case is dominated by the grain area in drained cells and thus increases monotonically during drainage. For the oil wet (weakly wetted) medium, though, the dependence is more complex: interfacial area reaches a maximum, while relative permeabilities remain monotonic. This behavior can not be explained by any simple relationship between these parameters. In fact it suggests that the interfacial area between the fluid phases does not influence relative permeability; instead the area of the fluid/solid interfaces is the primary factor. (Recall that this interface does not contribute to the measured area in the weakly wetted system).

For secondary imbibition, the absence of correlation is even more evident: relative permeability to the wetting phase in the strongly wetted system ($K_{r,water}$ in water wet medium) increases as interfacial area decreases, whereas the in weakly wetted system ($K_{r,oil}$ in oil wet medium) it increases as interfacial area *increases*. Relative permeability to the nonwetting phase likewise exhibits opposing trends as wettability changes. The results shown on Figs 14 and 15 suggest that there are no simple correlations between relative permeability and W-NW interfacial area (such as a power law, for instance). To use such a correlation in some empirical model, one would have to take into account a number of other factors that can influence this relationship (such as the wettability of the system).

The above qualitative analysis of the measurements of interfacial area simultaneously with the relative permeabilities allows us to identify a system as weakly or strongly wet.

CONCLUSIONS

Our analysis suggests qualitatively different behavior of interfacial area and relative permeabilities of two-phase flow in porous media, depending on whether the system is strongly or weakly wetted. This knowledge allows classifying the degree of the wettability of the system from measured trends of one parameter (interfacial area or relative permeability). Knowing the wettability of the system, it is possible to predict qualitative trends of both interfacial area and relative permeability. This idea was demonstrated in this paper, where interfacial area and relative permeability were measured simultaneously and were generally consistent with the predicted trends. An exception was the behavior of the NW phase during imbibition in oil-wet media.

ACKNOWLEDGEMENTS

Funding for this work was provided by the Department of Energy under grant DE-AC26-98BC15205 for the project "Characterization of Mixed Wettability at Different Scales and Its Impact on Oil Recovery Efficiency". Additional support was provided by EPA (R827116/01/0) and with funds from the State of Texas as part of the program of the Texas Hazardous Waste Research Center (THWRC, 069UTA0803). The contents do not necessarily reflect the views and policies of the sponsor nor does the mention of trade names or commercial products constitute endorsement or recommendation for use. This paper has not been subject to agency review and therefore does not necessarily reflect the views of the sponsoring agency, and no official endorsement should be inferred. Support for the first author was also provided by UT Austin's Center of Excellence in Formation Evaluation, jointly sponsored by Baker Atlas, Halliburton, and Schlumberger. The consortium web page is http://uts.cc.utexas.edu/~cefe/res/.

Nomenclature

A_g = total surface area of the grains, cm^2/cm^3
A_{film} = surface area of thin films of W phase, cm^2/cm^3
A_{total} = total interfacial area between phases, cm^2/cm^3
A = area of bulk interface, cm^2/cm^3
f_w = fractional flow of water, parts of unity
k_r = relative permeability, parts of unity
$k_{r,water}$ = relative permeability to water, parts of unity
$k_{r,oil}$ = relative permeability to oil, parts of unity
S = spreading coefficient, number
S_w = W phase saturation, parts of unity
S_{water} = water saturation, parts of unity

S^{r}_{nw} = residual NW phase saturation, parts of unity
W = wetting
NW = non-wetting
θ = contact angle, degree
γ = interfacial tension between W and NW phases, mN/m
γ_{WS} = interfacial tension between W phase and solid grain, mN/m
γ_{NS} = interfacial tension between NW phase and solid grain, mN/m

REFERENCES

1. Gray, W.: "Thermodynamics and Constitutive Theory for Multiphase Porous-Media Flow Considering Internal Geometric Constraints", *Adv. Wat. Res.* **22**, 521-547, 1999.
2. Alpak, F., Lake, L and Embid, S.: "Validation of a Modified Carman-Kozeny Equation to Model Two-Phase Relative Permeabilities", SPE 56479, prepared for presentation at the 1999 SPE Annual Technical Conference and Exhibition held in Houston, Texas, 3-6 October 1999.
3. Leverett, M.C.: "Capillary Behavior in Porous Solids", *AIME Pet. Trans.* **142,** 152-169, 1941.
4. Bradford S.A. and Leij, F.J.: "Estimating Interfacial Areas for Multi – Fluid Soil Systems", *J. Cont. Hydr.* **27**, 83 – 105, 1997.
5. Jain, V., Bryant, S. and Sharma, M.: "Influence of Wettability and Saturation on Liquid-Liquid Interfacial Area in Porous Media", *Environ. Sci. Technol*. **37**(3): 584 – 591, 2003.
6. Embid, S.: "Modeling Capillary Pressure and Relative Permeabilty for Systems with Heterogeneous Wettability." Ph. D. Dissertation. The University of Texas at Austin, 1997.
7. Bryant, S. and A. Johnson. "Prediction of Irreducible Wetting Phase Saturations in Simple Granular Media," in press, *J. Coll. Interfac. Sci.*, 2003.
8. Lewis, M. Masters Thesis, Department of Petroleum and Geosystems Engineering, The University of Texas at Austin, 1988.

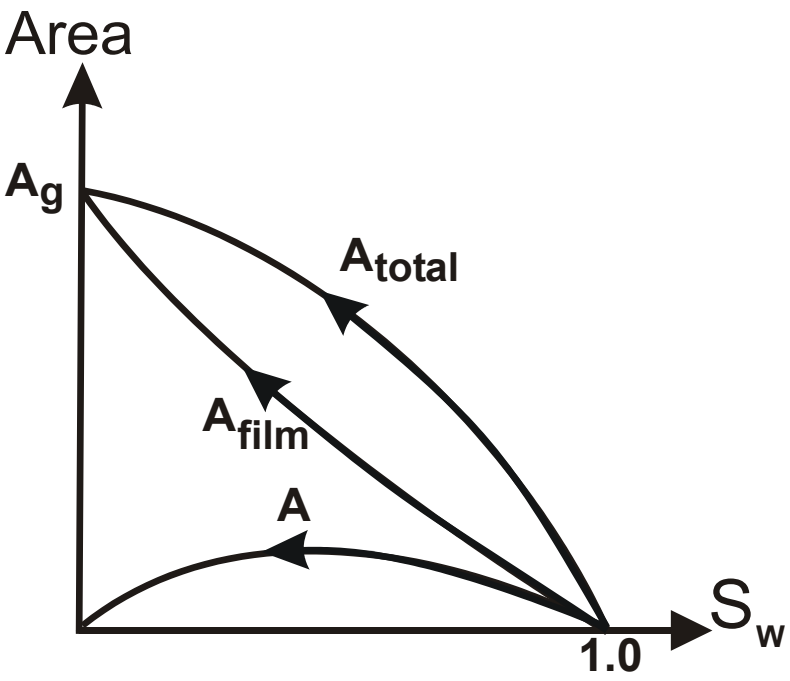

Figure 5.1 Schematic trends of interfacial areas during primary drainage for the case S<1 (strongly wetted).

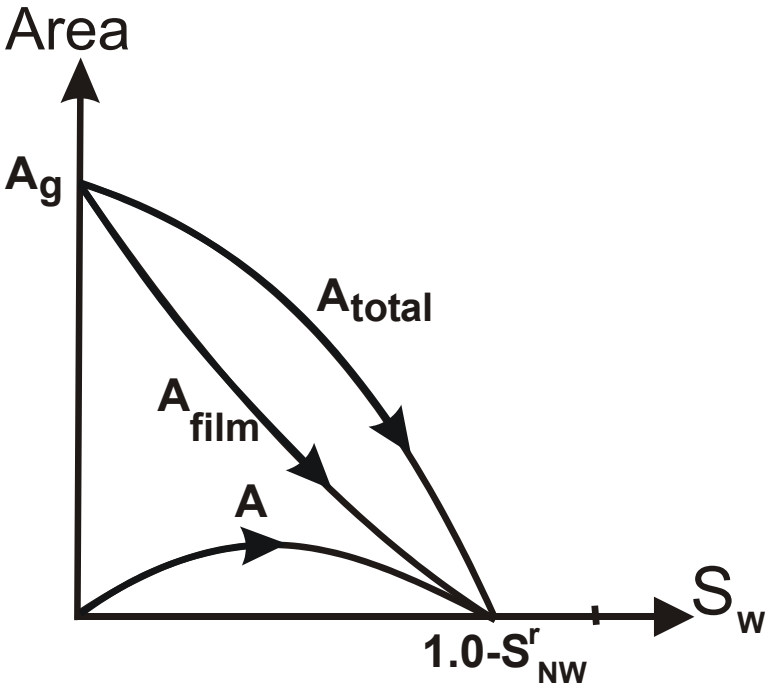

Figure 5.2 Schematic trends of interfacial areas during imbibition for these cases case S<1 (strongly wetted).

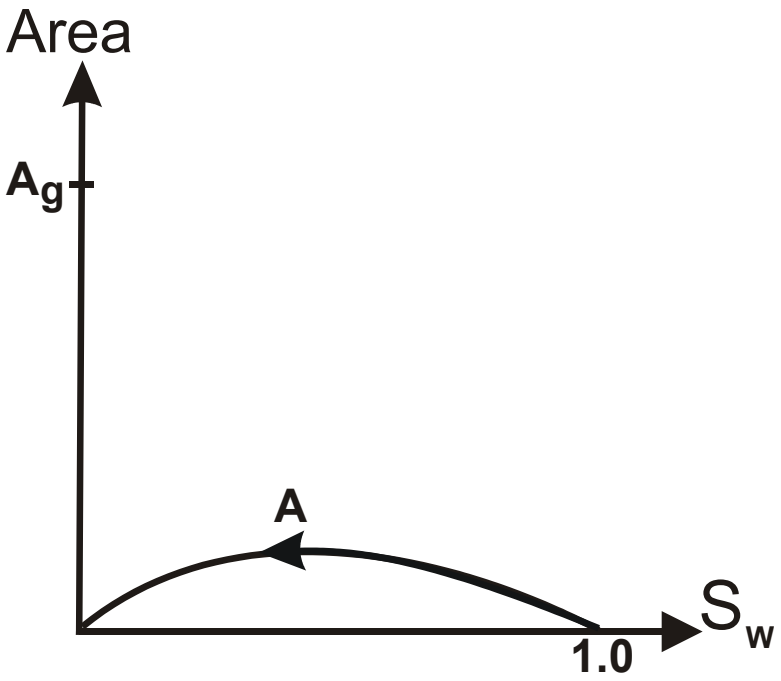

Figure 5.3 Schematic trends of interfacial areas during primary drainage for the case S>1 (weakly wetted).

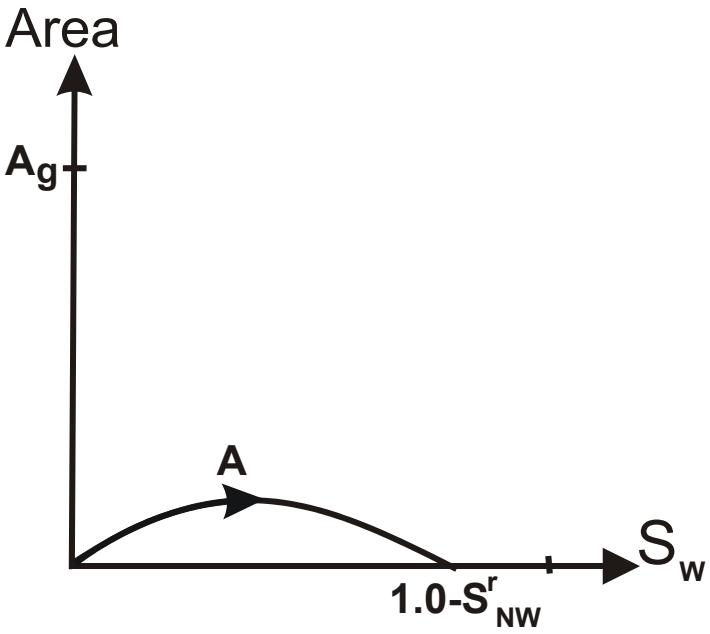

Figure 5.4 Schematic trends of interfacial areas during imbibition for the case S>1 (weakly wetted).

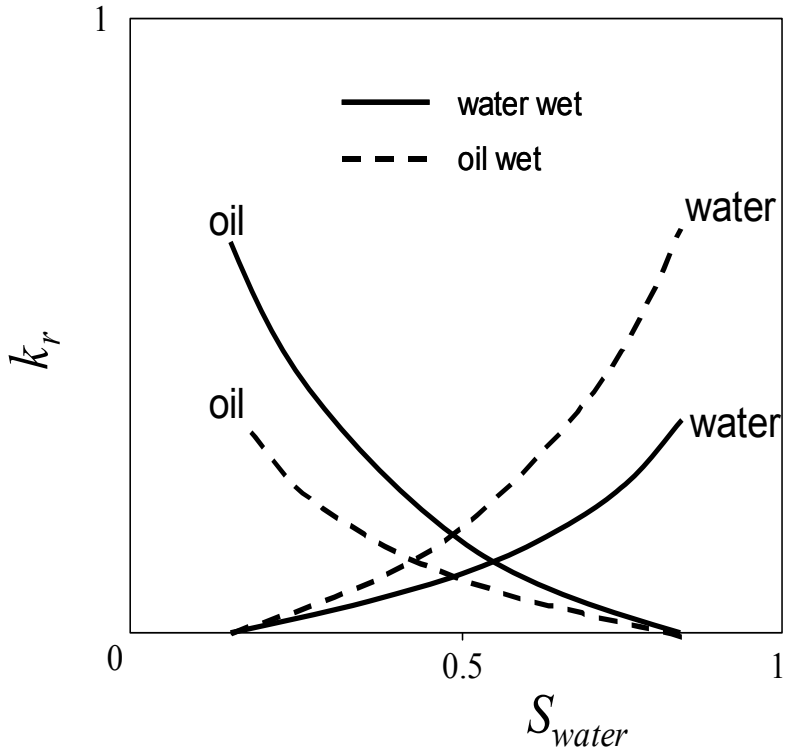

Figure 5.5 Effect of strong preferential wettability on relative permeabilities as functions of water saturation

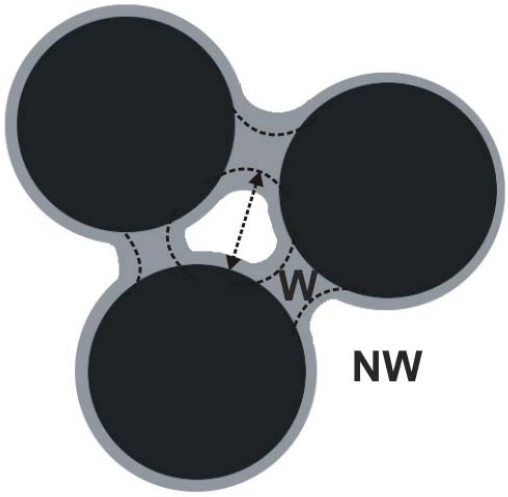

Figure 5.6Pendular rings of W phase restrict the size of the pore throat available for the NW phase flow, reducing relative permeability to NW phase. Pendular rings in a weakly wetted system are trapped and disconnected from the bulk so that they remain constant in size during drainage (shown by gray color). In a strongly wetted system they diminish in size as capillary pressure increases (shown by the dotted lines), thus increasing the size of the pore throat available for the flow of NW phase.

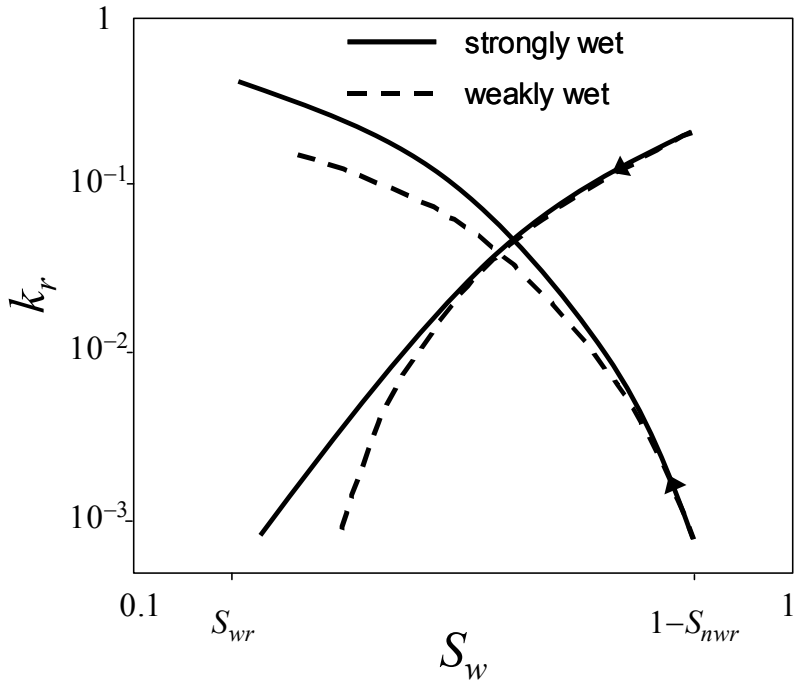

Figure 5.7Qualitative behavior of relative permeabilites of W and NW phases as a function of wetting phase saturation for primary drainage.

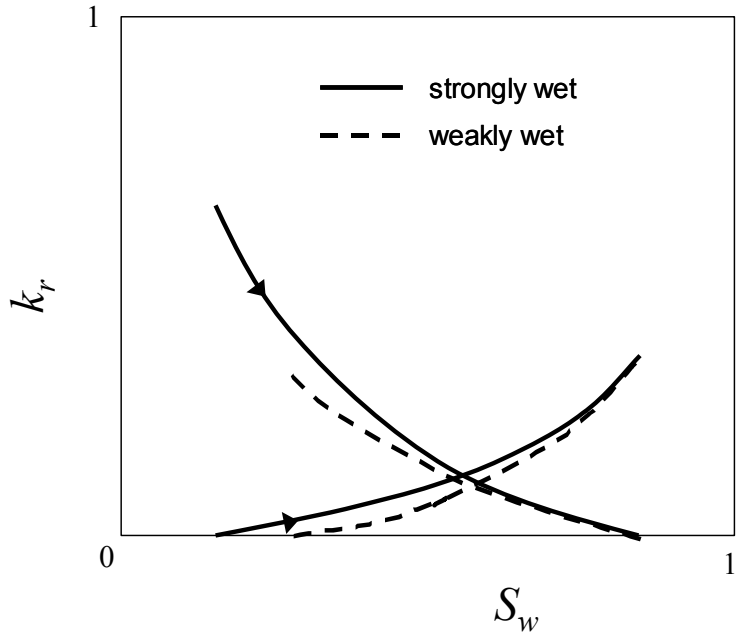

Figure 5.8Qualitative behavior of relative permeabilities of W and NW phases a function of wetting phase saturation for secondary imbibition.

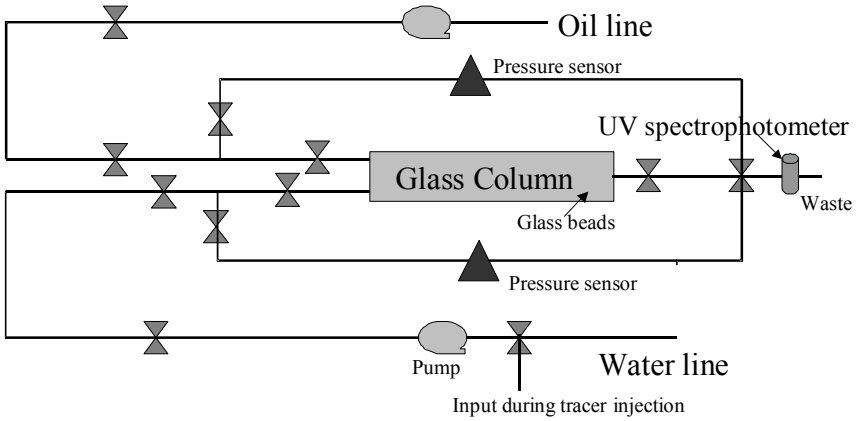

Figure 5.9 Setup for the column experiments

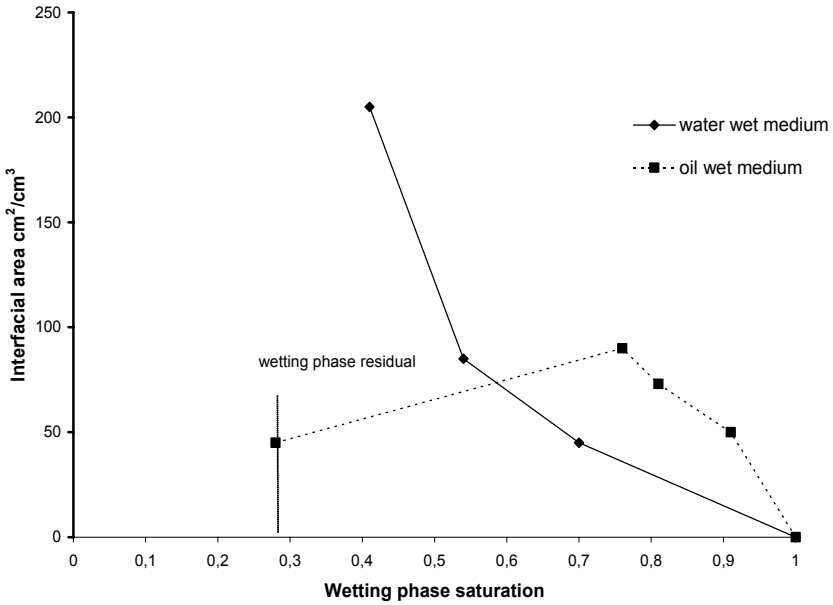

Figure 5.10 Interfacial area during primary drainage for water-wet (strongly wetted) and oil-wet (weakly wetted) conditions.

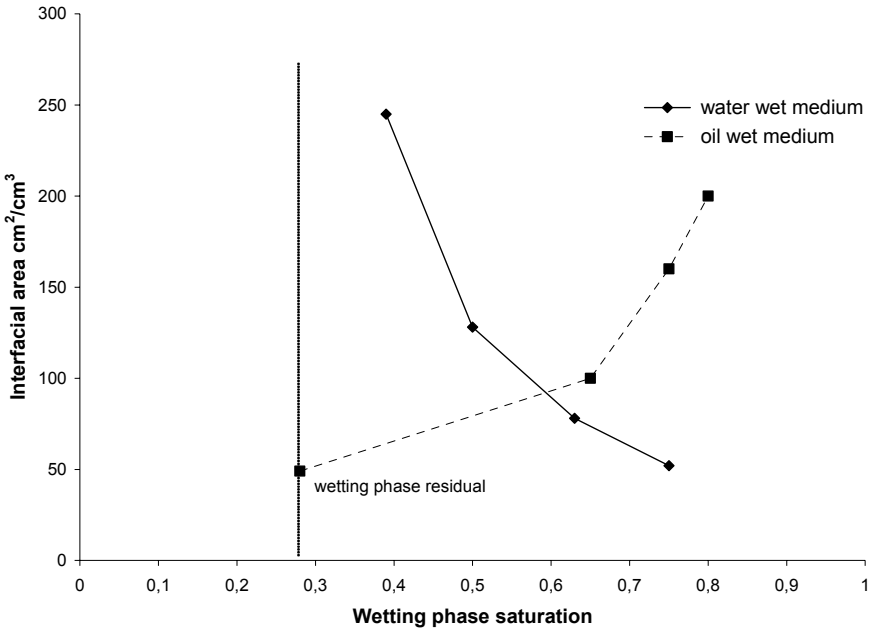

Figure 5.11 Interfacial area during secondary imbibition for water-wet (strongly wetted) and oil-wet (weakly wetted) conditions.

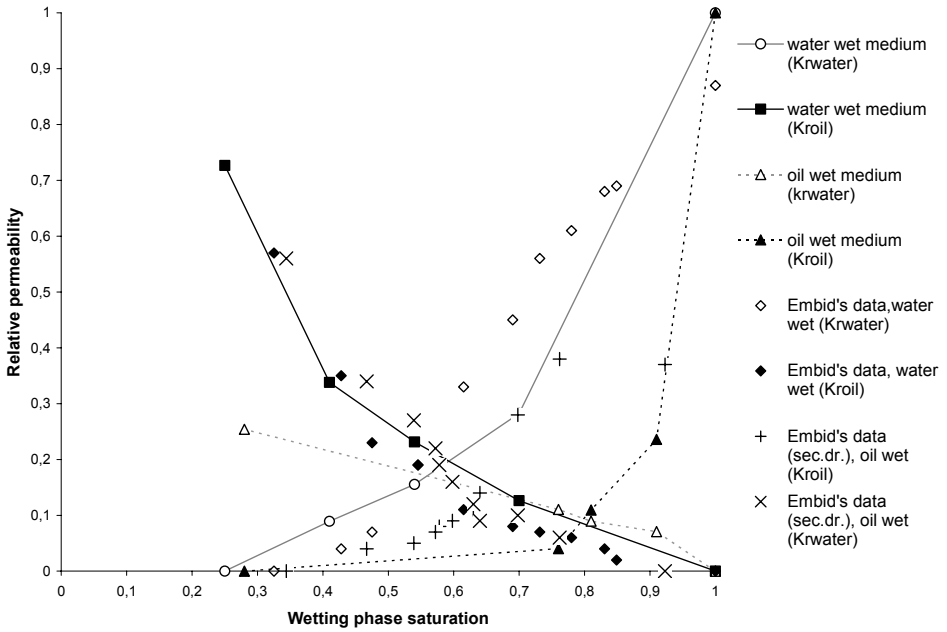

Figure 5.12 Relative permeabilities to W and NW phases during drainage for water-wet and oil-wet conditions. (Points joined with lines are this work; points without lines are from Embid[6]).

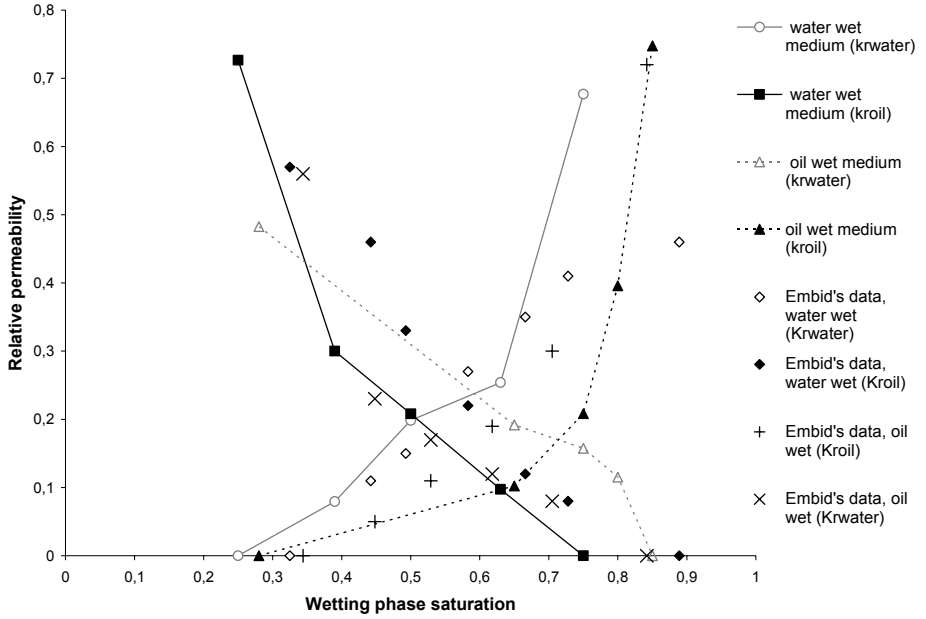

Figure 5.13Relative permeabilities to W and NW phases during secondary imbibition for water-wet and oil-wet conditions. (Points joined with lines are this work; points without lines are from Embid[6]).

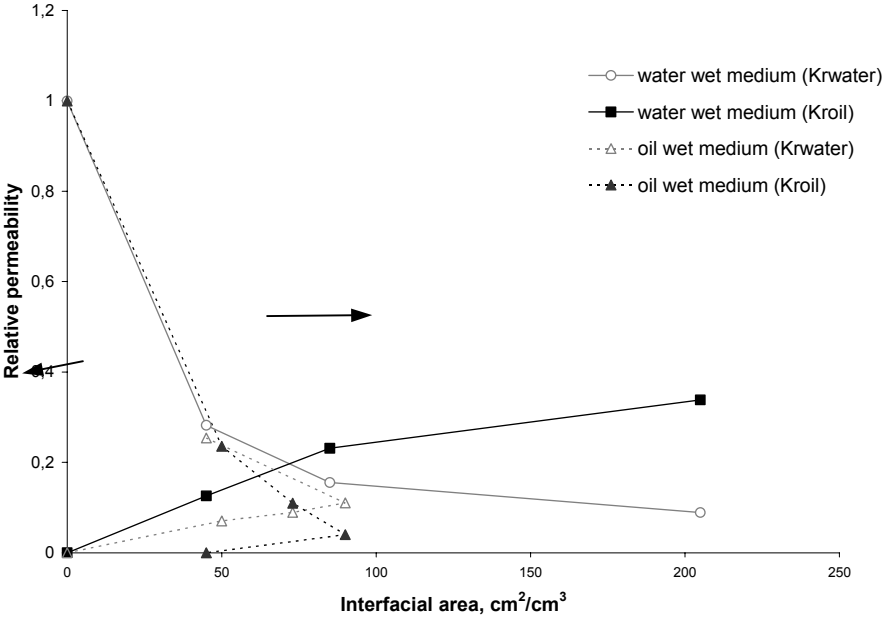

Figure 5.14Dependence between relative permeability and interfacial area during primary drainage for water-wet (strongly wetted) and oil-wet (weakly wetted) conditions. Arrows indicate the direction of decreasing wetting phase saturation for each experiment.

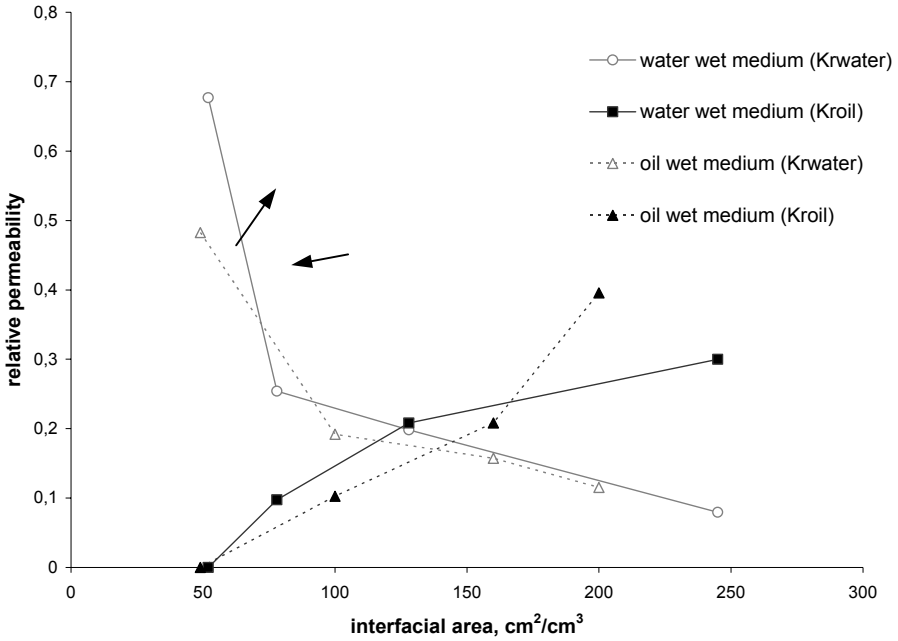

Figure 5.15Dependence between relative permeability and interfacial area during secondary imbibition for water-wet (strongly wetted) and oil-wet (weakly wetted) conditions. Arrows indicate the direction of increasing wetting phase saturation for each experiment. Note the opposite trends for the two wettabilities.

6. Phase Behavior Modeling of Hydrocarbon-Methanol-Water Mixtures by Peng-Robinson and SAFT Equations of State

Ayyalasomayajula, P., Sharma, R., Walker, J. G., Sharma, M. M., and Pope, G. A.

SPE 77575, presented at the SPE Annual Technical Conference and Exhibition held in San Antonio, Texas, 29th September–2th October 2002.

ABSTRACT

The phase behavior of mixtures of hydrocarbons, methanol and water is important in gas-condensate reservoirs as well as in gas hydrates. Gas-condensate wells frequently show reduced productivity when operated below the dew point due to the build up of condensate near the well. A combination of high water and condensate saturation results in a significant reduction in the gas relative permeability. Recently, methanol has been used to remove liquid blocking around such wells and restore well productivity. The phase behavior of such fluid mixtures is difficult to model using currently available equations of state.

In this study, phase behavior data were measured both to help interpret coreflood experiments and for testing of equation-of-state models used in compositional simulation studies of methanol well treatments. The Peng-Robinson equation-of-state and the SAFT equation-of-state were used to model this new phase behavior data. The Peng-Robinson equation-of-state does better than the SAFT equation-of-state for hydrocarbon mixtures. The binary interaction coefficients had to be adjusted in both models to match the experimental data when methanol and water are in the mixture. The SAFT EOS required less tuning to match data from hydrocarbon-methanol mixtures. SAFT EOS, as expected, agrees with the data better than the Peng-Robinson EOS when water is in the mixture.

INTRODUCTION

Hydrocarbon-water-methanol mixtures are important in diverse applications such as the productivity of gas-condensate wells[1,2] as well as gas hydrate inhibition.[3] In gas-condensate reservoirs, a liquid hydrocarbon phase (condensate) drops out when the bottomhole pressure falls below the dew point pressure. This results in a build-up of liquid near production wells and a corresponding decrease in the gas relative permeability and well

productivity. Afidick *et al.*[4] have reported field data from the giant Arun field in Indonesia that show a reduction in well productivity by a factor of 2 to 4 due to condensate accumulation.

The phase behavior of gas-condensate hydrocarbon mixtures has been extensively studied [Whitson *et al.*,[5] Wang *et al.*,[6] Sarkar *et al.*[7]]. However, there have been very few studies [Kokal,[8] Ng and Robinson[9]] on the influence of water on the phase behavior and properties of gas-condensate fluids. Recently, experimental coreflood studies have shown [Du *et al.*,[1] Walker[2]] that methanol treatments can significantly increase the gas relative permeability when condensate and/or water blocking is present. No phase behavior data or modeling under these conditions was available to aid in the interpretation of these experiments. Hydrocarbon-water-methanol mixtures have been studied at lower temperatures where hydrates form.[10, 11]

In this study, we present the pressure-volume relationships for a synthetic gas-condensate mixture and the effect of methanol and methanol-water mixtures at 145 ºF. We also model these phase behavior data using a Peng-Robinson equation-of-state and a theoretical equation-of-state, Statistical Associating Fluid Theory (SAFT). The most important property of interest in gas-condensate modeling is the liquid dropout. We also model the effect of the polar components water and methanol on the condensate dropout.

EXPERIMENTAL METHODS

The four hydrocarbons used to create the gas-condensate mixture were methane (C1), normal butane (nC4), normal heptane (nC7), and normal decane (nC10). The composition of the mixture is shown in Table 6.1 (Mixture 1). The C1 was from Air Liquide America Corp, and was stored in a high-pressure tank with unlisted purity. The nC4 was from Speciality Gas Concepts and was stored in a 24 pound tank with unlisted purity. The nC7 and nC10 were from Philips Petroleum Co., stored in 30 pound cans, each with 99 mol % percent purity. Methanol was from EM Science and was 99.9 mol % pure. Distilled water was taken from the building supply line.

Figure 6.1 shows the apparatus that was used to measure hydrocarbon-methanol-water phase behavior. A Ruska windowed cell with an internal volume of 93.7 cc was enclosed in a Ruska PVT oven and maintained at 145 °F. Mercury was used as the pistoning

fluid inside the windowed cell in contact with the experimental mixture (e.g., a hydrocarbon-methanol-water mixture). This mercury was reservoired in a high-pressure accumulator inside the oven and was driven by a Ruska proportioning pump using water as the hydraulic fluid. An Isco syringe pump, also using water as the hydraulic fluid, was used to drive hydrocarbon mixture from a high-pressure accumulator in an adjacent coreflood oven (Du *et al.*[1] gives an explanation of the coreflood apparatus). Using the Isco syringe pump to inject hydrocarbon mixture into the windowed cell while the Ruska proportioning pump simultaneously withdrew mercury, hydrocarbon mixture was transferred at constant pressure to the windowed cell above its dew point pressure. Another Ruska proportioning pump was used to inject methanol or water into the windowed cell above the dew point of the mixture. After the injection ports of the windowed cell were closed, mercury was withdrawn to decrease the pressure in the windowed cell. All liquid dropout experiments were constant composition expansion processes.

EQUATIONS-OF-STATE

Two equations-of-state were used to model the hydrocarbon-water-methanol mixtures. The Peng-Robinson equation-of-state (PREOS) [Peng and Robinson[12,13]] is a cubic equation-of-state that has been shown to accurately model hydrocarbons typically found in gas and oil reservoirs and is widely used in reservoir simulators. However, when water and methanol are added to hydrocarbon mixtures the binary interaction coefficients used with the PREOS must be adjusted to fit the data. The Statistical Associating Fluid Theory (SAFT) equation-of-state developed by Huang and Radosz,[14,15] and implemented by Ayyalasomayajula[16] to test its predictive capabilities for multi-component mixtures of hydrocarbon and polar components, was tested in the hope that it would have greater predictive capability for the hydrocarbon-water-methanol mixtures than the PREOS.

The PREOS can be expressed as follows:

$$P = \frac{RT}{v - b} - \frac{a}{v(v + b) + b(v - b)} \qquad (6.1)$$

For mixtures simple mixing rules are used to obtain a and b from pure component

parameters

$$a = \sum_{i=1}^{n} \sum_{j=1}^{n} x_i x_j a_{ij} \quad , \quad b = \sum_{i=1}^{n} x_i b_i \tag{6.2a}$$

$$a_{ij} = (1 - k_{ij}) \sqrt{a_{ii} a_{jj}} \tag{6.2b}$$

SAFT is an equation of state based on statistical mechanical theories and takes into account the intermolecular potential function. It is of special interest because it captures the major effect of the non-spherical nature and the association among molecules. We give the basic equations involved in SAFT in this section. The compressibility factor is given as

$$Z = 1 + Z^{hs} + Z^{chain} + Z^{assoc} + Z^{disp} \tag{6.3}$$

In the above expression Z^{hs} is the compressibility factor contribution due to the hard-sphere repulsion of the molecules and is given by the well-known Carnahan and Starling equation[14]

$$Z^{hs} = \frac{P_{CS}^{hs}}{\rho kT} \tag{6.4}$$

Z^{assoc} is the compressibility factor contribution due to association. The Helmholtz free energy for association has been proposed by Wertheim[17] and implemented by Huang and Radosz,[14,15]

$$Z^{assoc} = \sum_i x_i \frac{\mu_i^{assoc}}{RT} - \frac{a^{assoc}}{RT} \tag{6.5}$$

The Helmholtz free energy contribution due to association bonding is given by

$$\frac{a^{assoc}}{RT} = \sum_{i=1,n} x_i^B \left[\sum_{\lambda_i=1,M_i} \left\{ \ln(Y_{(\lambda_i,i)}^B) - Y_{(\lambda_i,i)}^B \right\} + \frac{M_i}{2} \right] \tag{6.6}$$

The most important term in the above expression is the $Y^{B}_{(\lambda i,i)}$ which is the mole fraction of molecules of i that are not bonded at the association bonding site λ_i, or in terms of Wertheim's terminology, the monomer density. The monomer density is dependent on the associating strength of the molecule, number of associating sites on each molecule as well as the molecular density of the mixture.

The non-spherical nature of the molecules is accounted for by Z^{chain} and is based on Chapman *et al*.,[18]

$$Z^{chain} = \sum_i x_i (1 - m_i) \rho \left[\frac{\partial \ln g_{ii}(d_i)^{hs}}{\partial \rho} \right]_{T, x_j} \qquad (6.7)$$

Finally, any additional intermolecular effects, (e.g., quadrupolar forces) are accounted as perturbations to the reference potential and are given by Z^{disp} based on Chen and Kreglewski.[19]

$$Z^{disp} = m \sum_j \sum_k k D_{jk} \left[\frac{u}{kT} \right]^j \left[\frac{\zeta_3}{\tau} \right]^k \qquad (6.8)$$

The complete and more detailed SAFT equations are given elsewhere.[9,10,11]

RESULTS AND DISCUSSION

A) Pure gas-condensate mixtures

The experimental liquid dropout data obtained at 145 °F by Walker[2] for the gas-condensate mixtures shown in Table 6.1. Figure 6.2 shows the total liquid volume fraction data for gas-condensate mixtures without any methanol or water (Mixture 1) and a comparison with the curves computed from the two equations-of-state. The binary interaction coefficients for the PR EOS were taken as zero in these calculations. On the other hand, the SAFT prediction for the same gas-condensate mixture without adjusting the binary interaction coefficients is not good. As shown in Figure 6.2, after adjusting the binary interaction coefficients, the SAFT equation does match the data. Table 6.2 shows the binary

interaction coefficients used to fit the liquid volume fractions. Since the PREOS was developed for hydrocarbons, it is not a surprise to see that the PR EOS fits the data better for pure hydrocarbon mixtures.

B) Gas-condensate-methanol mixtures

Figure 6.3 shows the variation in the experimental liquid volume fraction data with pressure at different methanol concentrations. Below 25 overall mole percent, the methanol increases the dew point pressure and the volume of liquid phase, but the behavior is still that of a retrograde condensate fluid. Above 25 mole percent methanol, a bubble point is observed rather than a dew point (i.e., the critical temperature of the mixture is now greater than the experimental temperature of 145 °F). At sufficiently high pressure, all of the hydrocarbons are miscible with the methanol (methanol is below its critical temperature and above its vapor pressure at 145 ºF and 3000 psia), so the entire mixture is observed to be a single-phase liquid. As the pressure is decreased, the lower molecular weight hydrocarbons form a gas phase and a bubble point is observed.

The binary interaction coefficients between methanol and the hydrocarbons in each EOS had to be adjusted to fit the data shown in Figure 6.3. Figure 6.4 shows the liquid volume fraction curves computed using the PR and SAFT equations-of-state for the overall composition corresponding to Mixture 2 in Table 6.1. The hydrocarbon-hydrocarbon binary interaction coefficients remain zero for the PR EOS and the same as those given in Table 6.2 for the SAFT EOS. Only the methanol-hydrocarbon binary interaction coefficients were adjusted to get a good fit to these data with both the PR and SAFT equations. After the methanol-hydrocarbon binary interaction coefficients were adjusted to those shown in Table 6.3, their dependence on temperature was less for the SAFT EOS than that for PR EOS.

After matching the liquid volume fraction curves for 10 mol % methanol with both the PR and SAFT EOS by adjusting the binary interaction parameters in each equation, the behavior of a 50 mol % methanol mixture with 50 mol % gas-condensate fluid with the composition given by Mixture 3 in Table 6.1 was predicted with each EOS. As shown in Figure 6.5, the PR EOS under-predicts the liquid volume fraction curves whereas the SAFT EOS slightly over-predicts the liquid volume fractions but captures the correct trend with pressure.

We should note here that when modeling the gas-condensate-methanol mixtures with the PR EOS we did only a two-phase flash rather than the more general multi-phase flash. This was done because we observed only two phases at all pressures in our experimental studies. When a phase stability test was done with the PR EOS, a spurious third phase at lower pressures was found over a wide range of binary interaction coefficients even with the Huron and Vidol mixing rules as well as the original PR EOS mixing rules. This clearly indicates one of the limitations of the PR EOS for mixtures with polar molecules and the advantage of the SAFT EOS since this problem was not observed with it.

C) Effect of methanol concentration on gas-condensate-methanol mixtures

Figures 6.6 and 6.7 show the changes in the liquid volume fraction curves with varying methanol concentration at temperatures 145 ºF and 250 ºF, respectively. These plots have been generated using the SAFT EOS with the binary interaction coefficients given by Table 6.2 and Table 6.3. As shown in Figure 6.6, at 10 and 15 mol % methanol concentrations the mixture exhibits retrograde behavior i.e. a liquid phase is formed as the pressure is lowered below the dew point pressure. There is a transition from dew-point behavior to bubble-point behavior as the methanol concentration is increased to about 20 %. Figure 6.7 shows the liquid volume fraction curves at 250 ºF. The transition now shifts to a higher methanol concentration of about 25-30 %. Also, the 0 % methanol dew point has decreased to 2600 psia from 2700 psia as the temperature is increased from 145 ºF to 250 ºF.

D) Water-methanol mixtures

In this section, we briefly present a study of the phase behavior of binary mixtures of methanol and water that are of particular significance in the context of methanol treatment of gas-condensate reservoirs with a substantial water saturation. Figure 6.8 shows the pressure-composition diagram at 39.9 ºC. By adjusting the binary interaction coefficients (BIC), the PR EOS gives a very good fit to the experimental data[20] even for these very highly associating species. Note that the binary interaction coefficient between methanol and water is a negative value of -0.1. When a positive BIC is used, two phases rather than one phase is calculated above the bubble point curve where there should only be one liquid phase. The BIC used to match these same data with the SAFT EOS is -0.15. Clearly, the use of a

negative BIC is needed to match these experimental data over a range of pressures and temperatures.

E) Gas-condensate-water-methanol mixtures

Figure 6.9 shows a comparison of the PR EOS predictions of the phase volume fractions with the measured data for a 30 mol % water, 17 mol % methanol and 53 mol % gas-condensate mixture with the overall composition of Mixture 4 in Table 6.1. The BICs given in Table 6.3 were used without adjustment. The PR EOS predicts the three-phase behavior reasonably well. Figure 6.10 shows the same comparison with the SAFT EOS, which also shows reasonably good agreement with the experimental three-phase data. The hydrocarbon-water BICs in this case have been adjusted to those shown in Table 6.3.

Figure 6.11 shows a comparison of the PR EOS predictions of the phase volume fractions with the measured data for a 13 mol % water, 65 mol % methanol and 22 mol % gas-condensate mixture with the overall composition of Mixture 5 in Table 6.1. The PR EOS captures the phase behavior qualitatively without any adjustment of the BICs, but it does not agree with the data quantitatively except it does predict the pressure for the transition between two and three phases rather well. Above pressures corresponding to the original gas-condensate dew point pressure of about 2700 psia, the data show a gas phase and an aqueous phase rather than just a gas phase as observed without the water and methanol components in the mixture. Figure 6.12 shows the same comparison for the SAFT EOS. The SAFT EOS shows good agreement with the experimental data without any adjustment of the BICs from those given in Tables 6.2 and 6.3. This indicates that the SAFT EOS may provide better predictions for mixtures with methanol and water as expected from theoretical considerations.

Finally, we have also made some comparisons with experimental composition data available in the literature for some hydrocarbon-water-methanol mixtures. Table 6.4 shows the PR and the SAFT predictions for a hydrocarbon-methanol-water mixture at 122 °F for which experimental Liquid-Liquid-Vapor equilibrium data were measured by Ng *et al*.,[10] in the context of gas-hydrate inhibition. Both equations give reasonably good predictions for the compositions of all three phases when using the same BIC given in Tables 6.2 and 6.3 i.e. without adjustment of the BICs.

CONCLUSIONS

A SAFT equation-of-state is presented that can model the phase behavior of water-methanol-hydrocarbon mixtures with somewhat better accuracy than the more commonly used Peng-Robinson equation-of-state. This is because the SAFT equation of state explicitly accounts for association bonding among polar molecules. The highly directional and strong intermolecular potential among associating molecules is of particular significance. The methanol-water and methanol-hydrocarbon binary interaction coefficients play a very important role in the phase behavior modeling of these mixtures using both the equations-of-state. We have also shown the effect of methanol concentration and temperature on the dew-point to bubble-point transition of a gas-condensate mixture. The transition from a bubble point to dew-point behavior occurs at a higher methanol concentration with increasing temperature. We have been able to tune the binary interaction coefficients of both the PR and SAFT equations to fit the experimental phase behavior data of hydrocarbon-water- methanol mixtures at a given temperature, but as would be expected the SAFT equation gives better predictions if the temperature is changed.

Nomenclature

P	*pressure*
V	*volume*
R	*Avogadro's constant*
T	*temperature*
a	*energy parameter of Peng-Robinson EOS*
b	*co-volume parameter of PR EOS*
a_{ii}	*pure component energy parameter of component i*
b_i	*pure component co-volume parameter of component i*
x_i	*mole fraction of component i*
k_{ij}	*binary interaction coefficient between component i and j*
Z	*compressibility factor*
Z^{hs}	*hard-sphere compressibility factor*
Z^{chain}	*chain compressibility factor*

Z^{assoc} *association compressibility factor*

Z^{disp} *dispersion compressibility factor*

P^{hs}_{CS} *Carnahan Hard-Sphere pressure*

ρ *density of the mixture*

a^{assoc} *association Helmholtz free energy*

μ_i^{assoc} *association chemical potential of component i*

$Y^{B}_{\lambda i,i}$ *mole fraction of molecules of i not bonded at associating site* λ_i

M_i *number of associating sites available on molecule i*

m_i *chain length of component i*

g_{ii} *radial distribution function of component i*

m *average chain length of mixture*

u_{ii} *dispersion energy of component i*

D_{jk} *Chen and Kreglewski constants for dispersion potential*

ξ_3 *reduced density*

τ *closed packing density limit (0.74048)*

REFERENCES

1. Du, Liangui, Walker, J.G., Pope, G. A., Sharma, M. M., Wang, P.: "Use of Solvents to Improve the Productivity of Gas Condensate Wells", Paper SPE 62935 presented at the SPE Annual Technical Conference and Exhibition, Dallas, TX (October 1-4, 2000).
2. Walker, J.G. : "Laboratory Evaluation of Alcohols and Surfactants to Increase Production from Gas-Condensate Reservoirs", MS Thesis, The University of Texas at Austin, December 2000.
3. Sloan Jr., E.D.,: "Clathrate Hydrates of Natural Gases" , 2nd Edition, Marcel Dekker Inc., 1997.
4. Afidick, D., Kaczorowski N. J., and Bette: "Production Performance if a Retrograde Gas: A Case Study of the Arun Field", paper SPE 28749 presented at the 1994 Asia Pacific Oil & Gas Conference, Melbourne, Australia, Nov. 7-10.
5. Whitson, C.H. and Brule, M.R.: "Phase Behavior", SPE Monograph Vol. 20, 2000.
6. Wang, P, Pope, G.A., Sepehrnoori, K.,: "Development of Equations of State for Gas condensate for Compositional Petroleum Reservoir Simulation", *In Situ*, **24** (2&3) 2000.

7. Sarkar, R., Danesh A.S., and Todd A.C.,: "Phase Behavior Modeling of Gas-Condensate Fluids Using an Equation of State", paper SPE 22714 presented at the 66th Annual Technical Conference and Exhibition of the Society of Petroleum Engineers, Dallas, Texas, October 6-9, 1991.
8. Kokal, S., Al-Dokhi, M., and Sayegh, S.,: "Phase Behavior of Gas Condensate/Water System", paper SPE 62931 presented at the 200 SPE Annual Technical Conference and Exhibition held in Dallas, Texas, October 2000.
9. Ng, H.J., Robinson, D.B.,: "The Influence of Water and Carbon Dioxide on the Phase behavior and Properties of a Condensate Fluid", paper SPE 15401 prepared for presentation at 61st Annual Technical Conference and Exhibition of the Society of Petroleum Engineers held in New Orleans, Louisiana, October 5-8, 1986.
10. Ng, H.J., Robinson, D.B.,: "The solubility of methanol or glycol in water-hydrocarbon systems", Gas Proc. Assn. Rsch. Rpt 117, March, 1988.
11. Ng, H.J., Robinson, D.B.,: "Vapour-Liquid and Vapour-Liquid-Liquid equilibria for H_2S, CO_2, selected light hydrocarbons and a gas condensate in aqueous methanol or ethylene glycol solutions", Gas Proc. Assn. Rsch. Rpt 149, March, 1995.
12. Peng, D.Y., Robinson, D.B.,: "A New Two Constant Equation of State", Ind. Engg. Chem. Fundam., 1976, Vol. 15, No. 1, 59 – 64.
13. Peng, D.Y., Robinson, D.B.,: "The Characterization of the Heptanes and Heavier Fractions for the GPA Peng- Robinson Programs", GPA Research Report RR-28, 1978.
14. Huang, S.H., and Radosz, M.,: "Equation of State for Small, Large, Polydisperse, and Associating Molecules", Ind. Eng. Chem. Res. 1990, 29, 2284-2294.
15. Huang, S.H., and Radosz, M.,: "Equation of State for Small, Large, Polydisperse, and Associating Molecules: Extension to Fluid Mixtures", Ind. Eng. Chem. Res. 1991, 30, 1994-2005.
16. Ayyalasomayajula, P.,: "Prediction of Bulk and Interfacial Thermodynamic Properties of Polar Mixtures by Statistical Associating Fluid Theory", Technical Report, DOE, August 2001.
17. Wertheim, M.S., "Fluids with Highly Directional Forces. III. Multiple attraction sites", J. Stat. Phys., 1986a, 42, 459-476.
18. Chapman, W.G., Gubbins, K.E., Jackson, G., and Radosz, M.,: "New Reference Equation

of State for Associating Liquid", Ind. Eng. Chem. Res., 1990, 29, 1709-1721.

19. Chen, S.S., Kreglewski, A., Ber. Bunsen-Ges. Phys. Chem., 1977, 81, 1048.
20. Sentenac, P., Bur, Y., Rauzy, E., and Berro, C.,: "Density of Methanol+Water between 250 K and 440 K and up to 40 Mpa and Vapor-Liquid Equilibria from 363 K to 440 K", J. Chem. Eng. Data., 1998, 43, 592-600.

Table 6.1 Overall composition of gas-condensate for various mixtures used in this study.

Component	Mixture 1	Mixture 2	Mixture 3	Mixture 4	Mixture 5
Water	0.000	0.0000	0.000	0.307	0.128
Methanol	0.000	0.1000	0.500	0.173	0.654
Methane	0.800	0.7200	0.400	0.416	0.174
Butane	0.150	0.1350	0.075	0.078	0.033
Heptane	0.038	0.0342	0.019	0.020	0.008
Decane	0.012	0.0108	0.006	0.006	0.003

Table 6.2 Binary interaction coefficients, k_{ij}, between hydrocarbons used in the SAFT Equation of state.

	Methane	Butane	Heptane	Decane
Methane	0			
Butane	0.025	0		
Heptane	0.13	0.05	0	
Decane	0.16	0.1	0	0

Table 6.3 Binary interaction coefficients, k_{ij}, between methanol and water with other components with the PR and the SAFT equations-of-state.

	Binary Interaction Coefficients With Methanol		Binary Interaction Coefficients With Water	
	PR	SAFT	PR	SAFT
Methane	0.2	0	0.50	0.2
Butane	0.4	0	0.47	0.15
Heptane	0.1	0.05	0.47	0.05
Decane	0.2	0.05	0.45	0
Methanol	0	0	-0.1	-0.15

Table 6.4 PR and SAFT EOS predictions of compositions of liquid-liquid-vapor phase equilibrium of a synthetic hydrocarbon-methanol-water mixture at 122 °F and 1026 psia.

Component	Overall Composition	Vapor Phase			Liquid Hydrocarbon Phase			Aqueous Phase		
		Expt	PR	SAFT	Expt	PR	SAFT	Expt	PR	SAFT
Water	0.3917	0.0017	0.0016	0.0018	0.0015	0.0012	0.0011	0.7705	0.7838	0.7705
Methanol	0.1188	0.0043	0.0041	0.0039	0.0105	0.0349	0.0092	0.2261	0.2161	0.2291
Methane	0.2937	0.9846	0.9832	0.9861	0.2890	0.2936	0.2260	0.0032	3e-5	2e-4
Heptane	0.1958	0.0093	0.0109	0.0080	0.6990	0.6701	0.7533	9e-5	5e-15	2e-6
Volume %		62.70	59.67	65.76	27.80	29.04	25.18	9.50	11.28	9.05

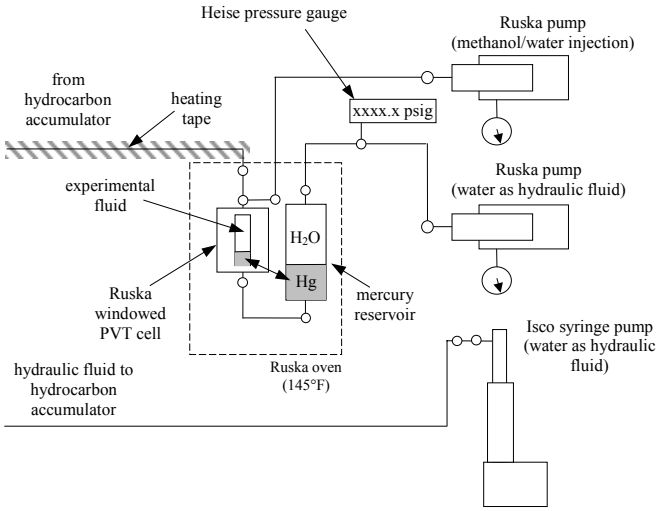

Figure 6.1 Schematic of PVT apparatus in Ruska oven and associated pumps.

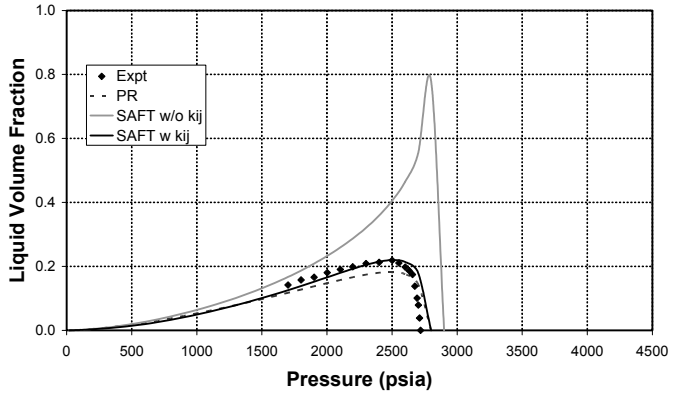

Figure 6.2 Liquid volume fraction curves for Mixture 1 of Table 6.1 at 145 ºF.

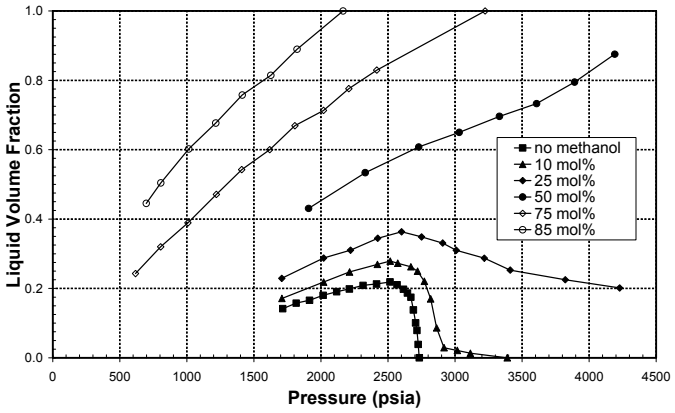

Figure 6.3 Experimental liquid volume fractions of hydrocarbon-methanol mixtures at 145 °F.

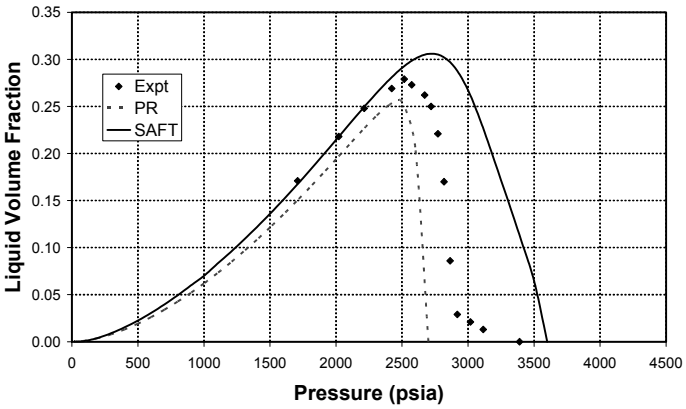

Figure 6.4 Liquid volume fraction curves for Mixture 2 of Table 6.1 (10 % methanol) at 145 ºF.

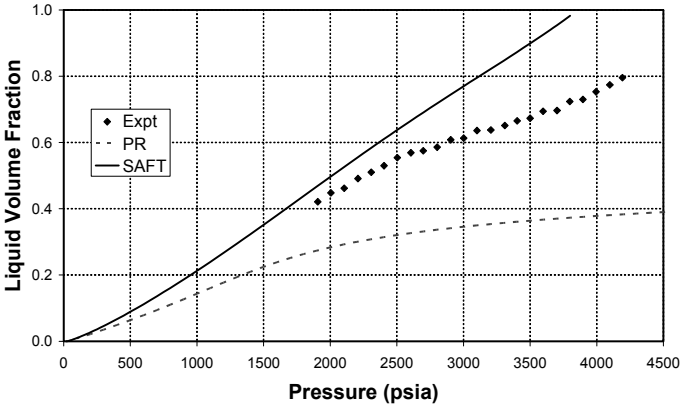

Figure 6.5 Liquid volume fraction curves for Mixture 3 in Table 6.1 (50% methanol) at 145 ºF.

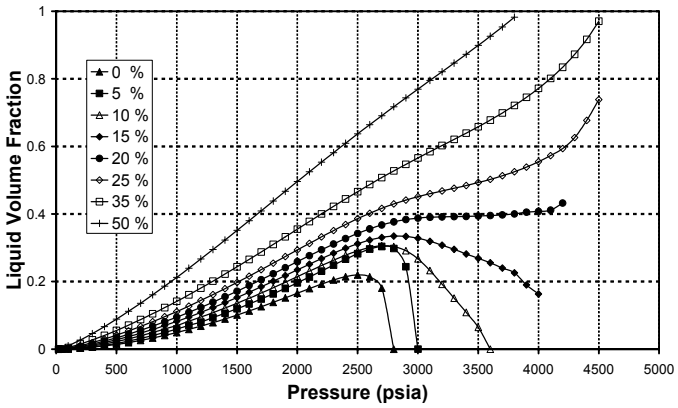

Figure 6.6 SAFT predictions of liquid volume fractions of hydrocarbon-methanol mixtures at 145 °F.

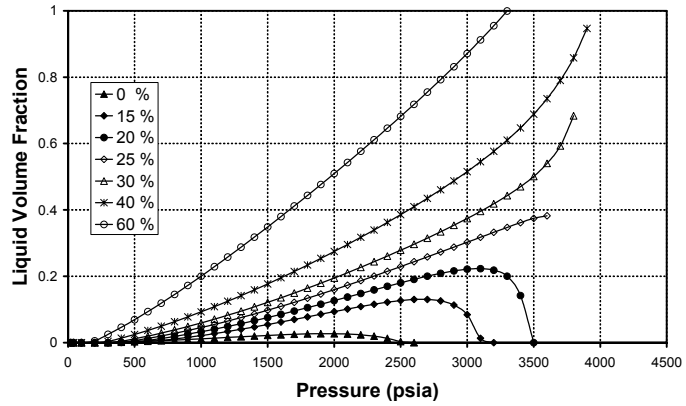

Figure 6.7 SAFT predictions of liquid volume fractions of hydrocarbon-methanol mixtures at 250 °F.

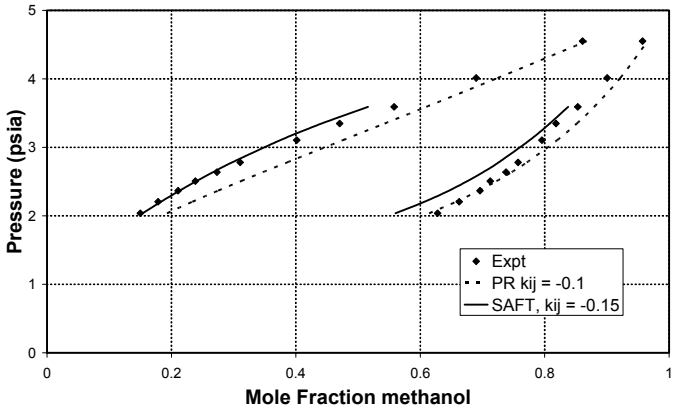

Figure 6.8 Pressure composition diagram for methanol-water mixtures at 39.9 ºC.

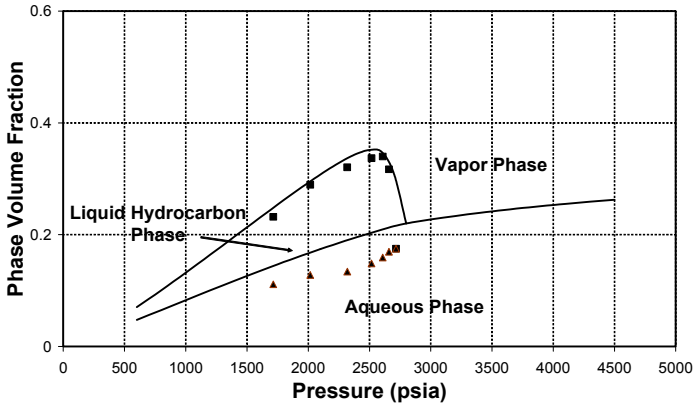

Figure 6.9 Volume fraction curves for Mixture 4 in Table 6.1 at 145 °F with PR equation.

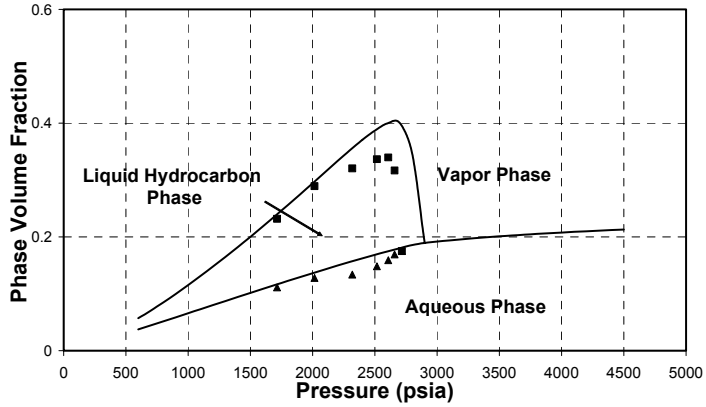

Figure 6.10 Volume fraction curves for Mixture 4 in Table 6.1 at 145 °F with SAFT equation.

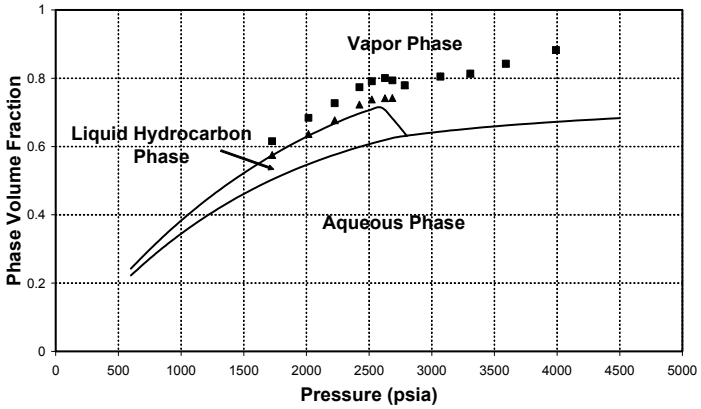

Figure 6.11 Volume fraction curves for Mixture 5 in Table 6.1 at 145 °F with PR equation.

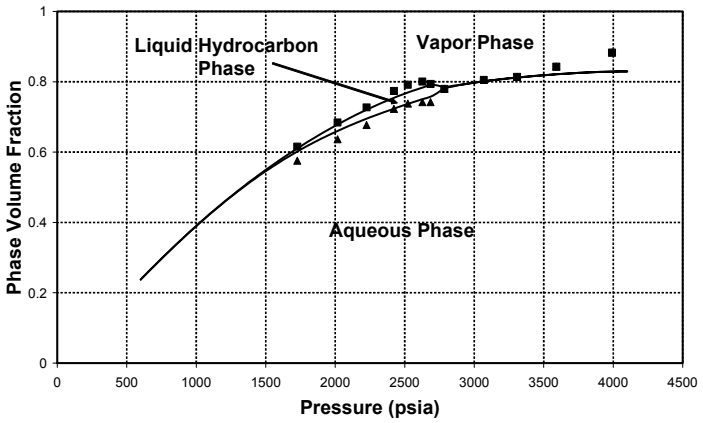

Figure 6.12 Volume fraction curves for Mixture 5 in Table 6.1 at 145 °F with SAFT equation.

7. SAFT Based Interfacial Tension Model with Gradient Theory

Padmakar Ayyalasomayajula and Mukul M. Sharma

ABSTRACT

SAFT equation of state is used with the generalized van der Waals gradient theory to evaluate the inhomogeneous influence parameter c for several non-polar and polar mixtures, which give an excellent agreement with the pure component interfacial tensions. Interfacial tensions of several binary mixtures are also computed. A mixing interaction coefficient similar to the binary interaction coefficient for bulk fluids had to be introduced in certain cases so as to obtain better predictions. The effect of high temperature and pressure on the interfacial tension of methane-water and CO2-water mixtures is also presented.

INTRODUCTION

The earliest theoretical models for describing the forces acting near a fluid interface were studied as far back as the early 19^{th} century. Laplace [1] was the first to describe the intermolecular forces and their effect on capillary phenomena. He introduced a concept of internal pressure, which is the force per unit area needed to separate an infinite body of liquid into two semi-infinite bodies bounded by their surfaces. The quantity that arises is the work per unit area that is done to separate the two surfaces which is equal to twice the interfacial tension because of the creation of two new surfaces.

Van der Waals [2] presented the earliest gradient based model, which was later extended by Cahn and Hilliard [3]. Since then gradient theory has been used by various authors [4,5,6,7] to predict interfacial tensions of various mixtures with varying success. Carey et. al. [4,5], have used the Peng-Robinson equation of state as the underlying model for free energy and the chemical potential calculation whereas Cornelisse et al.[6] had used both the PR and APACT equation of state. Sanchez et al., [7] have used lattice fluid models with the gradient theory to predict interfacial tensions. In this study we have used the SAFT equation of state as it is widely considered [8] as a very accurate and realistic representation for polar mixtures.

GRADIENT THEORY

The gradient theory of inhomogeneous fluids has been discussed extensively in the literratue. Here we presently briefly the outline of the gradient theory as formulated by Davies et al., [9]. The Helmholtz's free energy can be divided into the ideal and the excess parts.

$$F[\rho(\mathbf{r})] = F^{id}[\rho(\mathbf{r})] + F^{ex}[\rho(\mathbf{r})] \tag{7.1}$$

The capital F denotes that we are referring to the total Helmholtz energy of the mixture. The ideal gas functional is known exactly.

N_i is the total number of molecules of component i and ρ is the total mixture density at the point r in space. The Helmholtz free energy across the interface is given by free energy gradient approximation obtained by assuming that the molar free energy f(r) is a function of the local density n(r) and all its derivatives at r and expanding about the homogeneous state to obtain gradients in the Cahn-Hilliard form:

$$F = \int \left[f(n) + \sum_{i,j} \frac{1}{2} c_{i,j} \nabla n_i \nabla n_j \right] d^3 r \tag{7.2}$$

The chemical potential of species i given by

$$\mu_i = \frac{\partial F}{\partial n_i} \tag{7.3}$$

The chemical potential of component i computed from the integral equation (1) with minor rearrangement can be written as

$$\sum_j \nabla.(c_{ij} \nabla n_j) - \frac{1}{2} \sum_{k,j} \frac{\partial c_{kj}}{\partial n_i} \nabla n_k \nabla n_j = \frac{\partial \omega}{\partial n_i} \tag{7.4}$$

where ω is a thermodynamic potential defined by

$$\omega(n) \equiv f(n) - \sum_i n_i \mu_i \tag{7.5}$$

Equation (7.3) above is a non-linear ordinary differential equation with appropriate boundary conditions, which can be solved to obtain the interfacial profile of components. The microstructure of the interface, whether it is planar, spherical or a thin-film is determined by the total Helmholtz free energy function (ω).

For a planar system, the interfacial density is a function of only the interfacial distance $n_i = n_i(x)$, which reduces the partial differential equation (7.3) to the one-dimensional form,

$$\sum_{j=1}^{n} c_{ij} \frac{\partial^2 n_i}{\partial x^2} = \mu_i^0(n) - \mu_i(n) \quad i = 1, n \tag{7.6}$$

from which the interfacial tension of the system is given as

$$\gamma = \sum_{i,j} \int_{-\infty}^{\infty} c_{ij} \frac{dn_i}{dx} \frac{dn_j}{dx} dx \tag{7.7}$$

Gradient theory is comparatively mathematically simple and presents the physics of interfaces very clearly. The homogeneous system free energy and the influence parameters for the inhomogeneous fluid are separated clearly.

If we consider a one component fluid for a planar interface, the boundary conditions are $n(x) \to n^{(1)}$ as $x \to -\infty$ and $n(x) \to n^{(2)}$ as $x \to +\infty$, where $n^{(i)}$ is the bulk composition of phase i. For a one-component system, the above boundary conditions simplify as follows,

$$dx = \sqrt{\frac{c}{2}} \frac{dn}{\sqrt{\Delta \omega(n)}} \tag{7.8}$$

where $\Delta \omega(n) \cong \omega(n) - \omega_B$.

With the above simplification the interfacial tension for a pure component is given by

$$\gamma = \sqrt{2} \int_{n_g}^{n_l} \left[c \, \Delta \omega(n) \right]^{1/2} dn \tag{7.9}$$

Geometrically $\Delta\omega(n)$ can be represented as the vertical line between the curve of $f_0(n)$ versus n and a straight line touching f_0 at the vapor and liquid densities, n_g and n_l.

Another simplifying assumption to the above expression is that the cross interaction parameter also known as the influence parameter is taken to be independent of the density and hence can be taken outside of the integral.

One of the most elegant approaches which has been found to be extremely useful is the space transformation first suggested by Carey et al., [10].

$$y = \tanh x \tag{7.10}$$

Using this transformation the governing equations above can be written as

$$\sum_{j=1}^{n} c_{ij}\left[(1-y^2)^2\frac{\partial^2 n_i}{\partial y^2}-2y(1-y^2)\frac{\partial n_i}{\partial y}\right]=\mu_i^0(n)-\mu_i \quad i=1,n \tag{7.11}$$

The boundary conditions in the transformed conditions are

$$\begin{aligned} n &\to n^{I} \quad \text{from } y \to -1 \\ n &\to n^{II} \quad \text{from } y \to 1 \end{aligned} \tag{7.12}$$

It is to be noted that the boundary condition is now over a finite domain rather than over the infinite domain in the original formulation.

The cross interaction coefficient c_{ij} for mixtures is obtained from the pure component interaction coefficient by the following equation.

$$c_{ij}=(1-\chi_{ij})\sqrt{c_{ii}\,c_{jj}} \tag{7.13}$$

χ_{ij} is the mixing interaction coefficient defined for the interfaces. Usually, the binary interaction coefficient (k_{ij}) for the bulk phases is taken as the mixing interaction coefficient χ_{ij} for most cases. In some cases, however, the mixing interaction coefficient had to be adjusted to get a good prediction of the experimental interfacial tension values.

SAFT EQUATIONS OF STATE

The Statistical Associating Fluid Theory (SAFT) is an equation of state based on statistical mechanical theories and takes into account the intermolecular potential function. It is of special interest because it captures the major effect of the non-spherical nature and the association among molecules. We give the basic equations involved in SAFT in this section. The compressibility factor is given as

$$Z=1+Z^{hs}+Z^{chain}+Z^{assoc}+Z^{disp} \tag{7.14}$$

In the above expression Z^{hs} is the compressibility factor contribution due to the hard-sphere repulsion of the molecules and is given by the well-known Carnahan and Starling equation [11]

$$z_0^{hs}=\frac{P_{CS}^{hs}}{m\rho\,kT} \tag{7.15}$$

Z^{assoc} is the compressibility factor contribution due to association. The Helmholtz free energy for association has been proposed by Wertheim [13] and implemented by Huang and

Radosz [11,12],

$$Z^{assoc} = \sum_i x_i \frac{\mu_i^{assoc}}{RT} - \frac{a^{assoc}}{RT} \qquad (7.16)$$

The Helmholtz free energy contribution due to association bonding is given by

$$\frac{a^{assoc}}{RT} = \sum_{i=1,n} x_i^B \left[\sum_{\lambda_i=1,M_i} \left\{ \ln(Y^B_{(\lambda_i,i)}) - Y^B_{(\lambda_i,i)} \right\} + \frac{M_i}{2} \right] \qquad (7.17)$$

The most important term in the above expression is the $Y^B_{(\lambda i,i)}$ which is the mole fraction of molecules of i that are not bonded at the association bonding site λ_i, or in terms of Wertheim's terminology, the monomer density. The monomer density is dependent on the associating strength of the molecule, number of associating sites on each molecule as well as the molecular density of the mixture.

The non-spherical nature of the molecules is accounted for by Z^{chain} and is based on Chapman *et al*., [14]

$$Z^{chain} = \sum_i x_i (1 - m_i) \rho \left[\frac{\partial \ln g_{ii}(d_i)^{hs}}{\partial \rho} \right]_{T,x_j} \qquad (7.18)$$

Finally, any additional intermolecular effects, (e.g., quadrupolar forces) are accounted as perturbations to the reference potential and are given by Z^{disp} based on Chen and Kreglewski [15].

$$z^{disp} = m \sum_j \sum_k k D_{jk} \left[\frac{u}{kT} \right]^j \left[\frac{\zeta_3}{\tau} \right]^k \qquad (7.19)$$

The complete and more detailed SAFT equations are given elsewhere [11,12,13,14].

PARACHOR METHOD FOR EVALUATION OF SURFACE TENSION

We have also compared the results of the interfacial tension calculation by the Gradient Theory with the parachor calculations for mixtures. This is especially useful because parachors are very widely used especially in the petroeleum engineering community for the calcualation of interfacial tension in reservoir simulators. The earliest empirical model for prediction of interfacial energy is due to Macleod and Sugden using parachors [16,17,18]. The method developed by Macleod in 1923 and modified by Sugden in 1932 is given for pure fluids.

$$\gamma = [\Lambda (\Delta \rho)]^4 \tag{7.20}$$

where Λ is the parachor of the fluid and $\Delta\rho$ is the density difference between vapor and liquid of pure species. The above correlation can be extended to mixture [5].

$$\gamma = \sum_{i=1}^{n} [\Lambda_i \, (\rho_{ii} \, x_i - \rho_i \, y_i)]^4 \tag{7.21}$$

where n is the number of species i, Λ_i, is the parachor of species i, ρ_{II} is the density of denser phase and ρ_I is the density of the lighter phase. x_i and y_i are the compositions of the respective phases.

RESULTS AND DISCUSSION

A) Pure Components

Figure 7.1 shows the interfacial tension of some pure non-polar compounds like CO_2 and n-alkanes. We observe that SAFT is able to predict the interfacial tension using the gradient theory fairly accurately. We note that the interaction parameter (c_{ij}) has been obtained by fitting the experimental interfacial tension value at a single temperature for each compound. The average absolute deviation between the predicted values and experimental interfacial ranges from about 1.1 % for Nitrogen to less than 10 % for decane. Similarly Figure 7.2 shows the interfacial tension calculation for polar compounds like n-alcohols and water. Since the SAFT equation of state has been shown to do particularly well for polar compounds, we observe that the interfacial tension predictions for the polar compounds are also very good. The average absolute deviation ranges for 1.7 % for ethanol to about 10 % for water over a wide range of temperatures.

Table 7.1: Pure component interaction parameter with the SAFT equation

Mixtures

B) CO_2 – Decane Mixture

Next we present the SAFT-GT predictions of the interfacial tensions of mixtures. Figure 7.3 shows the interfacial profile for a CO_2 – decane mixture at 344 K and 0.94 MPa. The interfacial tension for this mixture predicted is 8.29 mN/m which compares very well

with the experimental values. We observe that for all compositions of the equilibrium mixture the interfacial profile of decane is monotonically increasing. CO_2 on the other hand shows increased surface concentration at intermediate as well as high concentrations of CO_2. Figure 7.4 shows the interfacial tension of the mixture as a function of CO_2 concentration in the liquid phase. We see that the SAFT based IFT model does a fairly good job of predicting the interfacial tension of this mixture. The mixing interaction coefficient for the interface (χ_{ij}) used in this case is same as the bulk phase binary interaction coefficient. We also show the parachor calculations of interfacial tension for this mixture and we observe that the parachor predictions are off at very low CO_2 concentrations in the liquid phase.

C) Ethanol – Heptane Mixture

Figure 7.4 shows the interfacial profile of an ethanol-heptane mixture, which is a non-polar-polar mixture. Note that this is essentially a three component mixture as nitrogen is added to the mixture to form a gas-liquid interface. At the system pressure of 0.101 MPa and temperature of 298.15 K ethanol and heptane form a single-phase binary mixture over the entire heptane concentration range, so that we measure the interfacial tension over nitrogen. The interfacial profiles of heptane is monotonously increasing whereas ethanol exhibits slight interfacial activity. On the other hand, we observe that when there is significantly small amount of ethanol present in the liquid phase (Figure not shown) the interfacial profiles of ethanol are monotonously increasing and heptane exhibits a slight interfacial activity. At intermediate ethanol concentrations it is interesting to note that; ethanol shows an increased interfacial activity whereas the heptane concentration is suppressed in the interfacial region. This is because ethanol is a polar molecule so that the polar sites tend to be localized near the interface. We observe that SAFT together with gradient theory provides very good predictions of interfacial tension of the ethanol-heptane mixture as shown in Figure 7.6. The mixing interaction coefficient for the interface (χ_{ij}) used in this case is again the same as the bulk phase binary interaction coefficients. On the other hand, we observe that the parachor calculatons significantly over predict the interfacial tension of this mixture.

D) Methanol-Water Mixture

Next we present the results for a methanol-water mixture at 263.15 K and 0.101 MPa.

Here again we introduce nitrogen in the mixture so as to be able to calculate the tension of the vapor-liquid interface. In this case the cross-interaction parameter for the binary mixture (χ_{ij}) for predicting the interfacial profiles of this mixture. It is interesting to note, however, that even for two very different values of mixing interaction coefficients (χ_{ij} = 0 and 1), we have been able to predict the interfacial tension of the mixture accurately as shown in Figure 7.7. Again, the SAFT predictions are much better than the parachor calculations.

E) Ethanol-Water Mixture

Figure 7.9 show the interfacial tension predictions with both SAFT – Gradient Theory and the parachor calculations for ethanol-water mixture at 288.15 K and 0.101 MPa. Nitrogen is present as a third component to provide a vapor-liquid interface. The behavior observed in the interfacial profiles is similar to what we have seen earlier in the methanol water mixtures. As low concentrations of ethanol the profiles are monotonic. As we increase the water concentration the water profile is monotonic whereas ethanol shows increased interfacial activity as shown in Figure 7.8. The mixing interaction coefficient of the interface (χ_{ij}) is set to zero, which results in very good interfacial tension predictions. The parachor predictions on the other hand are not very accurate.

F) Methane-Water Mixture

Figure 7.10 shows the SAFT predictions of the interfacial tension variation with pressure for a methane-water mixture at 25 C along with experimental data and parachor predictions. The mixing interaction coefficient for interfaces (χ_{ij}) had to be adjusted to 0.35 so as to obtain a reasonable match with the experimental measured values. We observe that SAFT predicts the interfacial tension very well with the adjustment of mixing interaction coefficient at this temperature whereas the parachor predictions are very poor especially at high pressues, which are typically experienced in underground gas reservoirs. Next we study the effect of temperature on the interfacial tension for this same mixture. Figure 7.11 shows the interfacial tension of methane-water mixtures at 106 C and 176.6 C using the mixing interaction given earlier for the 25 C case. The interfacial tensions predictions with the mixing interaction coefficient of are fairly accurate without further adjusting the mixing interaction coefficient for this case

CONCLUSIONS

We have used the SAFT equation of state with the gradient theory to predict the interfacial tension of pure components and mixtures. We have shown that this model predicts the interfacial tension of both non-polar and polar, pure components very accurately. We have introduced the pure component interaction parameters for the calculation of interfacial tension with the SAFT equation. We have also presented interfacial tension calculations for non-polar and polar mixtures. We have shown that SAFT with the gradient theory does a fairly good job of predicting interfacial tension of these mixtures. The interfacial tension of water-ethanol, water-methanol and a few other mixtures have been satisfactorily predicted .by the SAFT equation of state by introducing a mixing interaction coefficient. We have studied the effect of temperature and pressure on a methane-water mixture with this and have found that the theory holds well at different temperatures and pressures although we need to adjust the mixing interaction coefficients for interfaces (χ_{ij}) initially.

NOMENCLATURE

$F(\rho)$ *Helmholtz free energy functional*

γ *Surface tension/ interfacial tension (N/m)*

μ *chemical potential (J/mol)*

c_{ij} *cross-interaction coefficient between species i and j*

χ_{ij} *mixing interaction coefficient for interfaces between species i and j*

n_i *molar density (mol/m^3)*

x_i *mole fraction of component i*

k_{ij} *binary interaction coefficient between component i and j*

Z *compressibility factor*

Z^{hs} *hard-sphere compressibility factor*

Z^{chain} *chain compressibility factor*

Z^{assoc} *association compressibility factor*

Z^{disp} *dispersion compressibility factor*

$P^{hs}{}_{CS}$ *Carnahan Hard-Sphere pressure*

ρ *density of the mixture*

a^{assoc} *association Helmholtz free energy*

μ_i^{assoc} *association chemical potential of component i*

$Y^{B}{}_{\lambda i,i}$ *mole fraction of molecules of i not bonded at associating site* λ_i

M_i *number of associating sites available on molecule i*

m_i *chain length of component i*

g_{ii} *radial distribution function of component i*

m *average chain length of mixture*

u_{ii} *dispersion energy of component i*

D_{jk} *Chen and Kreglewski constants for dispersion potential*

ξ_3 *reduced density*

τ *closed packing density limit (0.74048)*

REFERENCES

1. Laplace, P.S. , Traite de Mecanique Celeste; Supplement au dixieme livre, Sur l Action Capillaire, 1806, Courcier, Paris.
2. Van der Waals, J.D., and Kohnstamm, P., *Lehrbuch der Thermodynamik*, Vol. 1. Leipzig, 1908.
3. Cahn, J.W., and Hilliard, J.E., Free Energy of a Nonuniform System. I. Interfacial Free Energy, *J. Chem. Phys*., 28, 258, 1958.

4. Carey, B.S., Scrivenn, L.E., and Davis, H.T., Semiempirical theory of surface tensions of pure normal alkanes and alcohols, *AIChE Journal*, 24, 6, 1076 (1978).

5. Carey, B.S., Scrivenn, L.E., and Davis, H.T., Semiempirical theory of surface tensions of Binary Systems, *AIChE Journal*, 24, 6, 1076 (1978).

6. Cornelisse, P.M.W., Peters, C.J., and de Swaan Aarons, J., Application of the Peng-Robinson Equation of State to Calculate Interfacial Tensions and Profiles at Vapour-Liquid Interfaces, *Fluid Phase Equilibria*, 82, 119 (1993).

7. Poser, C.I., and Sanchez, I.C., Interfacial tension theory of low and high molecular weight liquid mixtures, *Macromolecules*, 14, 361 (1981).

8. Muller, E.A., and Gubbins, K.E., Molecular-Based Equations of State for Associating Fluids: A Review of SAFT and Related Approaches, *Ind. Eng. Chem. Res*., 40, 2193 (2001).

9. Davis, H.T., and Scriven, L.E., Stress and structure in fluid interfaces, Chapter in *Advances in Chemical Physics*, Vol. XLIX, Wiley & sons, New York, (1982).

10. Carey, B.S., *Molecular thermodynamics of multicomponent interfaces*, Ph.d Thesis, University of Minnesota, (1979).

11. Huang, S.H., and Radosz, M.,: "Equation of State for Small, Large, Polydisperse, and Associating Molecules", Ind. Eng. Chem. Res. 1990, 29, 2284-2294

12. Huang, S.H., and Radosz, M.,: "Equation of State for Small, Large, Polydisperse, and Associating Molecules: Extension to Fluid Mixtures", Ind. Eng. Chem. Res. 1991, 30, 1994-2005.

13. Wertheim, M.S., "Fluids with Highly Directional Forces. III. Multiple attraction sites", J. Stat. Phys., 1986a, 42, 459-476.

14. Chapman, W.G., Gubbins, K.E., Jackson, G., and Radosz, M.,: "New Reference Equation of State for Associating Liquid", Ind. Eng. Chem. Res., 1990, 29, 1709-1721.

15. Chen, S.S., Kreglewski, A., Ber. Bunsen-Ges. Phys. Chem., 1977, 81, 1048.

16. Macleod, D.B., "On a relation between surface tension and density", *Trans. Faraday Soc*., **19**, 38 (1923).

17. Sugden, S., "The variation of surface tension with temperature and some related functions", *J. Chem. Soc*., **125**, 32 (1924).

18. Sugden, S.; "A relation between surface tension, density, and chemical composition", *J. Chem. Soc*., **125**, 1177 (1924).

19. Vargaftik, N.B., Tables on the Thermophysical properties of Liquids and Gases, John Wiley & Sons, New York, 1970.

20. Hsu, J-C., Nagarajan, N., and Robinson Jr., R.L., , "Equilibrium Phase Compositions, Phase Densities, and Interfacial Tension for CO_2 +Hydrocarbon Systems. 2. CO_2 + n-Decane", *J. Chem. Eng. Data*., 30, 485 (1985).

21. Papaioannou, D., Panayiotou, C.G., *J. Chem. Eng. Data*, 39(3), 457 (1994).

22. Teitelbaum, B. Ya., Gortalova, T.A., Ganelina S.G., "The surface layer of liquid systems. I. Surface tension of binary liquid systems in the instance of surface separation of layers", *Kolloid. Zhur.,* 12, 294, (1950).

23. Birumshaw, L.L., *J. Chem. Soc.,* 121, 887 (1922).

24. Sachs, W., and Meyn, V., "Pressure and temperature dependence of the surface tension in the system natural gas/water. Principles of investigation and the first precise experimental data for pure methane/water at 25 C up to 46.8 M Pa", *Colloids and Surfaces, A: Physicochemical and engineering Aspects*, 94, 291, (1995).

Component	Interfacial Tension Parameter (c_{ii}), J/m^5mol^2	% Average Absolute Deviation	Parachor
Nitrogen	1.38e-20	1.0	35.00
CO_2	2.33e-20	3.5	77.50
Methane	2.79e-20	5.0	77.90
Propane	2.33e-20	2.6	
Butane	2.33e-20	4.4	
Heptane	4.63e-19	6.9	311.36
Decane	7.52e-19	10.0	431.20
Methanol	2.77e-20	7.9	89.60
Ethanol	5.26e-20	1.8	126.80
Butanol	1.29e-19	7.6	
Water	9.32e-21	1.7	52.60

Table 7.1: Pure component interaction parameter with the SAFT equation.

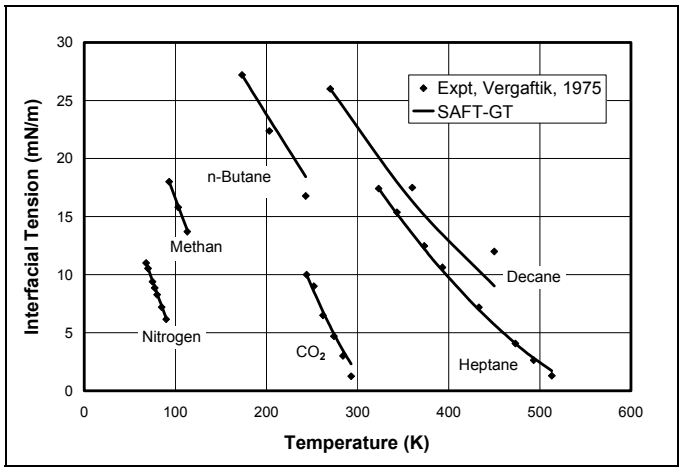

Figure 7.1: Interfacial tension calculations of non-polar compounds

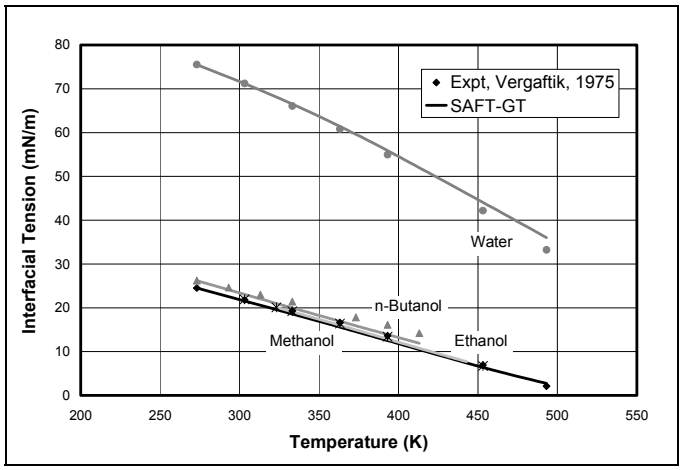

Figure 7.2: Interfacial tension calculations of polar compounds

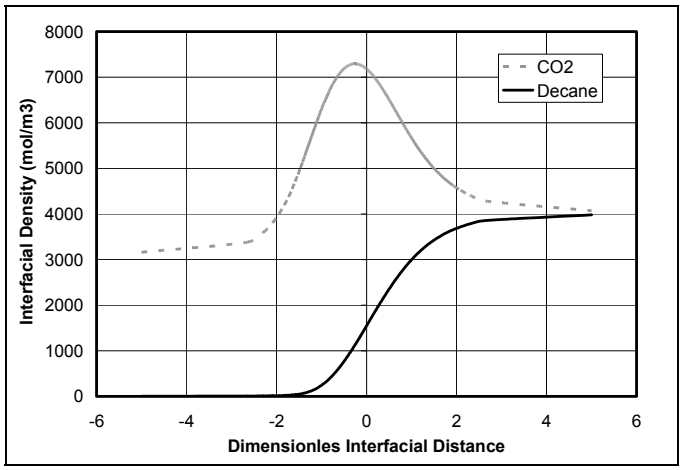

Figure 7.3: Interfacial profile of CO_2 -Decane mixture at 344 K and 0.94 MPa

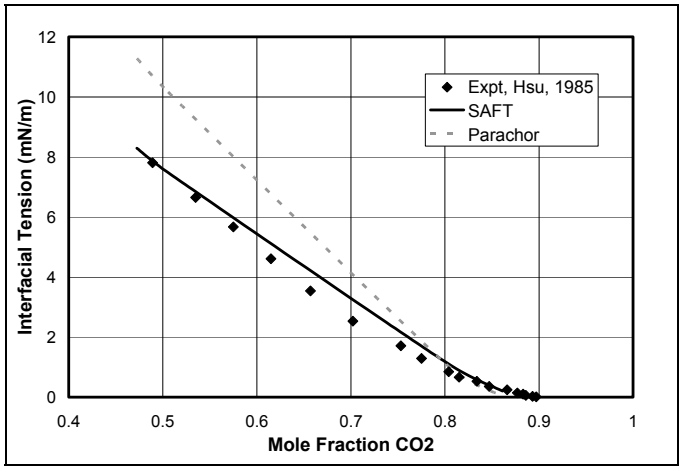

Figure 7.4: Interfacial Tension of CO_2 – Decane mixture with equilibrium CO_2 composition

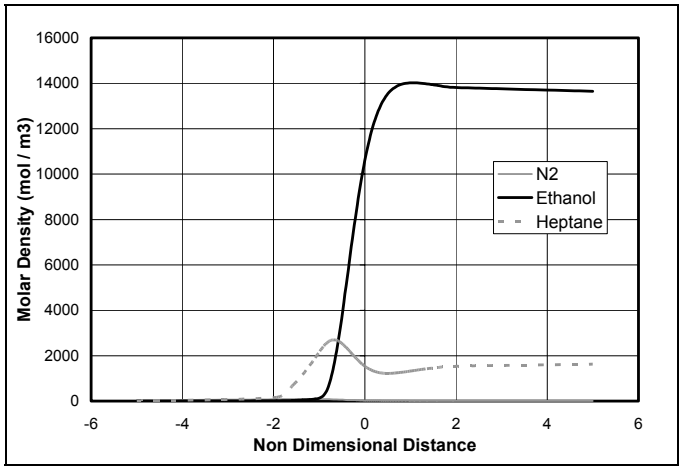

Figure 7.5: Interfacial Tension Profile for 87.7 % Ethanol - 7.47 % Heptane Mixture at 0.101 Mpa, 298.1 K

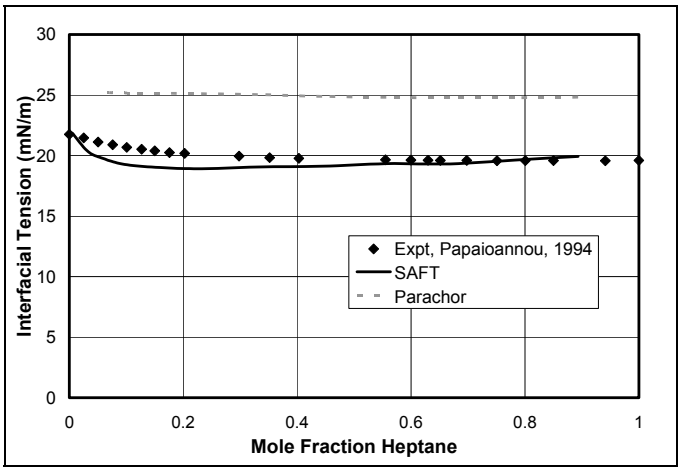

Figure 7.6: Interfacial Tension of Ethanol – Heptane mixture with equilibrium liquid ethanol composition

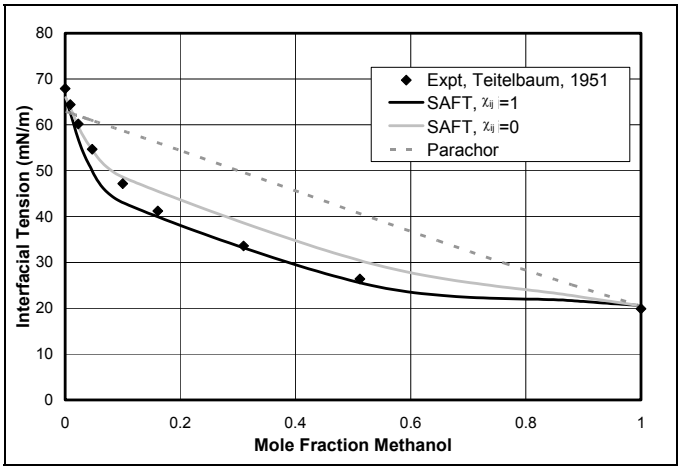

Figure 7.7: Interfacial Tension of 10.25 % Methanol – 89.75 % Water Mixture at 0.101 MPa, 298.1 K

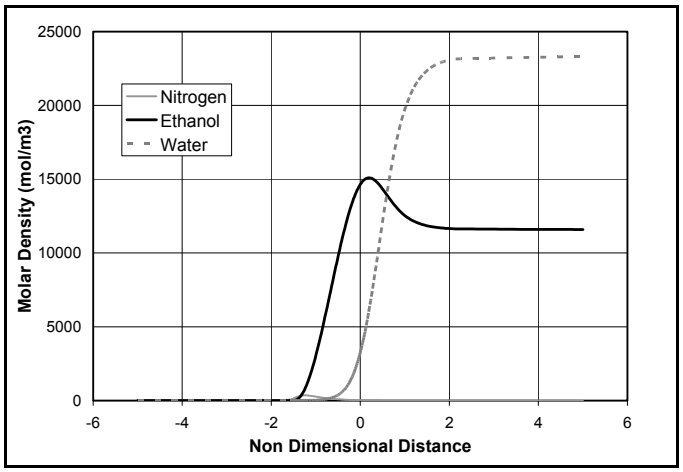

Figure 7.8: Interfacial profile of 33.7 % Ethanol – 66.2 % Water mixture at 0.101 MPa and 288.1 K

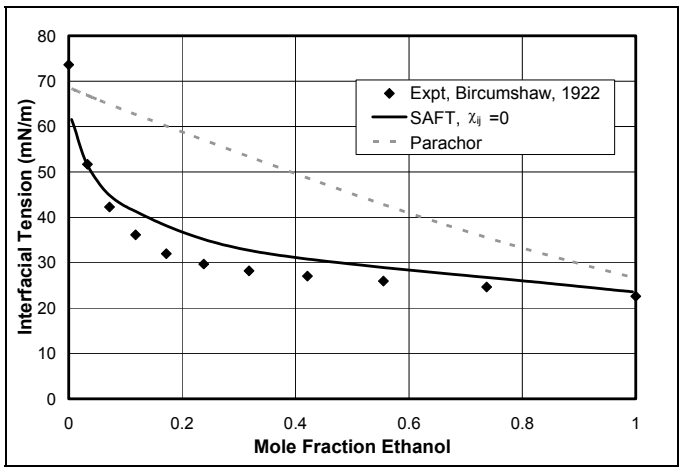

Figure 7.9: Interfacial tension of ethanol-water mixture at 0.101 MPa and 288.1 K

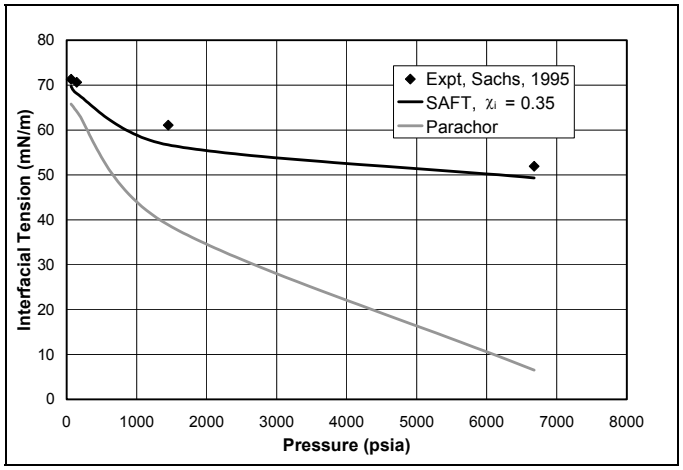

Figure 7.10: Interfacial tension variation with pressure for mthane-water mixture at 25 C

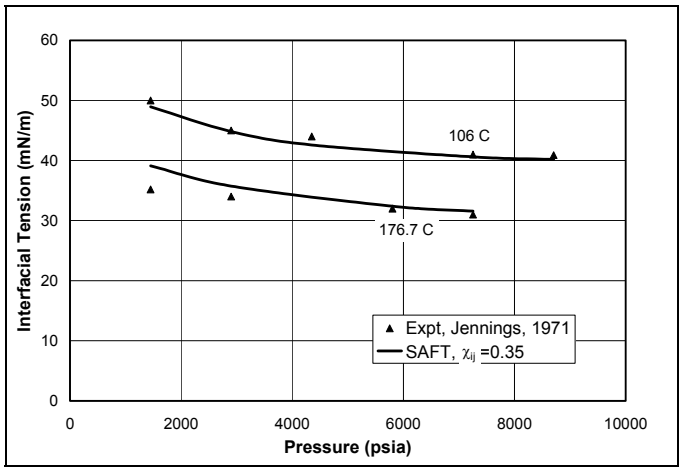

Figure 7.11: Interfacial tension variation with temperature for mthane-water mixture

8. Estimation of Relative Permeability Curves and Wettability from Transient Pressure Drop Measurements

ABSTRACT

In this chapter a method is provided for the rapid determination of relative permeability curves and wettability from simple displacement experiments. The results for core flood experiments conducted on Texas Cream limestone and Berea sandstone are presented that illustrate the methodology.

The peak in the transient pressure drop response during displacement is found to be a very sensitive indicator of the curvature of the relative permeability curves. A simple curve-fitting algorithm is used to obtain the best fit to the transient pressure response during primary drainage and imbibition to obtain the water and oil exponents in a Corey type relative permeability model. It is shown that these exponents of the relative permeability curves provide a good initial estimate of the curvature of the relative permeability curves, which, in addition to the relative permeability end-points, can be used in reservoir simulators.

The ratio of dimensionless end-point pressure drop during primary drainage, normalized by viscosity ratio, to the dimensionless pressure drop during secondary imbibition is defined as a new wettability indicator. For oil-wet rocks, the Relative Permeability Wetting Index (RPWI) is greater than one, whereas, for water-wet rock the RPWI is less than one. For intermediate wet rock, the wetting index is observed to be close to one.

The methodology provided in this paper gives a rapid and convenient way of estimating both wettability and relative permeability curves without having to conduct capillary pressure or steady state relative permeability experiments, which can be very time consuming.

INTRODUCTION

The relative permeability to oil and water in rocks is measured either by an unsteady state method (1) or by a steady state displacement method. The wettability of a rock is measured by one of three quantitative methods: contact angle, Amott method, and the U. S. Bureau of Mines (USBM) method. Both wettability and relative permeability are strongly correlated for a given rock sample (2).

The steady-state experiments required to measure the relative permeability curves are time consuming and tedious. The end-point pressure drop as well as the fractional flow as a function of time is measured when using the JBN (1) method for obtaining the relative permeability from unsteady state data. Although the unsteady state method is faster than the steady-state method, measuring the fractional flow of water as a function of pore volumes injected can be challenging since only a few samples are obtained where oil and water both are produced during the displacement experiment. This provides poor resolution over the course of the displacement experiment. Measurement of the volumes of oil and water recovered is a discrete sampling process and can have large errors. At high mobility ratios and in high rate displacements, the experiment is affected by viscous instability (3).

An alternative strategy is to measure the pressure drop across the core continuously and use this as an indication of the relative permeability of the core. This strategy has been followed in this paper and it is shown that good estimates of relative permeability are obtained using the method. It should be noted that the methodology illustrated in this paper assumes a Corey (4) type saturation dependence for the relative permeability. This assumption can in principle be relaxed. If, however, this assumption is used, the relative permeability obtained may only be approximate particularly for rocks that do not follow a Corey type relative permeability relationship. The relative permeability curves obtained may be used as a first estimate in reservoir simulators because of the simplicity of the method and the fact that results can be obtained in a relatively short period of time.

The proposed method of determining the relative permeability from transient pressure drop measurements provides a simple alternative for approximately measuring the relative permeability curves and defining the wettability of the core using relatively simple displacement experiments. The method takes advantage of the fact that pressure drop can be measured continuously and much more accurately than the fractional flow of oil at the outlet of a core.

The wettability of reservoir core samples is traditionally measured using capillary pressure curves. The combined Amott-USBM index (5) has been extensively used as an indicator of wettability in core samples. The procedure involves conducting spontaneous and forced imbibition and drainage cycles that are typically conducted in a centrifuge. Although good indications of wettability that distinguish between water-wet, oil-wet, intermediate wet

and mixed wet conditions are obtained, this process is time consuming and may require several days of experimentation to complete. A comprehensive review of the trends in wettability measurement is available in a paper by Anderson (6).

Contact angle measurements (7) require thoroughly clean and smooth sample surfaces. The measurements are localized and do not give a representative value for the reservoir rock. The Amott method suffers from its insensitivity at neutral wetting states and the USBM is time consuming. In this paper, we present a method that allows us to obtain a wettability index directly inferred from displacement experiments that need to be conducted for obtaining the relative permeability curves. The wettability index is defined on the basis of pressure drops measured during the drainage and imbibition displacement processes.

OBTAINING RELATIVE PERMEABILITY CURVES

The relative permeability model assumed is the Corey type model where the relative permeability is a function of the normalized saturation as detailed below.

$$k_{ro}\left(\overline{S_o}\right) = k_{ro}{}^{\max} \overline{S_o}^{no}$$

$$k_{rw}\left(\overline{S_o}\right) = k_{rw}{}^{\max} \left(1 - \overline{S_o}\right)^{nw}$$

where $\overline{S_o} = \dfrac{S_o - S_{or}}{1 - S_{or} - S_{wr}}$.

Mass conservation equations are used to describe the multi-phase fluid flow in the core and a relationship is derived between the saturation and the distance along the core, the pressure drop across the core and the time elapsed from injection of displacing fluid. The derivations of these relationships are discussed in Appendix A. The transient pressure drop across the core is dependent on the endpoint relative permeability, and the exponent of the Corey model. The pressure drop across the core is related to the spatial integral of fractional flow and the relative permeability by the following equation (see Appendix A for derivation),

$$\Delta p = \frac{q\mu_o}{kA} \int_0^{X_{sof}} \frac{f_o}{k_{ro}} dx + \frac{q\mu_w}{kA} \int_{X_{sof}}^{L} \frac{f_w}{k_{rw}} dx .$$

A numerical routine was programmed to automatically history match the pressure history curves from experimental data and obtain the Corey exponents. These exponents together with the end-point relative permeabilities and the residual saturations (which are

obtained from the experiments) completely define the oil and water relative permeability curves.

Figure 1 shows the pressure drop across a core during primary imbibition for different Corey exponents. It is evident that the pressure drop transient curve is very sensitive to the Corey exponents. Any match to the pressure drop data will, therefore, provide and excellent estimate of the Corey exponents.

INFERRING WETTABILITY

The pressure drop transient history also gives us a good estimate of the wettability of the rock. The end-point pressure drop is the pressure drop measured across the core after a large number of pore volumes of displacing fluid have been flowed through it and the pressure drop does not show any change with additional injection of the displacing fluid. It is made dimensionless by dividing the measured pressure drop by the single-phase (brine) pressure drop ΔP_{1-p}.

The end-point pressure drop for drainage (oil displacing brine) measured from experiment is denoted by, $\Delta P^{o}{}_{o/w}$ (which is equal to $\frac{q_o \mu_o L}{k k^{o}_{ro}}$). The dimensionless oil displacing water pressure drop is then given by $\frac{\Delta P^{o}{}_{o/w}}{\Delta P_{1-p}}$. This is further normalized with the ratio of water to oil viscosities to give $\frac{\Delta P^{o}{}_{o/w}}{\Delta P_{1-p}} \frac{\mu_w}{\mu_o}$.

The dimensionless end-point pressure drop for imbibition (brine displacing oil) is similarly defined as $\frac{\Delta P^{o}{}_{w/o}}{\Delta P_{1-p}}$.

The ratio of the dimensionless end-point pressure drops is defined as a relative permeability wettability index,

$$RPWI = \left[\frac{\Delta P^{o}{}_{o/w}}{\Delta P^{o}{}_{w/o}} \frac{\mu_w}{\mu_o} \right].$$

This indicator of wettability (RPWI) is significantly less than one if the core is water-wet and is significantly greater than one if the core is oil-wet. A RPWI close to one indicates that the core is intermediate-wet.

EXPERIMENTAL METHODS

Experiments were conducted on fluid flow through cylindrical cores, which were either oil-wet or water-wet (details of the experimental procedure are presented in the following subsection). The pressure drop across the core was obtained at various points in time. Also, the end-point saturations were measured from the volumetric data collected during the experiments. This enables us to determine the end-point relative permeability and residual saturation for both the oil and the water phases.

FLUIDS USED

The fluid system-3 wt% brine/decane was chosen for Berea sandstone with the objective of obtaining near equal mobility ratio displacement and also minimize the pressure drop across the core. The 3-wt% brine/crude oil (AK-93 Prudhoe Bay) system is used to perform displacements in the Texas Cream limestone.

CORE PREPARATION

Two cylindrical cores (1 inch in diameter and 6 inches in length) were cut from a homogenous slab of Berea sandstone using tap water as the cutting fluid. The cores were dried in an air-oven at 100°C for at least 24 hours and then evacuated and saturated directly in the Hassler apparatus, which is later used for the core flooding experiments.

Berea sandstone in its original state is water-wet. To artificially render the cores oil-wet the cores were treated with a wettability-altering agent, a 1% v/v solution of OTS (octadecyltrichlorosilane). Details of the core treatment procedure are given in Appendix B.

A limestone core was cut from a slab of rock after making sure there were no vugs or any major inconsistencies. The core is then cut into lengths of 2 inches and left in an oven for drying for at least 24 hours at 100 ^{o}C. These cores are then evacuated in the Hassler apparatus and vacuum saturated in the Hassler apparatus.

COREFLOOD EXPERIMENTS

Water-Wet Rock

3-wt% brine is first de-aerated to eliminate any dissolved gases. This brine is stored in an airtight container and later used to saturate the evacuated cores using a burette. The volume of brine used to saturate the core is read from the burette and is used to calculate the porosity of the core.

In primary drainage, decane displaces the brine. Decane is injected at a constant flow rate. The pressure drop is recorded across the core continuously and the displaced brine is collected at the outlet end of the core. The flooding is carried out for more than 25 pore volumes until the change in volume of brine collected is negligible. The residual saturation of brine is also calculated using a simple volume balance.

The primary drainage is followed by an imbibition step where brine is injected into the core from the same inlet end at a constant rate. The flow rate is maintained the same as that during primary drainage and the pressure drop across the core is recorded continuously. The displaced decane is collected at the outlet. Brine injection is performed for more than 25 pore volumes until the change in volume of decane collected is negligible. Secondary drainage is performed by injecting decane at the same flow rate and the pressure drop across the core is recorded continuously. The displaced brine is collected at the outlet to calculate the residual saturation of brine in the core.

The above procedure was repeated for a 3-wt% brine/crude oil system instead of decane. In addition to the other measurements listed above, the outlet fluid was collected in a fractional collector periodically to measure the oil-to-water ratio.

Another set of experiments was conducted on Berea sandstone with the same sequence as above but with an ageing step of 20 days after primary drainage (the core was left for 20 days at residual water saturation).

Oil-Wet Rock

Berea sandstone cores were made oil-wet by saturating with OTS solution as described in Appendix B. The oil-wet core was saturated with brine. Decane was then used to displace the brine. The pressure drop across the core is measured and the volume of brine collected at the outlet is used to calculate the residual saturation.

Mixed-Wet Rock

Primary imbibition in the limestone rock was carried out in the same manner as the Berea sandstone core. The brine is displaced by crude oil injected at constant rate through an accumulator. The outlet fluid was collected in a fractional collector periodically in addition to the other measurements listed above. The core was left to age in the core holder for 20 days after primary drainage after which secondary imbibition and secondary drainage steps were conducted.

RESULTS AND DISCUSSION

OBTAINING RELATIVE PERMEABILITY FROM PRESSURE DROP TRANSIENT CURVES

Figures 1 to 4 show the effect of Corey exponents and the mobility ratio on the shape of the pressure drop history for a Berea sandstone core. The shapes show large sensitivity to the Corey exponents and the mobility ratio. Increasing the value of the exponents signifies an increase in the curvature of the relative permeability curves. As the value of the exponent increases, the magnitude of the peak (in the case of a drainage process in a water-wet core) increases. An increase in both water and oil exponents results in an increase in magnitude of the peak pressure drop with the water exponent showing a larger effect (Figure 1a) than the oil exponent (Figure 2a). Figures 1b and 2b show the effect of changing the exponents on the position of the peak. An increase in the water exponent advances the occurrence of peak slightly (Figure 1b) while an increase in oil exponent delays the occurrence of the peak (Figure 2b). Figure 3 shows the effect of increasing both the oil and water exponents. The effect of increase of oil and water exponents appear to be additive in creasing the pressure drop peak magnitude. The magnitude of the peak also varies with the mobility ratio. When the end-point oil mobility ratio is increased, the magnitude of the peak, in the case of a drainage process in a water-wet core, decreases (Figure 4).

Figures 5 and 6 show a history match of the experimental pressure drop data for a water-wet Berea sandstone core (secondary imbibition and secondary drainage). The pressure drop approaches a constant value after injection of many pore volumes and this gives us the end-point relative permeability to water and decane respectively. In this sample, the end-point pressure drop for decane (Figure 5) is low so that the end-point relative permeability of decane is high. The opposite is true for the water relative permeability. An automatic history match of the pressure drop transient with equation A-16 gives the Corey exponents. The only

parameters varied for the match are the exponents (n_o and n_w), since the mobility ratio is fixed by the experiment. Two sets of exponents can be obtained from each of the displacement sequences.

Similarly, Figures 7 and 8 show the theoretical simulation of the pressure drop history for the secondary imbibition process and secondary drainage process in an oil-wet core. Here the end-point pressure drop for decane is high (Figure 7) i.e. the end-point relative permeability to decane is low. The Corey exponent parameters, which were estimated using the numerical history match routine, are listed in Table 1.

The relative permeability curves for water-wet and oil-wet cores can be obtained using the exponents from history matching and the end-point relative permeability from experiment and are shown in Figures 9 and 10. Figure 9 shows that, as expected, the relative permeability to water in a water-wet core is lower than the relative permeability to oil. On the contrary the relative permeability to water in an oil-wet core is higher than the relative permeability of oil. The curves also show hysteresis in the non-wetting phase, with the non-wetting phase imbibition curves showing lower relative permeabilities.

INFERRING WETTABILITY FROM PRESSURE DROP TRANSIENT CURVES

Figure 11 shows the pressure drop versus time data for primary drainage when decane is displacing the imbibed brine from a water-wet sandstone core. The pressure drop achieves a peak value at breakthrough and subsequently flattens out at large pore volumes injected.

Figures 12 and 13 show the pressure drop history for secondary imbibition and secondary drainage. The pressure drop for secondary imbibition is high due to the water-wet nature of the rock. For water-wet rocks, the flow of brine faces more resistance from the permeable media than does the oil flow.

Figures 14, 15 and 16 show the primary drainage, secondary imbibition and secondary drainage for the case of oil-wet Berea. Note that the three curves are similar to the trends observed for the same processes in a water-wet core. This is because the flow of a wetting fluid faces more resistance than a non-wetting fluid in permeable media irrespective of whether the fluid is oil or brine.

Figures 17, 18 and 19 show drainage and imbibition sequences in both oil-wet and water cores. The purpose of this sequence of fluids is to enable comparison of the pressure

drop profiles for rocks, which differ only in wettability. It is evident that not only are the equilibrium pressure drops dramatically different, but even the transient response is qualitatively different.

Figure 20 shows a plot of dimensionless pressure drop across a water-wet core versus pore volumes of fluid injected for primary drainage and secondary imbibition. The plot shows that the end-point pressure drops after injection many pore volumes of fluid differ significantly. Figure 21 shows a plot of dimensionless pressure drop across an oil-wet core versus pore volumes injected. The end-point pressure drop for primary drainage is significantly different from the end-point pressure drop for secondary drainage. However, in the oil-wet case, primary drainage end-point pressure drop is higher than the secondary drainage end-point pressure drop as compared to the water-wet case. This shows that the wetting liquid faces greater resistance to flow than the non-wetting liquid.

Figure 22 shows the comparison of dimensionless pressure drop for the limestone core that has been converted to mixed-wet by ageing in crude oil for tertiary drainage and tertiary imbibition. In the case of the mixed-wet core, the end-point pressure drops are close to each other, which indicates that, both the liquids face about equal flow resistance.

There is a significant difference in the ratio of end-point pressure drops among the three cases. This difference between the ratios of the pressure drops is an indication of the wettability. The Relative Permeability Wetting Index (RPWI) for each of the cores is given in Table 2.

Figure 23 shows the relative permeability curves (calculated using JBN method from fractional flow data) before ageing. Figure 24 shows the relative permeability curves after ageing between primary drainage and tertiary drainage in a limestone core. There is a marked increase in the end-point relative permeability to water and a decrease to that of oil. The residual saturation of water after tertiary drainage is lower than that after primary drainage. This observation leads us to believe that there has been a significant change in wettability from water-wet to a mixed-wet core because of ageing of the core at residual water saturation.

CONCLUSIONS

1) The results for core flood experiments conducted on Texas Cream limestone and Berea sandstone show that the pressure drop across the core increases to a peak value

and then drops to a steady state value gradually. In the case of a drainage process the end-point pressure drop is lower than for an imbibition process.

2) An analytical expression for the pressure drop across a core sample was derived as a function of Corey exponents and end-point relative permeabilities. It is shown that the pressure drop profile is significantly affected by the value of the Corey exponents and the end-point mobility ratio.
3) A method for automatic history matching of the pressure drop transient history with the analytical model is used to obtain the Corey exponents and hence the relative permeability curves.
4) A relative permeability based wetting indicator called RPWI is obtained from the pressure drop curves in displacement experiments. For oil-wet rocks, the wetting index (RPWI) is greater than one whereas for water-wet rock the RPWI is less than one. For intermediate wet (or mixed wet) rock, the wetting index is observed to be close to one. The proposed method to determine wettability is rapid, does not require time consuming capillary pressure measurements and is measured simultaneously with relative permeability curves. The method also easily accommodates cores of any length that are representative of the reservoir.
5) As expected a change in wettability from water-wet to oil-wet increased the water relative permeability and decreased the oil relative permeability for a Berea sandstone core. The residual oil saturation decreased and the residual water saturation remained approximately the same.
6) The relative permeability to oil is decreased and the relative permeability of water is increased when Texas cream limestone rock is aged at S_{wr}. The residual saturation of oil and the residual water saturation decrease slightly when the core is aged at S_{wr}. This reduction of residual water saturation at the end of a drainage process is desirable as the oil relative permeability increases with decreasing residual water saturation.

NOMENCLATURE

S_i - Saturation in phase i
ω_{ij} - Mass fraction of species i in j

ρ_i - Density of phase i

$\overrightarrow{\overrightarrow{K_{ij}}}$ - Dispersion tensor

$\overrightarrow{\overrightarrow{k_{ij}}}$ - Permeability tensor

p_i - Pressure in phase i at a given location

ϕ - Porosity of the permeable medium

p_c - Capillary pressure between two phases

Np - Number of phases(=2)

R_i - Reaction in phase i (=0)

f_i - Fractional flow of phase I

M_x - Mobility ratio of 'x'

q_w - Brine flow rate in cm^3/s

μ_w - Brine viscosity in cP

k_{rw} - Brine relative permeability

q_o - Oil flow rate in cm^3/s

μ_o - Oil viscosity in cP

k_{ro} Oil relative permeability

k - Absolute permeability of the core sample in mD

REFERENCES

33. Johnson, E. F., Bossler, D. P., and Naumann, V. O.: "Calculation of Relative Permeability from Displacement Experiments," Transactions of the American Institute of Mechanical Engineers (AIME) (1959) **216**, 370-372.
34. Anderson, G. W.: "Wettability Literature Survey - Part 5: The Effects of Wettability on Relative Permeability," *JPT* (November 1987) 1453.
35. Peters, E. J. and Khataniar, S.: "The Effect of Instability on Relative Permeability Curves Obtained by the Dynamic-Displacement Method," Society of Petroleum Engineers Reservoir Engineering Journal (Dec. 1987) 469-474.
36. Corey, A. T.: "Mechanics of Heterogeneous Fluids in Porous Media," Water Resources Publications, Fort Collins, Colorado, 1977.
37. Sharma, M. M. and Wunderlich, R. W.: "The Alteration of Rock Properties Due to Interactions With Drilling Fluid Components," Society of Petroleum Engineers (SPE) paper 14302, presented at the 60th Annual Conference and Exhibition of the SPE held in Las Vegas, NV, September 22-25,1985.
38. Anderson, G. W.: "Wettability Literature Survey - Part 2: Wettability Measurement," *JPT* (November 1986) 1246.
39. Neumann, A. W. and Good, R. J.: "Techniques of Measuring Contact Angles," Surface and Colloid Science,R.J. Good and R.R. Stromberg (eds.), Plenum Press, New York City (1979) 11, 31-91.

APPENDIX A

Derivation of equation describing the saturation distribution and pressure drop in a one-dimensional two-phase immiscible displacement (oil displacing brine).

Constitutive equations:

Mass conservation equation:

$$\frac{\partial W_i}{\partial t} + \vec{\nabla} \cdot \overrightarrow{N_i} = R_i \quad \text{(A-1)}$$

$$W_i = \phi \sum_{j=1}^{Np} \rho_j S_j \omega_{ij} + (1-\phi)\rho_s \omega_{is} \quad \text{(A-2)}$$

$$\overrightarrow{N_i} = \sum_{j=1}^{Np} \left(\rho_j \omega_{ij} \overrightarrow{u_j} - \phi \rho_j S_j \overrightarrow{\overrightarrow{K_{ij}}} \cdot \overrightarrow{\nabla \omega_{ij}} \right) \quad \text{(A-3)}$$

Momentum conservation equation:

$$u_j = -\lambda_{rj} \vec{\vec{k}} \cdot \left(\overrightarrow{\nabla p_j} + \rho_j \vec{g} \right) \quad \text{(A-4)}$$

$$p_j - p_n = p_{cjn}(S, \omega, x) \quad \text{(A-5)}$$

Consider a one-dimensional flow and neglecting the effect of capillary pressure, gravity and adsorption, we have for an immiscible displacement,

$$\omega_{oo} = 1$$

$$\omega_{wo} = 0$$

$$\omega_{ww} = 1$$

$$\omega_{ow} = 0$$

and making $u_i = u f_i$, where f_i is the fractional flow of phase i, we get,

$$\phi \frac{\partial S_o}{\partial t} + u \frac{\partial f_o}{\partial x} = 0 \quad \text{(A-6)}$$

$$\phi \frac{\partial S_w}{\partial t} + u \frac{\partial f_w}{\partial x} = 0 \quad \text{(A-7)}$$

Solving one of the above equations by method of characteristics gives the saturation distribution of both the phases.

Therefore we solve for the oil phase saturation distribution.

$$X\big|_{So} = \frac{qt}{A\phi}\frac{\partial f_o}{\partial S_o} \qquad \text{(A-8)}$$

The fractional flow derivative in the above equation can be estimated analytically by assuming a relative permeability model. In this case we assume the Corey[13] model as detailed below.

$$k_{ro}\left(\overline{S_o}\right) = k_{ro}{}^{\max}\,\overline{S_o}^{\,no} \qquad \text{(A-9)}$$

$$k_{rw}\left(\overline{S_o}\right) = k_{rw}{}^{\max}\left(1-\overline{S_o}\right)^{nw} \qquad \text{(A-10)}$$

$$\textbf{where } \overline{S_o} = \frac{S_o - S_{or}}{1 - S_{or} - S_{wr}}$$

We know that fractional flow of oil is given by,

$$f_o = \frac{\dfrac{k_{ro}\mu_w}{\mu_o k_{rw}}}{1+\dfrac{k_{ro}\mu_w}{\mu_o k_{rw}}} \qquad \text{(A-11).}$$

Substituting for the relative permeability expressions and after algebraic manipulations we get,

$$f_o = \frac{M_o\,\overline{S_o}^{\,no}}{\left(1-\overline{S_o}\right)^{nw} + M_o\,\overline{S_o}^{\,no}} \qquad \text{(A-12)}$$

Where M_o is called the mobility ratio of oil and is given by,

$$M_o = \frac{k_{ro}{}^{\max}\mu_w}{\mu_o k_{rw}{}^{\max}}.$$

Writing equation for saturation distribution as,

$$X\big|_{So} = \frac{qt}{A\phi}\frac{\partial f_o}{\partial \overline{S_o}}\frac{\partial \overline{S_o}}{\partial S_o} \qquad \text{(A-13)}$$

and after substituting for the derivatives we get,

$$X\big|_{So} = \frac{qt}{A\phi}\frac{M_o\,\overline{S_o}^{\,no-1}\left(1-\overline{S_o}\right)^{nw-1}\left[no+\overline{S_o}(nw-no)\right]}{\left[\left(1-\overline{S_o}\right)^{nw}+M_o\,\overline{S_o}^{\,no}\right]^2}\frac{1}{\left(1-S_{or}-S_{wr}\right)} \qquad \text{(A-14)}$$

From the above, after assuming suitable values of exponents and residual saturations, we can determine the saturation distribution with respect to distance and also time. However the above solution gives triple valued result for saturation, which can be corrected by doing a material balance around the displacing front. The position of the displacing oil front, $X\big|_{sof}$ is given by solving for $\overline{S_{of}}$ from the equation,

$$\frac{M_o \overline{S_{of}}^{n_o-1}\left(1-\overline{S_{of}}\right)^{n_w-1}}{\left[\left(1-\overline{S_{of}}\right)^{n_w}+M_o\overline{S_{of}}^{n_o}\right]^2}=\frac{M_o\overline{S_{of}}^{n_o}}{\left[\left(1-\overline{S_{of}}\right)^{n_w}+M_o\overline{S_{of}}^{n_o}\left[\overline{S_{of}}+\frac{S_{or}}{\left(1-S_{or}-S_{wr}\right)}\right]\right.} \quad \text{(A-15)}$$

The pressure drop in the permeable medium is then given by,

$$\Delta p=\frac{q\mu_o}{kA}\int_0^{X_{sof}}\frac{f_o}{k_{ro}}dx+\frac{q\mu_w}{kA}\int_{X_{sof}}^{L}\frac{f_w}{k_{rw}}dx \qquad \text{(A-16).}$$

A similar exercise for the brine displacing oil case gives the position of the displacing water front as,

$$X\big|_{Sw}=\frac{qt}{A\phi}\frac{M_w\overline{S_w}^{n_w-1}\left(1-\overline{S_w}\right)^{n_o-1}\left[n_w+\overline{S_w}\left(n_o-n_w\right)\right]}{\left[\left(1-\overline{S_w}\right)^{n_o}+M_w\overline{S_w}^{n_w}\right]^2}\frac{1}{\left(1-S_{or}-S_{wr}\right)} \quad \text{(A-17)}$$

Where $M_w=\dfrac{k_{rw}^{\max}\mu_o}{\mu_w k_{ro}^{\max}}$.

As earlier, the above solution gives triple valued result for saturation, which can be corrected by doing a material balance around the displacing front. The position of the displacing oil front, $X\big|_{swf}$ is given by solving for $\overline{S_{wf}}$ from the equation,

$$\frac{M_w \overline{S_{wf}}^{n_w-1}\left(1-\overline{S_{wf}}\right)^{n_o-1}}{\left[\left(1-\overline{S_{wf}}\right)^{n_o}+M_w\overline{S_{wf}}^{n_w}\right]^2}=\frac{M_w\overline{S_{wf}}^{n_w}}{\left[\left(1-\overline{S_{wf}}\right)^{n_o}+M_w\overline{S_{wf}}^{n_w}\left[\overline{S_{wf}}+\frac{S_{wr}}{\left(1-S_{or}-S_{wr}\right)}\right]\right.} \quad \text{(A-18)}$$

The pressure drop across the core at any time is then given by,

$$\Delta p=\frac{q\mu_o}{kA}\int_{X_{swf}}^{L}\frac{f_o}{k_{ro}}dx+\frac{q\mu_w}{kA}\int_o^{X_{swf}}\frac{f_w}{k_{rw}}dx \qquad \text{(A-19).}$$

APPENDIX B

PREPARATION OF OIL-WET CORES

The procedure for preparation of oil-wet core sample is described below. This procedure was used for making both Berea sandstone and Texas Cream limestone oil-wet.

1) The cores required to be made oil-wet are cleaned, dried in an oven for 24 hours and placed in the Hassler apparatus (with Viton Sleeve to prevent damage from Chloroform used later).
2) The cores are evacuated for 2 hours until the vacuum attains 30mmHg.
3) The cores are saturated with Decane by directly flowing it into the evacuated cores.
4) The decane imbibed is displaced with 50 pore volumes of a 1% by wt solution of OTS (Octadecyltrichlorosilane) in Chloroform.
5) The cores are allowed to sit in with the solution for about 15 minutes and then flushed with 50 pore volumes of chloroform.
6) The cores are removed from the core holders and placed in an oven to heat-dry at 80 degc.

Table 8.1 Calculated relative permeability's, residual saturation and Corey exponents.

	Water-wet (Decane-Water in untreated Berea)	Oil-wet (Decane-Water in treated Berea)	**Crude Oil-Water in Limestone**
k^o_{ro}	**0.730**	**0.061**	**0.540**
k^o_{rw}	**0.091**	**0.568**	**0.342**
S_{or}	**0.303**	**0.514**	**0.474^{+} (0.374^{++})**
S_{wr}	**0.4**	**0.25**	**$0.24^{\#}$ ($0.19^{\#\#}$)**
n_o	**2.4* (2.1**)**	**2* (2.8**)**	
n_w	**1.6* (1.9**)**	**3* (2**)**	

* -Calculated from the experimental transient pressure drop data for wetting liquid displacing non-wetting liquid (secondary imbibition).

** -Calculated from the experimental transient pressure drop data for non-wetting liquid displacing wetting liquid (secondary drainage).

\+ -Residual saturation of oil before ageing.

++ -Residual saturation of oil after ageing.

\# -Residual saturation of water before ageing.

-Residual saturation of water after ageing.

Table 8.2: Wettability inference from the ratio of end-point pressure drops (WI)

	Water-wet core (Berea)	**Oil-wet core(Treated Berea)**	**Mixed wet core (aged Limestone)**
Wettability Index (RPWI)	**0.124**	**6.295**	**0.963**

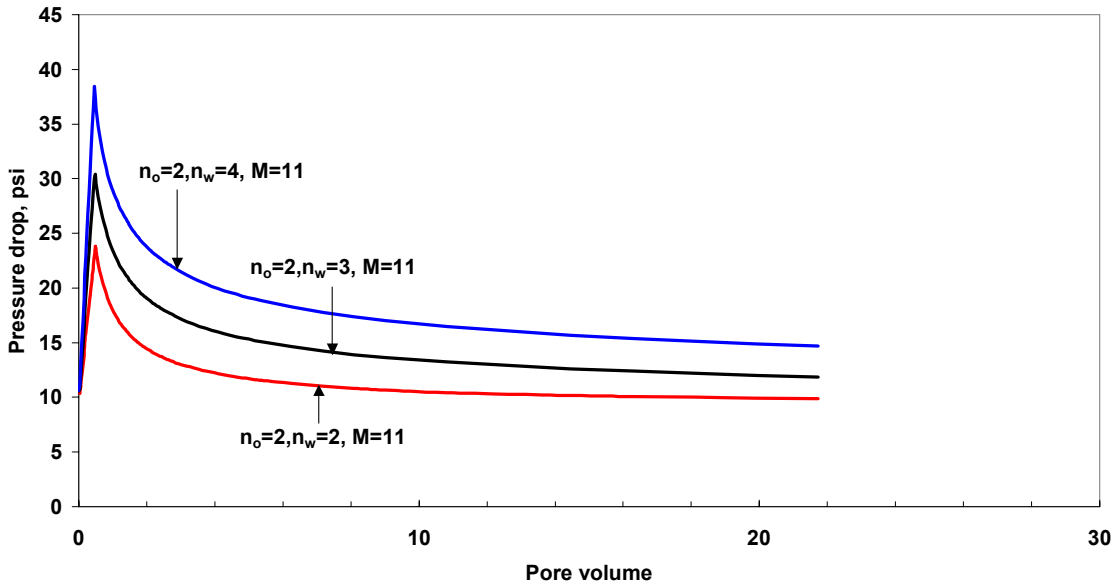

Figure 8.1a: Effect of Corey water exponent on pressure drop history of water-wet core (primary drainage).

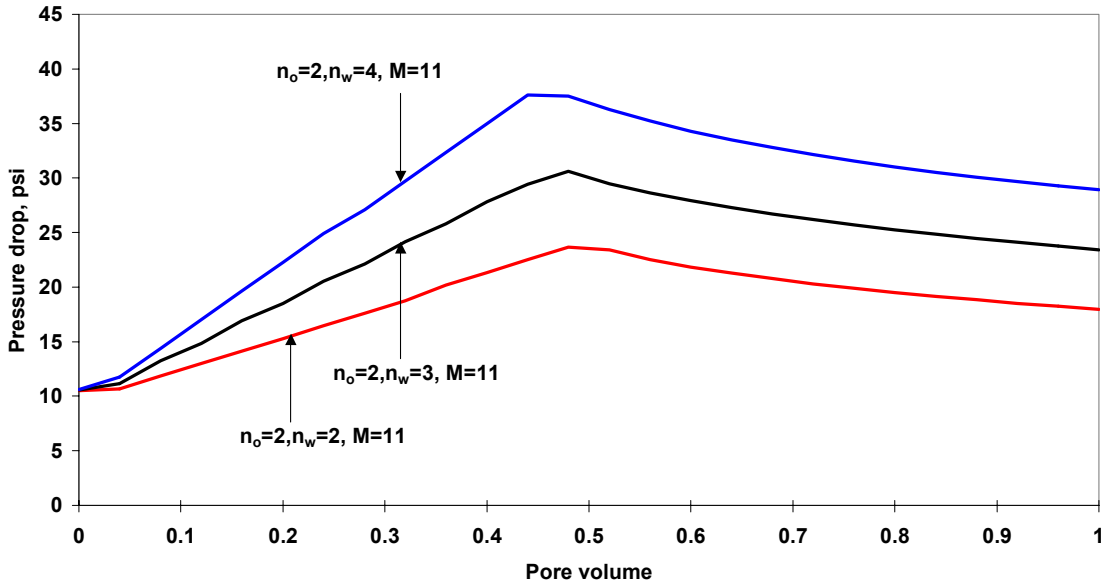

Figure 8.1b: Effect of Corey water exponent on pressure drop history of water-wet core (primary drainage) showing variation of position of peak.

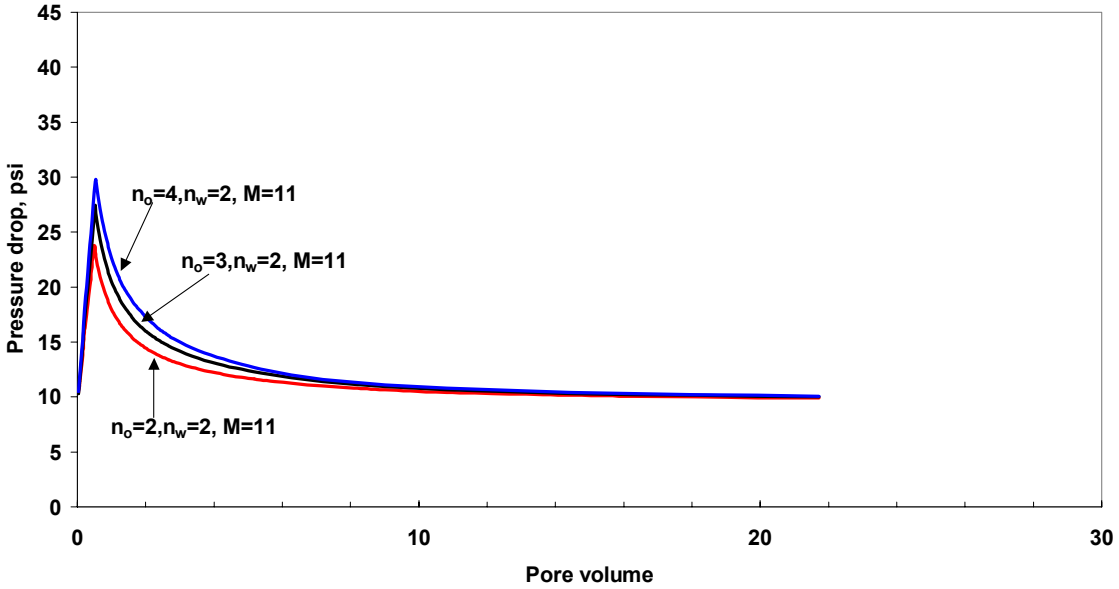

Figure 8.2a: Effect of Corey oil exponent on pressure drop history of water-wet core (primary drainage).

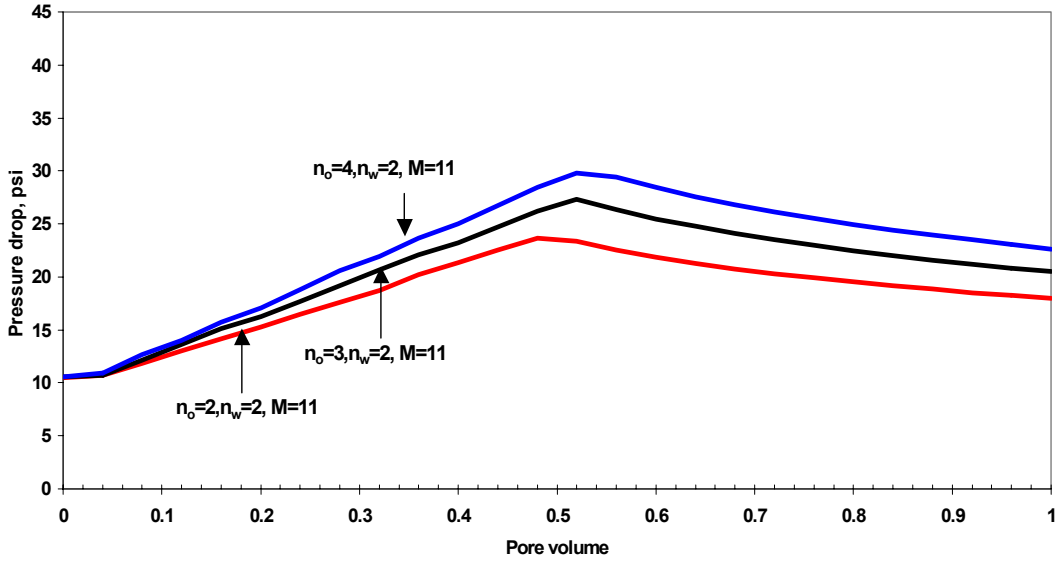

Figure 8.2b: Effect of Corey oil exponent on pressure drop history of water-wet core (primary drainage) showing variation of position of peak.

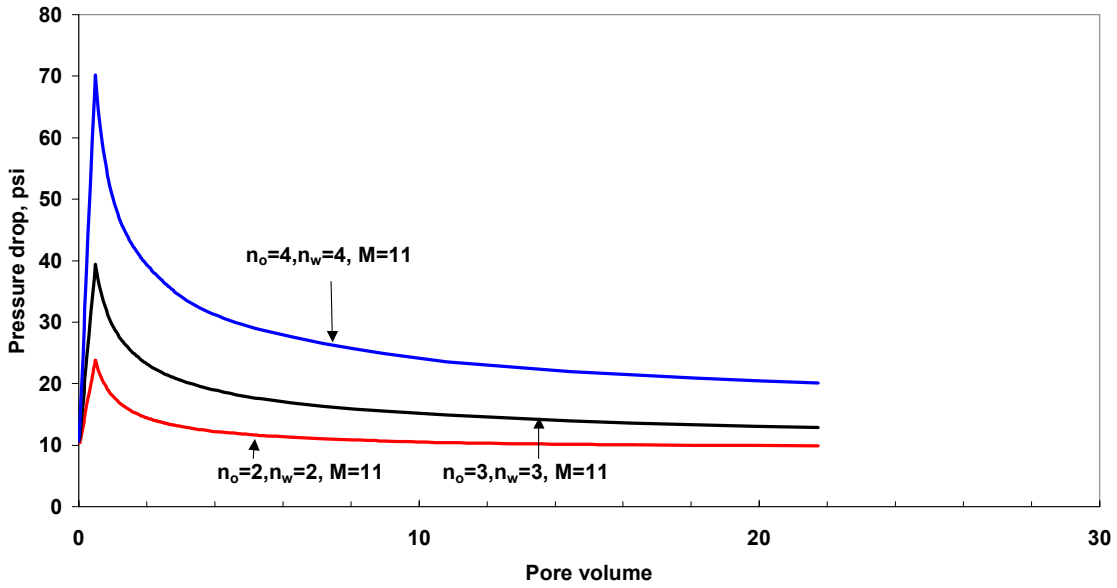

Figure 8.3: Effect of Corey oil and water exponents on pressure drop history of water-wet core (primary drainage).

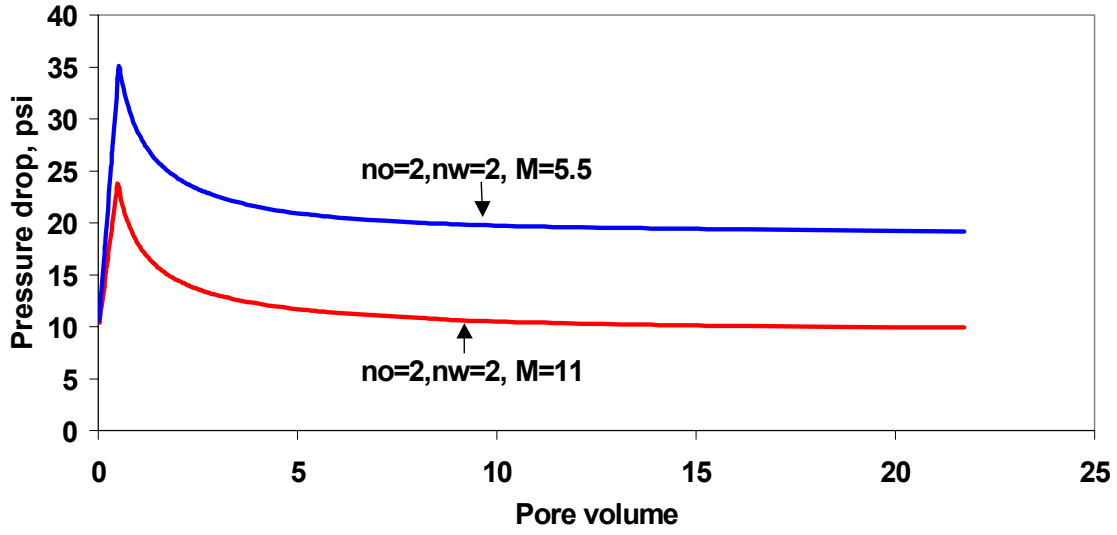

Figure 8.4 Effect of mobility ratio on pressure drop history of water-wet core (primary drainage).

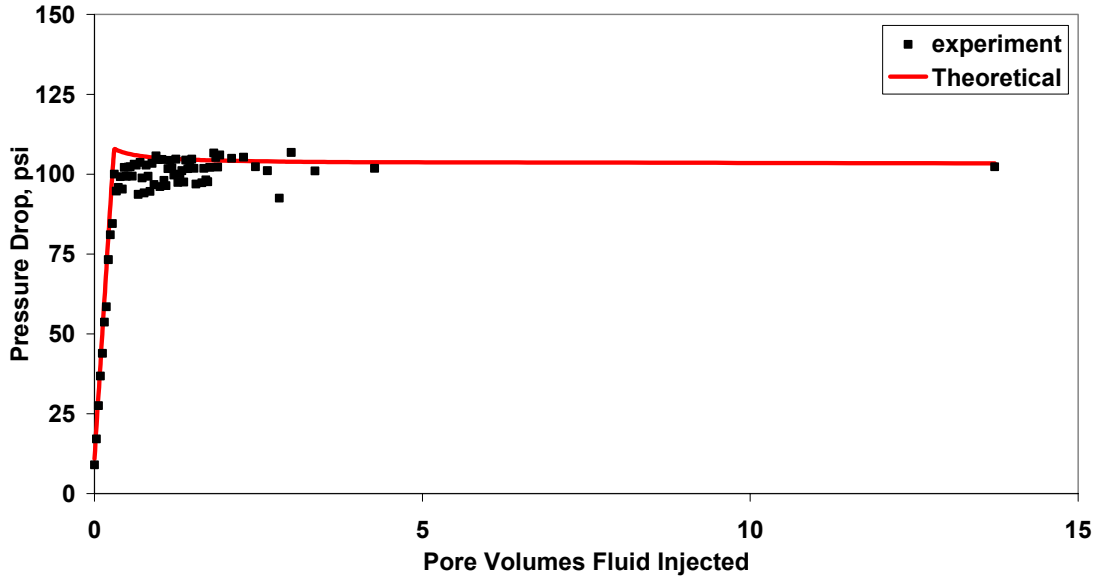

Figure 8.5 History match of secondary imbibition (brine displacing decane) pressure drop data for a water-wet Berea sandstone core.

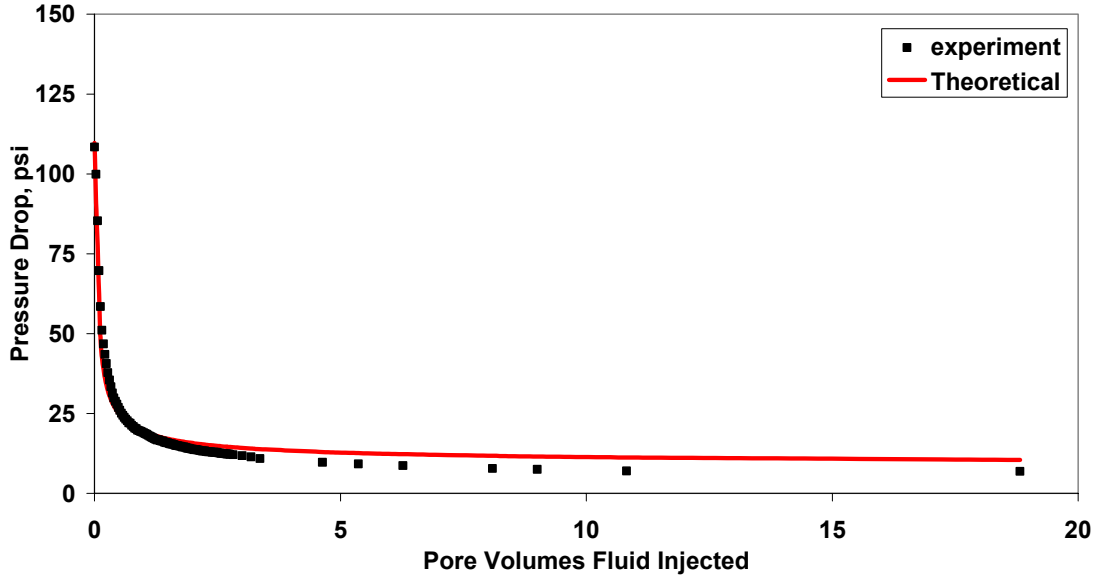

Figure 8.6 History match of secondary drainage (decane displacing brine) pressure drop data for a water-wet Berea sandstone core.

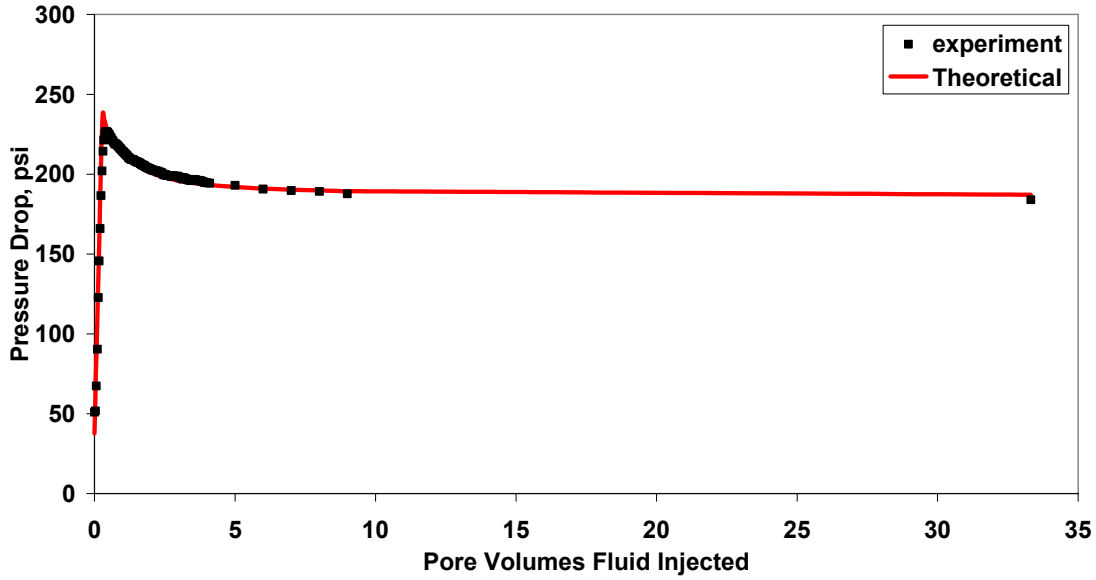

Figure 8.7 History match of secondary imbibition (decane displacing brine) pressure drop data for an oil-wet Berea sandstone core.

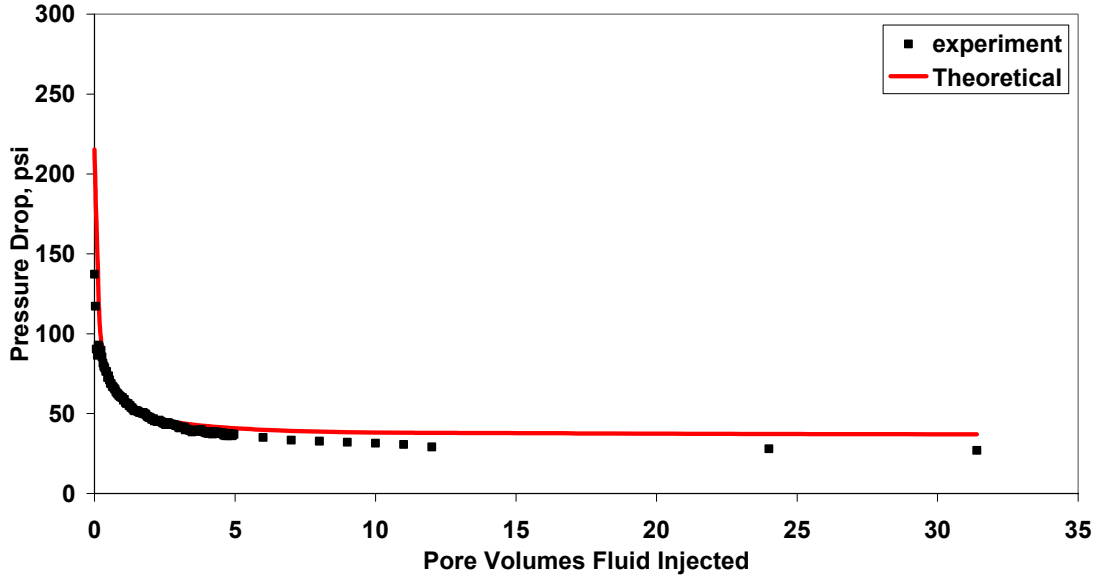

Figure 8.8 History match of secondary drainage (brine displacing decane) pressure drop data for an oil-wet Berea sandstone core.

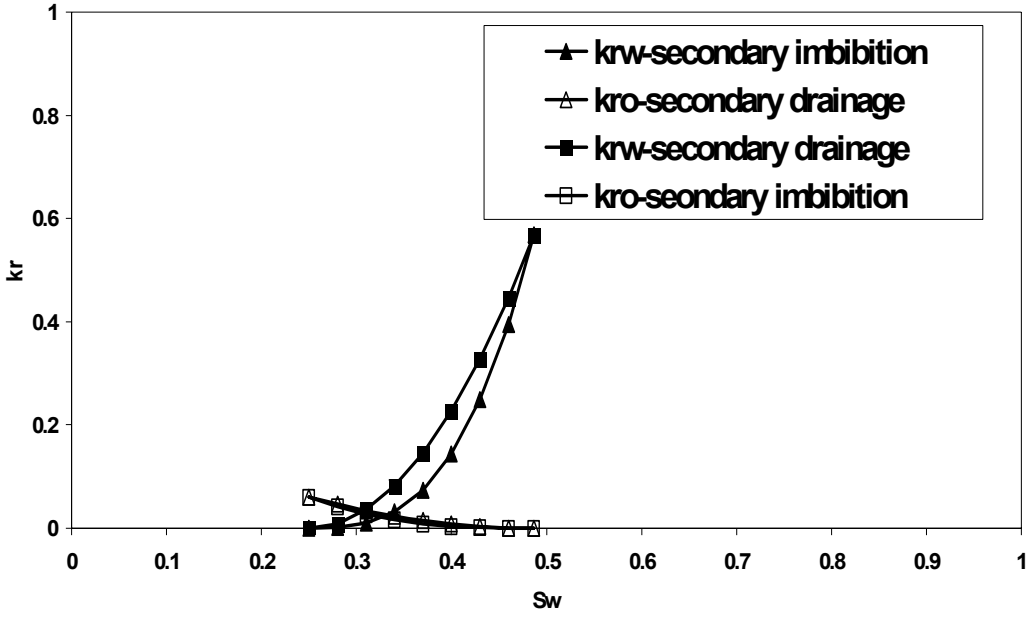

Figure 8.9 Oil-water relative permeability for oil-wet core.

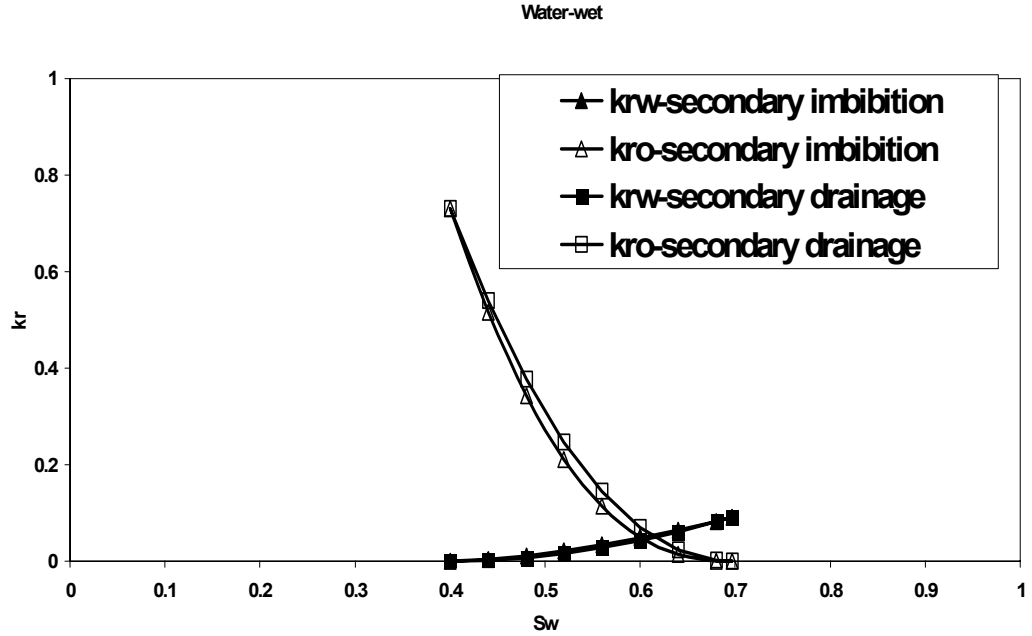

Figure 8.10 Oil-water relative permeability for water-wet core. These curves were generated by using end-point relative-permeability, residual saturation and Corey exponents obtained by history matching the experimentally measured pressure drop profiles and residual saturation.

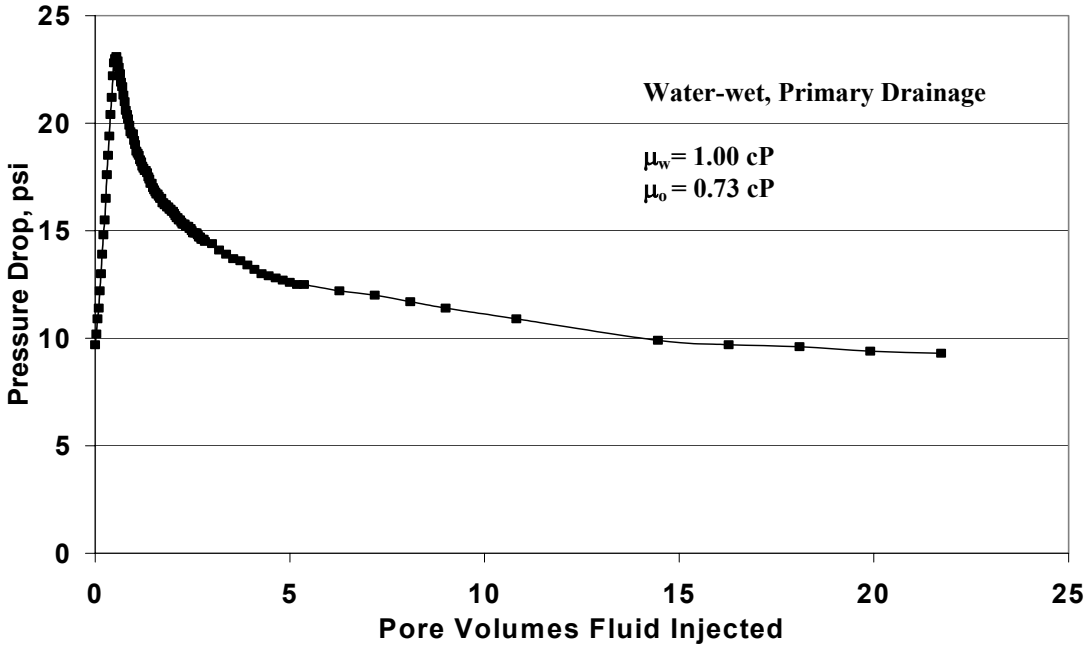

Figure 8.11 Transient pressure drop across a water-wet Berea sandstone core (primary drainage, decane displacing brine).

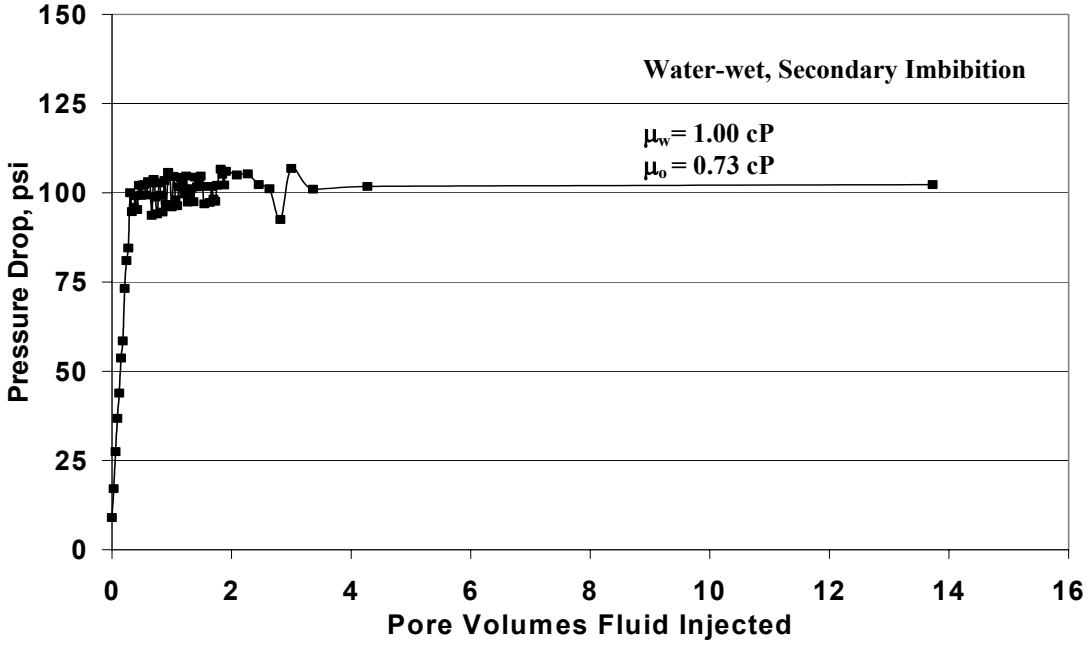

Figure 8.12 Transient pressure drop across a water-wet Berea sandstone core (secondary imbibition, brine displacing decane).

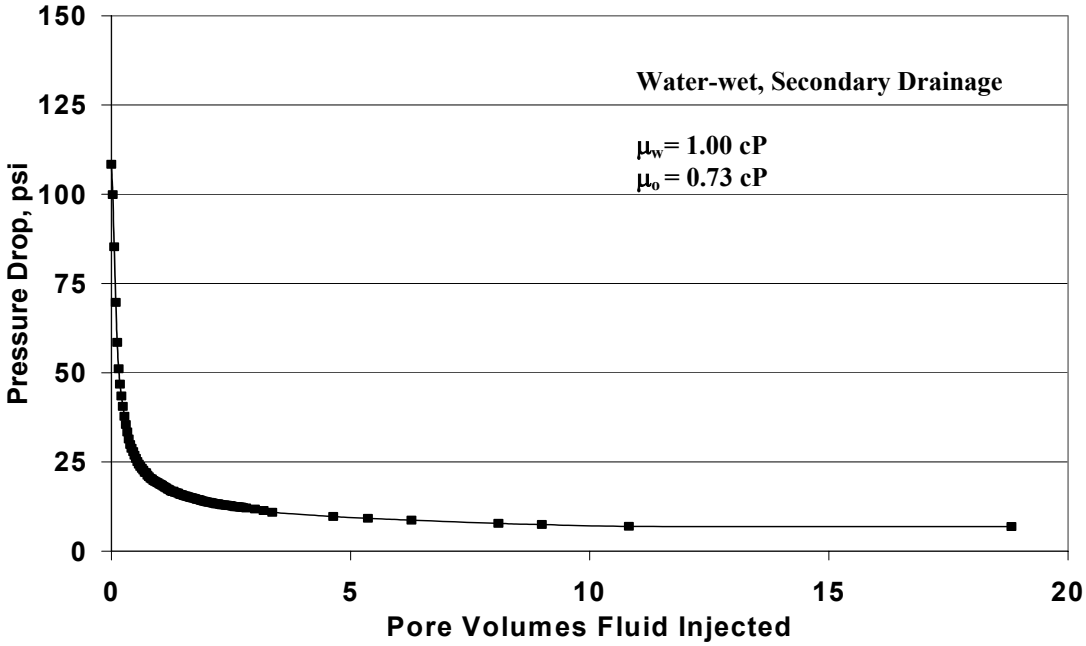

Figure 8.13 Transient pressure drop across a water-wet Berea sandstone core (secondary drainage, decane displacing brine).

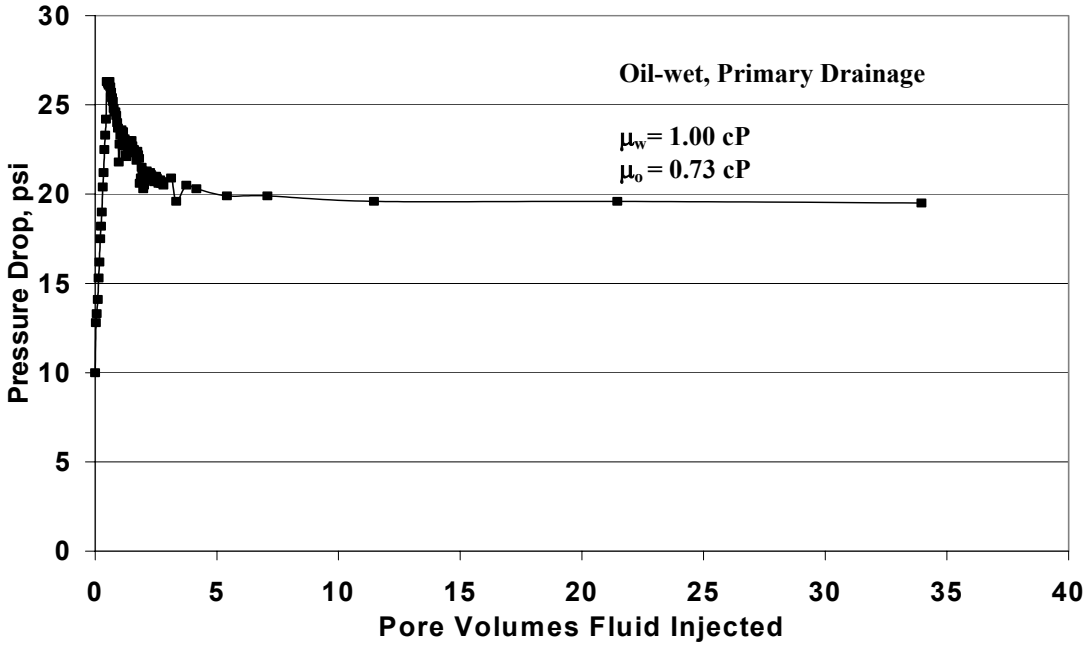

Figure 8.14 Transient pressure drop across an oil-wet Berea sandstone core (primary drainage, brine displacing decane).

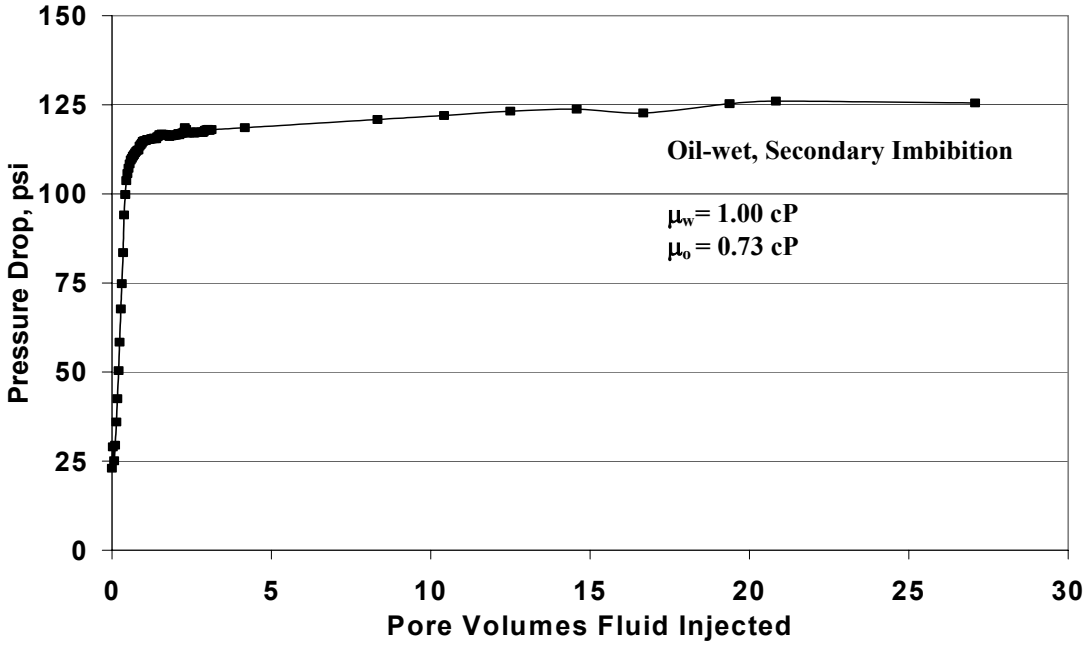

Figure 8.15 Transient pressure drop across an oil-wet Berea sandstone core (secondary imbibition, decane displacing brine).

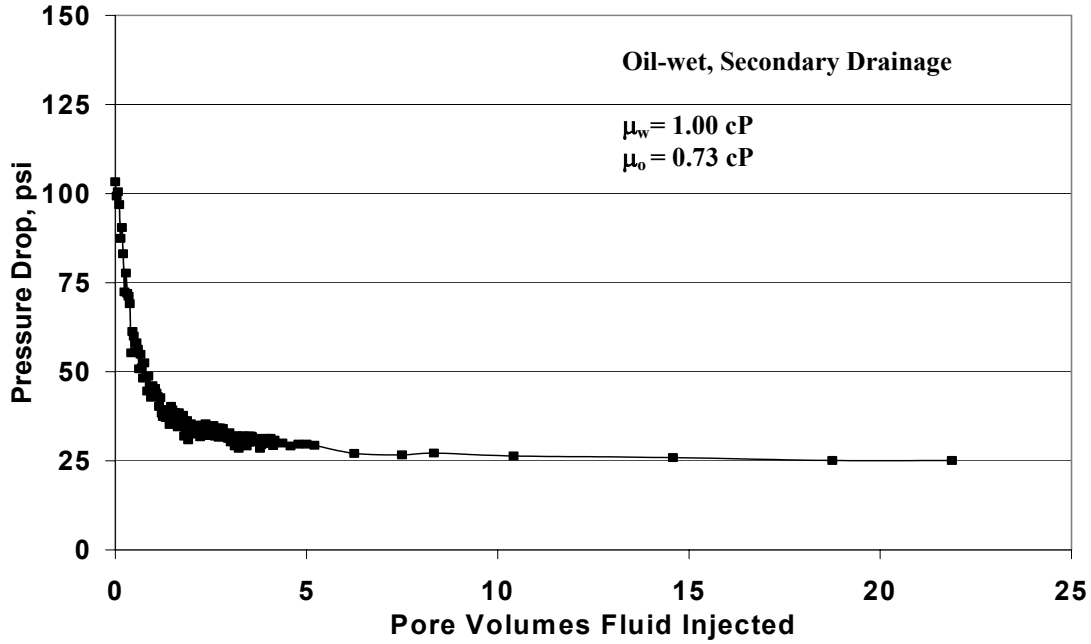

Figure 8.16 Transient pressure drop across an oil-wet Berea sandstone core (secondary drainage, brine displacing decane).

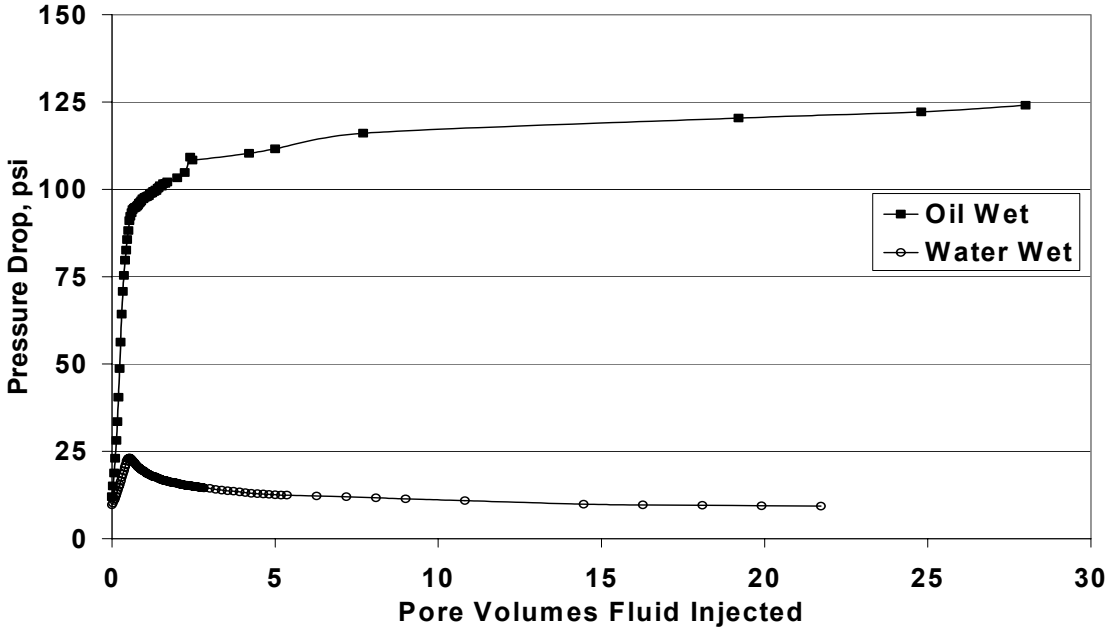

Figure 8.17 Comparison of pressure drop (across the core) history of oil-wet and water-wet cores (decane replacing brine).

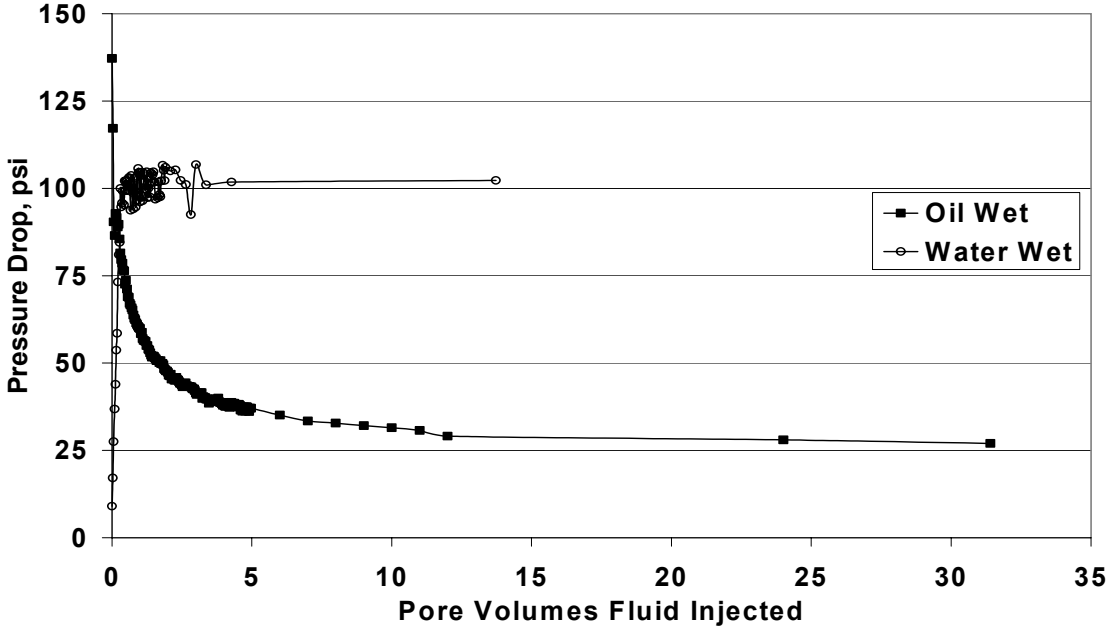

Figure 8.18 Comparison of pressure drop (across the core) history of oil-wet and water-wet cores (brine displacing decane). The core is initially at residual water saturation.

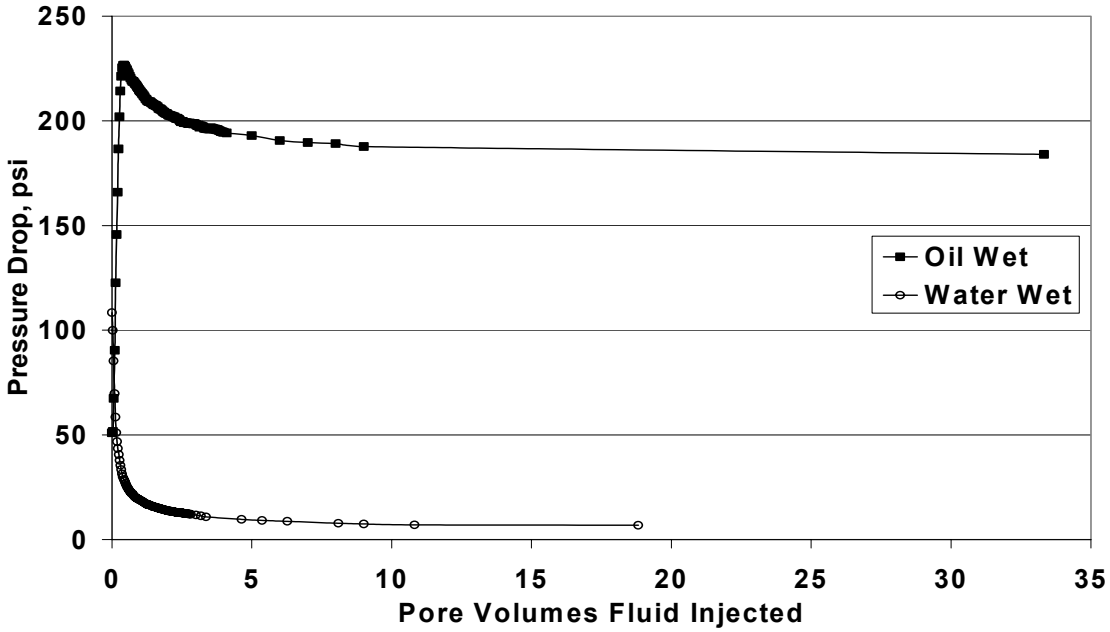

Figure 8.19 Comparison of pressure drop (across the core) history of oil-wet and water-wet cores (decane displacing brine). The core is initially at residual decane saturation.

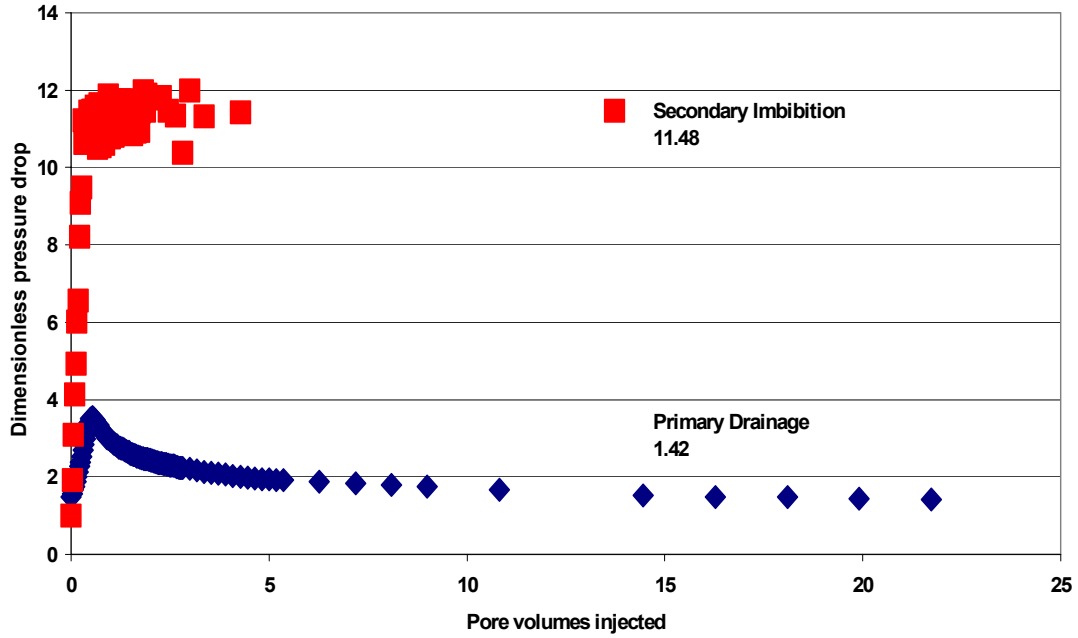

Figure 8.20 Comparison of pressure drop (across the core) history of water-wet Berea core (primary and secondary imbibition).

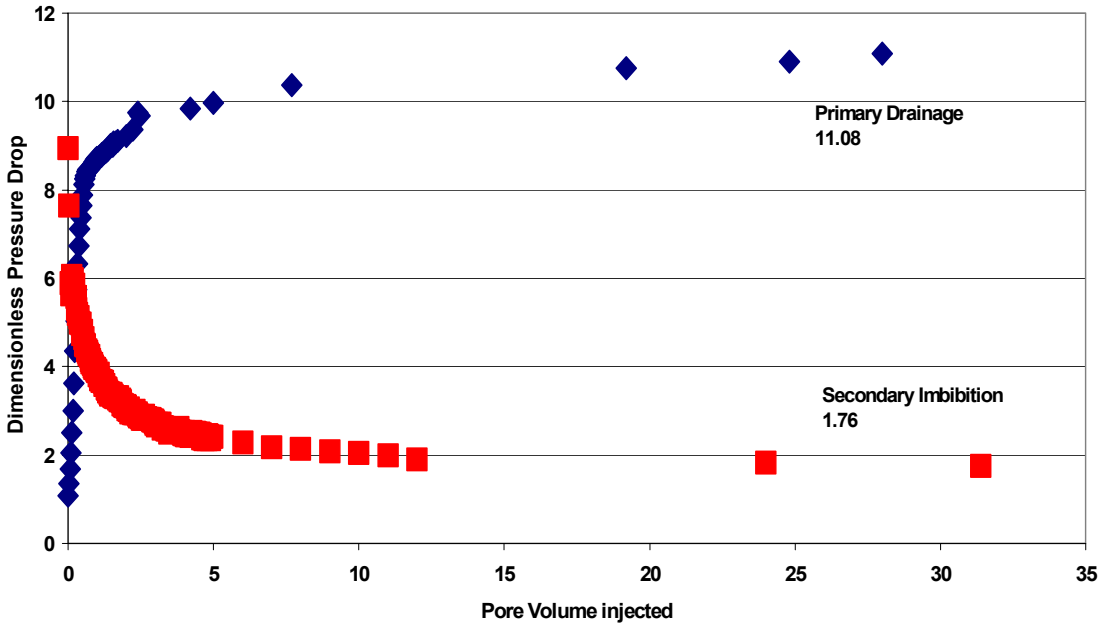

Figure 8.21 Comparison of pressure drop (across the core) history of oil-wet Berea core (primary drainage and secondary imbibition).

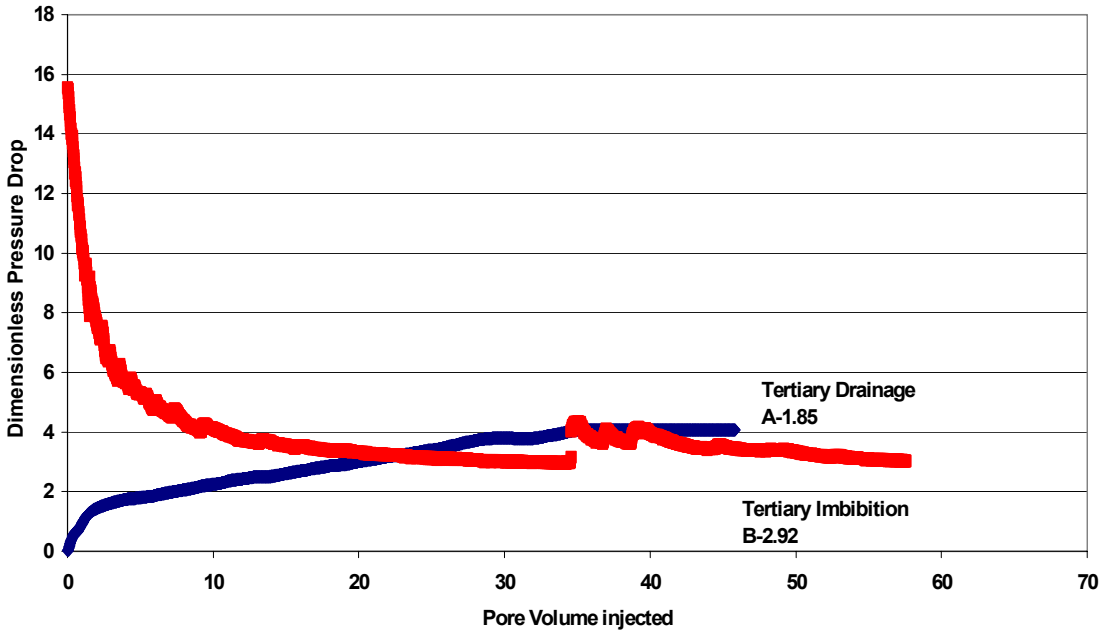

Figure 8.22 Comparison of pressure drop (across the core) history of mixed-wet limestone core (tertiary drainage and tertiary imbibition). The core is initially at residual water saturation.

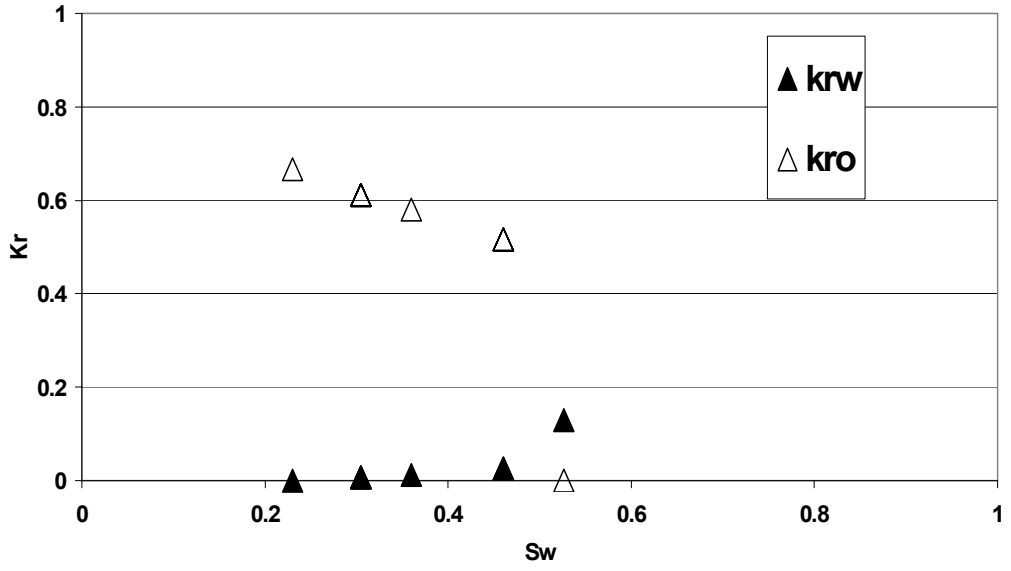

Figure 8.23 Oil-water relative permeability for limestone core. These curves were generated by using the unsteady state measurement (JBN[12]) method. The plot shows the relative permeability curves before ageing with crude oil.

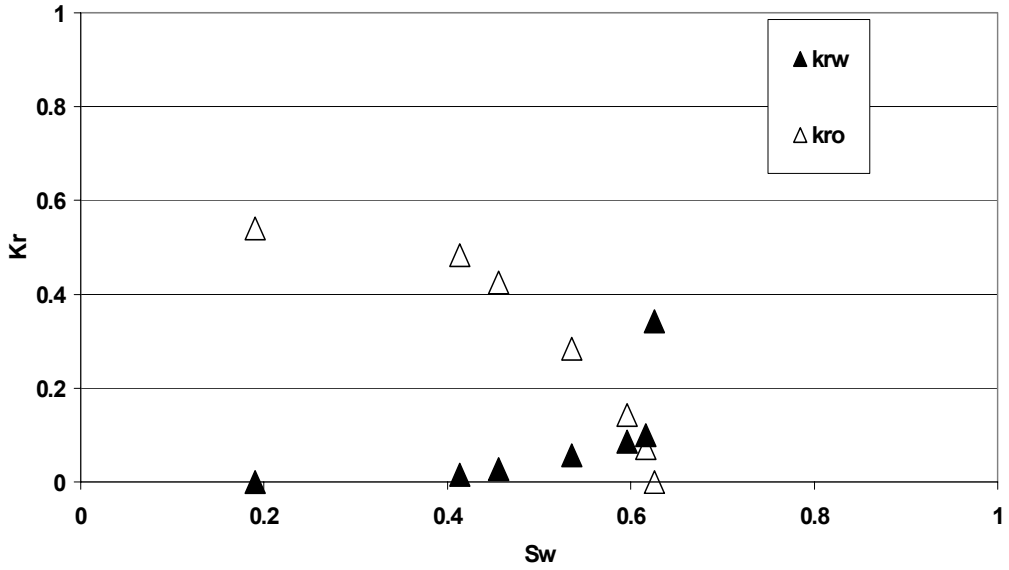

Figure 8.24 Oil-water relative permeability for Limestone core. These curves were generated by using the unsteady state measurement (JBN[12]) method. The plot shows the change in relative permeability curve after ageing with crude oil (aged for 20 days at residual water saturation).

9. Enhanced Imbibition into Oil-Wet Matrix

Zhang, L. D. and Hirasaki, G.

Presented at the 2003 SPE International Oilfield Chemistry Symposium

ABSTRACT

Oil recovery by water flooding in fractured formations is often dependent on spontaneous imbibition. However, spontaneous imbibition is usually insignificant in oil-wet, carbonate rocks. Sodium carbonate and anionic surfactant solutions are evaluated for enhancing oil recovery by spontaneous imbibition from oil-wet carbonate rocks. Crude oil samples must be free of surface-active contaminants to be representative of the reservoir. Calcite, which is normally positively charged, can be made negative with sodium carbonate. The ease of wettability alteration is a function of the aging time and temperature and the surfactant formulation.

INTRODUCTION

Much oil remains in fractured, carbonate oil reservoirs after waterflooding and in some cases in paleo-transitions zones, which result from the oil/water contact moving upward before discovery. The high remaining oil saturation is due to a combination of poor sweep in fractured reservoirs and the formation being preferentially oil-wet during imbibition[1,2]. Poor sweep is not an issue in paleo-transition zones but yet the remaining oil saturation may still be significant.

There are several reasons for high remaining oil saturation in fractured, oil-wet, carbonate formations. Poor sweep was mentioned earlier. If the formation is preferentially oil-wet, the matrix will retain oil similar to an oil-wet blotter and high oil saturation transition zones will exist where the upward oil film flow path is interrupted by fractures. This is illustrated in Fig. 9.1, which shows the oil retained by oil-wet capillaries of different radii. The height of the capillary retained oil column is greater for the smaller pores. In oil-wet systems, oil is the phase contacting rock surfaces, and surface trapping is likely to be particularly important in rocks with highly irregular surfaces and large surface areas[1], Fig. 9.2.

The objective of this investigation is to develop a process to overcome the mechanisms for oil retention illustrated by Figs. 9.1 & 9.2. Oil is retained by wettability and capillarity. Thus altering the wettability to preferentially water-wet conditions and reducing the interfacial tension to ultra-low values can overcome these mechanisms. Introducing an injected fluid into the matrix of a fractured formation is challenging because the injected fluid will flow preferentially in the fractures rather than through the matrix. Thus the process must spontaneously imbibe the injected fluid from the fracture system into the matrix, as illustrated in Fig. 9.3. Spontaneous capillary imbibition may no longer be important because of low interfacial tension. However, if wettability is altered to preferentially water-wet and/or capillarity is diminished through ultra-low interfacial tensions, buoyancy will tend to allow oil to flow upward and out of the matrix into the fracture system. The injected fluid will replace the displaced oil in the matrix and thus the spontaneous imbibition will continue as long as oil flows out of the matrix.

Spontaneous imbibition is an important mechanism in oil recovery from fracture reservoirs. A recent survey by Morrow and Mason reviews the state-of-the-art[3]. They state that imbibition rates with different wettability can be several orders of magnitude slower and displacement efficiencies range from barely measurable to better than very strongly water-wet. The primary driving force for imbibition in strongly water-wet conditions is the capillary pressure. Reduction of interfacial tension reduces the contribution of capillary imbibition. Buoyancy, as measured by the Bond number then becomes the dominant parameter governing the displacement, even of the wetting phase[4].

Application of surfactant to alter wettability and thus enhance spontaneous imbibition has been investigated by Austad, et al.[7-11] with chalk and dolomite cores. Chen, et al.[12], investigated enhanced imbibition with nonionic surfactants. Spinler, et al.[13], evaluated 46 surfactants for enhanced imbibition in chalk formations. Standes, et al.[11] and Chen, et al.[12] used either nonionic or cationic surfactant with a strategy to alter wettability but avoiding ultra-low tensions. The work presented here differs from the previous work in that sodium carbonate and anionic surfactants are used to alter wettability and reduce interfacial tension to ultra-low values.

CRUDE OIL SAMPLES

It is important to have a representative crude oil sample when designing an EOR process. Since the process is based on surface phenomena, it is important that the crude oil is free of surface-active materials such as emulsion breaker, scale inhibitor, or rust inhibitor. A simple test for contamination is to measure the transient interfacial tension (IFT) of the crude oil sample with synthetic brine. Fig. 9.4 is a plot of the transient oil/brine IFT of several crude oil samples from the same field. These measurements were made with a pendant drop apparatus with automatic video data acquisition and fit to the Young-Laplace equation. Samples MY1 and MY2 have low initial IFT and the value decreases with time. This is an indication that these samples contain a small amount of surface-active material, which slowly diffuses to the interface and reduces the IFT. Samples MY3 – MY6 have a much larger initial IFT and the value does not change significantly with time. Some early experiments were made with MY1 but the later experiments were made with MY3.

The properties of the crude oil samples are listed in Table 9.1. The higher acid number and viscosity for MY1 compared to the other samples suggest that it may be an outlier. The wettability of the oil samples were compared by pressing an oil drop in brine against a calcite (marble) or glass plate for 5-10 minutes, withdrawing the drop, and measuring the water advancing contact angle after motion has ceased. The water advancing contact angles of MY1 and MY3 against calcite or glass after aging time of 5-10 minutes are compared in Fig. 9.5. Clearly, MY1 and MY3 have different wettability properties.

FORMATION WETTABILITY

Spontaneous imbibition in carbonate formation usually does not occur or is slow compared to sandstone formations. Treiber, Archer, and Owens[14] measured the equilibrated water advancing contact angles of fifty crude oils. They found that of the carbonate reservoir-crude oil-water systems tested, 8% were water-wet; 8% intermediate; and 84% oil-wet. This is in contrast to 43% water-wet; 7% intermediate-wet; and 50% oil-wet for silicate formation reservoirs.

Freedman, et al.[15], evaluated the wettability of Bentheim sandstone, Berea sandstone, and the dolomite formation of the present investigation. A common crude oil from the North Sea was used for the evaluation. Water would spontaneously imbibe into the sandstone

formation materials but no measurable spontaneous imbibition occurred in the dolomite formation during 24 hours. The dolomite cores were partially water flooded to an intermediate saturation and the NMR relaxation time distribution of the remaining oil was measured. The relaxation time distributions of the oil in the sandstones were identical to that of the bulk oil but that of the carbonate was shortened, indicating surface relaxation due to oil making contact with the pore walls. This is evidence of oil wetting the pore walls.

The wettability of the MY3 crude oil was evaluated by measuring the water advancing contact angle of calcite (marble) plates. The plates were solvent cleaned, polished on a diamond lap to remove the surface layer, aged in 0.1 M NaCl brine overnight, and aged in the crude oil for 24 hours, either at room temperature or 80° C. The reservoir is close to room temperature but the elevated temperature aging was done to compensate to the short aging time compared to geological time. Photographs of an oil drop on the upper calcite surface after all motion had stopped are shown in Fig. 9.6. It is clear that the water advancing contact angle is near 180°, i.e., it is oil-wet. It should be noted that MY3 aged for only 5-10 minutes, shown earlier, had an advancing contact angle of only 50°. These results demonstrate the importance of both aging time and temperature on wettability.

One of the most important factors in the determination of the wettability of crude oil-brine-mineral systems is the electrical or zeta potential of the crude oil/brine interface and of the mineral/brine interface[16-18]. The zeta potentials of these interfaces as a function of pH are shown in Fig. 9.7. The zeta potential of the MY1 crude oil is negative for pH greater than 3. This is due to the dissociation of the naphthenic acids in the crude oil with increasing pH. The surface of calcite is positive for pH less than 9 when the only electrolytes are 0.02 M NaCl and $NaHCO_3/Na_2CO_3$. The opposite charge between the two surfaces results in an electrostatic attraction between the two interfaces, which tend to collapse the brine film and bring the oil in direct contact with the mineral surface. Thus this system can be expected to be non-water-wet around neutral pH[19-20]. However, this figure also shows that the zeta potential of calcite is negative down to neutral pH when the brine is 0.1 N $Na_2CO_3/NaHCO_3$ plus HCl to adjust pH. This is because the potential determining ions for the calcite surface are Ca^{2+} and CO_3^{2-}. An excess of the carbonate anion makes the surface negatively charged. If both the crude oil/brine and calcite/brine interfaces are negatively charged, there will be an electrical repulsion between the two surfaces, which tends to stabilize a brine film between

the two surfaces. Thus a system with brine containing sufficient excess carbonate ions may be expected to have a preference to be water-wet, compared to in the absence of excess carbonate ions.

Figs. 9.8 and 9.9 illustrate the effect of alkaline surfactant on wettability alteration of a calcite (marble) plate that has been aged in crude oil either at room temperature or 80° C. The oil-wet system with brine is the same as that shown in Fig. 9.6. The displacement of oil by reduction of the interfacial tension and the alteration of the wettability upon replacement of the brine with 0.05% CS-330 and 0.5 M Na_2CO_3 are shown as a function of time. Both systems showed the oil streaming from the surface at early times as a result of the reduction in interfacial tension. Later, small oil drops are observed with higher magnification and the change in contact angle can be observed.

An oil drop on the upper surface of a solid immersed in brine is not stable for drop dimensions such that the Bond number is the order of unity or greater. Fig. 9.10 illustrates possible equilibrium shapes of axisymmetric oil drops [21,22]. The length scales are made dimensionless with respect to the capillary constant, $\sqrt{\sigma/(\Delta\rho g)}$. The interface intersects the flat solid at the point where the angle is equal to the equilibrium contact angle. This figure shows that the maximum stable oil drop size is proportional to the square root of the interfacial tension. Also, oil drops with small contact angles are smaller than those with larger contact angles. Thus the oil drop size being 10^2 smaller implies that the IFT is 10^4 smaller.

Alteration of wettability also contributes to the displacement of the oil. Fig. 9.8 shows the wettability being altered from strongly oil-wet to preferentially water-wet for the plate that was aged in crude oil at room temperature. An oil drop becomes unstable and detaches after the contact angle approaches a small value. Fig. 9.9 shows that the plated that was aged in crude oil at 80° C altered to intermediate water-wet conditions during the period of observation. No further change was observed over a period of 4 days.

The observations with 0.05% TDA-4PO in 0.3 M Na_2CO_3 aged at room temperature and at 80° C are shown in Figs. 9.11 and 9.12. With this formulation, the wettability only alters to intermediate wettability, even for the system aged at room temperature. These figures show the oil on an oil-wet surface being displaced by buoyancy as interfacial tension is reduced and wettability is altered to more water-wet conditions. The degree of wettability

alteration is very dependent on whether the system was aged at room temperature or elevated temperature and the surfactant formulation.

SPONTANEOUS IMBIBITION

Spontaneous imbibition is most commonly associated with counter-current capillary imbibition in systems that are preferentially water-wet[3]. If the interfacial tension is very low, capillarity becomes less important compared to buoyancy[4]. However, for systems that are preferentially oil-wet, spontaneous imbibition of brine does not occur and capillarity is the mechanism that retains oil in the matrix, as illustrated in Fig. 9.1. Buoyancy is an omnipresent driving force for displacement of oil by water. Reduction of interfacial tension and alteration of wettability inside the matrix will reduce the tendency for capillarity to retain the oil. Thus a low-tension process has the process fluids entering the matrix to replace the oil that is leaving by buoyancy[4], as illustrated in Fig. 9.3.

The effect of buoyancy displacing oil from between two parallel surfaces is demonstrated with the system in Fig. 9.13. A calcite (marble) plate was aged in crude oil at room temperature. It is placed in an optical cell with a plastic film as a spacer to create a 15 μm gap between the plate and the front wall of the cell. The glass of the front of the cell has been treated with a dilute solution of hexadecyltrimethylammonium bromide to make the glass preferentially oil-wet. Oil in the gap is not displaced when the cell is filled with brine. The buoyancy forces cannot overcome the capillary entry pressure to displace the oil from the gap. However, when the brine is replaced with 0.05% CS-330 and 0.3 M Na_2CO_3, the displacement of oil is rapid, Fig. 14. The alkaline surfactant solution both lowers the interfacial tension and alters the wettability. Only isolated drops of oil remain after 7 hours.

One qualitative difference between displacement of oil from a gap between parallel surfaces and a porous rock is that the gap has 100% oil saturation while a porous rock has formation brine occupying the pore space along with the oil, Fig. 9.15. Buoyancy may displace the mobilized oil but may not displace the formation brine unless there is a significant density difference between the formation brine and the alkaline surfactant solution. This will result in accumulation of a bank of formation brine ahead of the alkaline surfactant solution. Dispersive mixing is necessary for the alkaline surfactant solution to

penetrate past the bank of formation brine and contact the trapped oil. Also, the alkaline surfactant solution must remain active as it mixes with the formation brine.

SURFACTANT FORMULATIONS

It was mentioned earlier that nonionic and cationic surfactants have been previously evaluated for wettability alteration in carbonate formations[5-13]. This investigation focuses on the use of anionic surfactants and sodium carbonate. It builds on the previous understanding developed for alkaline surfactant flooding[23,24]. Also, this technology has found many applications during the past decade when it was commonly thought that surfactant flooding was not economical because of the expense of the surfactant[25-40].

There are a number of reasons for choosing sodium carbonate as the alkali. We mentioned earlier that the carbonate ion is a potential determining ion for carbonate minerals and thus is able to impart a negative zeta potential to the calcite/brine interface, even at neutral pH. A negative zeta potential is expected to promote water-wetness. Other reasons for choosing sodium carbonate include:

- The moderately high pH generates natural surfactants from the naphthenic acids in the crude oil by in situ saponification;
- Sodium carbonate suppresses calcium ion concentration;
- Sodium carbonate reduces the extent of ion exchange and mineral dissolution (in sandstones) compared with other alkali[27, 41];
- Adsorption of anionic surfactants is low with the addition of an alkali, especially with sodium carbonate[23, 41-43];
- Carbonate precipitates do not adversely effect permeability as compared to hydroxide and silicates[41];
- Sodium carbonate is an inexpensive alkali since it is mined as the sodium carbonate – bicarbonate mineral, trona.

The phase behavior of MY3 crude oil and different concentrations of sodium carbonate solution is shown in Fig. 9.16. The aqueous phase is most turbid at a concentration of 0.1 M and becomes clear at a concentration of 0.2 M. Based on an acid number of 0.2 mg KOH/g, a concentration of 0.003 M Na_2CO_3 is required to neutralize the acid to soap and $NaHCO_3$. The pH of the equilibrated solutions exceed 10 with a Na_2CO_3 concentration of 0.05 M. The

clear aqueous phase at a concentration of 0.2 M indicates that a Winsor Type II microemulsion has formed at this concentration. This is an oil-continuous microemulsion, or is commonly called as "over-optimum". Thus a concentration of alkali large enough to transport through a reservoir is often over-optimum in electrolyte strength. Some crude oil-brine-mica systems, which were water-wet at high pH and low salinity, became oil-wet at high pH and high salinity[44-45]. Thus, the over-optimum phase behavior must be avoided if water-wet conditions are desired. Also, over-optimum conditions result in high surfactant retention in conventional surfactant flooding[46].

The choice of surfactants to use for an alkaline surfactant process for carbonate formation was guided by the experience with sandstone formations but recognizing that adsorption is going to be on the carbonate minerals, calcite and dolomite. Thus internal olefin sulfonates, which are effective for sandstones[24], were not considered since they are very sensitive to calcium ions. Rather, ethoxylated and propoxlated sulfate surfactants were evaluated[47-50] because of their tolerance to divalent ions. Sulfates rather than sulfonates were evaluated because of their greater availability and because the target application is at a low temperature where the sulfate hydrolysis should not be a problem. The surfactants evaluated are identified in Table 9.2. CS-330 is similar to NEODOL 25-3S, used previously[23]. The propoxylated surfactants are calcium tolerant such that $CaCl_2$ has been used as the electrolyte to achieve optimal salinity[50].

The phase behavior of the MY3 crude oil with alkaline surfactant solutions as a function of Na_2CO_3 concentration with 0.05% (active material) surfactant is shown in Figs. 9.17-9.20. CS-330 is shown in Fig. 9.17; C12-3PO in Fig. 9.18; TDA 4PO in Fig. 9.19; and ISOFOL14T-4.1PO in Fig. 9.20. Only Na_2CO_3 was used as the electrolyte rather than a mixture of NaCl and Na_2CO_3 to reduce a degree of freedom in the comparisons. The spinning-drop interfacial tensions of the equilibrated phases are shown in Fig. 9.21. All systems have interfacial tension in the range 10^{-3} – 10^{-2} mN/m for a range of Na_2CO_3 concentrations. Nelson ,et al.[23] pointed out that amount of oil relative to the amount of synthetic surfactant is an important parameter since the natural surfactant from the naphthenic acids and the synthetic surfactant have different optimal salinities. This is illustrated by the dependence of the interfacial tension on the water/oil ratio, Fig. 9.22, since the synthetic surfactant is in the water and the natural surfactant comes from the oil. While

each system had ultra-low tension at a water/oil ratio of 1:1, the tension increases with increase in water/oil ratio. This increase is rapid for CS-330 but much less for TDA-4PO. The phase behavior of the systems with increased concentrations of TDA-4PO of 0.2% (active material) and 1% are shown in Figs. 9.23 and 9.24. Compared to a concentration of 0.05%, the corresponding phase behavior has moved to higher Na_2CO_3 concentrations. The interfacial tensions, shown in Fig. 9.25, have optimal conditions at higher Na_2CO_3 concentrations. Also, the minimum tension is lower with the higher surfactant concentrations. Apparently, the optimal salinity changes to higher electrolyte strength since the ratio of the synthetic surfactant to natural surfactant increases with increasing surfactant concentration. These dependencies must be considered in optimizing a system for oil recovery[23, 49].

MIXING WITH FORMATION BRINE

Mixing with formation brine has always been an important issue with surfactant flooding, but new considerations are needed because of the presence of sodium carbonate. Hard water cannot be used to prepare the solutions for injection because of precipitation of $CaCO_3$. Also, premature production of injected fluids should be minimized to avoid production well scaling and produced emulsions. Fig. 9.15 shows that there will be mixing with the formation brine as the alkaline surfactant solution invades the formation matrix. Besides dilution, alkalinity will be lost due to precipitation of divalent ions in the formation brine. The surfactant formulation should be formulated such that the diluted system is active in altering wettability and lowering IFT at the low concentration "toe[49]" of the concentration profile illustrated in Fig. 9.15. This will require evaluating changes in: electrolyte strength, alkalinity and pH, surfactant concentration, and ratio of synthetic/natural surfactants.

ALKALI CONSUMPTION AND SURFACTANT ADSORPTION

Alkali consumption is an important issue in sandstones because of ion exchange with clays, dissolution of silicate minerals, mixing with formation brine, and neutralization of the acids in the crude oil. Soluble calcium minerals such as gypsum or anhydrite can contribute to alkali consumption. However, Cheng[41], found no significant consumption of Na_2CO_3 on dolomite. Olsen, et al.[25], reported 5.8 meq of alkalinity consumed per kg of carbonate rock

with an ASP system using Na_2CO_3 and sodium tripolyphospate. Measurement of alkali consumption of the system of interest is needed to determine how much of the electrolyte strength can be accomplished with NaCl rather than Na_2CO_3.

Addition of an alkali significantly reduces surfactant adsorption in sandstones[23]. Al-Hashim, et al.[42], showed surfactant adsorption on limestone to be decreased in the presence of 1:1 $NaHCO_3$:Na_2CO_3 for low surfactant concentrations. The adsorption of the alkaline surfactant systems introduced here is yet to be evaluated.

OIL RECOVERY

Spontaneous imbibition experiments were conducted for two systems. The properties of the dolomite cores and experimental conditions are listed in Table 9.3. There was no further extraction or cleaning of the cores. The composition of the formation brine is in Table 9.4. Core B showed no spontaneous imbibition after it was immersed in formation brine for 9 days. The recovery from the enhanced spontaneous imbibition with alkaline surfactant solutions was faster and greater for Core A compared to Core B, Fig. 9.26. The primary reason for the difference is thought to be due to Core A not being aged and Core B being aged at 80° C for 24 hours. Other differences that could be contributing to the recovery performance include: surfactant systems, initial oil saturation, and length of the core.

FUTURE WORK

The work to date has been to identify the important factors affecting the enhanced recovery with alkaline surfactant solution rather than to optimize the system. A practical system will have only enough Na_2CO_3 to satisfy the alkali consumption and use NaCl for the remainder of the electrolyte strength. The frontal advance rate of the alkali and surfactant should be matched. A possible approach to optimization of a surfactant formulation is to design the system such that with the changing concentrations and saturations, the system changes from being optimum or over-optimum at the front of the displacement front to being under-optimum behind the displacement front[51].

The different surfactants need to be systematically characterized. Fundamental questions remain about mixtures of dissimilar surfactant. For example, one system appeared to have two local minimums in interfacial tension.

One alkaline surfactant system shown here altered a calcite plate that was aged at room temperature to preferentially water-wet conditions. However, the system that was aged at 80° C only altered to intermediate-wet (~90° contact angle). The mechanisms governing the wettability alteration and methods to make the elevated temperature system more water-wet will be sought[52].

The long-term stability of a surfactant formulation at the condition of application should be evaluated. Talley[53] shows that ethoxylated sulfates as those shown here are unstable at low pH and high temperatures. They were more stable at neutral and high pH provided a significant concentration of calcium ions was not present. Na_2CO_3 should suppress the calcium ion concentration in the alkaline surfactant systems discussed here.

The spontaneous imbibition experiments shown were in small cores. The controlling displacement mechanism needs to be identified and be scaled to the rate of displacement from matrix blocks of dimensions typical of actual reservoirs.

The scope of the work discussed here is limited to a single matrix block. Sweep efficiency is an equally important factor in oil recovery, especially in fractured formations. Fracture systems generally have a broad distribution of fracture widths. The wider fractures will act as thief zones for the injected fluid and little of the injected fluid will reach the narrower fractures. Favorable mobility ratio displacement aids in the distribution of injected fluids in heterogeneous systems. Polymer has commonly been used for mobility control of surfactant flooding processes. However, polymer will also retard the invasion of the surfactant solution into the matrix. An alternative process of mobility control for surfactant flooding is foam[40,54]. Foam mobility control has been field demonstrated for aquifer remediation[55] and since then, applied to full-scale expansions.

CONCLUSIONS

1. Crude oils used for interfacial research should be screened for contamination.
2. Calcite, which is normally positively charged at neutral pH can be made negatively charged through the presence of $NaHCO_3/Na_2CO_3$ in the brine.

3. The wettability of crude oil on calcite and the ease of wettability alteration with alkaline surfactant solution is a function of aging time, temperature, and surfactant formulation. The degree of wettability alteration observed here ranged from preferentially water-wet to intermediate-wet.
4. Oil is retained in oil-wet pores by capillarity. Oil displacement can occur by buoyancy since alkaline surfactant solution reduces interfacial tension and alters wettability to more water-wet conditions.
5. Oil recovery from oil-wet cores has been demonstrated by spontaneous imbibition of an alkaline anionic surfactant solution.

ACKNOWLEDGMENT

The authors acknowledge Maura Puerto and Clarence Miller for their advice and assistance; Larry Britton and Upali Weerasooriya for the surfactants, and Jill Buckley for the crude oil analysis. Hung-Lung Chen and Marathon Oil Company are acknowledged for the crude oil, core samples and the imbibition apparatus. The financial support of the Consortium on Processes in Porous Media and the U.S. DOE are gratefully acknowledged.

NOMENCLATURE

g = acceleration of gravity, m/s^2

IFT = interfacial tension, mN/m

σ = interfacial tension, N/m

$\Delta\rho$ = density difference, kg/m^3

REFERENCES

1. Wardlaw, N.C.: “Factors Affecting Oil Recovery from Carbonate Reservoirs and Prediction of Recovery,” in *Carbonate Reservoir Characterization: A Geologic-Engineering Analysis, Part II*, Chilingarian, G.V., Mazzullo, S.J., and Rieke, H.H., ed., Elsevier, New York, (1996) 867.

2. Van Golf-Racht, T.D.: "Naturally-Fractured Carbonate Reservoirs," in *Carbonate Reservoir Characterization: A Geologic-Engineering Analysis, Part II*, Chilingarian, G.V., Mazzullo, S.J., and Rieke, H.H., ed., Elsevier, New York, (1996) 683.

3. Morrow, N.R. and Mason, G.: "Recovery of oil by spontaneous imbibition," *Current Opinion in Colloid & Interface Science*, (2001) **6,** 321.

4. Schechter, D.S., Zhou, D., and Orr, F.M., Jr.: "Low IFT drainage and imbibition," *J. Pet. Sci. & Eng*., (1994) **11** 283.

5. Miller, J. and Austad, T.: "Chemical flooding of oil reservoirs. 6. Evaluation of the mechanisms for oil expulsion by spontaneous imbibition of brine with and without surfactant in water-wet, low permeability, chalk material," *Colloids and Surfaces A: Physicochemical and Engineering Aspects*, (Aug 10, 1996) **113**, No. 3 269.

6. Miller, J. and Austad, T.: "Chemical flooding of oil reservoirs. 7. Oil expulsion by spontaneous imbibition of brine with and without surfactant in mixed-wet, low permeability chalk material," *Colloids and Surfaces A: Physicochemical and Engineering Aspects*, (Oct. 5, 1996) **117**, No. 1-2 109.

7. Austad, T., Matre, B., Milter, J., Saevaried, A., and Oyno, L.: "Chemical flooding of oil reservoirs. 8. Spontaneous oil expulsion from oil- and water-wet low permeability caulk material by imbibition of aqueous surfactant solutions," *Colloids and Surfaces A: Physicochemical and Engineering Aspects*, (June 15, 1998) **137**, No. 1-3 117.

8. Austad, T. and Milter, J.: "Spontaneous imbibition of water into low permeability chalk at different wettabilities using surfactants," Proceedings – SPE International Symposium on Oilfield Chemistry, (1997) 257.

9. Standes, D.C. and Austad, T.: "Wettability alteration in chalk 1. Preparation of core material and oil properties," *J. Pet. Sci. Eng*., (2000) **28**, 111.

10. Standes, D.C. and Austad, T.: "Wettability alteration in chalk 2. Mechanism for wettability alteration from oil-wet to water-wet using surfactants," *J. Pet. Sci. Eng*., (2000) **28**, 123.

11. Standnes, D.C., Nogaret, L.A.D., Chen, H.-L., and Austad, T.: "An evaluation of spontaneous imbibition of water into oil-wet reservoir cores using a nonionic and a cationic surfactant," *Energy and Fuels*, **16**, No. 6 (Nov./Dec. 2002) 1557.

12. Chen, H.L., Lucas, L.R., Nogartet, L.A.D., Yang, H.D., and Kenyon, D.E.: "Laboratory Monitoring of Surfactant Imbibition Using Computerized Tomography," SPE 59006 presented at the 2000 International Petroleum Conference and Exhibition, Villahermosa, Mexico (1-3 February 2000).

13. Spinler, E.A., Zornes, D.R., Tobola, D.P., and Moradi-Araghi, A.: "Enhancement of Oil Recovery Using a Low Concentration of Surfactant to Improve Spontaneous and Forced Imbibition in Chalk," SPE 59290 presented at the 2000 SPE/DOE Improved Oil Recovery Symp., Tulsa, OK (3-5 April 2000).

14. Treiber, L.E., Archer, D.L., and Owens, W.W.: "A Laboratory Evaluation of the Wettability of Fifty Oil-Producing Reservoirs," *SPEJ* (December, 1972) 531.

15. Freedman, R., Lo, S.-W., Flaum, M., Hirasaki, G.J., Matteson, A., and Sezginer, A.: "A New NMR Method of Fluid Characterization in Reservoir Rocks: Experimental Confirmation and Simulation Results," *SPEJ* (December, 2001) 452.

16. Dubey, S.T. and Doe, P.H.: "Base Number and Wetting Properties of Crude Oils," *SPERE* (August, 1993) 195.

17. Hirasaki, G.J.: "Wettability: Fundamentals and Surface Forces," *SPEFE* (June, 1991) 217.

18. Buckley, J.S., Takamura, K., and Morrow, N.R.: "Influence of Electrical Surface Charges on the Wetting Properties of Crude Oils," *SPERE* (August, 1989) 332.

19. Morrow, N.R., Cram, P.J., and McCaffery, F.G.: " Displacement Studies in Dolomite with Wettability Control by Octanoic Acid," *SPEJ* (August, 1973) 221.

20. Hansen, G, Hamouda, A.A., and Denoyel, R.: "The effect of pressure on contact angles and wettability in the mica/water/n-decane system and the calcite+stearic acid/water/n-decane system," *Colloids and Surfaces A: Phtsicochemical and Engineering Aspects*, (2000), **172**, 7.

21. Hartland, S. and Hartley, R.W.: *Axisymmetric Fluid-Liquid Interfaces*, Elsevier, New York (1976).

22. Finn, R.: *Equilibrium Capillary Surfaces*, Springer-Verlag, New York, 1986.

23. Nelson, R.C., Lawson, J.B., Thigpen, D.R., and Stegemeier, G.L.: (1984) "Cosurfactant-Enhanced Alkaline Flooding," SPE/DOE 12672 presented at the SPE/DOE Fourth Symp. EOR, Tulsa, OK, April 15-18.

24. Falls, A. H., Thigpen, D. R., Nelson, R. C., Ciaston, J. W., Lawson, J. B., Good, P. A., Ueber, R. C., and Shahin, G. T.: "A Field Test of Cosurfactant-Enhanced Alkaline Flooding," SPE/DOE 24117, paper prepared for presentation at the SPE/DOE Eighth Symposium on Enhanced Oil Recovery (April 22-24, 1992) Tulsa, OK.

25. Olsen, D.K., Hicks, M.D., Hurd, B.G., Sinnokrot, and Sweigart, C.N.: "Design of a Novel Flooding System for an Oil-Wet Central Texas Carbonate Reservoir," SPE/DOE 20224 presented at the SPE/DOE Seventh EOR Symp., Tulsa, OK (22-25 April, 1990).

26. Clark, S. R., Pitts, M. J., and Smith, S. M.: "Design and Application of an Alakaline-Surfactant-Polymer Recovery System for the West Kiehl Field," *SPE Advanced Technology Series*, **1**, No. 1 (1993) 172.

27. Baviere, M., Glenat, P., Plazanet, V., and Labrid, J.: "Improved EOR by Use of Chemicals in Combination," *SPERE* (August, 1995) 187.

28. Gao, S., Li, H., and Li, H.: "Laboratory Investigation of Combination of Alkali/Surfactant/Polymer Technology for Daqing EOR," *SPE Reservoir Engineering*, (August 1995) 195.

29. Gao, S., Li, H., Yang, Z., Pitts, M. J., Surkalo, H., and Wyatt, K.: "Alkaline-Surfactant-Polymer Pilot Performance of the West Central Saetu, Daqing Oil Field," SPE/DOE 35383, paper prepared for presentation the 1996 SPE/DOE Tenth Symposium on Improved Oil Recovery (April 21-24, 1996) Tulsa, OK.

30. Gu, H., Yang, R., Guo, S., Guan, W., Yue, X., and Pan, Q.: Study on Reservoir Engineering: ASP Flooding Pilot Test in Karamay Oilfield," SPE 50918, paper prepared for presentation at the 1998 SPE International Conference and Exhibition (November 2-6, 1998) Beijing, China.

31. French, T.R. and Burchfield, T.E.: Design and Optimization of Alkaline Flooding Formulations, " SPE/DOE 20238 presented at the SPE/DOE Seventh Symp. On EOR, Tulsa, OK (April 22-25, 1990)

32. Meyers, J. J., Pitts, M. J., and Wyatt, K.: "Alkaline-Surfactant-Polymer Flood of the West Kiehl, Minnelusa Unit," SPE/DOE 24144, paper prepared for presentation at the SPE/DOE Eighth Symposium of Enhanced Oil Recovery (April 22-24, 1992) Tulsa, OK.

33. Qiao, Q., Gu, H., Li D., and Dong, L.: "The Pilot Test of ASP Combination Flooding in Karamay Oil Field," SPE 64726, paper prepared for presentation at the SPE International Oil and Gas Conference and Exhibition in China (November 7-10, 2000) Beijing, China.

34. Qu, Z., Zhang, Y., Zhang, X., and Dai, J.: A Successful ASP flooding Pilot in Gudong Oil Field," SPE 39613, paper prepared for presentation at the 1998 SPE/DOE Improved Oil Recovery Symposium (April 19-22, 1998) Tulsa, OK.

35. Surkalo, H.: "Enhanced Alkaline Flooding," SPE 19896, SPE Technology Today Series (January 1990), *JPT*.

36. Tong, Z., Yang, C., Wu, G., Yuan, H., Yu, L., and Tian, G.: "Study of Microscopic Flooding Mechanism of Surfactant/Alkali/Polymer," SPE 39662, paper prepared for presentation at the 1998 SPE/DOE Improved Oil Recovery Symposium (April19-22, 1998) Tulsa, OK.

37. Vargo, J., Turner, J., Vergnani, B., Pitts, M. J., Wyatt, K., Surkalo, H., and Patterson, D.: "Alkaline-Surfactant-Polymer Flooding of the Cambridge Minnelusa Field," *SPE Reservoir Eval. & Eng.* (December 2000), **3**, No. 6, 552.

38. Wang, D., Zhang, Z., Cheng, J., Yang, J., Gao, S., and Li, L.: "Pilot Tests of Alkaline/Surfactant/Polymer Flooding in Daqing Oil Field," *SPERE* (November, 1997) 229.

39. Wang, C., Wang, B., Cao, X., and Li, H.: "Application and Design of Alkaline-Surfactant-Polymer System to Close Well Spacing Pilot Gudong Oilfield," SPE 38321,

paper prepared for presentation at the 1997 SPE Western Regional Meeting (June 25-27) Long Beach, CA.

40. Zhang, Y., Yue, X., Dong, J., and Yu, L.: "New and Effective Foam Flooding to Recover Oil in Heterogeneous Reservoir," SPE 59367, paper prepared for presentation at the 2000 SPE/DOE Improved Oil Recovery Symposium (April 3-5, 2000) Tulsa, OK.
41. Cheng, K. H.: "Chemical consumption during alkaline flooding: a comparative evaluation," paper 14944 presented at the SPE/DOE Fifth Symposium on Enhanced Oil Recovery, Tulsa, OK. (1986)
42. Al-Hashim, H. S., Obiora, V., Al-Yousef, H. Y., Fernandez, and F. Nofal, W.: "Alkaline surfactant polymer formulation for Saudi Arabian carbonate reservoirs," paper 35353 presented at SPE/DOE Tenth Symposium on Improved Oil Recovery, Tulsa, OK. (1996).
43. Krumrine, P. H., Campbell, T. C., and Falcone, J. S. Jr.: "Surfactant flooding 1: the effect of alkaline additives on IFT, surfactant adsorption, and recovery efficiency," paper 8998 presented at SPE Fifth International Symposium on Oilfield and Geothermal Chemistry, Stanford, CA, (1980).
44. Israelachvili, J. and Drummond, C., "Fundamental Studies of Oil-Surface-Water Interactions and Its Relationship to Wettability," The 5th International Symposium on Evaluation of Reservoir Wettability and its effect on oil recovery, Trondheim, Norway, (22-24 June 1998).
45. Yang, S.-Y., *Mechanisms of Wettability for Crude Oil/Brine/Mica System*, Ph.D. thesis, Rice University, Houston, TX. (2000).
46. Glover, C.J., Puerto, M.C., Maerker, J.M., and Sandvik, E.L.:, "Surfactant Phase Behavior and Retention in Porous Media," *SPEJ*, (June, 1979) 183.
47. Gale, W.W. Puerto, M.C., Ashcraft, T.L., Saunders, R.K., and Reed, R.L.: "Propoxylated Ethoxylated Surfactants and Method of Recovering Oil Therewith," U.S. Patent 4,293,428 (October 6, 1981).

48. Osterloh, W.T. and Jante, Jr., M.J.: "Surfactant Polymer Flooding with Anionic PO/EO Surfactant Microemulsions Containing Polyethylene Glycol Additives," SPE/DOE paper 24151 presented at the Eighth Symp. On EOR, Tulsa, OK (April 22-24, 1992).

49. Wellington, S.L. and Richardson, E.A.: "Low Surfactant Concentration Enhanced Waterflooding," SPE 30748 paper presented at the SPE ATCE, Dallas, TX (22-25 October, 1995).

50. Aoudia, M., Wade, W.H., and Weerasooriya, V.: "Optimum Microemulsions Formulated with Propoxylated Guerbet Alcohol and Propoxlated Tridecyl Alcohol Sodium Sulfates," *J. Dispersion Sci. Tech*., **16**, No. 2 (1995) 115.

51. Hirasaki, G.J., van Domselaar, H.R., and Nelson, R.C. "Evaluation of the Salinity Gradient Concept in Surfactant Flooding", *Soc. Pet. Eng. J.* (June 1983), 486.

52. Reed, R.L. and Healy, R.N.: "Contact Angles for Equilibrated Microemulsion Systems," SPE 8262 presented at the 54th SPE ATCE, Las Vagas, NV (Sept. 23-26, 1979).

53. Talley, L.D.: "Hydrolytic Stability of Alkylethoxy Sulfates," SPE/DOE 14912 presented at the SPE/DOE Fifth Symp. On EOR, Tulsa, OK (April 20-23, 1986).

54. Lawson, J.B. and Reisberg, J.: "Alternate Slugs of Gas and Dilute Surfactant for Mobility Control During Chemical Flooding," SPE 8839 presented at the First Joint SPE/DOE Symp. On EOR, Tulsa, OK (April 20-23, 1980).

55. Hirasaki, G.J., Miller, C.A., Szafranski, R., Tanzil, D., Lawson, J.B., Meinardus, H., Londergan, J.T., Jackson, R.E., Pope, G.A., and Wade, W.H.: "Field Demonstration of the Surfactant/Foam Process for Aquifer Remediation," SPE 39292 presented at the 1997 SPE ATCE, San Antonio (5-8 October 1997).

Table 9.1 Crude oil properties (Jill Buckley, private communication)

Oil ID	°API	RI@20°C	ρ@20°C	Acid#	Base #	IEP	B/A	Sat.	Arom.	Resins	Asph.	Visc.(cp)
MY1	27.2	1.4979	0.8887	0.50	1.17	3.2	2.34	64.02	24.59	9.67	1.71	22.6
MY2	28.9	1.4941	0.8789	0.17	1.16	3.7	6.82	62.52	23.72	12.68	1.08	18.1
MY3	28.2	1.4955	0.8830	0.20	1.17	3.3	5.85	61.86	24.83	12.22	1.09	19.1
MY4	28.4	1.4943	0.8818	0.22	1.23	3.4	5.59	65.28	23.69	9.94	1.10	18.8

Table 9.2 Surfactant identification

Trade name	Structural name
CS-330	Sodium dodecyl 3EO sulfate
C12-3PO	Sodium dodecyl(Guerbet) 3PO sulfate [50]
TDA-4PO	Ammonium iso-tridecyl 4PO sulfate[50]
ISOFOL14T-4.1PO	Sodium tetradecyl(Guerbet) 4PO sulfate [50]

Table 9.3 Core properties and results

Property	Core A	Core B
diameter, inch	1.5	1.5
length, inch	8	3.5
porosity, %	11	20
Permeability, md	7.3	90
brine	Table 9.4	Table 9.4
crude oil	MY1	MY3
oil saturation, %	36	71
aging	none	80° C, 24 hr
surfactant	CS-330	TDA-4PO
surf. conc., %	0.05	0.05
Na_2CO_3, M	0.3	0.3
Recovery, % OOIP	37	>18

Table 9.4 Formation brine composition

Element	mg/L	mmole/L
sodium	2024	88.0
calcium	802	20.0
magnesium	243	10.0
strontium	21	0.2
chloride	3899	110.0
sulfate	164	1.7
bicarbonate	2110	34.6
ppm TDS	9265	
ionic strength		180.2

$$\Delta\rho\, g\, h = -2\sigma\cos\theta / R$$

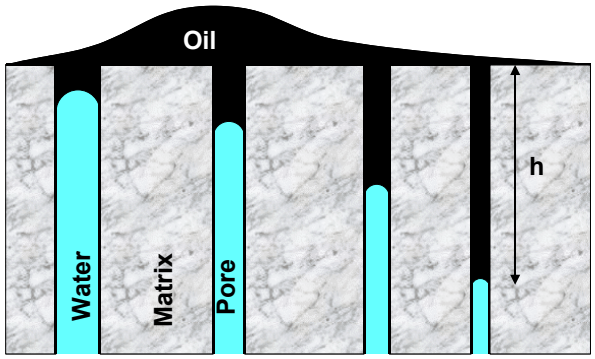

Fig. 9.1 The height of the retained oil in oil-wet matrix blocks is a function of the pore radius, interfacial tension, and contact angle.

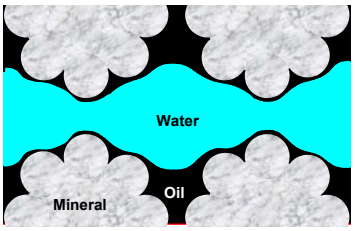

Fig. 9.2 Oil is trapped by surface trapping in oil-wet and small pores of oil-wet systems.

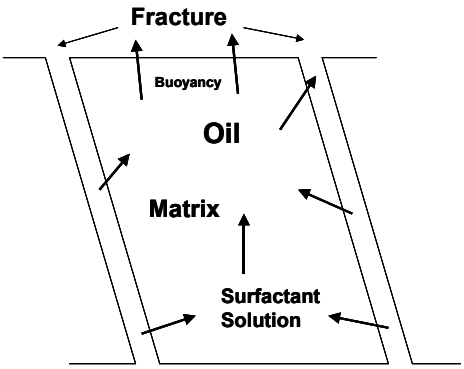

Fig. 9.3 Spontaneous imbibition of surfactant solution from the fracture system into the matrix occurs to replace the oil that flows out of the matrix by buoyancy.

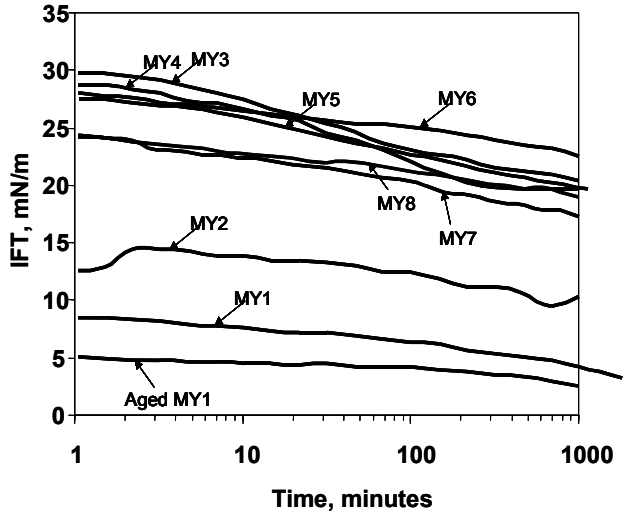

Fig. 9.4 Transient crude oil/brine IFT is an indication of whether of not the crude oil is contaminated with surface-active materials.

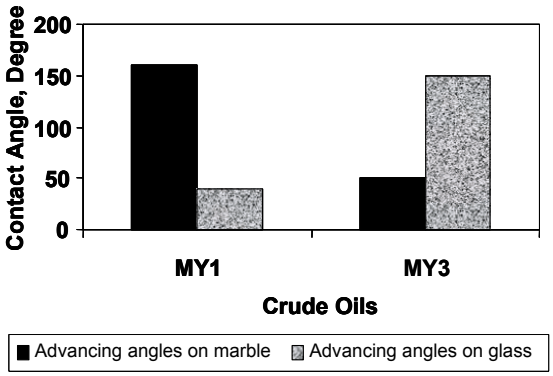

Fig. 9.5 Water advancing contact angles of MY1 and MY3 crude oils on calcite and glass with 5-10 minutes aging time.

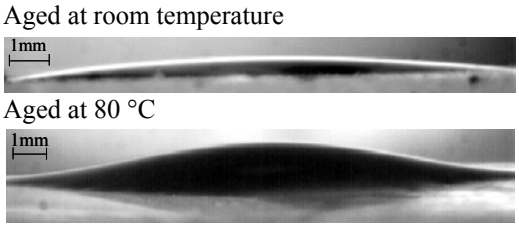

Fig. 9.6 Water advancing contact angle of MY3 crude oil in 0.1 M NaCl brine after aging for 24 hours either at room temperature or 80 °C.

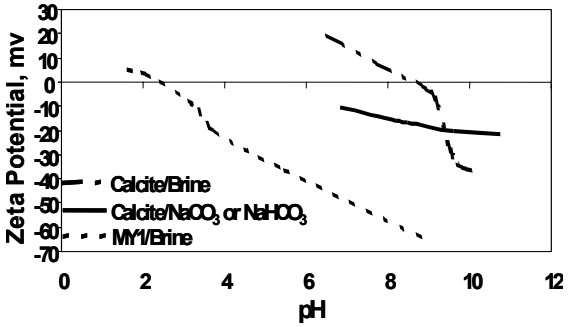

Fig. 9.7 Zeta potential of MY1 crude oil/brine and calcite/brine interfaces in 0.02M NaCl as a function of pH without and with added Na_2CO_3 / $NaHCO_3$ and pH adjusted with HCl.

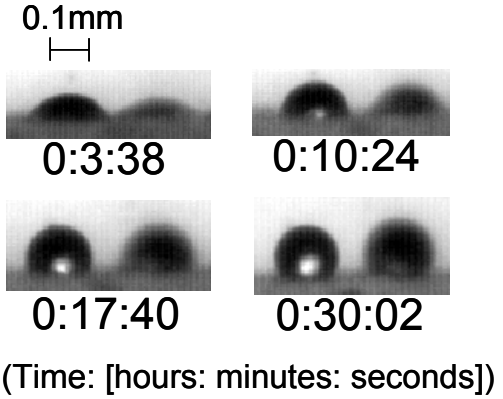

Fig. 9.8 Wettability alteration of calcite plate aged at room temperature with 0.05% CS-330 and 0.5 M Na_2CO_3.

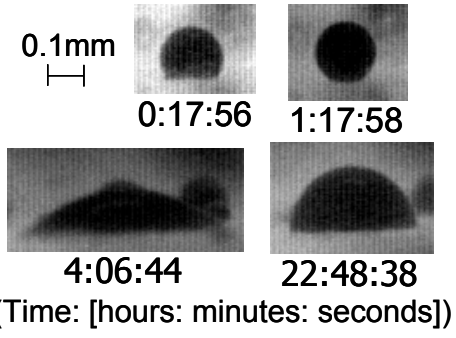

Fig. 9.9 Wettability alteration of calcite plate aged at 80 °C with 0.05% CS-330 and 0.5 M Na_2CO_3. (Two different drops show different wettability.)

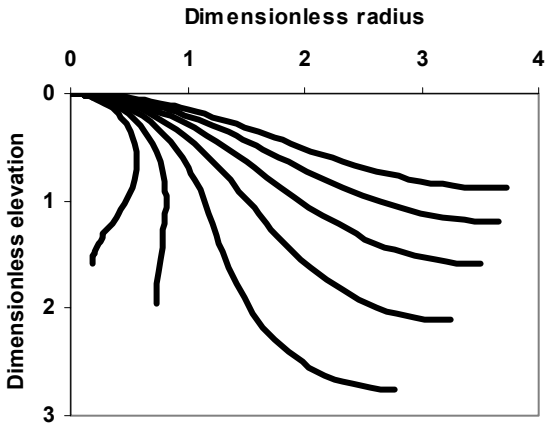

Fig. 9.10 Family of axisymmetric oil interfaces for an oil drop immersed in water. Each curve has a different curvature at the apex of the drop. The distances are normalized by $\sqrt{\sigma/(\Delta\rho g)}$.

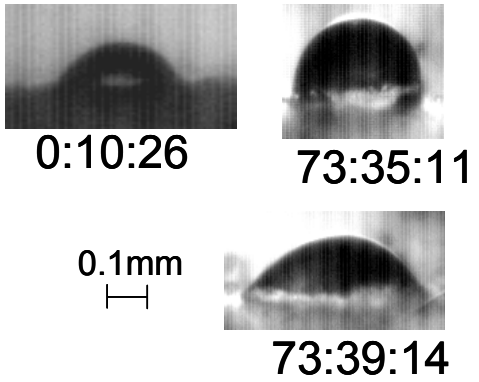

Fig. 9.11 Wettability alteration of calcite plate aged at room temperature with brine and with 0.05% TDA-4PO and 0.3 M Na_2CO_3. (These are different drops.)

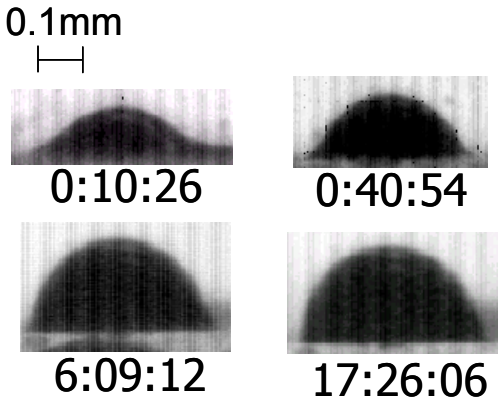

Fig. 9.12 Wettability alteration of calcite plate aged at 80° C with brine and with 0.05% TDA-4PO and 0.3 M Na_2CO_3.

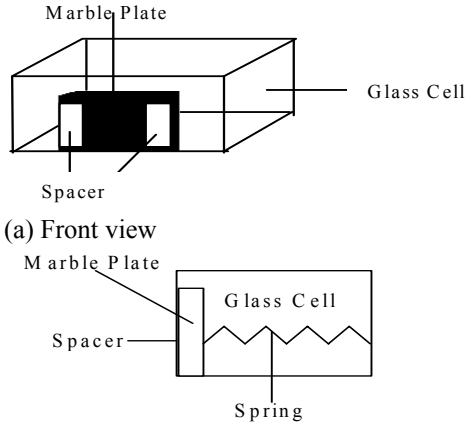

Fig. 9.13 A calcite (marble) plate has two plastic films to create a 15 μm gap between the plate and the front of an optical cell

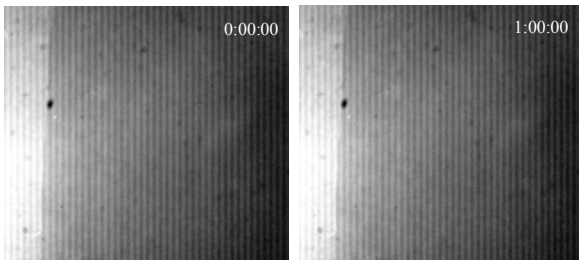

(a) Oil Displacement in Brine

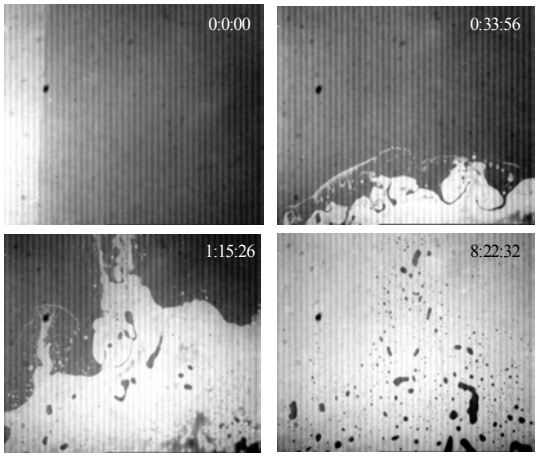

(b) Oil Displacement in 0.05 % CS-330/0.3 M Na_2CO_3
(Time: hours: minutes: seconds)

Fig. 9.14 Displacement of crude oil in narrow gap with brine or with alkaline surfactant solution.

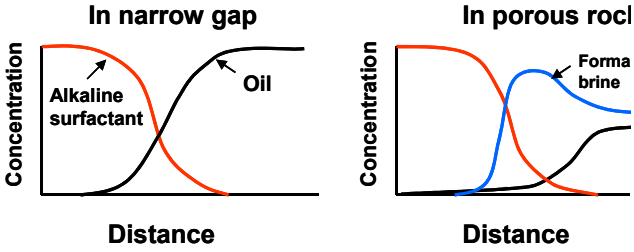

Fig. 9.15 Saturation/concentration profiles in a narrow gap or in a porous rock during displacement of oil by buoyancy.

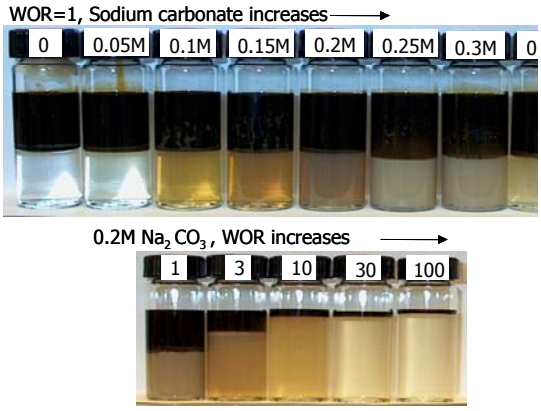

Fig. 9.18 Phase behavior of MY3 crude oil with 0.05% (AM) C12-3PO.

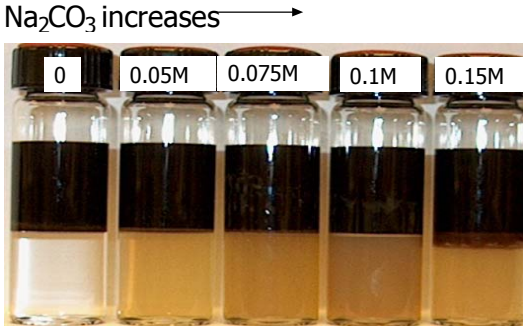

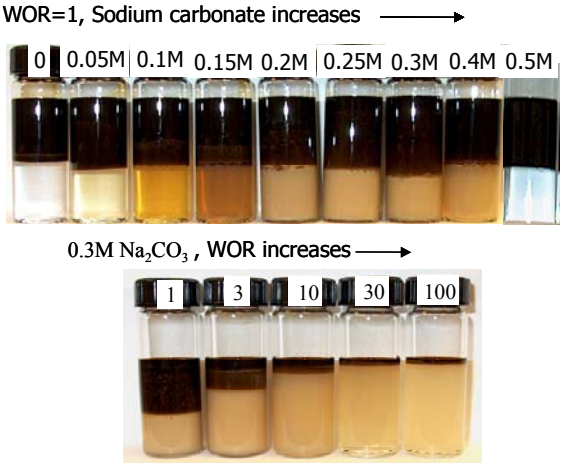

Fig. 9.19 Phase behavior of MY3 crude oil with 0.05% (AM) TDA-4PO.

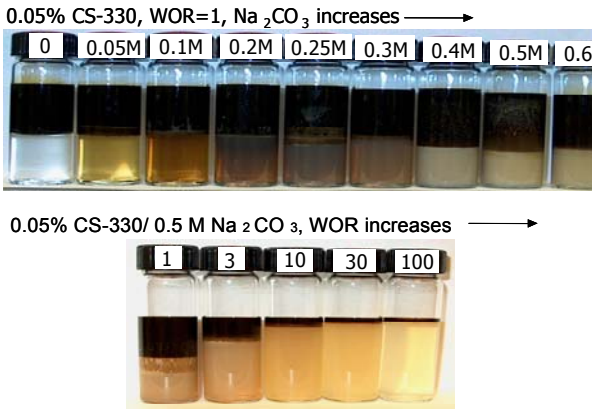

Fig. 9.17 Phase behavior of MY3 crude oil with 0.05% (AM) CS-330.

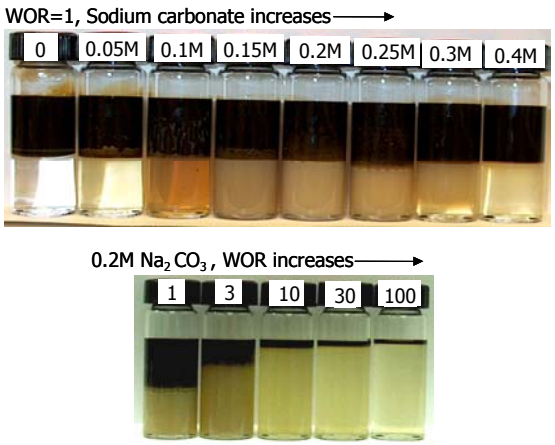

Fig. 9.20 Phase behavior of MY3 crude oil with 0.05% (AM) ISOFOL 14T-4.1PO.

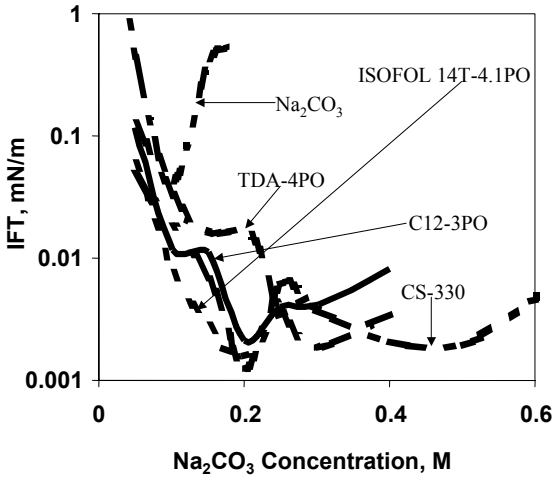

Fig. 9.21 IFT of MY3 crude oil with 0.05% (AM) surfactant solution as a function of Na_2CO_3 concentration. Water/Oil ratio = 1:1

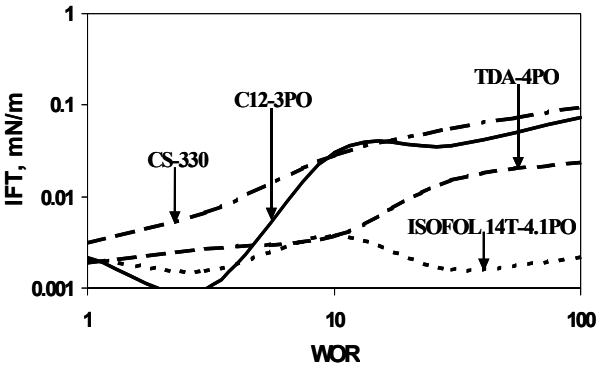

Fig. 9.22 IFT of MY3 crude oil with 0.05% (AM) surfactant solution as a function of water/oil ratio. Optimum Na_2CO_3 concentration corresponding to WOR=1.

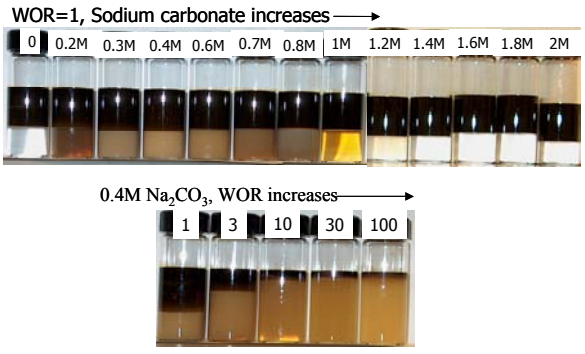

Fig. 9.23 Phase behavior of MY3 crude oil with 0.2% (AM) TDA-4PO

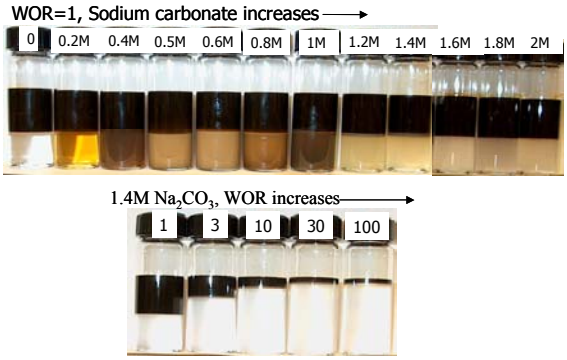

Fig. 9.24 Phase behavior of MY3 crude oil with 1% (AM) TDA-4PO.

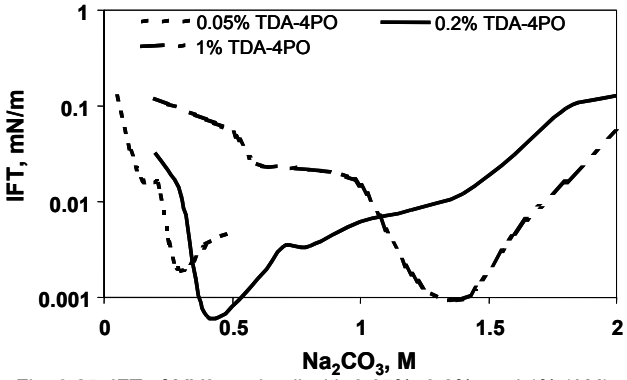

Fig. 9.25 IFT of MY3 crude oil with 0.05%, 0.2%, and 1% (AM) TDA-4PO as a function of Na_2CO_3 concentration. Water/oil ratio = 1:1.

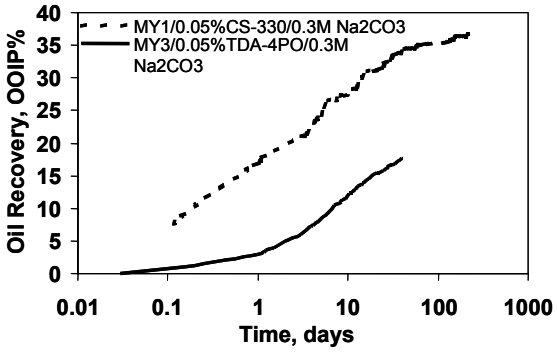

Fig. 9.26 Oil recovery by spontaneous imbibition of the two systems described in Table 3.

10. Effects of Asphaltene Polydispersity on its Phase Behavior In Oil

P.D. Ting, G.J. Hirasaki, and W.G. Chapman

INTRODUCTION

By using a proposed oil and asphaltene equation-of-state (EOS) characterization scheme, Ting, *et al.* (2003) has shown that the Statistical Associating Fluid Theory (SAFT) equations of state can adequately describe asphaltene phase behavior in model live oil and recombined oil systems under reservoir conditions. The results presented by these authors were calculated by treating asphaltenes as a single, monodisperse component in oil. Since asphaltenes are, in actuality, a polydisperse class of compounds with resins as their lowest molecular weight sub-fractions, the effects of asphaltene polydispersity need to be incorporated.

The goal of this investigation is to examine the effects of asphaltene polydispersity on its thermodynamic phase behavior in oil. One of the questions we will try to answer is whether the lowest molecular weight asphaltenes (including the resins) can stabilize, via nonpolar interactions, the higher molecular weight asphaltenes. Another question we will try to address is whether SAFT can describe the correct partitioning of the asphaltene pseudo-components between the oil and the precipitated phases at equilibrium. Since deposition tendencies onto pipeline surfaces have often been associated with variations in the morphology and the composition of the precipitated asphaltene phase, an understanding of the molecular weight distribution of polydisperse asphaltenes in equilibrium phases will help us estimate asphaltene's deposition tendencies.

At this stage of the research, polydisperse asphaltene will be represented as four pseudo-components in SAFT: the n-C_{3-5}, the n-C_{5-7}, the n-C_{7-15}, and the n-C_{15+} n-alkane insoluble sub-fraction. The reader should keep in mind that, traditionally, the n-C_{3-5} fraction is called resins and that conventional asphaltene extraction techniques generally identify asphaltenes as the n-C_{5+} or n-C_{7+} insoluble fractions of heavy organics. All asphaltene sub-fractions in this work are soluble in aromatic solvents.

SELECTION OF SAFT PARAMETERS FOR POLYDISPERSE ASPHALTENES

In experiments performed by Wang (2000), the asphaltenes for Lagrave oil (the oil modeled in this study) were first separated into various solubility fractions using excess n-pentane, n-heptane, and n-pentadecane precipitants; these sub-fractions are called n-C_5 insoluble asphaltenes (7.5 g/100 mL oil), the n-C_7 insoluble asphaltenes (6.7 g/100 mL oil), and the n-C_{15} insoluble asphaltenes (5.1 g/100mL oil), respectively. The asphaltene instability onsets for mixtures of asphaltenes, toluene, and n-alkanes (at ambient condition and initially with an asphaltene/toluene ratio of 1 g per 100mL toluene) were then measured for each asphaltene fraction. The experimental asphaltene fractionation and instability onset data that we used to fit the SAFT model are those for Lagrave oil and were taken from Wang (2000).

The method used to obtain the SAFT parameters for polydisperse asphaltenes was similar to the monodisperse SAFT asphaltene characterization procedure given in Ting, et al. (2003). Within the SAFT model, polydisperse asphaltenes were modeled as three or four pseudo-components (depending on whether the resin fraction, which is the n-C_{3-5} asphaltene sub-fraction, was included): an n-C_{15+} sub-fraction, an n-C_{7-15} sub-fraction, an n-C_{5-7} sub-fraction, and an n-C_{3-5} sub-fraction. SAFT parameters were fit for the n-C_{15+} asphaltene sub-fraction to reproduce the experimental data on the minimum volume fraction precipitant needed to induce asphaltene instability (ϕ_v^{ppt}) for mixtures of n-C_{15} insoluble asphaltene, toluene, and various n-alkanes. The asphaltene made from the combination of n-C_{15+} and n-C_{7-15} sub-fractions were assumed to represent the n-C_7 insoluble asphaltenes; a second set of SAFT parameters were fit for the n-C_{7-15} sub-fraction to reproduce (together with the previously fitted n-C_{15+} sub-fraction) the experimental ϕ_v^{ppt} data for a mixture of n-C_7 insoluble asphaltene, toluene, and n-alkane. Finally, a third set of SAFT parameters were fit to the n-C_{5-7} sub-fraction so that the combination of the n-C_{15+} (previously fit), n-C_{7-15} (previous fit), and n-C_{5-7} sub-fractions represented the n-C_5 insoluble asphaltenes and reproduced the experimental ϕ_v^{ppt} data for a mixture of n-C_5 insoluble asphaltene, toluene, and n-alkanes. Due to lack of precipitation data, the SAFT parameters for the resin (n-C_{3-5}) sub-fraction were obtained by decreasing the SAFT parameters (m and ε/k) of the n-C_{5-7} asphaltene sub-fraction until a set of parameter was obtained that would make the resins insoluble in propane (tested at 10 bars) and soluble in n-pentane.

A comparison of the equation-of-state fitted and the experimental ϕ_v^{ppt} data is shown in Figure 10.1, with the fitted SAFT asphaltene parameters listed in Table 10.1. As seen in the

figure, the agreement between SAFT calculated and measured ϕ_v^{ppt} is qualitative. SAFT is able to describe the change in magnitude (and to a lesser extent, the curvature) of the ϕ_v^{ppt} vs. n-alkane carbon number curve between n-C_{15} insoluble and n-C_5 insoluble asphaltenes. For the precipitation onsets with n-C_7 and n-C_5 extracted asphaltenes, SAFT does not accurately describe the experimental ϕ_v^{ppt} data in cases where larger n-alkanes (undecane and higher) are used to induce asphaltene precipitation; SAFT consistently under-predicts the volume fraction of n-alkane precipitants needed to induce asphaltene instability.

A comparison of SAFT and measured mass distribution of the asphaltene sub-fractions is shown in Figure 10.2. For the column labeled "experimental", the mass of each asphaltene sub-fraction was inferred from the difference in the measured amount of asphaltenes precipitated with different precipitants. Within the SAFT model, the amount of each asphaltene sub-fraction was optimized (together with the sub-fraction's asphaltene SAFT parameters) to fit the experimental ϕ_v^{ppt} data in Figure 10.1. It is interesting to note the large discrepancy in the amount of n-C_{5-7} asphaltene sub-fraction between experimental inferred and SAFT calculated n-C_5 extracted asphaltenes; to get a reasonable fit to experimental ϕ_v^{ppt} data, SAFT requires three times as much low molecular weight asphaltenes (n-C_{5-7} sub-fraction) as was inferred from experiments.

Several factors may contribute to the poor agreement in the amount of low molecular weight asphaltenes in the asphaltene fraction shown in Figure 10.2. Experimentally, the measured amount of asphaltenes precipitated may contain not only asphaltenes that should precipitate with the precipitant used but also small amounts of entrained resins, oil, and other asphaltene fractions; variations in the amount of asphaltenes precipitated exist even for the same oil using the same extraction procedure. On the modeling side, because there are insufficient data to uniquely fit all of the model parameters for polydisperse asphaltenes, certain approximations and relationships have to be made. For instance, the molecular weights of all SAFT asphaltene sub-fractions were set to be linearly dependent on chain length. This was done because the experimental molecular weight of each asphaltene sub-fraction is not known and because the SAFT chain length is roughly linearly dependent on molecular weight for polynuclear aromatics. The constant of proportionality (MW=*m*/0.0216) used in this work was set to give the n-C_{15+} asphaltene sub-fraction a molecular weight of 2,500. In another approximation, the segment diameters of all asphaltene sub-fractions were set to 4 Angstroms.

The rationale behind setting the segment diameter to 4 was that for most polynuclear aromatics and polynuclear aromatics derivatives, the average value for the SAFT parameter σ is about 4.

A plot of the SAFT parameters ε/k vs. m for the various SAFT asphaltene fractions and resin (the n-C_{3-5} sub-fraction) shows a well-defined trend between ε/k and m (Figure 10.3). The asphaltenes precipitated by the lower molecular weight n-alkanes tend to be smaller in size and have lower segment energy.

EFFECTS OF ASPHALTENE POLYDISPERSITY AND RESIN ADDITION

To investigate the roles resins and asphaltene polydispersity play on asphaltene phase behavior in oil, the asphaltene solubility behavior of four model oil mixtures with monodisperse or polydisperse asphaltenes are compared. In these model systems, toluene is used as the model oil (with different amounts of n-alkane precipitants added) and the asphaltene parameters were fit to experimental ϕ_v^{ppt} data for Lagrave asphaltenes. The properties and asphaltene/resin contents of these systems are listed in Table 10.2 and are discussed in the following paragraph. We use a mixture of 7.5g asphaltenes in 100mL of toluene in these investigations because the total amount of n-pentane insoluble asphaltenes in Lagrave oil is 7.5g. Following Ting, *et al.* (2003), all binary interaction parameters between all species are set to zero.

The biggest difference between the various systems in Table 10.2 is that asphaltenes in Systems 1 and 2 are monodisperse, while the asphaltenes in Systems 3 and 4 are polydisperse. More specifically, the asphaltene used in Model System 1 is monodisperse and was fit to experimental ϕ_v^{ppt} data for the n-C_{15} insoluble Lagrave asphaltenes (also called the n-C_{15+} asphaltene fraction in this work). The asphaltene used in Model System 2 is monodisperse and was fit to experimental ϕ_v^{ppt} data for the n-C_5 insoluble Lagrave asphaltenes. The asphaltene used in Model System 3 is polydisperse and the SAFT parameters for each asphaltene sub-fraction was fit to the experimental ϕ_v^{ppt} data of the fractionated asphaltenes. Model System 4 is similar to Model System 3 with the exception that 10g of resin per 100mL oil (approximately 1-2 moles resin/100moles toluene) is added to the system. The amount of resin added (10g resin per 100mL oil) is arbitrary because the actual amount of resin in the oil is not available in literature.

The effects of n-alkane addition on the amount of asphaltenes precipitated (at 20°C and 1 bar) for the four model oil mixtures are shown in Figures 10.4 and 10.5. For systems containing monodisperse asphaltenes (Figure 10.4), the change in asphaltene solubility is dramatic:

asphaltenes go from completely soluble to almost completely insoluble in the model oil when the volume fraction of the n-alkane precipitant is increased slight past the asphaltene instability onset point. As expected, the lower molecular weight asphaltenes (the monodisperse asphaltene fit to the n-C_5 insoluble asphaltenes ϕ_v^{ppt} data) are more soluble than the higher molecular weight asphaltene (the monodisperse, n-C_{15} insoluble asphaltene) in terms of the amount of precipitant needed to induce asphaltene instability. When sufficiently large amount of n-alkanes are added to the model oil, all asphaltenes will precipitate.

A large change in the amount of precipitated asphaltenes vs. precipitant volume fraction can be seen when the effect of asphaltene polydispersity (and resin addition) is taken into consideration (Figure 10.5). By treating asphaltene as a polydisperse specie, the amount of asphaltenes precipitated increases much more gradually with precipitant addition. A significant amount of asphaltenes will stay in solution even at high precipitant volume fractions, and more asphaltenes can be precipitated using lower molecular weight n-alkanes. It is interesting to note that when n-C_{15} is used as the precipitant, SAFT predicts the existence of a solubility minimum around $\phi_v^{ppt} = 0.9$.

A comparison of the saft-predicted behavior of polydisperse asphaltenes with and without resins show that the presence of resins will increase the amount of precipitant needed to induce the onset of asphaltene instability (figure 10.5). Furthermore, at lower precipitant volume fractions in the oil, the amount of asphaltenes that will precipitate is less when resins are present. Even though only dispersion interactions are considered in our models, the lower molecular weight asphaltenes and especially resins will stabilize the heavier asphaltenes in the oil. It can be seen in figure 5 that the effects of resins on asphaltene phase behavior in the oil become less pronounced, as the oil becomes more dilute with precipitants.

A plot of the mass distribution of the asphaltene sub-fractions as a function of precipitant volume fraction is shown in Figure 10.6. As seen in the figure, near the initial asphaltene instability onset, the precipitated phase is composed mostly of the heaviest asphaltene fractions (in this case, the n-C_{15+} sub-fraction). As the amount of precipitant is increased further, more and more lower molecular weight asphaltenes will precipitate.

SUMMARY

In this study, we investigated the effects of asphaltene polydispersity on the thermodynamic phase behavior of oil. At this stage of the research, we represented polydisperse asphaltene in SAFT with four pseudo-components: the n-C_{3-5} (the resins), the n-C_{5-7}, the n-C_{7-15}, and the n-C_{15+} sub-fractions. Using an extension of the monodisperse SAFT asphaltene parameter fitting procedure, we were able to assign a set of SAFT parameters to represent each of the four sub-fractions. The volume fractions of precipitants at asphaltene instability onset calculated using these parameters qualitatively agree with experimental findings.

SAFT calculations show that the lower molecular weight asphaltenes and resins play a large role in stabilizing higher molecular weight asphaltenes in oil. This is despite the inclusion of only dispersion interactions in the SAFT model. Resin's stabilizing effects on polydisperse asphaltene is greatest in the region of incipient asphaltene instability; when sufficiently large amounts of n-alkane precipitants are added, similar amounts of asphaltenes would precipitate regardless of the presence of resins in the oil. An analysis of the mass distribution of the asphaltene sub-fractions in the precipitated phase shows that the largest asphaltenes will precipitate first, followed by the precipitation of smaller asphaltenes upon further oil dilution.

REFERENCES

1. Ting, P.D., Hirasaki, G.J., and Chapman, W.G. *Modeling of Asphaltene Phase Behavior with the SAFT Equation of State*. Pet. Sci. Tech. 21: 647-661 (2003).
2. Wang J.X. *Predicting Asphaltene Flocculation in Crude Oils*. Ph.D. Thesis. New Mexico Institute of Mining & Technology. Socorro, New Mexico (2000).

Table 10.1. SAFT parameters for the various asphaltene sub-fractions (including resins)

	SAFT Parameters					
asph sub-fraction	MW	*m*	σ (A)	*ε/k* (K)	δ ($MPa^{0.5}$)	ρ (g/cm^3)
n-C_{15+}	2500	54	4.00	350.5	22.17	1.150
n-C_{7-15}	1852	40	4.00	340.0	21.52	1.137
n-C_{5-7}	1806	39	4.00	335.0	21.25	1.133
resin	556	12	4.00	330.0	20.41	1.103

Table 10.2. Oil and asphaltene properties of four representative model oils tested to study the effects of asphaltene polydispersity and resin addition.

Model System 1	
Ratio of asphaltene/toluene:	7.5 g/100mL (20°C, 1 bar)
Asphaltene type:	Monodisperse, fitted n-C_{15+} asphaltene (see Table 1 for parameters)
Resins in system:	No
Model System 2	
Ratio of asphaltene/toluene:	7.5 g/100mL (20°C, 1 bar)
Asphaltene type:	Monodisperse, n-C_5 asphaltene (m = 46; σ = 4.0 A; ε/k = 350.5 K; MW = 2080; ρ = 1.12 g/cm^3; δ = 22.13 $MPa^{0.5}$) This asphaltene was fitted to experimental ϕ_v^{ppt} data for n-C_5 insoluble Lagrave asphaltenes
Resins in system:	No
Model System 3	
Ratio of asphaltene/toluene:	7.5 g/100mL (20°C, 1 bar)
Asphaltene type:	Polydisperse with 3 sub-fractions: n-C_{15+}, n-C_{7-15}, and n-C_{5-7} Lagrave asphaltenes (see Table 1 for parameters)
Mass ratio of asph fractions:	4.5 : 2.0 : 3.5 (n-C_{15+}:n-C_{7-15}: n-C_{5-7})
Resins in system:	No
Model System 4	
Ratio of asphaltene/toluene:	7.5 g/100 mL (20°C, 1 bar)
Asphaltene type:	Polydisperse with 3 sub-fractions: n-C_{15+}, n-C_{7-15}, and n-C_{5-7} Lagrave asphaltenes (see Table 1 for parameters)
Mass ratio of asph fractions:	4.5 : 2.0 : 3.5 (n-C_{15+}:n-C_{7-15}: n-C_{5-7})
Resins in system:	Yes (see Table 1 for parameters)
Ratio of resin/toluene:	10 g/100 mL (20°C, 1 bar)

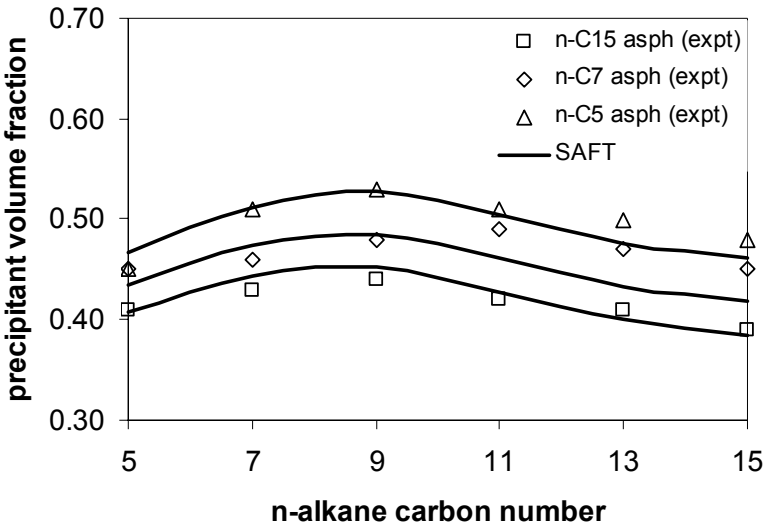

Figure 10.1. Comparison of SAFT and measured precipitant volume fraction at asphaltene instability onset for asphaltene-toluene-n-alkane mixtures at 20°C and 1 bar. The initial asphaltene/toluene ratio is 1g/100mL. Experimental data are from Wang (2000).

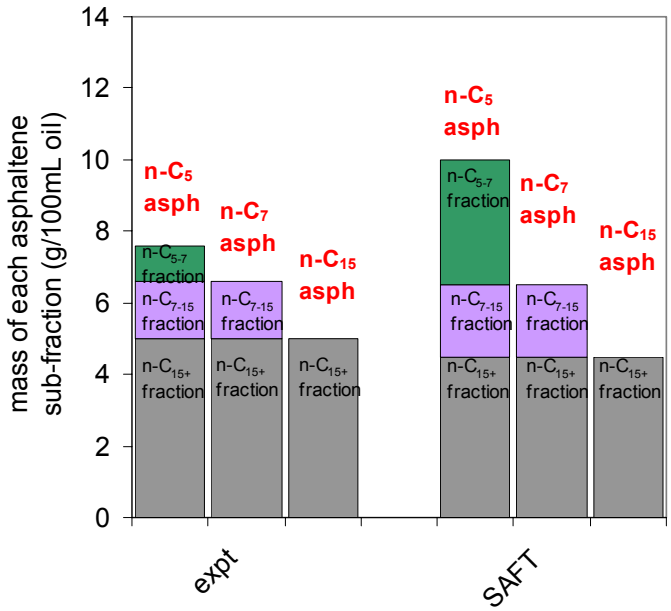

Figure 10.2. Comparison of saft and experimental mass distribution of each asphaltene sub-fraction in lagrave asphaltenes. The red column labels identify the precipitants used to extract the asphaltenes. Experimental data are from wang (2000).

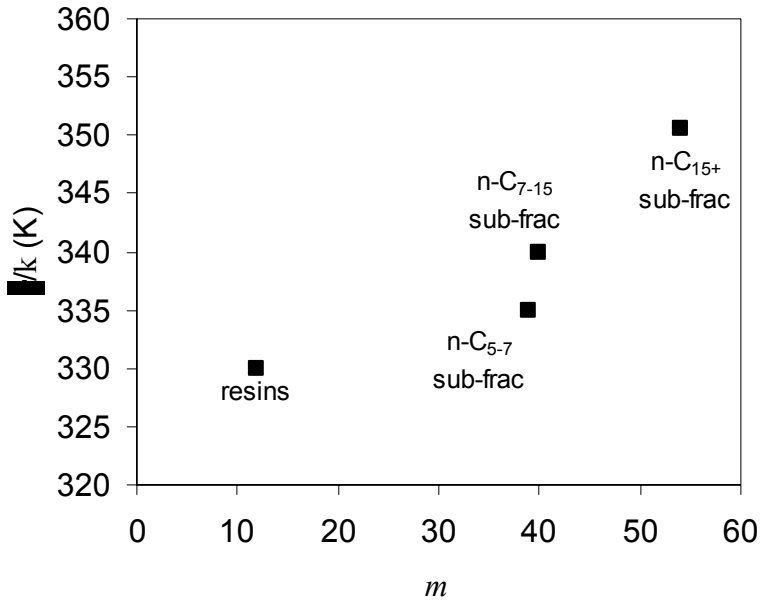

Figure 10.3. Plot of ε/k vs. m for the various SAFT asphaltene sub-fractions and resin.

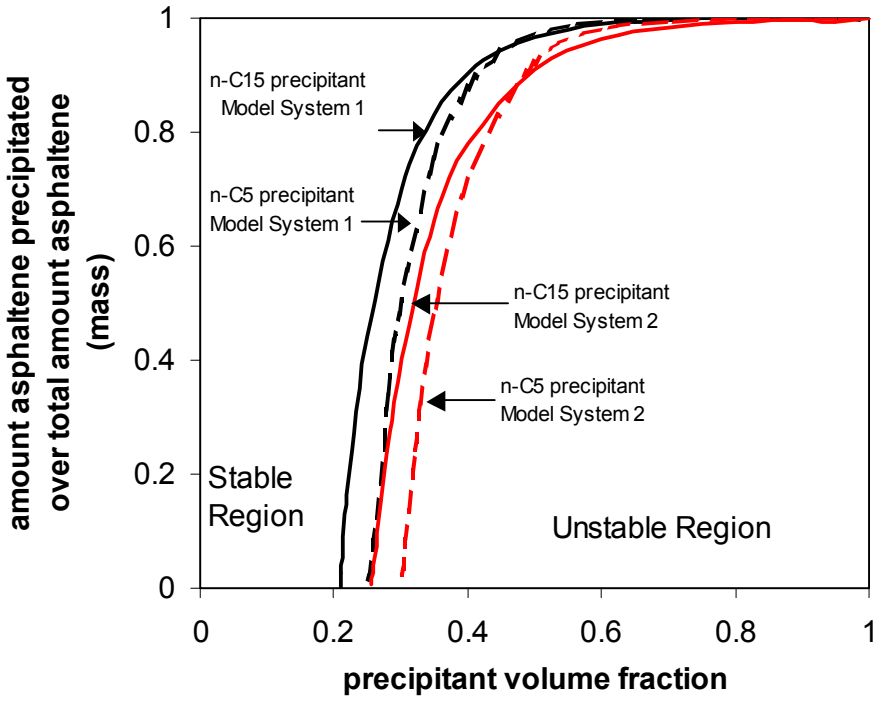

Figure 10.4. Solubility of monodisperse asphaltenes in model Lagrave oil (7.5g asphaltene/100mL toluene) mixed with n-alkanes at 20°C and 1 bar.

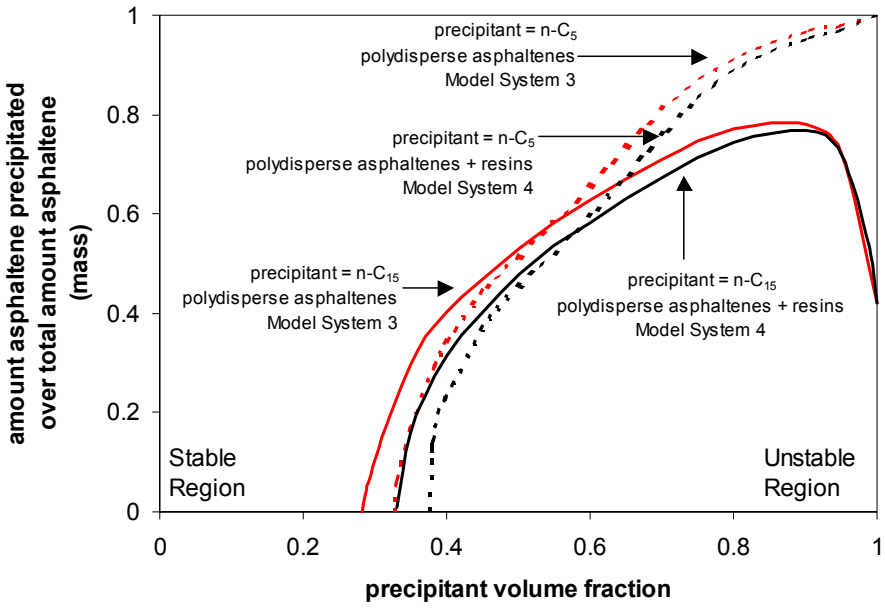

Figure 10.5. Solubility of polydisperse asphaltenes (with or without resins) in model Lagrave oil (7.5g total asphaltene/100mL toluene) mixed with n-alkanes at 20°C and 1 bar.

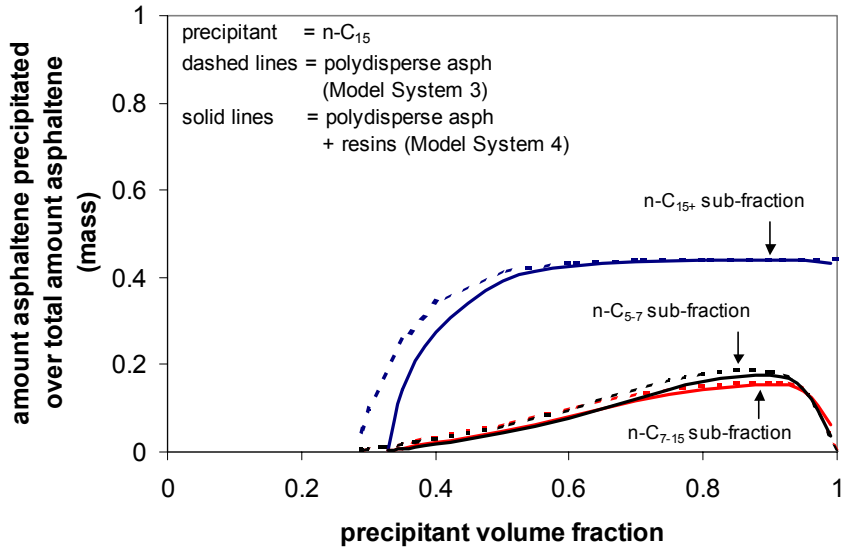

Figure 10.6. Normalized distribution of the asphaltene sub-fractions in the precipitated phase as a function of volume fraction precipitant in the model oil mixtures.